Radionuclides and heavy metals concentrations in particulate matter around uranium and gold mining towns of Erongo region, Namibia

Munyaradzi Zivuku

orcid.org / 0000-0002-6220-977X

Thesis submitted in fulfilment of the requirements for the degree
Doctor of Philosophy in Physics
at the North-West University

Promoter: Prof VM Tshivhase
Co-promoter: Prof NA Kgabi

Graduation ceremony: April 2020
Student number: 22622926

Abstract

The aim of the study was to measure the activity concentrations of naturally occurring radioactive materials (NORM) and these are: ^{226}Ra, ^{210}Pb , ^{238}U, ^{232}Th and ^{40}K and levels of toxic heavy metals in particulate matter (PM) and soil associated with mining activities in the two towns of Karibib and Arandis in Erongo region, Namibia. Furthermore, the radionuclides concentrations and toxic heavy metals were evaluated for their impact on human health and the environment. In both locations, some PM samples were collected with soil samples. Radioactivity measurements were performed with **γ-**ray spectrometer coupled with a high purity germanium detector (HPGe) while toxic heavy metal concentrations were determined by inductively coupled plasma mass spectrometry (ICP/ Ms). The activity concentrations from this study revealed higher levels of radionuclides associated with ^{238}U series and these were unevenly distributed among the sites. The most dominant concentration was found in ^{226}Ra, which ranged from 19.76 $\pm$ 0.47 to 135.29 $\pm$ 12.82 Bq.kg^{-1}. The activity concentrations in the samples were within the acceptable figures given by worldwide ranges of 11 to 64 for ^{238}U, 17 to 60 for ^{232}Th and 140 to 850 Bq kg^{-1} for ^{40}K (UNSCEAR, 2000). It is also interesting to note that the activity concentrations in PM was higher than the corresponding soil samples because the radioactivity concentrations increase as the average grain size decreases.

The radiological parameters associated with the measured radionuclides were: absorbed dose (D), annual effective dose equivalent (AEDE), radium equivalent activity concentrations (Ra_{eq}), external hazard index (H_{ex}) and internal hazard index (H_{in}) and excess lifetime cancer risk (ELCR) and the results showed that the mean radiological parameters in most samples were within the permissible limits with Ra_{eq} < 370 Bq.kg^{-1}, which corresponds to an upper safe limit of AEDE of 1 mSv.yr^{-1}, the prescribed acceptable limit by International Commission on Radiological Protection (ICRP) and thus, the potential radiological health effects may not be significant. However, some sites have hazard index closer to a unit which may imply that prolonged exposure to NORM in soil and PM in those mining areas may pose a health hazard to members of the public. Furthermore, the ELCR was found to be greater than 0.29 x 10^{-3}, the safe limit recommended by ICRP in all the samples, which may be a health risk to individuals as the chances of developing cancer due to radionuclides could be high.

The average indoor radon concentrations from the two mining towns was found to be 88 Bq.m^{-3}, which corresponds to an annual effective dose of 2.22 mSvy^{-1}. The mean values

due to exposure to radon and its decay daughter is two times higher than the worldwide average annual effective dose of 1.26 mSv (UNSCEAR, 2000).

The toxic heavy metals concentrations measured in this study were Fe, Mn, Cr, Zn, Cu, Ni, Pb, As, and Cd. The results for the average toxic metals concentrations were compared with the FAO/WHO soil guidelines and other countries to determine whether they were within the allowable limits. The results showed that most of the measured values were found to be within the permissible limits. Pollution contamination indicators were applied to quantify the level of contamination and it was found that contamination factors for most of the samples in the towns of Arandis and Karibib show a low level of contamination while the pollution load index (PLI) and the Geoaccumulation Index (Igeo) illustrate that the soils are not polluted. Similarly, the elemental composition was determined by a scanning electron microscope attached to an energy dispersion X-ray (SEM/EDX) and the major particles identified in the samples were: biogenic particles, soot, aggregates, aluminosilicates, mineral particles, quartz particles, clay particles, and non-biogenic C rich particles.

The non-carcinogenic risk of heavy metals of the soil samples in the two towns of Karibib and Arandis was assessed and the total HQ in Arandis town was $1.52x10^{-1}$ and $7.04x10^{-1}$ for adults and children respectively, while in Karibib town, it was $8.83x10^{-2}$ for adults and $3.86x10^{-1}$ for children. These values were less than 1 and therefore, not significant. The computed total carcinogenic risk due exposure to heavy metals in Arandis town was also found to be 1.40×10^{-3} for adults, and 1.30×10^{-2} for children. In Karibib town, the cancer risk value for adults was found to be 4.25×10^{-4} and in children it was 3.97×10^{-3}. Since these values were higher than the worldwide average Excess Lifetime Cancer Risk due to exposure to radionuclides from terrestial origin (0.29×10^{-3}) (Taskin et al, 2009) and thus there higher chances of increase in cancer among the inhabitants of these mining towns due to heavy metal exposure.

Key words

Radioactivity, particulate matter, annual effective dose, toxic heavy metals, excess lifetime cancer risk

Declaration

I, Munyaradzi Zivuku hereby declare that this research dissertation titled “Radionuclides and heavy metals concentrations in particulate matter around uranium and gold mining towns of Erongo region, Namibia”, is my own work executed at the North-West University. This work has not been submitted in any form in order to be awarded a degree at any other institution, nor has it been previously published. All the resources that were consulted in the preparation of this work has been cited and acknowledged.

Signature: _  _ _____ Date: _05 December 2019___

Acknowledgements

I would like to thank my two supervisors, Prof VM Tshivhase and Prof NA Kgabi, for their patient guidance, encouragement and advice they have provided throughout my Phd studies. Most importantly, I would like to thank Dr T Dlamini for his guidance and constructive criticism. I have been extremely lucky to have supervisors who took me through each step and responded timely to my questions and queries without them this research would not have been completed. I would like to thank North West University for providing the Bursary scheme and a conducive environment that made it possible to complete my studies.

My gratitude also goes to the Centre for Applied Radiation Science and Technology (CARST) for their assistance and technical support in many areas of my studies. Special attention goes to Mr Sam Thaga, Monde Kakula for administrative support in securing the much-needed resources promptly and Mr Tobias Mawase technical support in analysis of my samples. I would also like to thank the Municipalities of the two of Arandis and Karibib for granting me the opportunity to collect particulate matter (PM) and soil samples within their jurisdiction. I must express my gratitude to Thembinkosi, my wife, for her patience, continued support and encouragement throughout my studies.

Completing this work could have been a daunting task were it not for the support and friendship provided by colleagues and peers at both the North West University (NWU) and Namibia University of Science and Technology (NUST) who have continuously showered me with words of encouragement. In particular, I would like to thank Mr Markus Hitila, Dr Sylvanus Onjefu and Dr Casper Kamunda for their technical support throughout my studies.

List of Abbreviations

µm	Micrometer
ADC	Analogue to digital converter
AEDE	Annul effective dose equivalent
ALARA	As low as reasonably achievable
ASTM	American Society for Testing and Materials Standard Method
BC	Black carbon
BM	Building material
DNA	Deoxy ribonucleic acid
ELCR	Excess lifetime cancer risk
FWHM	Full width at half maxima
GeV	Giga electron volt
GPS	Geographical positioning system
Gy	Gray
HPGe	High purity germanium detector
IAEA	International Atomic Energy Agency
ICP-MS	Inductive couple plasma mass spectroscopy
ICRP	International committee on radiation protection
K	Kelvin
LET	Linear energy transfer
MDA	Minimum detection activity
MeV	Mega electron volt
NAA	Neutron activation analysis
NCRP	National Council on Radiological Protection
NGM	Novachab gold mine
nm	Nanometre
NORM	Naturally occurring radioactive material
NPC	National Population Commission
NUST	Namibia University of Science and Technology
OC	Organic carbon
PAE	Potential alpha energy

PAEC	Potential alpha energy concentration
PM	Particulate matter
$PM_{2.5}$	Particles with aerodynamic diameter less than 2.5 microns
Ra_{eq}	Radium equivalent
RF	Radio frequency
RF	Risk factor
RUM	Rössing uranium mine
SEA	Strategic environmental assessment
SEM/ EDX	Scanning electron microscopy energy dispersion X -ray
Sv	Sievert
UNSCEAR	United Nations Scientific Committee on the effects of Atomic Rad
USEPA	United State Environmental Protection Agency
WHO	World Health Organization
WLM	Working level month
WNA	World Nuclear Association
WSRA	World surface rock average

Table of Figures

List of Tables

TABLE OF CONTENTS

CHAPTER 1 : INTRODUCTION AND PROBLEM STATEMENT

1.1 Introduction

Environmental radionuclides can be divided into three groups: radionuclides of primordial origin, radionuclides generated by cosmic-ray interaction in the atmosphere and radionuclides generated by human activities. These are inherently present in small but measurable quantities in rocks, soil, water and the atmosphere that constitute the earth's surface (Tzortzis & Tsertos, 2004). Human beings are exposed to radiation through various pathways such as ingestion of radionuclides present in the food, soil and water, and sometimes through the inhalation of radon gas and its progeny and/or radioactive particulate matter (PM), which may contain solid short lived alpha-emitters or long lived radionuclides. Indirect contamination by radionuclides can occur through an extremely complicated path, passing right down to the food chain. For this reason, it is necessary to examine the potential contamination of the atmosphere by naturally occurring radioactive materials (NORM). With this information in mind then it will become easy to assess the harmful effects on organs of the human body.

Extensive work has been done in many countries to quantify radioactivity and toxic heavy metals in environmental samples including soil, water and food. In Namibia, there is very little research on environmental radioactivity. Some few research studies done are only concentrating on few geographical locations. For example, a handful of researchers have evaluated the soils of Erongo region for radioactivity (Oyedele et al., 2006; Zivuku et al., 2016) while Onjefu et al., 2017 have examined the soils of Henties Bay and Swakopmund for toxic heavy metals and radionuclides concentrations. However, to all these studies, there was very little attention being given in measurement of radionuclides and toxic heavy metals in particulate matter associated with mining activities. Thus, this study was undertaken with the aim of investigating radionuclides concentrations and toxic heavy metal levels in PM and evaluate the health risk due exposure to these pollutants to the inhabitant's of uranium and gold mining towns of Erongo region of Namibia.

1.2 Overview on radon as a carcinogen in modern societies

Research conducted by many groups such as the Centre for Disease Control, the American Lung Association, the American Medical Association and the Public Health Association has confirmed radon to be a known human carcinogen that can cause some

negative human health effects. Consequently, the risks from indoor radon exposure have been a major concern for the general population (EPA, 1992). Furthermore, epidemiological studies conducted in many countries have shown strong and compelling evidence of close association between indoor radon concentration and lung cancer (WHO, 2014). The exposure to indoor toxicity comes from the isotopes of ^{222}Rn and ^{220}Rn and these have short lived-lived decay products, these are formed as ions and they have an affinity for water molecules or air where they form aerosols. These radon progenies which are solids, short-lived alpha energy emitters are inhaled into the lungs where they settle on the delicate alveolar linings and emit radiation which cause multiple radiation damage to the DNA .

Assessment of radiation dose due to radon exposure is achieved by considering the amount of alpha energy released when radon and its short-lived alpha emitter undergoes transformations. These are the potential alpha (PAE) which relates to the total alpha energy emitted during the decay of ^{222}Rn and its daughters to ^{210}Pb or the decay of ^{220}Rn and its daughters to ^{208}Pb. The potential alpha concentration (PAEC) which is PAE per unit volume i.e. linked to the mixture of ^{222}Rn and ^{220}Rn progeny in the air.

Indoor radon concentration can be affected by several factors such the concentration of uranium in the soil, building material (BM), the outdoor air, water supply to a building and natural gas. Radon in the soil and the BM permeates the buildings through diffusion and advection air flow currents. Similarly, a building water supply may contain a considerable amount of radon which contributes to the total radon exposure while the radon gas from natural gas is generally neglible. Additionally, the concentration of indoor radon can vary due to air exchange between the indoor and outdoor air.

1.3 Problem statement and motivation

The worldwide increase in population and the technological advancement have led to massive exploitation of natural resources which in turn have left a permanent footprint to the environment. Activities such as mineral mining and exploration involve removal or clearance of vegetation, drilling and excavation of land which lead to significant pollution of the atmosphere by emission of particulate matter (PM) containing dust, smoke, fumes and aerosols, gases (sulfur dioxide, nitrogen dioxides, and hydrocarbons), radioactive materials (Rana et al., 2016; Bhaskar & Mehta, 2010). Airborne particulate matter that contains radionuclides and heavy metals are considered as a public health concern as it can enter the human respiratory system (Csavina et al., 2012). These studies were further supported

with epidemiological studies conducted in many countries which have established a close link between PM and the occurrence of respiratory and cardiovascular diseases (O'Toole et al.,2008). Radioactive substances may increase human exposure to radiation through inhalation, ingestion and skin contact leading to the development of cancer.

Studies on radionuclides levels and heavy metals concentrations have been performed in different countries to determine the dose to members of the public and the workers and in order to establish the degree of contaminations and hence chemical toxicity due to heavy metals (Watson et al, 2005; Tzortis and Tsertos, 2004). These studies were concentrating on matrix such as soil, water and to a lesser extent on food with little attention being given to characterisation of particulate matter (PM) in terms of its radiological and chemical toxicity. The main pathway by which human beings are exposed to radionuclides (and heavy metals to a lesser extend) is through inhalation of radon gas and its progeny. It is estimated that more than 50% of the total dose received by the world's population is associated with inhalation of radioactive particles in the form of particulate matter (Charles, 2001). The deposition of aerosols in the human respiratory system depends on aerosol size and its distribution. Large particles (PM_{10}) do not travel deeper into the respiratory track because they are trapped by cilia and mucus upon entering the respiratory system whereas fine particles ($PM_{2.5}$) are able to reach the pulmonary alveoli (Ny & Lee, 2011).

Background levels of radionuclides in PM can be elevated due to industrial process involving naturally occurring radioactive materials (NORM) work activities such as mining of uranium and gold. The Erongo region of Namibia is host to Rössing uranium mine and Novachab gold mine and these mines generate large amounts of PM which could disperse into the atmosphere. The PM may contain toxic metals and naturally occurring radioactive materials (NORM) which may pose a radiation hazard to the workers and the population residing nearby these mining sites. The town of Arandis is situated 16 km from Rössing uranium mine and Karibib town is 10 km from Novachab Gold in the Erongo region. Since most mining activities are concentrated in the Erongo region, this study was undertaken to investigate the radionuclides and toxic metals levels in particulate matter (PM) as the people residing nearby these mines are susceptible to adverse health effects emanating from the mining activities.

The major industrial activity in Erongo region of Namibia is mining and it has been demonstrated that mining is the greatest contributor to environmental pollution due to the emission of vast amounts of wastes containing particulate matter, toxic heavy metals and polycyclic hydrocarbons (Wahl et al, 2007; Kamunda et al, 2016). Although the Erongo region of Namibia has shown as an area with high background radiation, research on radioactivity has not been growing at a fast pace and hence data related to environmental radioactivity is limited. Even if the data is available, it is usually concentrated to few geographical areas and /or is mainly on soil radioactivity. Data on radioactivity and heavy metals pollution in PM associated with mining activity has been neglected and as a result the general population are not aware or have very little knowledge of the potential health hazards of these pollutants to their communities. It is important to investigate environmental radioactivity and heavy metals in Erongo region so as to provide base line values. The information can assist Namibia Radiation Protection Authority (NRPA) in formulating dose limits to which the general population and workers can receive radiation dose and thus protecting human health and the environment.

1.7 Research aim and objectives

1.7.1 Aim

The aim of the study was to investigate radionuclides levels and heavy metals concentrations in particulate matter (PM) associated with uranium and gold mining in the Erongo region of Namibia.

1.7.2 Objectives

The objectives of the study were to:

- evaluate the activity concentrations in PM and soil associated with mining activities,
- determine the indoor radon concentrations in selected households nearby the mining sites,
- assess the radiological health risk due to NORM in soil,
- investigate the concentrations of heavy metals in soil associated with mining activities,
- conduct morphological analysis of particulate matter (PM) associated with mining activities and,
- evaluate toxicological risk due to toxic heavy metal associated with mining activities.

CHAPTER 2 : LITERATURE REVIEW

2.1 Mining in the Erongo region of Namibia

Mining is the biggest contributor to Namibia' economy in terms of revenue and it accounts for 25% of Namibia 's income with a contribution of 11.6 % in 2014 which makes it one of the largest economic sectors (https://www.npc.gov.na). There are many minerals being mined throughout Namibia and these include diamond, gold, cobalt, felspar, manganese, fluorspar and uranium. However, in Erongo region, the major resources mined is uranium followed by gold. As a result of the mining activities, several towns have been established to cater for the work force who work in these mines. The notable mines and their associated resources mined are Langer Heinrich Mine near Swakopmund town for Uranium mining, Husab mine near Arandis town for uranium mining, Rössing uranium Mine near Arandis for uranium mines and Navachab gold mine near Karibib town.

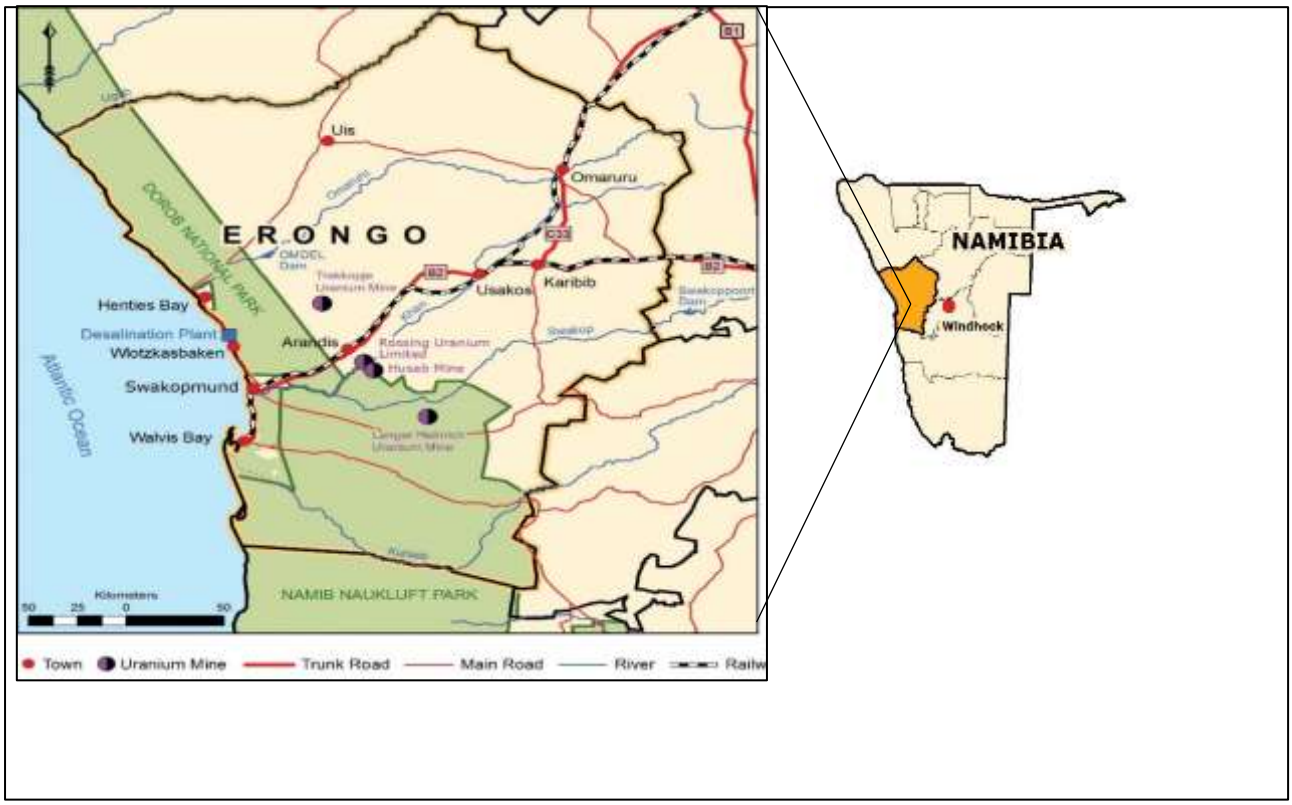

Figure 2.1 Map showing the sampled areas (https://www.rosing.com)

Furthermore, mineral processing involves addition of chemicals containing a multitude of heavy metals which end up as wastes and these are discharged into the environment where they may be in cooperated into soil or underground water systems. These pollutants

may be taken up by plants and join the food chain where they will eventually get ingested by human beings and cause negative health effects such cancers but may also induce non-cancer illness such as eye lens distraction, diabetes and radiogenic illness (Busby, 2010).

Mining operations also discharge large quantities of particulate matter (PM) which are generated during clearance of large, excavations, blasting and movement of vehicles and heavy machinery which can pollute the atmosphere. These pollutants may undergo physicochemical transformation as they are transported to remote places where they affect the nearby communities. The PM may contain toxic heavy metals and radioactive materials which have the potential to cause serious health effects to the people and the environment. The current study gives an overview of mining in the Erongo region of Namibia with specific focus on the two mining towns understudy: Karibib town and Arandis mine town in which gold and uranium are mined, respectively.

The Erongo region is geographically located at -23^0 06”60.00”S and 14^0 51’59.99” E and with about 150,400 inhabitants and a low population density 2.4 km^{-2} (http://www.gov.na/documents). Figure 2.1 shows a map of the Erongo region. The greater part of Erongo region is found in the Namib desert which characterised by low rainfall of less than 10 mm per year, high daily temperatures that can reach 60^{0}C and night temperatures below 0^{0}C.

2.2 Environmental pollution due to mining activities

Although it is well known that toxic heavy metals and radionuclides are inherently present in the biosphere in minute quantities, their concentration may be increased to levels that are detrimental to human health and the environment (Thakur et al., 2004). The atmospheric pollution or surface contamination due to heavy metals and radionuclides in urban environments is largely due to anthropogenic activities resulting from rapid pace of industrialisation, motorization and urbanisation (Tong and Lam, 1998). Mining activities have been the main sources of toxic heavy metals and radionuclides in the environment (Duruibi et al., 2007; Boampsonsem et al., 2010) and exposure to these pollutants pose the greatest threat to human health and the environment (Csavina et al., 2012). Excessive emissions of PM containing heavy metals, often in the form of insoluble particulates (Duzgoren-Aydin et al., 2006), contaminate the environment, as they become airborne where they can be carried to remote places and affect nearby communities. The heavy metals from the mining environment may become soaked in water bodies and carried to remote areas where they

can be deposited in soil and plant materials. These heavy metals are potentially hazardous to human health due to their persistence, toxicity and can be incorporated into food chains (Santos et al., 2005).

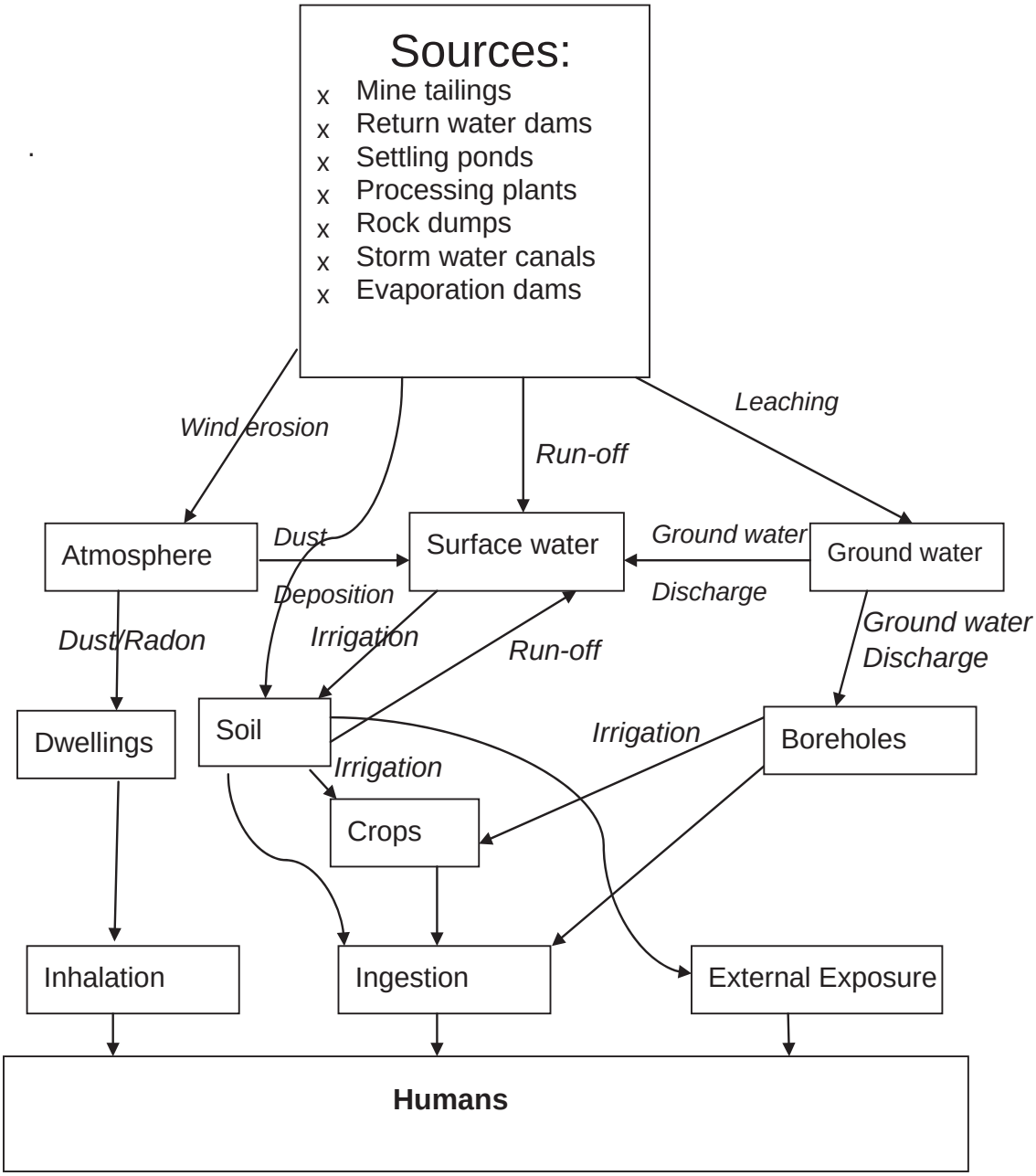

Figure 2.2 Human exposure pathways to heavy metals and radionuclides (Kamunda et al., 2016)

The major pathway by which radionuclides and heavy metals can enter the environment from a mining site is through airborne pathway. The other contribution is through external irradiation after authorised entry into the mine site, and by living in settlements adjacent to mines or abandoned mines (Sutton & Weiersbye, 2008).

2.3 Particulate matter (PM)

Particulate matter (PM) represents a complex mixture of organic and inorganic particles that are dispersed into air and these particles are heterogeneous in their physical characteristics, chemical composition, and origin and have toxic effects on human health. The inorganic components of particulate matter are mainly derived from both natural and anthropogenic sources (Shandilya et al., 2009). Depending on the aerodynamic diameter, PM can remain suspended for a long time enough to penetrate the pulmonary system (Li et al., 2013; Polichetti et al., 2009). The differences in physical and chemical characteristics of PM are largely due variability of emission sources, formation and the chemical transformations that these particles undergo during their lifetime. It is estimated that PM originating from agricultural and industrial practices contributes to about 30 to 50 % of the total dust burden of the atmosphere (Prospero et al., 2002).

Although PM_{10} and $PM_{2.5}$ are inhalable particles, $PM_{2.5}$ has demonstrated the greatest impact on human health due to its small size which allows it to easily travel deep into the alveolar lining of the respiratory system where it can illicit some anti-inflammatory response leading to the development of cancer, morbidity and cardiopulmonary mortality (Rashki, 2012). Radionuclides and toxic/heavy metals contained in PM travel from their source through various environmental exposure pathways to final receptor: the human body as illustrated in Figure 2.2.

2.4 Radioactivity and radiation

According to Choppin et al., (2002), radioactivity is defined as a statistical process by which an unstable atomic nucleus transforms to a more stable configuration. This process results in the element emitting particles (alpha, beta) or waves (gamma or X-rays) or any type of radiation. These emissions are collectively called ionising radiations because they can disrupt electrons from the outer shells of the atoms.

The disintegration rate is directly related to the number of radioactive nuclei of a type, N, at any given time, t. The probability of decay per unit time interval is called decay constant (λ). It is related to the time required for the decay of one half of the original number of its original nuclei present ($T_{1/2}$). The activity (A) is the number of decays per unit time interval and this can be expressed by the first order differential equation in 2.1 (Turner, 2007)

$$A = -\frac{dN}{dt} = \lambda \mathrm{N} \qquad (2.1)$$

where, A is the decay rate (activity) expressed in Becquerel (Bq) named after the French Physicist who discovered radioactivity Henry Becquerel (1852-1908). One Becquerel is equivalent to one transformation per second (1 Bq = 1 disintegration per second). For liquids and gases, the activity concentration is related to volume Bq/l, Bq/m^3. The activity concentration of each radionuclide is calculated using equation 2.2 (UNSCEAR, 2000)

$$A = \frac{C}{I\varepsilon mt} \tag{2.2}$$

where, A is the specific activity of the radionuclide,

C is the number of counts,

I is the intensity (emission probability) of the peak energy,

ε is the counting efficiency of the peak at the specific energy,

m is the mass of the sample in kg,

and t is the time of the measurement in s.

Radiation damage depends on the absorption of energy from the radiation and is approximately proportional to the mean concentration of absorbed energy in irradiated tissue. For this reason, the basic unit of radiation dose is expressed in terms of absorbed energy per unit mass of tissue, that is,

$$\text{Radiation absorbed dose (D)} = \frac{\Delta \text{E}}{\Delta \text{m}} \tag{2.3}$$

where, ΔE is the absorbed energy and Δm is the mass of the tissue (Cember, 2009). The unit for radiation absorbed in the SI system is called Gray (Gy) and is defined as follows:
one Gray is an absorbed dose of one joule per kilogram. However, the unit does not account for different radiations (Idaho State University, 2014). The biological effect of radiation depends not only on the energy deposited by radiation in an organism but also on the type of radiations, the tissue weighting factors and the sum of all radiation received by different tissues and the way in which energy is deposited along the path length and therefore another term that takes this action into account was introduced-the linear energy transfer (LET). LET describes the mean energy deposited per unit path length in the absorbing material. The unit

of LET is keV/µm and differs with the type radiation. For the same absorbed dose, the LET follows the following order alpha > neutrons >beta > gamma rays.

2.4.1 Sources of radiation

NORMs are inherently present in all environmental settings and they are the main ionising radiation to which human beings are exposed (Lilley, 2001). There are two main sources of radiation: natural sources which is composed of cosmic radiation formed as a result of the interactions of particles with heavy nuclei in the atmosphere and anthropogenic sources which are as a result of man's activities and these include medical applications, mining activities and to some extent agriculture activities. In a natural phenomenon, the radioactivity is in continuum with its environment, however, due to the action of human activities which disturb this environment by mining activities or addition of some radionuclides, this may lead to an increase in the background radiation to which man is exposed. The radionuclides may transported in various pathways through the air, water and soil until the reach the human being which is the ultimate sink where they can induce cancer and various ailments (Avwiri et al., 2007).

Cosmogenic origin

Cosmic radiation reaches the earth from interstellar space and the sun. Those cosmic radiations from the interstellar are referred to as galactic particles while those from the sun is called the solar particles (Martin et al., 2012). Cosmic radiation is composed of a wide variety of penetrating radiations which undergo many types of reactions with the element they encounter in the atmosphere. The primary highly energetic particles which impinges on the earth atmosphere are composed of 87% protons, 11 % alpha particles and 1 % heavy ions (Silberg & Tsao, 1990). Cosmic radiation is characterised by having extremely high energy and therefore highly penetrating with many of these particles falling in the range of 10 MeV to 100 GeV (Martin and Harbison, 2006).

The interaction of primary cosmic radiation with the atomic nuclei in atmosphere generates a cascade of secondary cosmic radiation such as electrons, gamma rays, neutrons and mesons. A considerable number of these cosmic radionuclides with half-life of few minutes to several millions years are produced, and these are ubiquitous. It is well documented that only four of these radionuclides contribute significantly to measurable dose of radioactivity in humans (Eisenbud & Gesell, 1997; UNSCEAR, 2000) and these radionuclides, their half-lives and inventory and distribution, are summarised in Table 2.1.

Table 2.1 Examples of cosmogenic radionuclides on earth (Martin et al., 2006)

Radionuclide	T ½ (years)	Global Inventory (Bq)	Inventory in the Biosphere	
			Distribution (%)	Activity (Bq)
^{3}H	12.3	1300	35	350
^{7}Be	0.146	37	8	3
^{14}C	5730	8500	4	340
^{22}Na	2.6	0.4	21	0.08

Terrestial origin

Terrestial radiation is external radiation from radionuclides that occur naturally in the earth's surface and on other materials on the earth. These radionuclides are characterised by long half-lives which are comparable to the age of the earth. Some of these primordial radionuclides have long transition series, while others are singly occurring radionuclides. These radionuclides and their half-lives include ^{238}U (T ½ = 4.5 x 10^{9} years), ^{235}U (T ½ = 7.04 x 10^{8} years), ^{232}Th (T ½ = 1.4 x 10^{10} years), ^{237}Np (T ½ = 2.14 x 10^{6} years) and ^{40}K (T ½ = 1.28 x 10^{9} years). The primordial radionuclides undergo transitions at a very slow rate to yield several radioactive products (progeny) in their respective transition cascades until a stable product is formed. Of these radionuclides, only three are of radiological concern and these are ^{238}U, ^{232}Th and ^{40}K because they have a significant contribution to the dose received by human beings ^{235}U contributes less than 1 % to the external gamma exposure to human and ^{237}Np is not present in nature anymore and thus two radionuclides are not considered in radiation protection measurements. It is worth mentioning that a radioisotope of the radioactive gas radon (Rn) is a member of every transition cascade.

Anthropogenic radionuclides

Mining operations such clearance of vegetation, excavation of soil, mineral extraction and processing may lead to the discharge of radioactive elements in the environment often making their concentrations higher than the normal background radiation. These radionuclides can either reach the human being at the site of discharge known as onsite or they can be dispersed away to remote places where they may join the food chain and they are called offsite. The discharged radionuclides may reach human settlements nearby the

mining sites where they may negatively affect the health of human being either directly through ionising radiation or internal exposure through inhalation of radioactive particulate matter (O'Brien and Cooper, 1998).

2.4.2 Forms of radioactive decay

Radioactive decay occurs by chance which leads to nuclear transformation with consequence formation of a new stable element which is usually preluded by the release of gamma energy in a quest to attain stability. More often than not, the daughter nuclide formed is unstable, this leads to a radioactive decay chain process until a stable nuclide is reached (Magill and Galy, 2004). The following subtopics discuss the main process by which radioactive elements decays.

Alpha decay (α)

Alpha emission is characteristic of many naturally occurring heavy radionuclides whose atomic number is greater than 82 but less than 92 (Lilley, 2009). Under those conditions, the heavy nuclei carries a neutron-to-proton ratio that is too low and this results in the emission of a highly energetic particle in the form of the helium nucleus (Cember and Johnson, 2009). This macroscopic particle carries a charge of +2 and consists of two protons and two neutrons. This process requires the conservation of elemental particles and the parent nuclide 's atomic number and its mass number will decrease by two and four respectively. The process can be demonstrated by the classical decay of ^{210}Po as illustrated in 2.4.

$$^{210}_{84}Po \rightarrow \ ^{206}_{82}\mathrm{Pb} + \alpha \qquad (2.4)$$

It can be deduced that the neutron to proton ratio of ^{210}Po is 1.5: 1 but following alpha particle emission a stable daughter nucleus, ^{206}Pb is formed and the ratio is 1.51:1 (Cember and Johnson, 2009). This can be explained in two folds: in heavy nuclei there is a general increase in electrostatic repulsive force which overcome the cohesive nuclear force and as result the nuclei disintegrate and secondly, the emitted heavy particle must have sufficient energy to overcome the high potential barrier at the surface of the nucleus due to the presence of positively charged nucleons as shown in Figure 2.3 (Cember and Johnson, 2009).

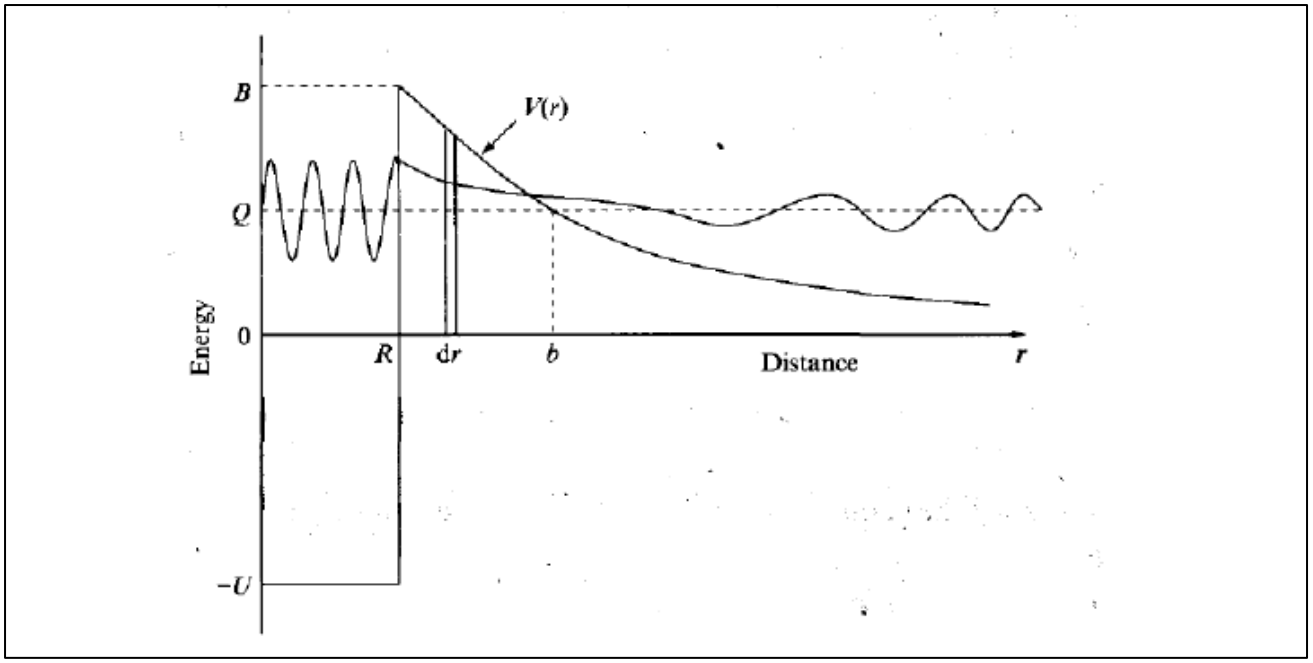

Figure 2.3 Schematic diagram of tunnelling of alpha particles through coulombic barrier (Gilmore and Hemingway, 2008)

By considering quantum physics and the idea of wave functions, it is easier to explain the emission probability using the quantum mechanical tunnelling. As can be seen in Figure 2.3, the macroscopic alpha particle is trapped in a potential barrier and has to tunnel through the barrier and emerge outside provided it has sufficient energy (Lilley, 2001). The shorter the half-life of the greater the probability of tunnelling through the barrier. The probability of tunnelling through the barrier increases with separation of energy of the particle (Krane, 1987).

Beta decay (β) and electron capture (EC)

Beta particles are derived from a nucleus having excess of neutrons which causes the atom to be unstable. A neutron can be converted into a proton and emit highly energetic negatively charged particle known as negatron. Alternatively, a proton is converted into a neutron, positron and a neutrino and thus a nucleus can attain stability as shown in expression 2.5. This process is known as positron emission and the result is positively charged electron.

Beta-plus decay $$p \rightarrow n + \beta^{+} + v \qquad (2.5)$$

Following emission, the positron comes under the influence of coulombic forces of the nucleus with consequence annihilation and two photons are emitted. An example of this decay is found in equation 2.6

$$22_{Na} \rightarrow 22_{\mathrm{Ne}} + \beta^{+} + v \tag{2.6}$$

Another form of beta decay is beta minus (β^{-}) in which a nucleus emits a negative electron from un unstable radioactive nucleus, and this is common with nuclides with excess neutrons. An example of negatron decay is shown in equation 2.7.

$$14_{C} \rightarrow 14_{\mathrm{N}} + \beta^{-} + v \tag{2.7}$$

Immediately after the emission of the beta particle, the daughter is positively charged having the same number of electrons as the parent atom and this positive charge is easily lost through capturing by the daughter of an electron within its vicinity.
The third type of beta decay is Electron Capture (EC) and this is analogous to (β^{+}), in fact the charge of the nucleus decreases. The process results in the ejection of neutrino and the emission of an X-ray when the electron is not filled by the surrounding electrons.

Gamma emission (γ)

This is not a form of decay like the alpha or beta in that there is no change in the number of nucleons in the nucleus; there is no change in Z, N or A. Gamma-rays are mono electromagnetic radiations that are emitted from the nucleus of an excited atom following a radioactive transformations (Gilmore and Hemingway, 2008) and they provide a means for the nuclei to attain stability. Following alpha or beta decay, an excited nucleus may lose energy in a transition to a state lower in energy in the same nucleus. When this happens, the transition energy ΔE, is defined by the difference in energy between the first and last and may appear as γ-ray photon (Lilley, 2001; Friedlander, 1981) and the energy released from gamma photons can be expressed by equation 2.8.

$$E_i = E_f + E_\gamma + E_R \tag{2.8}$$

where, E_i excited state of the nucleus and E_f, is the final state of the nucleus and energy is conserved and this equation can be rearranged as;

$$\Delta E = E_i - E_f = E_\gamma + E_R \quad (2.9)$$

During this process, recoil energy E_R , becomes infinitesimal and can be neglected (Debertina et al., 1988) and thus, the gamma-ray energy E_γ, is approximal equal to the energy of the de-excitation ΔE, which is the energy difference between the two states. (Lilley, 2001).

Branching ratio

During measurements of naturally occurring radioactivity, there are several possible decay schemes to describe the disintegration of nuclei. It has been shown that some nuclei may decay through a single decay mode while others decay only through different competing decay modes involving alpha and beta emission with different relative decay probabilities (Krane, 1988).

The branching ratio is defined as the probability of a nuclear decay by more than one mode. This occurs because there are a number of possible decay modes within a nucleus. An example of this decay mode is illustrated by ^{40}K which has a probability of 10.72% to decay to ^{40}Ar or it can decay by positron emission with a probability of 10.67% and electron capture with probability of 0.048 % (Bou-Rabee, 1997). It can also decay to ^{40}Ca by Beta minus with a probability of 89.28 % as depicted in Figure 2.4.

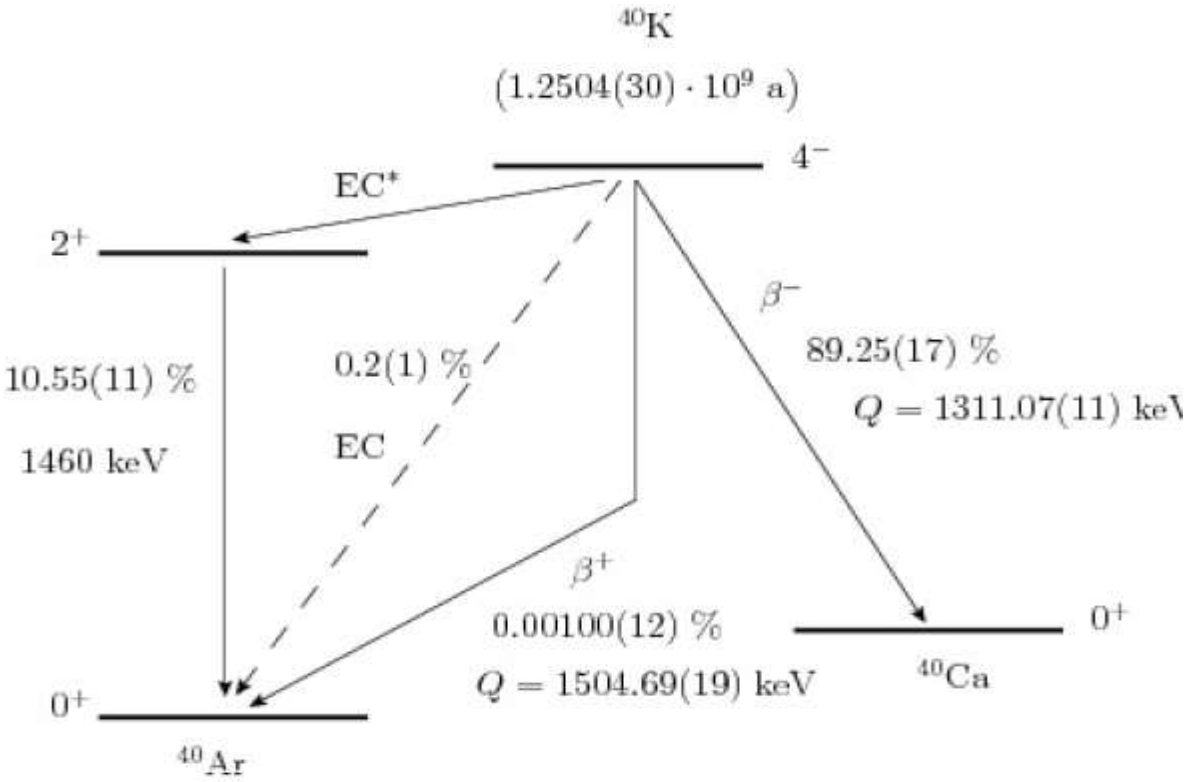

Figure 2.4 Branching decay scheme of ^{40}K (Pradler and Yavin, 2013)

2.4.3 NORM

Naturally occurring radioactive material refers to material containing primordial radionuclides and these include radiostopes of uranium, actinium, thorium decay series as well as potassium-40. These radionuclides are of radiological concern in radiation protection because of their potential to cause cancer to humans. It has been confirmed that there is a close association between inhalation of short-lived radioactive progeny of radon gas and lung cancer. Radon (Rn) is released from materials containing radium isotopes and accumulates where ventilation in compromised. The measurement of indoor radon concentrations and the activity concentrations of primordial radionuclides in materials are of interest for controlling the exposure emanating from these radionuclides.

Sources of NORM

Most of the radionuclides in NORM arise from the decay products of uranium and thorium. For example, the decay products of radium will give rise to a high concentration of radon and its decay products which are detrimental in human health. It is well documented that human activities and technological processes may increase the concentrations of

radionuclides in NORM (Faanu et al, 2011). These industrial activities may concentrate the radionuclides to a degree that can pose a risk to humans and the environment. Examples of industries associated with the processing of NORM with elevated concentrations of radioactive materials include mining and milling of metalliferous and non-metallic ores, production of coal, oil, and gas, extraction and purification of water, generation of geothermal energy and production of industrial minerals, including phosphate, clay and building materials. Since radioactive materials are responsible for ionising radiation, members of the public and workers may be exposed to these radionuclides and therefore it is important to monitor the doses to the population due to NORM to assess the potential health risk.

Decay chain series

A radioactive parent nuclide can decay leading to the formation of a stable nuclide (LÁnnunziata, 2007). For example, the ^{14}C nuclide decays to form a stable product of ^{14}N as indicated by the equation 2.9.

$$^{14}_{6}C \rightarrow {}^{14}_{7}N + \beta^{-1} + \bar{\nu} \qquad (2.9)$$

Several isotopes exhibit this characteristic decay mode and some of them are ^{3}H, ^{32}P, ^{36}Cl, ^{131}I (LÁnnunziata, 2007). However, the most common decay sequences result in the formation of a nuclide that is unstable which undergoes further radioactive decay (Krane, 1988). This can be illustrated by a schematic decay chain which starts with a radioactive parent nucleus P decaying with a constant $\boldsymbol{\lambda}_p$ into a daughter nucleus D, which in turn is radioactive and then subsequently decays with a decay constant $\boldsymbol{\lambda}_D$ into a stable grand-daughter nucleus, G, as shown below (Krane, 1988).

$$\mathrm{P} \xrightarrow{\boldsymbol{\lambda}_p} D \xrightarrow{\boldsymbol{\lambda}_D} G\ (stable)$$

Considering that the number of nuclear specie present are P, D and G at a given time t, we can derive some differential equations to express the decay and build-up of various nuclides as follows (Prince,1979).

$$dN_p = -\boldsymbol{\lambda}_p N_p \qquad (2.10)$$

$$\frac{dN_D}{dt} = \boldsymbol{\lambda}_p N_p - \boldsymbol{\lambda}_D N_D \qquad (2.11)$$

$$\frac{dN_G}{dt} = -\boldsymbol{\lambda}_D N_D \quad (2.12)$$

where, dN_p is the change in the quantity of radioactive parent nuclei and dN_D is the rate of change in the number of daughter nuclei which equals the difference between build-up of new daughter nuclei through the decay of the parent nuclei and the loss of the daughter nuclei from the decay of itself to a stable product (Halliday, 1955).

It is common that the grand-daughter of a radioactive decay is still unstable and continues with producing another radioactive product and thus, it is possible to have series or chains of radioactive decays (Lilley, 2001). There are three main limiting conditions that govern sequential radioactive decays and these are; (i) secular equilibrium (ii) transient equilibrium and (iii) no equilibrium (LÁnnunziata, 2007).

Series radionuclides

Many of the naturally occurring radioactive elements are members of the four long radioactive decay series, which are uranium, thorium, actinium and neptunium series (Lilley, 2001). These primordial radionuclides undergo transitions at a very slow rate to produce radioactive products (progeny) in their respective cascades until a stable isotope. These series are summarised in Table 2.2.

Table 2.2 Series radionuclides

Primordial radionuclide	Half-life (years)	Number of intermediates	Final product
^{238}U	4.5 x10^{9}	14	^{206}Pb
^{235}U	7.04 x10^{8}	12	^{207}Pb
^{232}Th	1.4 x10^{10}	10	^{208}Pb
^{237}Np	2.14 x10^{9}	12	^{209}Bi

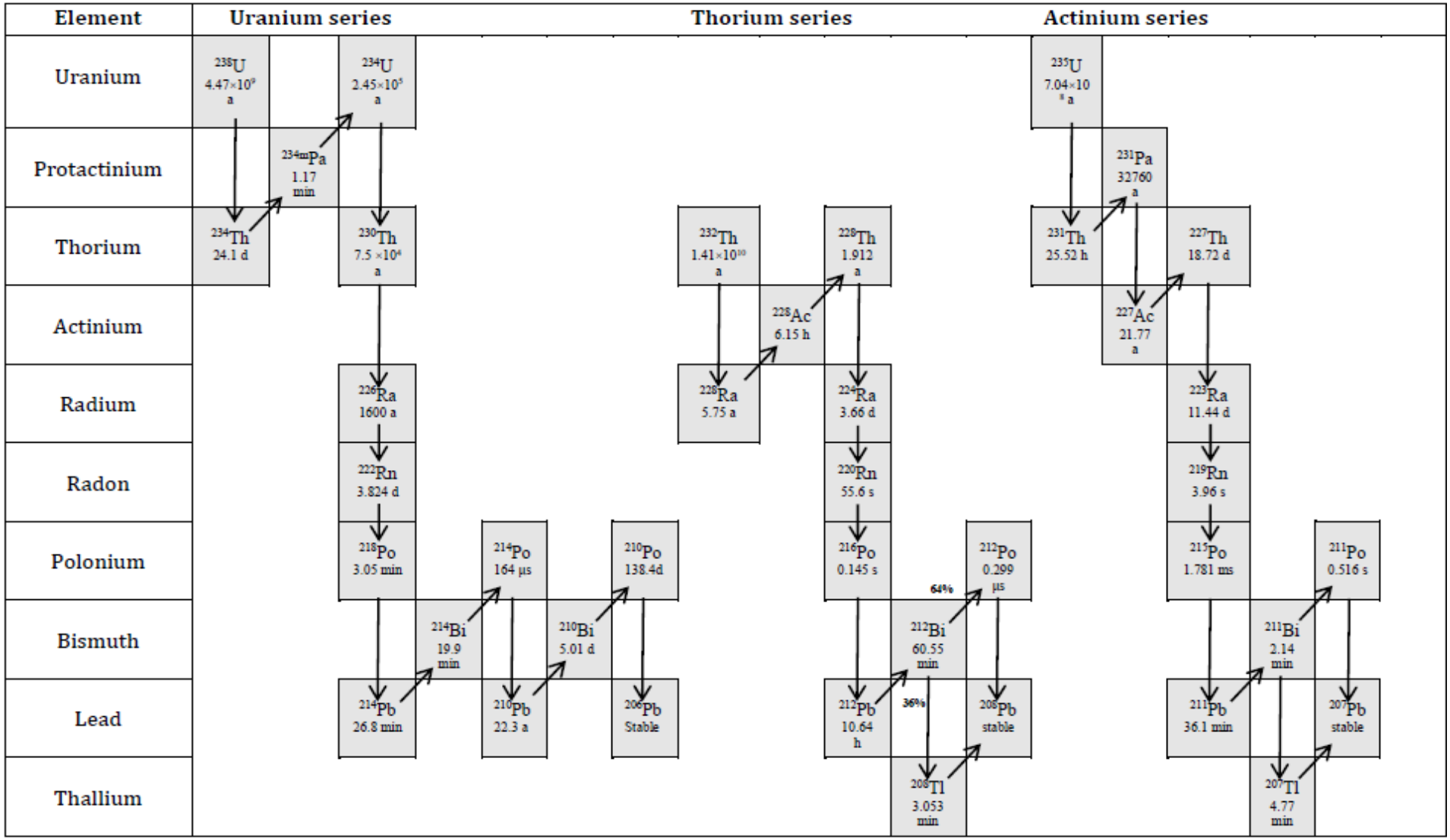

Figure 2.5 Uranium, thorium and actinium decay series (Alharbi, 2016)

The non- existence of the head of Neptunium series and the relatively short half-life daughters means that this series is not of radiological concern in radiation protection measurements (NCRP,1975). Uranium consist of two radioisotopes ^{238}U and ^{235}U which have an isotopic natural abundance of 99.3% and 0.7% respectively. ^{232}Th is the most abundant of all naturally occurring radioisotopes. The principal decay schemes of three radioactive series are ^{238}U, ^{235}U and ^{232}Th and the details of each radionuclide within the chain are presented in Figure 2.5.

Non-series radionuclides

These are nuclides that are not members of any series and they have extremely long half-lives and these are considered to be the same age as the earth (4.5 x 10^9 years). Most of these nuclides have low specific activity which makes their detection and identification very difficult except for ^{40}K and ^{87}Rb.

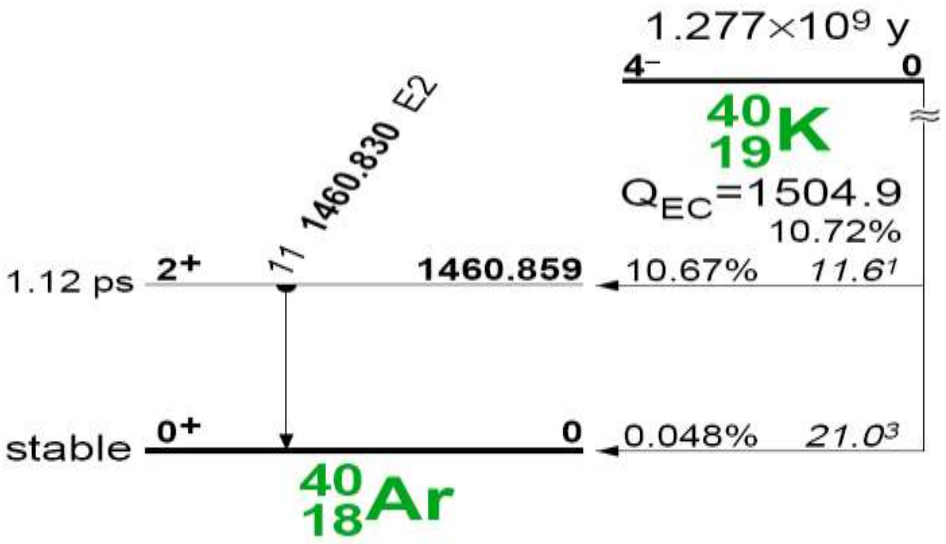

Figure 2.6 Schematic of the $^{40}_{20}K$ decay (Browne et al., 1986)

These two radionuclides are of interest in radiation protection because they are ubiquitous in the environment and have a significant contribution to human exposure (Watson et al., 2005). ^{40}K has a half-life of 1.28 x 10^9 years and contributes about 40% to natural radiation received by humans. It is available as natural potassium with an isotopic abundance of 0.0117% and can transmutate to Ar by β^{-1}decay accompanied with γ-ray emission while ^{87}Rb undergoes beta decay only (NRP, 1975) as demonstrated in Figure 2.6 which shows the decay of ^{40}K to ^{40}Ar (Browne et al., 1986).

Radioactive equilibrium

Radioactive equilibrium is described as a steady state condition in which the radioactive species and all its daughters have attained relative proportions that they disintegrate at the same numerical rate and therefore maintain their proportion constant (Prince, 1979). For the purpose of this study, the most useful state of equilibrium is what is termed secular equilibrium in which the activities of the parent and the daughter are the same and can only occur in a radioactive decay chain if the half -life of the daughter D is much shorter than that of the parent radionuclide P, therefore, $\boldsymbol{\lambda}_D \gg \boldsymbol{\lambda}_P$ (Burcham, 1973; Cember & Johnson, 2009; Faires & Boswell, 1981; Krane, 1988) . $\boldsymbol{\lambda}_P$ can be estimated to zero. Mathematically, the radioactive decay of the parent is given by equation 2.1 and that of the daughter nuclides follows equation 2.13 (Lilley, 2001; Lapp & Andrews, 1972).

$$N_D(t) = N_P(t_0)\frac{\boldsymbol{\lambda}_p}{\boldsymbol{\lambda}_{D-\lambda_p}}\left(e^{-\boldsymbol{\lambda}_P t} - e^{-\boldsymbol{\lambda}_D t}\right) \quad (2.13)$$

$$N_D(t) = N_P(t_0)\frac{\boldsymbol{\lambda}_p}{\boldsymbol{\lambda}_D}\left(1 - e^{-\boldsymbol{\lambda}_D t}\right) \quad (2.14)$$

$$N_D(t) = N_P(t_0)\frac{\boldsymbol{\lambda}_p}{\boldsymbol{\lambda}_D} \quad (2.15)$$

By rearranging equation 2.13, the equation can be simplified to equation 2.14 (Krane 1988). However, with time the term $e^{-\boldsymbol{\lambda}_D t}$ will become infinitesimally small and hence neglible and the daughter nuclei will decay at a constant rate and equation 2.14 reduces to equation 2.15. So it can be deduced that under those conditions, the activity of the daughter D is the same activity as the parent P, this is illustrated by the equation 2.16.

$$\boldsymbol{\lambda}_D N_D = \boldsymbol{\lambda}_p N_P \quad (2.16)$$

The ingrowth of radionuclide D increases until it reaches an equilibrium and full equilibrium usually takes several half-lives of radionuclide D to establish. This can be illustrated in Figure 2.7 with an example of secular equilibrium between ^{238}U with a very long half-life (half-life 4.9 billion years) and its progenies (^{234}U, ^{230}Th and all its descendants with short half-life) .

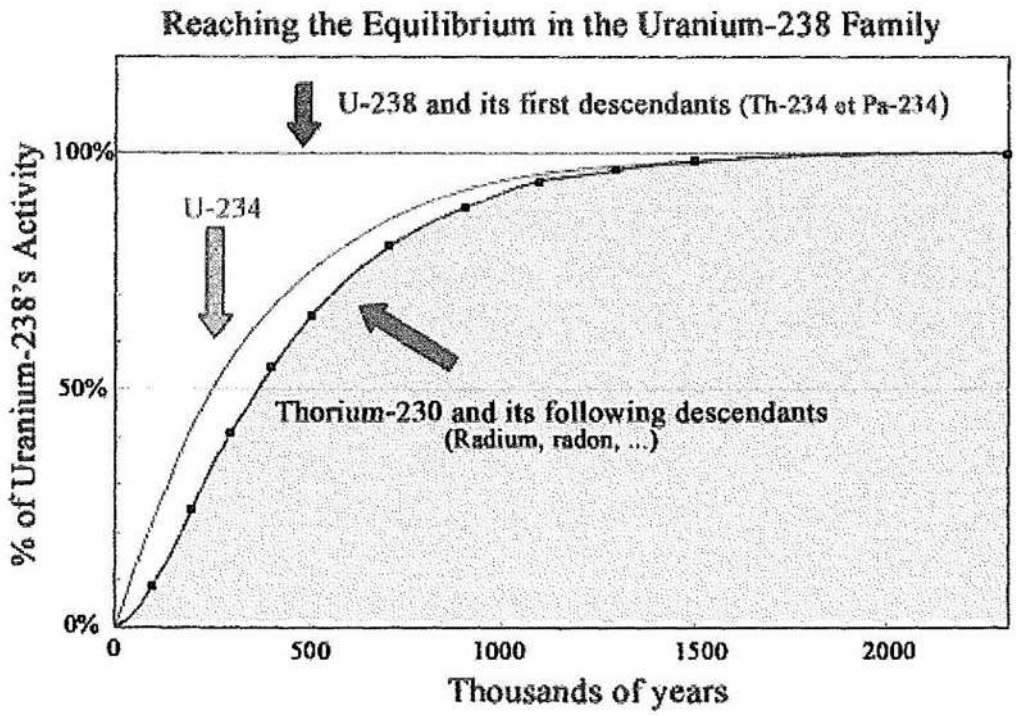

Figure 2.7 Secular equilibrium of ^{238}U and its progeny (Dlamini, 2015)

The understanding of secular equilibrium is important in terms of dose assesses due to naturally occurring radioactive materials (Lombardo and Mucha, 2008) and this is applicable when the radionuclide of interest cannot be directly determined by the detection method or to circumvent challenges in the measurements. In gamma spectrometry, for example, the activity concentration of ^{226}Ra is commonly determined through gamma rays emitted from its progenies, ^{214}Pb and ^{214}Bi after attaining secular equilibrium (Al-Masri and Aba, 2005; Landsberger et al., 2013, Sartandel et al., 2014) and this is more accurate than comparing the activity ratio ^{238}U/^{235}U (Dowdall et al., 2004). It also worth to mention that secular equilibrium varies with the radionuclide of interest and this is shown in Table 2.3.

The disadvantage of using secular equilibrium to extrapolate the activity concentration of the parent is the waiting period especially for those nuclides with very long half-lives. It is evident from Table 2.3 that the activity concentration of ^{238}U can be measured from ^{234}Th and ^{234}Pa after a waiting period of 4 months (Huy and Luyen, 2004). However, the equilibrium state can be disturbed, intentionally or accidentally and this occurs when members of the radioactive decay series are removed or added creating a condition of disequilibrium. Disequilibrium can be due to human activities such as back end uranium mineral mining activities which results in the separation of uranium isotopes from the primordial uranium series (Dejeant et al., 2014).

Table 2.3 Examples of radionuclides in equilibrium

Radionuclide of interest	Measured radionuclide	Typical delay time	Reference
^{238}U	^{234}Th and ^{234}Pa	4 months	Huy and Luyen, 2004; Lenka et al., 2009
^{226}Ra	^{214}Pb and ^{214}Bi	3 weeks	Dowdall et al., 2004; Landsberger et al., 2013, Murray et al., 1987)
^{228}Ra	^{228}Ac	36 hours	Lourtau et al., 2014; Xhixha et al., 2013)
^{228}Th ^{224}Ra	^{212}Pb and ^{208}Tl	3 weeks and 2 days	Awudu et al, 2012, Condomines et al., 2010)
^{227}Ac	^{227}Th and ^{223}Ra	3 months	Kohler et al., 2000; Van Beek et al., 2010
^{223}Ra	^{219}Rn	A minute	Desideri et al., 2008; El Afifi et al., 2006)

In the natural environment, disequilibrium is governed by the behaviour of individual nuclides, physicochemical properties such as leachability and mobility (Wang et al., 2012; Rajarethtnam and Spitz, 2000). Once the equilibrium is disturbed, it requires time ranging from days to thousands or even millions of years to be restored depending on the half-lives of the radionuclides.

Note that the activity only describes the number of disintegrations per second and does not mention the kind of radiations emitted or their energies (Faires and Boswell, 1981). The next section will describe the types of radiations and their characteristics.

Transient equilibrium

Transient equilibrium occurs when the half-life of the parent is a few times greater than the half-life of the daughter i.e. where $\lambda_p < \lambda_D$ (Magill & Galy, 2004) and during this period the parent will undergo radioactive decay while the daughter will build up. The daughter will build up until a state of equilibrium is reached. A close look at the decay equation shows that as the exponential term becomes smaller and smaller and the ratio of A_p/A_D approaches the limiting constant value $\lambda_D/(\lambda_D - \lambda_P)$ which is shown by equation 2.17.

$$N_D/N_p = \lambda_p/\lambda_D - \lambda_p \qquad \text{(Eq. 2.17)}$$

Transient equilibrium can be shown by the decay of ^{140}Ba ($T_{1/2}$ 12.75d), which decays to ^{140}La ($T_{1/2}$ 1.68 d) as shown in Figure 2.8.

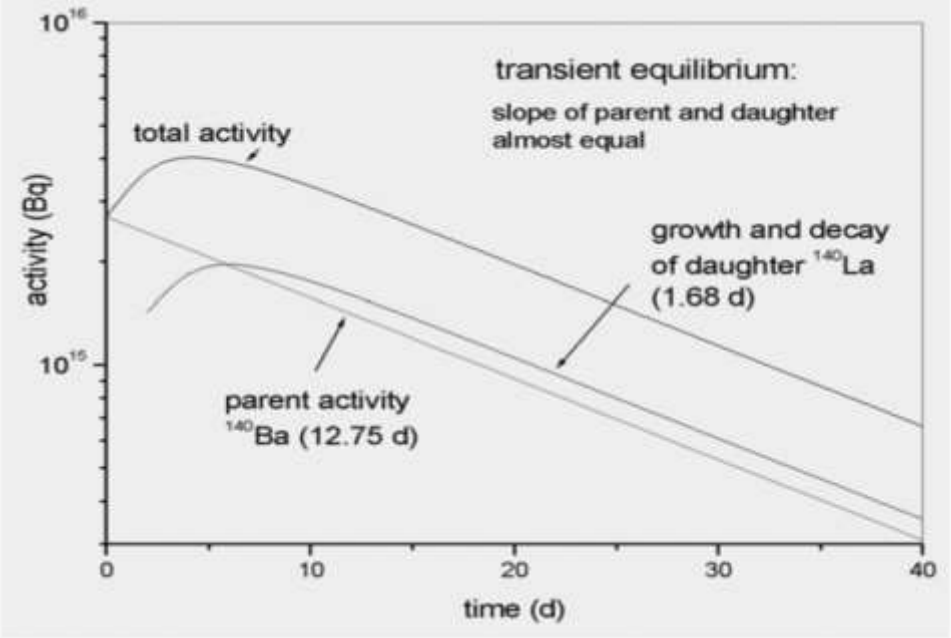

Figure 2.8 Example of transient equilibrium between ^{14}Ba and ^{140}La (Magill and Galy, 2004)

While the activities of both the parent and the daughter nuclides may appear to be almost the same, there will be some changes with time. As can be deduced from equation 2.17, a state of equilibrium will be attained and the proportions of nuclides becomes a constant value (Kaplan and Gugelot, 1955) and the parent and the daughter nuclides will decay at the same rate, related to the decay of parent.

2.4.4 The biological effects of ionising radiation in humans

The immediate consequence of the interaction of any radiation with matter is the deposition of an appreciable amount of energy causing the ionization and excitation of atoms and molecules. The extent of radiation damage in biological molecules is governed by the type of radiation and its energy, dose received, number of cells involved and sensitivity of organs (CPEP, 2003). Scientific studies have shown that the main target of radiation damage to the cell is the DNA, which may lead to cell mutation, carcinogenesis and sometimes cell death (UNSCEAR, 1998).

The radiation damage caused to the cells may sometimes be self-repaired by the body so that there is no apparent effect, but high doses of radiation received may result in harm.

Ionising radiation can cause two types of biological effects which are: (a) somatic effects which is type of damage that occurs in the irradiated person and may be further divided into acute if the individual receives large doses at the shortest possible time and this leads non stochastic effects. The other form is chronic effects in which low doses are received over a long time and this gives the body an opportunity to repair itself and recover from radiation damage. The results of chronic effects occur by chance and the symptoms may appear several years after the dose has been received. The second form of biological damage due to ionising radiation is (b) genetic defects which can be passed on to future generation through the changes in the chromosol structure of offspring. If the damage occurs in the young and undifferentiated cells, the changes in the hereditary material will be carried to subsequent generations.

Ionising radiation can cause an increase in the mutation rate and the number of abnormalities in the gene pool. Therefore, the population radiation exposure must be carefully controlled and minimized. While it can be argued that there are other sources which induce cancer in human beings, it is imperative to control radiation exposure even in low doses since it can induce cancer.

2.5 Radiation detection

Ionizing radiation is emitted as either alpha and beta particles or by waves (gamma rays, neutron) and these impart their energy to the absorbing medium and leave their signatures. The effects of radiation signatures can be measured with a suitable detector. Scintillation counters make use of special crystal materials which when activated will be able to give flashes of light photons (Choppin et al., 2002). Scintillation detectors are known for their high efficiency in acquisition but poor in their energy resolution (Bode, 1998). Depending on the availability of materials and cost, it is possible to manufacture solid, liquid or gas scintillator detectors.

The other type of detectors operate based on ionization where charge carriers are produced between the charged electrodes contained in the detector. Devices working on this principle can be solid semiconductor materials or gas filled, which are divided into ion chamber, proportional and Geiger-Muller tubes. Solid semiconductor has p-n junction diode (Gruber, 2009). When photons interact within the depleted region, charged carriers (positive holes and negative electrons) are freed and are swept to their respective collecting electrodes by high voltage supply. The collected charge is shunted into a preamplifier and converted to a voltage pulse with the amplitude proportional to the original photon energy.

The most common materials for semiconductor detectors are germanium (Ge) and (Si). Semiconductor detectors are frequently used because of certain advantages such as high energy resolution, good stability, excellent timing characteristics and simplicity of operation. The fundamental differences between Ge and Si based detectors rests on the energy gap, atomic number and mobility of the major carriers. The Ge requires less energy than Si detector which confers its use to room temperature. However, Ge must be cooled to 77K or -196 ^{0}C with liquid nitrogen to reduce the energy leakage current due to thermal generation of charged carriers to an acceptable level which is only achieved under vacuum conditions. The sensitive detector surfaces are protected from moisture and other contaminants. The gamma detector is made of high photoelectric cross section material to improve the efficiency.

2.5.1 Interaction of ionising radiation with matter

Ionising radiation is radiation that has enough energy knock out electrons out of their electron cloud around the atom and thus disturbs the electron/proton balance resulting in the formation of a positively charged atom and a free electron. The highly energetic electrons transfer their energy to the absorbing medium through ionisation and excitation. If the absorbing medium is composed of body tissues, sufficient energy may be deposited within cells, destroying their reproductive capacity. However, most of the absorbed energy is converted to heat, producing no biological effect (Chandrasekaran et al., 2015). There are two types of ionisation which are: direct ionisation which is due to charged particles (alpha particles, beta particles, electrons) and indirect ionisation which is mediated by neutral waves such as X-ray, gamma photons and neutrons). These are discussed in detail in the following subtopics.

Interaction of charged particles with matter

Charged particles such as protons, electrons and alpha particles are capable of direct ionisation provided they have enough kinetic to produce ionisation by collision as they penetrate matter (Bailey, 2014). It is well documented that a mono-energetic, parallel beam of charged particle has a well-defined distance through which they can travel before coming to a stop, whereas uncharged particles are attenuated more or less exponentially without a well-defined range (Turner, 2007). Charged particles interact with matter continuously and intensely and exhibit a well-defined range and because of this they have a low penetration ability as opposed to uncharged particles (Khan, 2010).

As charged particle traverse through matter the interact with material through two mechanisms: ionising slowing down and radiative slowing down.

During ionisation slowing down, the coulombic interaction of the charged particle with the atomic electrons may impart energy to the atom and excites to a higher energy state. If the energy is sufficiently high, one or more electrons may be ripped off the electron cloud leading to a cascade of ionising events. In every ionisation event, a small amount of energy is transferred from the charged particle to the atom being ionised so that the energy of the traversing particle decreases (Turner, 2007). and this can be explained in terms of linear energy transfer (LET i.e. the energy transferred per unit path length) of a heavy charged particle. The mechanism of ionisation slowing down is illustrated by in equation 2.12

$$LET = \frac{z^2 Z}{v} \qquad (2.12)$$

Where z is charge of the projectile, Z is the atomic number of the medium in which the interaction takes place and *v* is the speed of the heavy charged particle. The LET rate is the measure of the intensity with which the particle interacts with matter (Cember and Johnson, 2009) and the ionisation density (Jevremovic, 2009). From the given expression of LET, it can be deduced that:

- The z^2 term shows that the higher the charge, z, on a charged particle, the more intensely it will interact i.e. the more energy will be transferred and the more ion pairs will be produced per unit path length.
- The z term shows that the higher the atomic number Z of the medium in which the charged particle slows down, the more intense the interaction will occur i.e. the more energy will be transferred per unit path length.
- The 1/v term shows that slower-moving charged particles will interact more intensely than fast moving charged particles.

The second mechanism by which charged particles lose kinetic energy occurs via radiative slowing down in which a loosely bound charged particle enters the vicinity of an atomic nucleus where it will be deflected from its original direction by the electric field in the nucleus. This results in the instantaneous change of direction and speed of movement of the electrically charged particle. The charged particle is decelerated, and it emits photons known as bremsstrahlung (“braking radiation”) (Turner, 2007) and this only occurs to unbound

charged particles. Conversely, charged particles such as atomic electrons that are bound inside a well potential do not emit bremsstrahlung when they are accelerated as they have quantised energies.

The intensity of bremsstrahlung production is given by the approximate relationship (Zschornack, 2007).

$$I = \frac{z^2 Z^2}{m^2} \tag{2.13}$$

Where z is the charge of the particle, m is the mass of the particle and Z is the atomic number of medium. It can be deduced from equation 2.13 that:

- Bremsstrahlung and radiative slowing down does not play a significant role for heavy charged particles, as a result of the $1/m^2$ term. However radiative slowing down with associated bremsstrahlung production will play a role in the attenuation of low mass charged particles such as electrons.
- The slowing down of charged particles in a medium with a high atomic number Z will produce much more bremsstrahlung compared to a medium with a low Z on account of z^2 term.

Interaction of X-rays and gamma photons with matter

Uncharged particles such as neutrons and photons are indirectly ionising. Ionising photons interact with atoms of a material or absorber to produce high speed electrons by three major processes: Photoelectric effect, Compton scattering and Pair production. (Knoll, 2010)

Photoelectric absorption

During photoelectric absorption, a photon disappears being absorbed by an atomic electron and this results in ionisation with subsequent ejection of the electron from the atom. The energy of the liberated electron is the difference between the photon energy ($h\nu$) and the energy needed to knock out the electron from the atom (E_b) as shown by equation 2.14. (Kantele, 1995). Figure 2.9 depicts the process of photoelectric absorption.

$$E_{e-} = h\nu - E_b \tag{2.14}$$

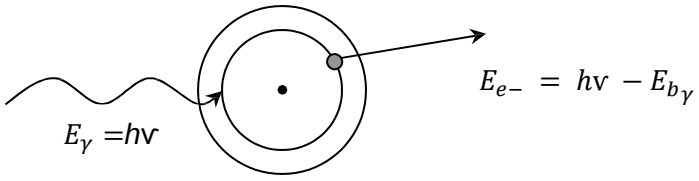

Figure 2.9 Schematic of the photoelectric absorption process (Gilmore and Hemingway, 2008)

The recoil momentum is absorbed by the nucleus to which the ejected electron was bound. If the released photoelectron has enough energy, it may generate secondary ionisation along its trajectory and in the case of a semiconductor material it may create electron hole pairs. If the electron does not leave the detector, the deposited energy corresponds to the energy possessed by the incident photon. The phenomenon of the photoelectric effect allows calibrating the gain of the detector attached to its readout system if the required energy to create electron hole pairs are known. The incident photons create an vacancy in the electron orbit, thus leaving an atom at higher energy state. The position can be filled by an outer orbital electron, resulting in emission of characteristic X-ray photons and fluorescence radiation (Lamarsh and Baratta, 2001). The excess energy, which is displayed as escape photons give rise to the so-called escape peaks in the measured spectrum. It should be noted that photon interaction depends on atomic number of the absorbing material. The optimum cross section increases as roughly Z^3 and for silicon, the photoelectric effect is dominant for photons below 100 keV.

Compton scattering

Compton scattering is collision in which an incoming gamma photon strike a loosely bound electron and the process results in the conservation of energy and momentum (Omole and Akanbi, 1997). During this process, some of the photon's energy is transferred to electron with consequential loss of energy and change in the trajectory in the incoming gamma-ray photon forming a recoil electron as shown in Figure 2.10 (Lamarsh and Baratta, 2001). The energies of the scattered photon and recoil electron are related to the angles at which they are emitted. By considering the equations for the conservation of energy and momentum, the energy of the scattered photon $h\nu'$ is related to the scattering angle θ by the expression given in equation 2.16 (Kaplan, 1962).

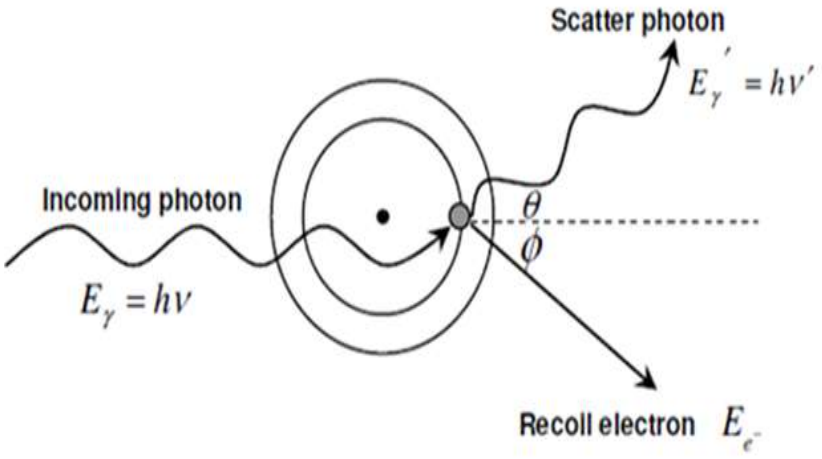

Figure 2.10 The electron energy and energy of scattered photon (Santawamaitre, 2012)

$$h\nu' = \frac{h\nu}{1+\left(\frac{h\nu}{m_0c^2}\right)(1-\cos\theta)} \tag{2.16}$$

where, $m_0c^2 = 511$ keV represents the rest mass energy of the bound electron. It thus, follows that the kinetic energy of the recoil electron is given by equation 2.17

$$E_{\overline{e}} = h\nu - h\nu' = h\nu\left(\frac{(h\nu/m_0c^2)(1-\cos\theta)}{1+(h\nu/m_0c^2)(1-\cos\theta)}\right) \tag{2.17}$$

The energy associated with the recoil electron can change from zero $(\theta = 0)$ up to a maximum value $(\theta = \pi)$ depending on the scattering angle. The maximum energy of the recoil electron is given by equation 2.18.

$$E_{\overline{e}} = \frac{2h\nu}{2+m_0c^2/h\nu} \tag{2.18}$$

The probability of Compton scattering taking place depends on the number of electrons per unit mass of the interacting material and the incoming gamma-ray energy as a function of $\frac{1}{E_\gamma}$ (Lilley, 2001).The Compton effect is one of the major ways in which a beam of X -rays and γ -rays is attenuated in passing through matter.

Pair production

A photon can interact in the field of a nucleus, annihilate and produce an electron-positron pair and this usually occurs in the presence of a third body which help in the conservation of energy and momentum as illustrated by the expression 2.19. The transformation energy required is above 1.022 MeV i.e. two times the rest mass of an electron.

$$E_e = E_\gamma - 2m_0c^2 \tag{2.19}$$

The excess photon energy greater than the minimum transformation energy is imparted to and distributed equally to the positron and electron as kinetic energy as shown by the equation 2.19 (Knoll, 2000). The electron and positron pair continue to interact with the surrounding transferring and losing kinetic energy along their path. Similarly, the β^+ can be moderated and because of its plus charge, it can combine with a negatively charged electron and subsequently annihilate to form two photons referred to as annihilation photons, each having energies $m_0c^2 = 0.511MeV$ and they traverse in opposite directions as is shown in Figure 2.11 (Gilmore and Hemingway, 2008). There exist no simple expression for the probability cross section of pair production per nucleus,K, but its size varies approximately as the square of the absorber atomic number as shown by the expression in 2.20 (Turner, 2007).

$$K \approx Z^2 f(E_\gamma, Z) \tag{2.20}$$

The variation of the K with the atomic size is dominated by the Z^2 term. The function $f(E, Z)$ is only slightly dependent on Z and increases continuously with energy from the threshold 1022 keV. The interaction scales up as Z^2 varies for different nuclei and thus materials containing high atomic number materials are more ready to convert photons into charged particles (Turner, 2007) and is the dominant interaction process for gamma energy greater than 10 MeV (Das and Ferbel, 2003). The relative importance of the three-interaction processes as a function of photon energy and the value of Z absorber is shown in Figure 2.12.

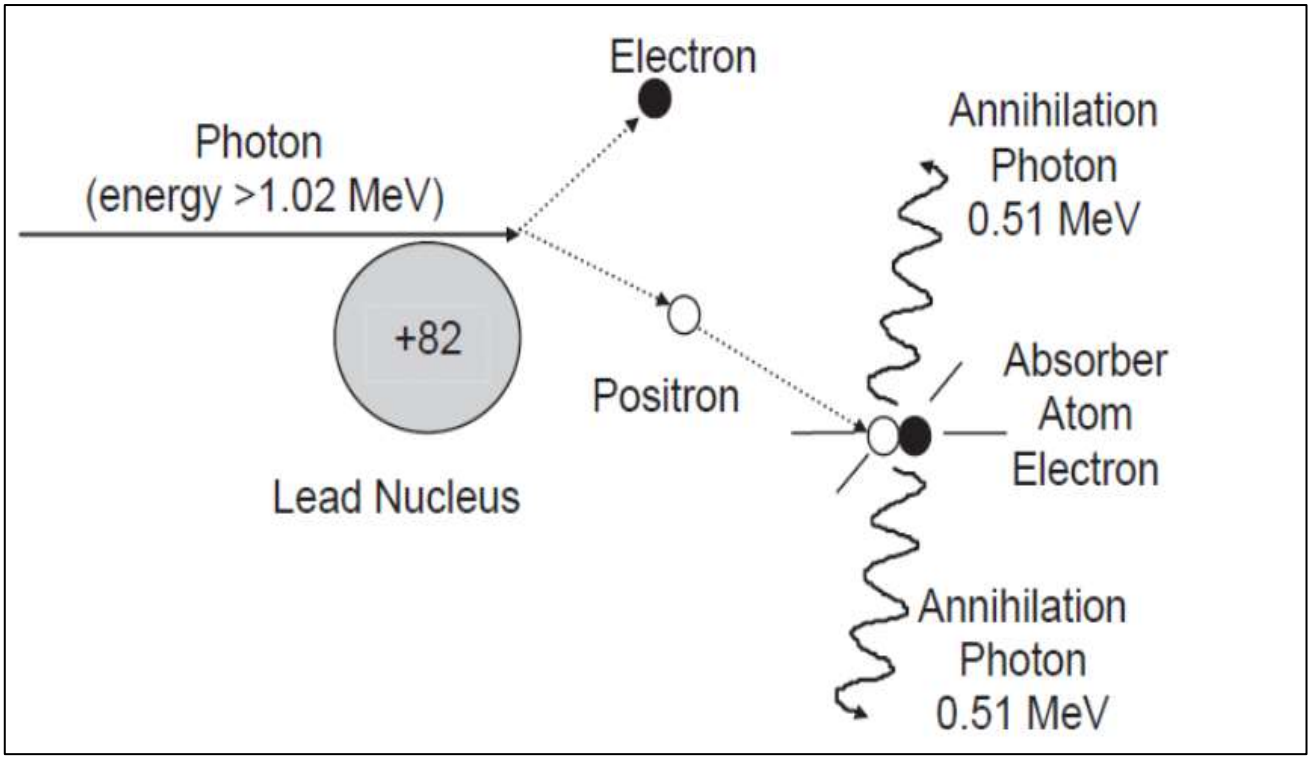

Figure 2.11 Schematic of the pair production process and annihilation (Kamunda, 2017)

2.5.2 Types of radiation detectors and principles of operations

There are several types of radiation detectors such as gas, scintillation or semiconductors detectors (Lilley, 2001) and the choice of a detector depends on information provided. Some detector can respond to high energy and high intensity and this depends on the type of radiation being measured. The main difference in detectors is based on the operating medium which can be gas, liquid or solid materials. In all detectors, the operating principles are universal which involves the generating of electrical signal which is as result of the interaction of radiation with the detector material. The detection methods are, in general based on the process of excitation or ionisation of the atoms in the detector by the passage of charged particle. There are a wide variety of detectors but currently three broad categories can be distinguished.

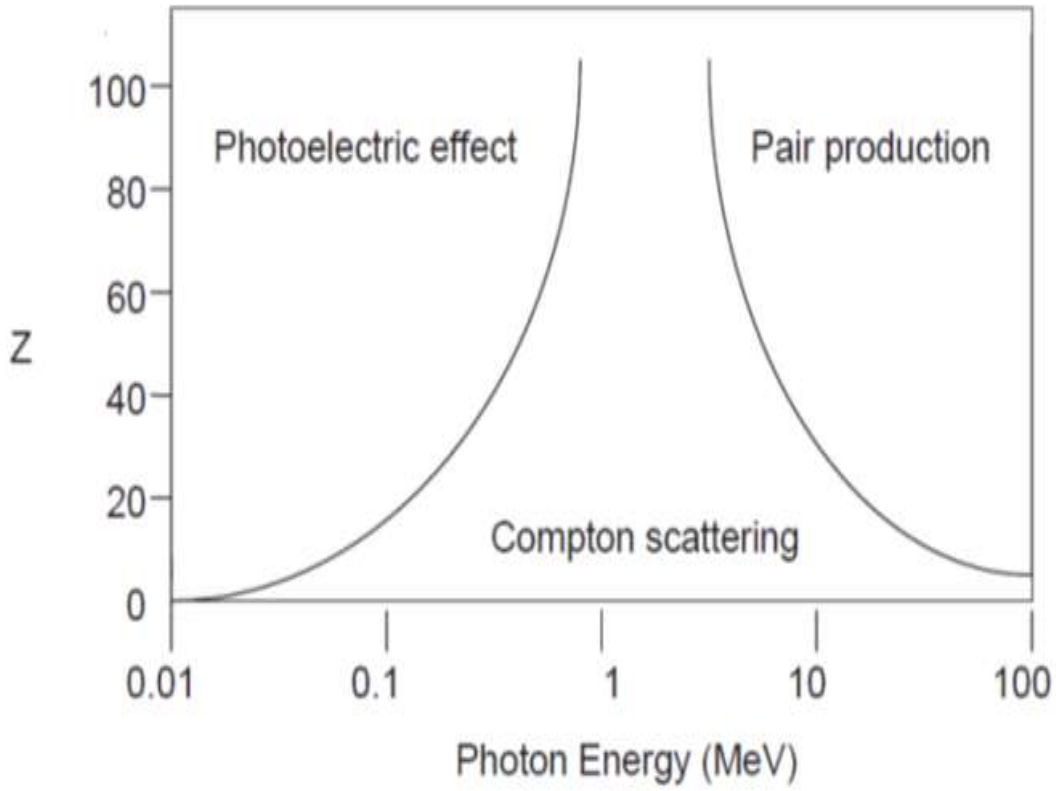

Figure 2.12 Interaction of three gamma ray photons and their region of dominance (Kamunda, Mathuthu, & Madhuku, 2016)

Gas filled detectors

In gas filled detectors the charged particles are passed through a gas in which the main mode of interaction involves ionisation and excitation of the gas along the particle track (Knoll, 1999). Although the excited molecules can at times give a signal that can be quantified, the majority of gas filled detectors are based on sensing the direct ionisation created by the passage of radiation. All the ionisation caused by a single particle of alpha, beta or gamma radiation inside a closed volume of gas is collected by applying a suitable electrical voltage across the container. The threshold energy needed to produce an electron ion pair is 30$\pm$ 10eV with slight dependence on the gas used and the energy of the incident particle (Martin, 2008). The electrons are attracted to the positive electrode and are swept from the gas before they can recombine with the positive ions. Figure 2.13 gives a schematic diagram of the gas filled detectors which are as primary detectors for measurements of alpha and beta particles. In gas filled radiation detectors, the amount of voltage across the electrodes and hence the

electrical field strength can be manipulated to give Ionisation chamber, Proportional counter or Geiger Muller counter (Bailey et al., 2014).

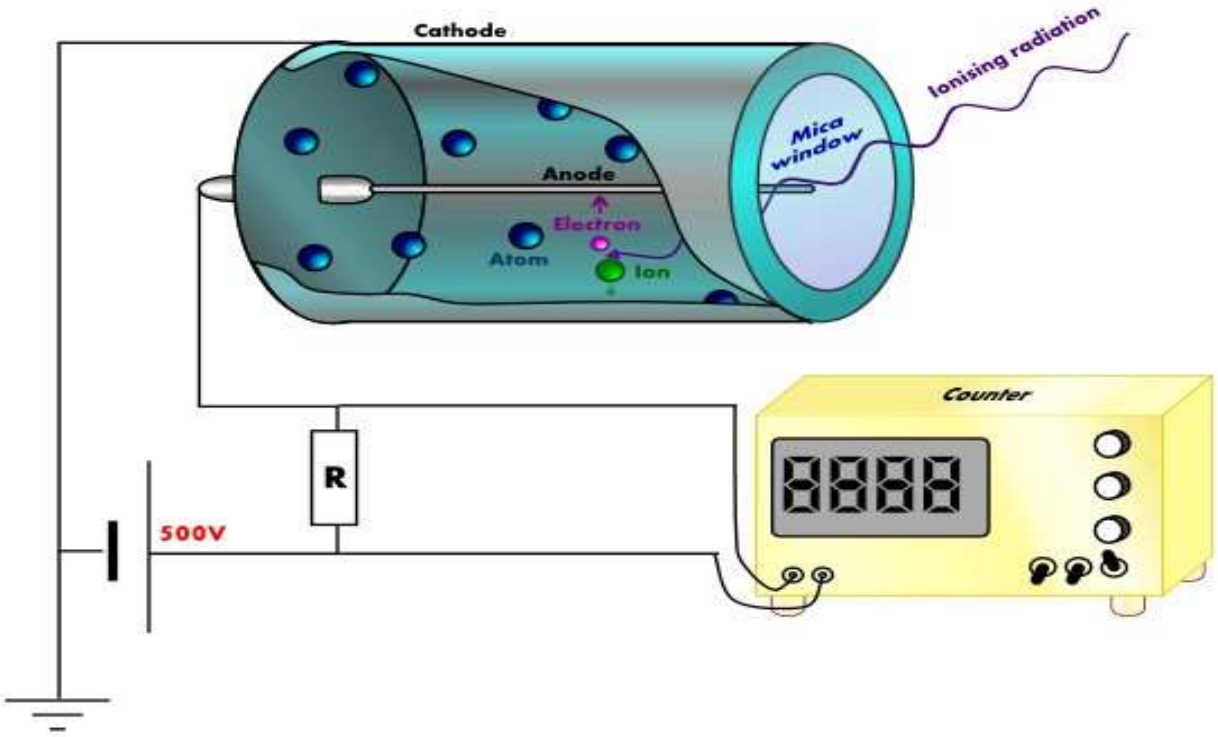

Figure 2.13 Gas filled detector (Lam, 2012)

It should be noted that gas filled detectors are ideal for counting low energy electrons, ions and photons due to the poor stopping capability of gas detection medium for gamma rays. Since low attenuation of photons implies poor detection efficiency for photons in gas detection medium, a higher atomic number and/or higher density liquid or solid materials are employed to measure higher penetrating radiations (Krane, 1988; Gilmore, 2008). Such detectors may be scintillation detectors or semi-conductors' detectors.

Scintillation Detectors

Scintillation detectors are one of the oldest and most useful techniques for the detection ionising radiation and spectroscopy of a wide range of radiations (Knoll, 2000). semiconductor detectors are used. Scintillation detectors are only sensitive to one type of radiation. Infact, NaI detectors will pick gamma radiation, but not alpha or beta while ZnS will only pick alpha radiation. In scintillator detectors, radiation strikes the scintillator and causes it to give off photons as visible light. These photons pass through the crystals and they strike

a thin metal called a photocathode- when this happens, the light enters a second part of the detector called a photomultiplier (PMT). The hitting of the photon on the photocathode causes it to be ejected from the cathode. Attached to the photocathode is a set of metal cups in which voltage is applied to each of them. The high voltage will accelerate the electron to strike the neighbouring cups leading to the knocking out of other loose electrons and this results in a cascading effect. Consequently, the PMT, the initial signal is multiplied by a factor of million or so. The amount of light generated every time a gamma hits the crystal culminates in pulse of electrons arriving at far end of the detector can be quantified on an electrical readout.

For gamma-ray spectrometry, Thallium activated sodium iodide scintillation detectors (NaI(*Tl*)) is the most frequently used because it has a high efficiency for detecting gamma radiation and does not require cooling. However, the major In this process the scintillation detector is a transducer that changes the kinetic energy of an ionising particle into a flash of light. limitation of scintillation detection is that they have poor energy resolution (Cember and Johnson, 2009). To achieve a good energy resolution, A germanium semiconductor detector was used in this experimental work and this is described in detail in the following section.

Semiconductor Detectors

Semiconductors detector are fabricated from either elemental or compound crystal material having a band gap in the range of approximately 1 to 5 eV (Knoll, 1999) and this may be Silicon or Germanium. These detectors have a P-I-N diode structure in which the intrinsic region (I) region created by depletion of charged carriers when a reverse bias is applied across the diode (Cember and Johnson, 2009). Semiconductors detectors are solid-state devices that operate in the same manner as ionisation chambers, however, the only difference is that in semiconductors, the charge carriers are not electrons and ions but are electrons and “holes”. When an incident photon strike upon the P-I-N junction in the depletion region, it produces electron-hole pairs as it passes through it . The electrons and holes are swept away under the influence of the electric field and with proper electronics the charge collected produces a pulse that can be recorded (Mirrion Technologies, 2017).

High Purity Germanium detector

It should be noted that these detectors do not consist only of semiconductor material and two electrodes but there exist several impurities atoms in these materials. The elements, Si and Ge have a valence 4 thus, when an impurity atom of valence 3 (acceptor) or 5 (donor) exists in the crystal, this tends to lower the energy necessary to create electron-hole pairs

and this results in the creation of much noise. In order to overcome this, p-n junctions are created at one electrode and then polarize it to prevent the passage of current through it when there is no ionizing radiation.

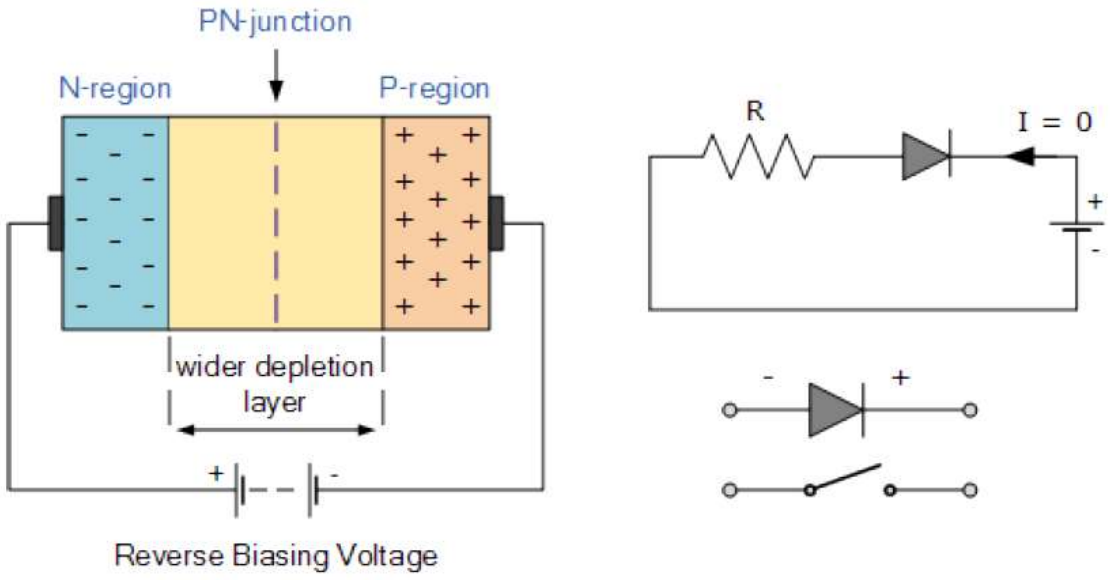

Figure 2.14 P-I-N junction (Anon, 2013)

This process is referred to as reverse bias. This process creates a region called the depletion layer. A step forward was ultimately achieved when high Germanium (Ge) material could be fabricated (Hansen, 1971; Khandaker, 2011), with impurity concentration of 10^{10} atoms/cm $^{-3}$ as against the 10^{13} atom/cm ^{3}, eliminating the need for Li compensation. This gives rise to high resistivity which is proportional to the square of the depletion layer's thickness. This achievement paved the way for the development and manufacture of a more efficient detector (Figure 2.14). Some major characteristics of HPGe detector are high atomic number, low impurity atom concentration, low ionizing energy requirement to generate electron-hole pair, compact size, high conductivity, high resolution, immediate response and the simplicity of operation (Khandaker, 2011).

The Germanium semiconductor is widely used by many researchers as the detector of choice for high energy-resolution gamma-ray spectrometric analysis due to its superior energy resolution (Knoll, 2000). The Germanium detector operates by collection of charges originating from the ionization process of the semiconductor material. On average, an electron-hole pair is produced for every 3 eV absorbed from the radiation. Subsequently, the

pair of electron-hole move under the influence of electric field to the electrodes where a pulse is generated.

2.6 Toxic heavy metals

Heavy metals are the most dangerous pollutants in the environment due to their non-biodegradability and their persistence in the environment and these are discharged into the environment through natural and anthropogenic sources. The term heavy metal refers to any metallic element that has a relatively high density usually more than 5.0 g/cm^3. Examples of these include mercury (Hg), cadmium (Cd), arsenic (As), chromium (Cr), lead (Pb), Copper (Cu), Nickel (Ni) and Iron (Fe). These metals are classified into three categories: toxic metals (Hg, Cr, Pb, Cu, Ni, Cd, As etc), precious metals such as Pd, Ag, Au, Ru etc and radionuclides such as U, Th, Ra, Am etc (Bishop, 2002). Some of the heavy metals have functional roles which are essential for a multitude of physiological and biochemical process in the mammalian bodies. Toxicity of heavy metals in the body depends on the type of element and the concentrations. Some heavy metals in high doses can be harmful to the body while others such as Cd, Hg, Pb and Cr even in very small quantities can have deleterious effects in the body causing acute and chronic toxicities.

Heavy metals are inherently present in the environment and they constitute an important class of toxic substances which are encountered in numerous occupational and environmental circumstances. The impact of these toxic agents on human health is a subject of intense interest due to their negative effects on health and the ubiquity of exposure (Jaishakar et al, 2014). These heavy metals can induce cancer through various pathways which depends on the type of metal and time of exposure. Heavy metal poisoning could result from consumption of contaminated food or soil or drinking contaminated water and in some cases may be as a result of exposure to ambient air contaminated with heavy metals.

2.6.1 The biological effects of toxic heavy metals

The ability of heavy metals to be mobilised and be transported between different environmental compartments and made potentially available is directly related to speciation. The forms of a metal that are available for uptake by organisms are considered to be the bioavailable fraction. Bioavailability is the degree to which a contaminate from a source is free for uptake and brings about site of action effect (Ownby et al., 2005), which may be toxic. The element speciation is critical regarding both the mobility and the metals toxicity. Studies have shown that bioavailability of toxic heavy metals in an ecosystem is brought about by

either direct absorption or food chain distribution. Exposure of the organism to contaminant concentration depends on its distance from the contaminant. The closer the organism the higher the chance of interaction with the contaminant in which case the organism may absorb, imbibe, ingest, or inhale the contaminant. In an environment where all the organisms are exposed to uniform conditions, the predominant pathway is direct absorption and similarly in terrestrial environment, the food chain mechanism is highly pronounced (Järup, 2003).

Toxicity of some heavy metals

The toxicity of heavy metals to mammalian systems is due to chemical reactivity of ions with cellular structural components such as enzymes and membrane systems. For a long time, in vivo studies have shown that the severity of specific metals is dependent on the concentration of the ions accumulating in a specific organ (Sakar et al, 2013). This is also governed by route of exposure and the chemical compound of the metal. i.e. valency state, volatility, solubility in lipids etc. Table 2.4 shows the target organ and clinical manifestations of chronic exposures to the metals. It should be noted that the main threat toxicities of metals lies on their potential to be carcinogenic.

Mercury toxicity is dependent on whether it takes the form of elementary mercury, inorganic mercury or organic mercury compounds. The ingestion of methyl mercury in sea foods is the major exposure scenario in human populations and about 80% of elementary mercury is inhaled as vapour where it is retained in the lungs and penetrate the blood brain barrier where it affects the neurons consequently leading to symptoms such as tremors, emotional liability, insomnia, memory loss, headaches and affecting the kidneys and the thyroid (Baishaw et al, 2007).

Copper is a naturally occurring metallic element that occurs in soil at an average concentration of 50 parts per million (ppm). It is required by both plants and animals in small concentrations. Copper is continuously discharged into the atmosphere through human activities such as mineral mining and exploration, smelting and refining of copper and copper downstream industries such as those making wire, sheet metals.

Short-term effects acute poisoning due to ingestion of excessive copper can cause temporary gastrointestinal distress with symptoms such as nausea, vomiting and abdominal pain. High levels of exposure to copper can cause destruction of red blood cells, possibly resulting in anaemia (Franchitto et al, 2008). On the other hand, on a long-term effect, mammalian cells have developed an efficient mechanism to protect themselves from

overexposure to copper. However, at high enough levels, chronic overexposure to copper can damage the kidneys and the liver.

Table 2.4 Clinical aspects of chronic toxicities

Toxic Heavy metals	**Main Source**	**Clinical manifestation**	
Lead	Industrial dust and fumes and polluted water and food	Nervous system, hematopoietic System, renal	Encephalopathy, peripheral neuropathy, central nervous Disorders, Anemia.
Nickel	Industrial dust, Aerosols	Pulmonary, skin	Cancer, dramatis
Tin	Medicinal uses, Industrial dusts	Nervous, pulmonary system	Central nervous system Disorders, visual defects And EEG changes, Pneumoconiosis.
Mercury	Industrial dust and fumes and polluted water and food	Nervous system, renal	Proteinuria

It is confirmed that lead is a major toxic heavy metal ion affecting the environment (Alloway & Ayres, 1997). The toxicity of lead poisoning results from the ingestion of lead containing materials such as paint or water containing traces of lead from pipes. Poisoning can also occur from inhalation of fumes from burning storage batteries. There is conflicting evidence in human subjects to confirm that lead is a serious poison (Benetou-Marantidou et al, 1988). Lead can enter the body through absorption and stored in the bones, blood or brain. In children, lead has been shown to cause brain damage, induce convulsions, mental retardation and even death. It is also known that lead is harmful to the kidney and permanent neurological injury (Snyder, 1971). Lead can pass through the placenta of the mother and can cause damage to the nervous system and brain to the unborn child.

2.6.2 Detection of toxic heavy metals in the environment

ICP-MS is a powerful technique for analysing heavy trace metals in environmental samples (Chakraborty et al., 2013). The ICP- MS can determine accurately the concentration of a specific element in the sample. The instrument first atomizes the sample followed by separation of different atoms (Jarvis, 2006). Figure 2.15 shows the schematic diagram of ICP-MS system. Most samples that are introduced into the ICP-MS system are liquids and the samples have to be vaporised and this is achieved by a nebulizer and spray chamber which volatizes the sample into fine aerosol droplets samples are introduced into an argon plasma as aerosol droplets

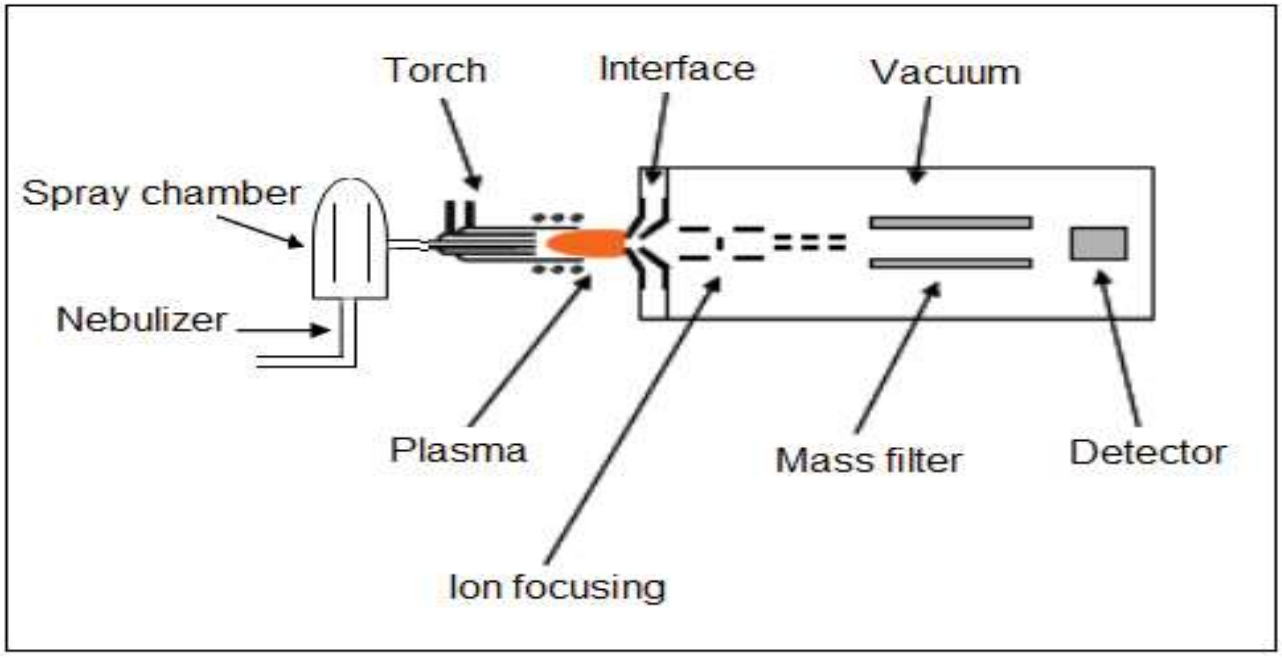

Figure 2.15 A diagrammatic schematic of quadrupole- ICP-MS (IAEA, 2014)

A stream of carrier gas, argon, breaks the liquid into small droplets that are injected into the spray chamber. The ICP torch together with the radio frequency (RF) coil together generates the argon plasma which creates a very high temperature of between 6000-10000 K environment for atoms, ions and electrons. The elements in the sample at such high temperature are ionized and are directed to a mass filtering device known as the mass spectrometer (MS) (PerkinElmer, 2004-2011).

The Interface then links the atmospheric pressure ICP ion source to high vacuum mass spectrometer. The interface allows the plasma and the ions system to coexist and the

ions generated by the plasma to pass into the ion lens region i.e. ions generated in the plasma are extracted and introduced to the mass spectrometer as an ion beam. The ion optics, quadrupole and the detector operate under vacuum and in this region, the sampled ions are accelerated and focused onto the mass filter by a set of charged plates or ion lenses.

The ion optics guide the desired ions into the mass analyser (quadrupole) while selecting against the neutral species and photons from the ion beam (PerkinElmer, 2004-2011). The ion beam then passes through the collision/reaction cell that is used to remove the interferences which can degrade the detection limit achievable. The MS then scans and sorts the ions according to their mass/charge ratio followed by directing them to an electron multiplier tube detector. At any given time only one mass-to-charge ratio will be allowed to pass through the mass spectrometer from the entrance to the exit. The impact of ions releases a cascade of electrons, which are amplified until they become a measurable pulse. The software compares the intensities of the measured pulses to those from standards, which make up the calibration curve, to determine the concentration of the element.

CHAPTER 3 : MATERIALS AND METHODS

3.1 Description of the study area

The town of Arandis in Erongo region covers an area of 29 square kilometres and is geographically located at latitude: 22.42^0S, longitude: 14.97^0E with an altitude of 585 m above sea level. The town is 15 km outside the world's largest pit mine: Rössing Uranium Mine (RUM) and was established in 1978 to cater for employees for RUM. Over the years, due to rural to urban migration and the availability of job opportunities in the mine and some associated industries, the town has grown its population to 7600 inhabitants (Namibia Census, 2011). The main activity at Rössing Uranium Mine is the extraction and mining of uranium ore. Figure 3.1 (a) shows the ariel view of the town of Arandis where the samples for soil, PM and radon measurements were collected.

On the other hand, Karibib is a satellite town for Navachab Gold mine in the Erongo region of Western Namibia and it is highly affected by mining activities from the mine operations. The town is located 10 km North of Navachab Gold Mine and has a population of 5132 inhabitants (Namibia Census, 2011). The area covers 97 square kilometres of town land. The town is situated on the Khan River, halfway between the capital city, Windhoek and the coastal town of Swakopmund. The main activities of this town are gold mining done at Novachab is also surrounded by commercial farms for cattle ranging. The town is known for its aragonite marble quarries and gold mining activities. Figure 3.1 (b) shows the layout of Karibib town.

3.2 Sample collection

Soil and PM samples were collected from the mining towns of Arandis and Karibib. The samples for PM, soil and radon gas were concurrently collected at the same geographical position. The position of the site was clearly marked with geographical position system (GPS) which was later used to locate the area using google earth. The sampling sites are illustrated in Figure 3.1 (a) Arandis town and Figure 3.1 (b) Karibib town.

About 50 soils samples were purposefully randomly sampled from each town in the vicinity of the mine. Each sampling location was carefully marked and cleared of debris and about 500 g of topsoil was scoped from the site using a shovel. Three samples from each marked site was thoroughly mixed and homogenised to make one sample as a representative

of that area. The soil samples were sieved to pass through a 2 mm sieve and placed in a polyethylene plastic bag and sealed. The sampled area was located with geographical

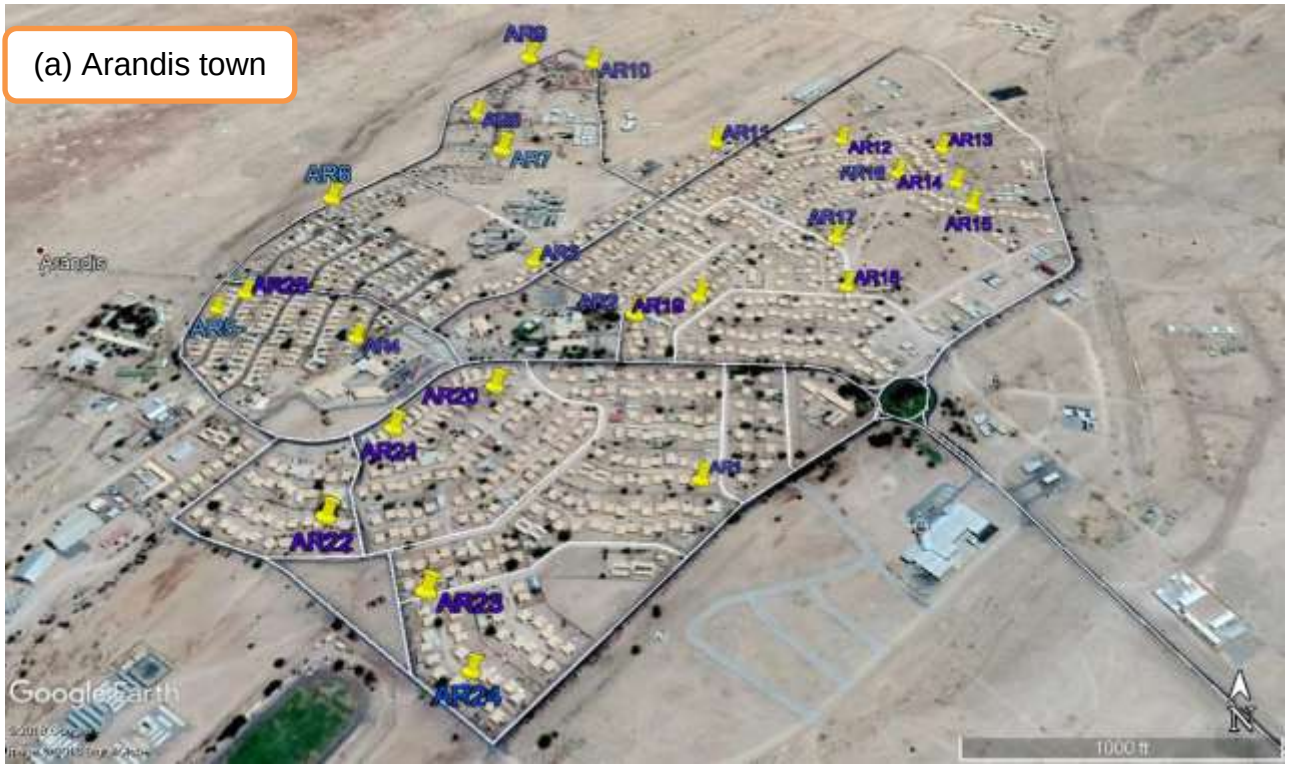

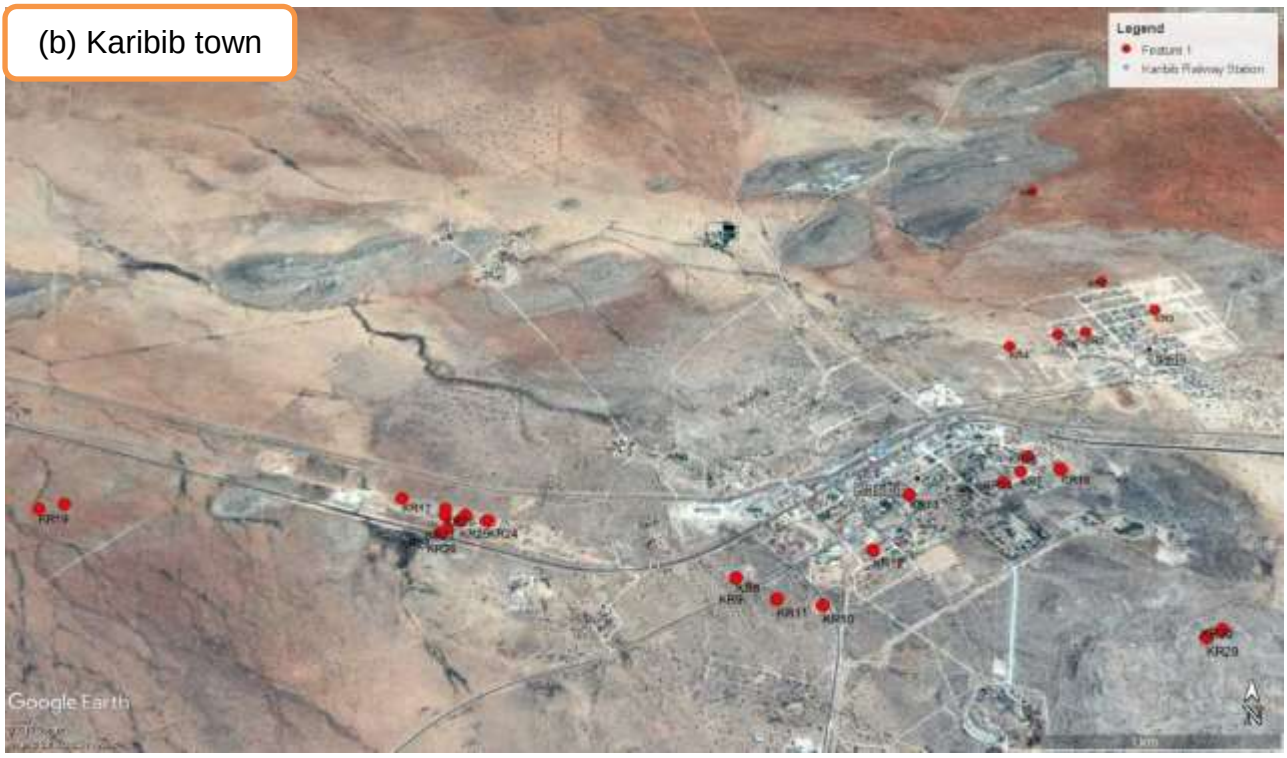

Figure 3.1 The map of Arandis town (a) and Karibib town (b) showing some sampling sites (www.googleearth.com)

positioning equipment (GPS) and the sampling bags were marked appropriately. The samples were taken to Namibia University of Science and Technology' Post graduate laboratory for analysis. Similarly, for particulate matter (PM), a total of twenty (20) single bucket dust monitors were deployed in each satellite mining town according to the procedure of American Society for Testing and Materials standard method (ASTM D1739). Dust fallout method is a known and accepted method used to monitor particulate matter including fallout dust from various sources (Kgabi et al., 2012). An open area with no obstructions from buildings and trees was selected at each sampling site. The sampling area was marked with a geographically position system (GPS) and the cylindrical buckets were tied to a metal pole and raised at least 1.5 m from the ground to avoid some water droplets and other debris from contaminating the contents of the bucket. The buckets were half filled with deionised water and it was treated with biocide to prevent algal growth and exposed for one calendar month. The amount of water to be filled in the bucket and the time was varied depending on prevailing conditions. The procedure was repeated for three consecutive months i.e. from May 2017 to July 2017. The contents of each bucket were taken to the laboratory where it was analysed using gravitational method, elemental concentration, morphological and radiological characteristics.

3.3 Assessment of radioactivity in particulate matter and soil

3.3.1 Soil sample preparation

At the laboratory the samples were dried in an oven to drive off all the moisture and they were transferred into sealable 500 ml Marinelli beakers. The samples were sealed and kept for 28 days to allow secular equilibrium to reach between uranium and its progenies and thorium with its progenies. The activity concentrations were measured using Canberra High Purity Germanium Detector (HPGe) and the results were used for the calculations of radiation parameters.

3.3.2 Particulate matter sample preparation

The buckets containing particulate matter samples were transferred to the laboratory. At the laboratory, the units were filtered with a Buchner filtration system. After filtration, the samples were attached to filter papers, air dried and placed in a desiccator to allow the mass to stabilise before weighing to determine the exact amount of settled particulate matter (PM) using gravitational calculations.

3.3.3 Gamma spectrometry

3.3.3.1 Detection system description

Gamma spectrometry is a non-destructive method for the measurements of activity of different radionuclides in environmental samples. Many radioactive sources will leave signatures that are used for quantifying them. i.e. they produce gamma rays of different energies (Lutz, 2001). A block diagram of High Purity Germanium detector (HPGe) coupled to a high vacuum cryostat Dewar system containing liquid nitrogen which creates a path for heat transfer from the reservoir to the detector is illustrated in Figure 3.2. The detector is shielded with a heavy lead material to prevent background radiation. The system is supplied with a high voltage power supply which can reach about 4000 V and supplies voltage to the rest of the electronic components. The system also has highly efficient electronics which include a preamplifier which produces a response proportional to the quantity of charge produced by the incident ray. The other element of the electronics is the amplifier whose main function is to amplify the signal. The last element is the multichannel analyser (MCA). The last part is critical in the experimental measurements.

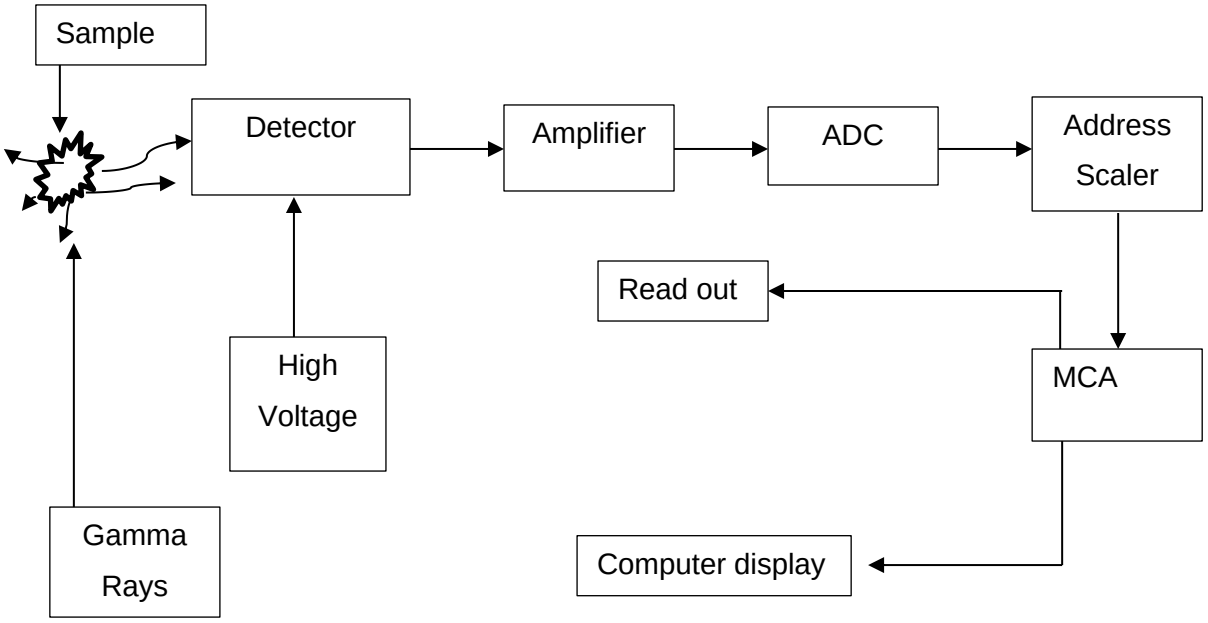

Figure 3.2 The schematic diagram of HPGe gamma spectrometry system (Faanu, 2011).

The MCA is composed of an analogue-to-digital converter (ADC), control logic, memory and display and its function is to collect pulses in all voltage ranges at once and displays this information in real time as final results or as data for further analysis (Reguigui, 2006). It is worth noting that the energy resolution and efficiency of the detector are two critical aspects of the detector and these are discussed briefly. Energy resolution of High Purity Germanium (HPGe) detector is a dominant characteristic in this type of detector and is responsible for enhancing the separation and resolving of various close energy gamma-ray peaks in a complex spectrum system. The energy resolution sometimes referred to as the full width at a level at half maximum of the full energy peak (FWHM) and this is expressed in keV for germanium detectors. The gamma peak energies of some standard radioactive sources such as ^{137}Cs and ^{60}Co are known i.e. the specific characteristic full energy peak of ^{137}Cs and ^{60}Co are 662 keV and 1332 keV respectively. The energy resolution of the germanium detector depends on the number of electron-hole pairs created in the detector, charge collection and electronic noise contribution. These three factors rely on the properties of the detector and the gamma-ray (Knoll, 2000). Similarly, the effectiveness of the detectors is inversely related to the log energy of the detector and depends on geometry. As a rule of thumb, the number of calibration points used in the analysis are important to produce an ideal calibration curve (IAEA, 1989).

3.3.3.2 Energy and efficiency calibration for high purity germanium detector (HPGe)

The calibration of energy-to-channel number was performed using International Atomic Energy Agency (IAEA) composite standards of Cadmium-109, Strontium-85 and cobalt-60 before sample measurements. These composite sources were chosen because they contain nuclides that emit photons covering the desired energy region.

The composite source was placed in a lead shielded detector and ran for 12 hours and the true position of every full energy peak was determined accurately, and the energy of the photon was plotted against the channel number as shown in Figure 3.3. The produced peaks were used to determine the energy of a photon that is responsible for an unknown peak in the spectrum. The IAEA composite standard used for energy calibration was also used for the efficiency calibration and these were counted for 12 hours. The net counts for each of the full energy events in the spectrum was determined and their corresponding energies were used in the determination of the efficiencies and this follows the expression given in 3.1 as follows (Darko et al., 2007).

$$\eta(E) = \frac{N_T - N_B}{P_E A_{STD} T_{STD}} \quad 3.1$$

where;

$\eta(E)$ is the efficiency of the detector,

P_E is the gamma emission probability for a given energy,

N_T is the total count under the photopeak,

N_B is the background count,

A_{STD} is the activity (Bq) of the radionuclide in the calibration standard at the time of calibration,

T_{STD} is the counting time of the standard.

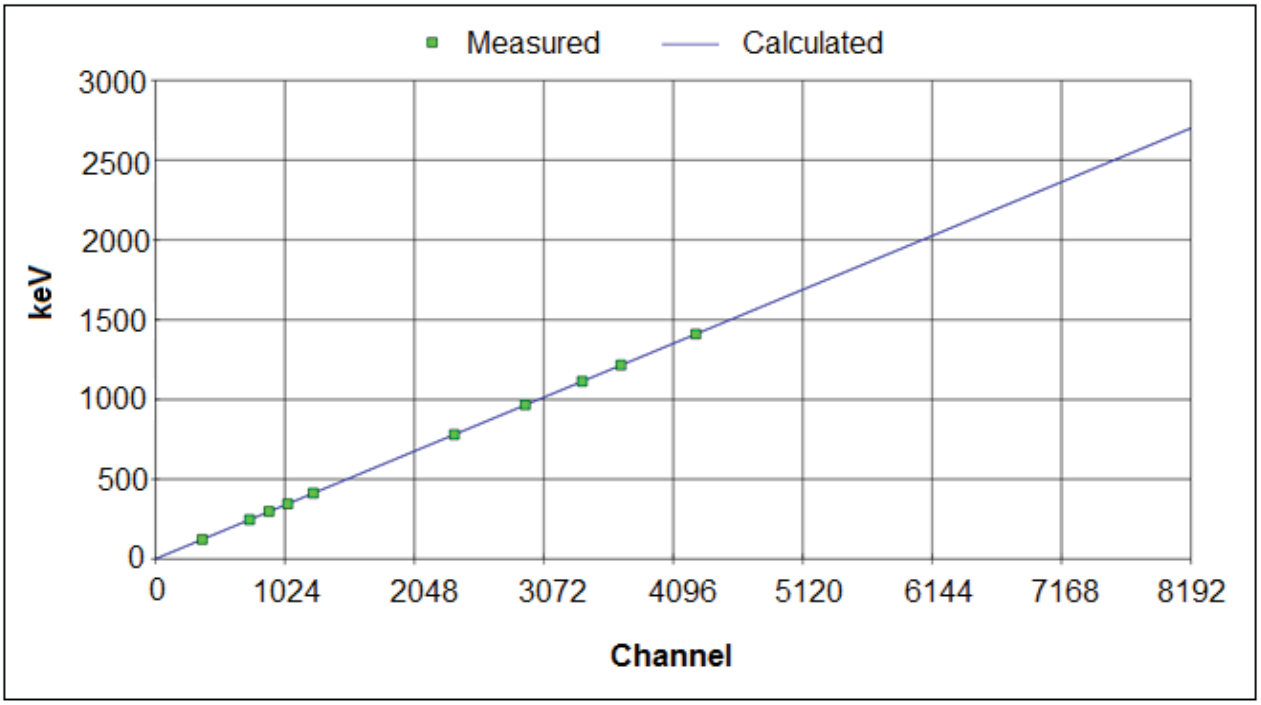

Figure 3.3 The energy calibration curve for the HPGe detector

The measured results were then plotted on a graph after taking into account a simplified geometry for the marinelli beakers such as physical parameters of the sample (fill height, material matrix, density and distance of the detector). The efficiency calibration curve was used to produce qualitative and quantitative results. Figure 3.4 shows a dual efficiency calibration curve for the HPGe detector.

3.3.3.3 Measurements of activity concentrations in soil samples

The beakers were tightly closed to prevent escape of radon gas and kept for at least twenty-eight days before measurements to allow radionuclides to attain secular equilibrium

with their progeny. According to Thorne and Mitchell (2011), who reviewed the behavior of ^{238}U in soils, following the disturbance of stability in its natural environment, the attaining of secular equilibrium occurs in an isolated system. The radionuclides in the decay chain can be differentiated on the basis of chemical properties mainly controlled by distribution coefficient (K_d) of ^{230}Th and ^{226}Ra or the formation of ^{222}Rn which may lead to disequilibrium of the progeny. Contrary to most calculations in ^{238}U which assumes that after 28 days the radionuclide will be at equilibrium with its daughters, it takes 10^6 years in most environments Chiozzi, Pasquale, & Verdoya (2002) to establish this equilibrium and as such measurement of ^{238}U is performed from first principle with the shorter -lived members of ^{238}U assumed to be in secular equilibrium with their immediate long lived ancestor. This follows that ^{238}U is measured from ^{234}Th and ^{234m}Pa while ^{226}Ra and ^{210}Pb is measured from their respective progenies.

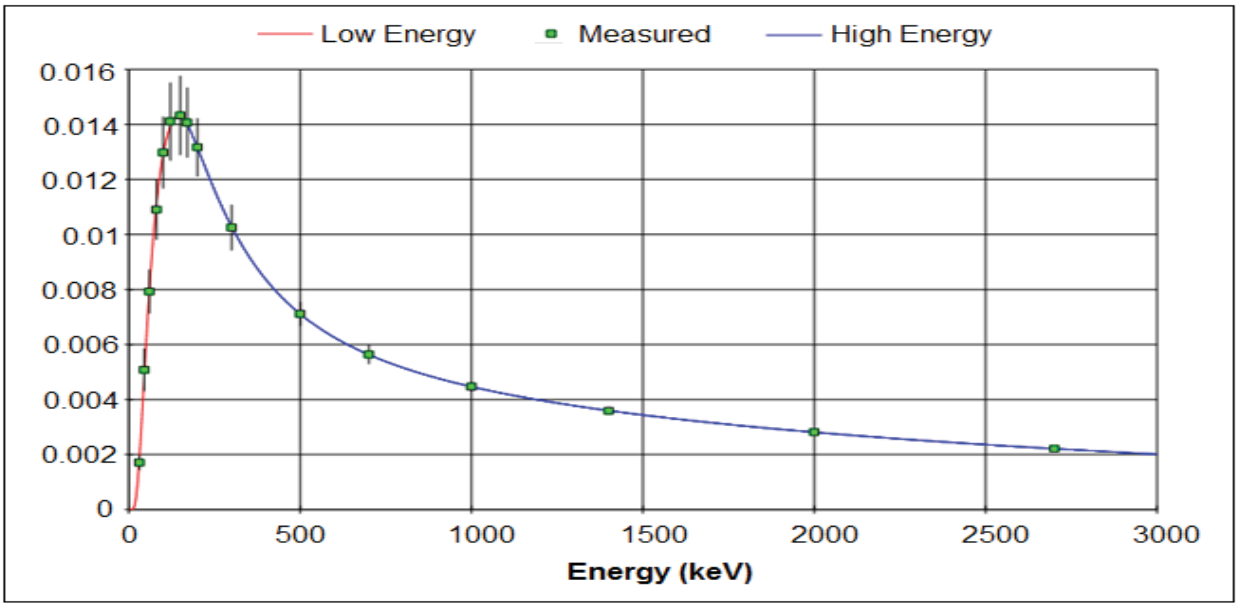

Figure 3.4 The dual efficiency calibration curve for the HPGe detector

The activity concentrations of each radionuclide was determined by considering the weighted mean activity concentrations of the daughters in each series at the given photo peak except where there was interference. i.e. ^{238}U was determined using photopeak 63.20 keV (4.1%) and 92.60 (2.39%) keV from ^{234}Th and 1001.03 keV (0.84%) from ^{234m}Pa and ^{226}Ra was determined with photopeak 295.2 keV (19.7%) and 351.9 (38.9%) from ^{214}Pb, 609.3 keV (46.1%) and 1120.3 keV (15.7%) from ^{214}Bi. Similarly, ^{232}Th activity was determined from the gamma-rays of 238.6 keV (44.6%) from ^{212}Pb and 338.3 keV (11.4%),

911.6 keV (27.7%) and 969.1 keV (16.6%) from ^{228}Ac, while ^{210}Pb and ^{40}K activities were determined from a single gamma energy photon line at 46.54 keV (4.25%) and 1460.2 keV (10.7 %) respectively. This is summarised in Table 3.1. The activity concentrations of radium, thorium and potassium in Bq kg^{-1} of the radionuclides in the composite soil samples were calculated using equation (3.2) (Hamby & Tynybekov, 2002).

$$A_{Bq.kg^{-1}} = \frac{C_{NP}}{B.I \times \varepsilon(E_\gamma) \times m} \quad (3.2)$$

where, C_{NP} is the net peak counts for a given energy line, *B.I* is the branching intensity, $\varepsilon(E\gamma)$ is the absolute photo-peak efficiency of the detector and m is the mass of the sample in kg.

Table 3.1 Summary of nuclear data of radionuclides used in the analysis.

Parent nuclide	Daughter nuclide	Gamma Energy (KeV)	Gamma Ray Abundance (%)
^{238}U	^{234}Th	63.20	4.1
	^{234}Th	92.60	2.39
	^{234m}Pa	1001.03	0.84
^{226}Ra	^{214}Pb	351.9	38.9
	^{214}Pb	295.2	19.7
	^{214}Bi	609.3	46.10
	^{214}Bi	1120.3	15.7
^{232}Th	^{212}Pb	238.6	44.6
	^{228}Ac	338.3	11.4
	^{228}Ac	911.6	27.7
	^{228}Ac	969.1	16.6
^{40}K	-	1460.20	10.67
^{210}Pb	-	46.54	4.25

3.3.3.4 Measurements of activity concentrations in PM samples

The activities of the investigated radionuclides (^{226}Ra, ^{238}U, ^{232}Th, ^{40}K and ^{210}Pb) in particulate matter from the two mining towns were determined by direct gamma spectrometry, using a well-type high purity germanium (HPGe) detector, with an efficiency of 30 % relative

to a 3”x 3” Na(TI) scintillator and an energy resolution (FWHM) of 1.8 KeV for 1.33 MeV ^{60}Co reference standard. The samples were stored for 4 weeks in a 1.5 ml Eppendorf tubes which were tightly closed to allow equilibrium to be established in uranium and thorium series. The prepared Eppendorf tubes together with the samples were placed in a well-type detector and run for 12 hours. Both the sample and the detector were lead shielded to supress background radiation. The ambient background radiation was determined by running an empty Eppendorf tube under identical conditions with the sample. The latter was subtracted from the measured spectra to obtain the net radionuclides activities using the gamma energy lines given in the previous topics. The data was acquired, stored and displayed by Genie 2000 software.

Detection limit for gamma analysis of ^{238}U, ^{232}Th and ^{40}K

Detection limit is defined as the estimate for the lowest amount of activity of a specific gamma-emitting radionuclide that can be detected at the time of measurement and can be calculated from several expressions. One such expression is what is known as the lower limit of detection (LLD) which contains a pre-selected risk of 5 % of concluding falsely that activity and a 95 % degree of confidence for detecting the presence of an activity i.e. lower limit of detection is defined as the true signal which may be expected to lead to a detection and is expressed as in equation 3.3. The detection limit sometimes called the critical level was introduced to give certain degree of confidence in measuring radioactivity concentrations in samples.

$$LLD = 2.706 + 4.653_{N_B} \quad (3.3)$$

where, σ_{N_B} is the standard deviation of count number when a blank sample is measured to determine the background level. The detection limit provides a means of determining the operating capability of a gamma measuring system without the influence of the sample and assumes that the count rate in the energy area taken for the radionuclide and the count rate in the region taken for background are independent.

Minimum limit of detection (MDA)

The minimum detection activity is a criterion for measuring performance of gamma-ray spectrometric counting. The minimum detectable amount of activity can be obtained from detection limit in equation 3.4.

$$MDA = \frac{L_D}{\varepsilon_f P_\gamma T} \quad (3.4)$$

where, LD is the detection limit, ε_f is the counting efficiency of the specific nuclide's energy; and P_γ is the absolute transition probability by gamma decay through the selected energy as for $\varepsilon_f \leq 1$. The MDA in Bq/kg used for determination of ^{238}U, ^{232}Th and ^{40}K in this study are given in Appendix A.

3.4 Determination of indoor radon concentrations in selected households

3.4.1 Sample site selection criteria

The radon gas monitors were randomly deployed in the selected households in mining towns and the sites were marked by geographical positioning system. These households are single floor apartments, free standing houses and semi-detached houses constructed of concrete, sand, and cement bricks and the roofs are at a height of 2.5 -3.5 m above ground. Short term radon measurements were carried out to evaluate the concentration of radon in dwellings in each of the two mining towns using Radon Passive Alpha CR-39 detectors. The duration of deployment of radon gas monitors ranged from 2 days to 90 days and this study was done over a period of three months to improve reliability. The dosimeters were installed at 2 metres above the ground exposed to ambient air in each dwelling (Asumadu-Sakyi et al., 2012). Precaution was taken not to install the dosimeters directly to the source of sunlight or closer to windows and other electronic gadgets that that can disturb the flow of currents.

3.4.2 Indoor radon detective device

Figure 3.5 is an illustration of the CR-39 radon gas monitors that was used in this study. There are slits around the dosimeter that allows the radon gas to diffuse into its chamber. The alpha particles generated from the decay of radon and its daughter in the air volume of the chamber can interact with the CR-39 film leaving microscopic ionization tracks which can be etched by an optical amplification readout device. After three months of exposure, the CR-39 dosimeters, were retrieved and chemically etched at a laboratory at Radon Gas Monitor (RGM) company in South Africa.

3.4.3 Interpretation and analysis of data

The number of tracks generated on each solid-state nuclear track detector (SSNTD) was counted and these were used to calculate the density i.e. tracks per given area (tracks/cm^2) denoted by the symbol, ρ according to the equation 3.5 (Aniagyei et al.,1996)

$$\rho = \frac{\sum N_i}{\mathrm{n}A} \tag{3.5}$$

where, N_i is the number of tracks counted in the field of vision i, A is the surface area (cm^2); n is the total number of fields on vision.

Figure 3.5: An illustration of CR-39 radon gas monitors

The concentration C_{Rn} of radon in each room was correlated to the track densities on the CR-39 detector using the following formula in equation 3.6 (Al-Bataina et al, 1997; Durani & Bull, 1987; Thabayneh, 2015).

$$C_{Rn} = \frac{\rho - \rho_0}{k\,.t} \tag{3.6}$$

where, C_{Rn} is the indoor radon activity concentration (Bq/m^3); ρ_o is the background track density; t is the exposure time of the detectors and equals to 2160 hours (90 days) in our study; k is the dosimeter calibration factor (tracks.cm^{-2}/kBqm^{-3} h). The calibration factor of the detector used was assumed to be 1 track.cm^{-2}/kBqm-^{3}h and ρ_o = 0. It has been shown that passive radon gas monitors are subject to systematic errors (Mishra et al, 2014)

Assessment of dose due to radon and its progeny

When it was realised that most of the dose due to radon come from its short-lived progeny, a conservative limit value was established, and this is known as the working level (WL). This was based on the energy that inhaled progeny would deposit in the lungs. In the traditional uranium mines, ventilation was often poor, and the radon progeny were close to equilibrium with radon (ICRP, 1993). It was also found that the radon progeny equilibrium with 3,700 Bqm^{-3} radon gas would release approximately 130,000 MeV of alpha energy as it decays and thus 1 WL is defined as;

1 WL = 130 000 MeV alpha energy per liter of air
= 0.0208 millijoules (mJ) alpha energy per m^3 in air (mJm^{-3})

The average working hours per month of a miner at that time was 170 hours and so the working level month (WLM) was introduced to simplify record keeping. The working level month (WLM) was calculated using equation 3.7 (EPA, 2003); the annual effective dose from radon and its progeny (H_E: mSv/y) using the equation 3.8 (UNSCEAR, 2000) respectively.

$$E_R = C_{Rn} \times F \times 2.7 \times 10^{-4} \times \frac{T}{170} \quad (3.7)$$

$$HE(mSv/y) = C_{Rn} \times E \times F \times T \times D \quad (3.8)$$

where, E_R is the average annual radon progeny exposure rate, C_{Rn} is the radon concentration (Bq/m^3), E is the equilibrium factor between radon and its progeny (0.4 indoor and 0.6 for outdoor), F is the occupancy factor (0.8 for indoor and 0.2 for outdoor), T is the time in hours per year (8,760 h); D is the dose conversion factor (9 x 10^{-6} mSv/Bq hr/m^3). Similarly, the excess lifetime cancer risk, ELCR, due to radon and its progeny was calculated using equation 3.9 (EPA, 2003)

$$ELCR = E_R \times LE \times F_R \quad (3.9)$$

where, LE is the average lifetime expectancy (70 years) and F_R is the risk coefficient for the exposure to radon in equilibrium with its progeny and is equals to 5 x 10^{-4} per WLM (ICRP, 2009).

3.5 Determination of toxic heavy metals in soil

3.5.1 Sample collection and pre-treatment

A total of 50 triplicate surface soil samples were obtained from the same point where the bucket dust monitors were deployed in the two towns of Karibib and Arandis. The mass of each surface soil sample collected was 200 g. Each area where the soil sample was collected was marked with geographical information system (GPS) which was used for identification of that area using google map. Triplicate samples were collected from each site and these were thoroughly mixed to yield a true representative. The representative sample was sieved through a mesh size of 1 mm and placed into pre-labelled, sterile disposable plastic bag. It has been reported that a mesh size of 1 mm is enough to contain most of the heavy metals (Ward et al., 2004). The samples were taken to the laboratory where they were dried in the oven at 100 ^{0}C to drive out all the moisture. The samples were later transported to North West University, Potchefstroom Campus for further processing and analysis using ICP- MS.

3.5.2 Microwave digestion for heavy metals in soil samples

For extraction of heavy metals from soil and dust samples, microwave digestion method was used. About 1 g of the sample was measured. A mixture of mixed HNO_3 and HCl was added to the sample in the ratio of 1: 3 respectively. A further 1 g of H_2O_2 was added to sample as a catalyst and the mixture was digested in a microwave at 120 ^{0}C for 45 minutes. After digestion, the mixture was cooled and then transferred into a 100 ml volumetric flask. 2 % of HNO_3 was added and the solution was made up to the 100 ml mark using deionised water. The solution was allowed to stand over night after which it was filtered using Whatmann-40 filter paper and it was ready for ICP-MS analysis.

3.5.3 Detection of heavy metals

The ICP-MS is a destructive method in which the digested sample is decomposed into atomic constituents followed by ionisation in an argon plasma at elevated temperature of between 6000-8000 K (Perkin Elmer, 2004-2011). The positively charged ions are accelerated from the plasma through a vacuum of mass spectrometer where they are separated by mass filter before being measured by an ion detector. The resident time of each sample is 60 seconds and each sample is run twice (USEPA, 2007). The TotalQuant method was used with a standard solution to improve the accuracy of the results and to be able to detect contamination and drift. Calibration of the method was achieved using 200 ug/l of solutions of Al, Pb, Cr, Cd, Ce, Cu, Co, Mg, Ni, Mn, Li, U and Zn. For quality control, two blanks were included with each standard sample. The calibration process updates internal response data that correlates measured ion intensities to the concentrations of the element in the solutions. The samples were analysed for levels of lead (Pb), arsenic (As), mercury (Hg), cadmium (Cd), chromium (Cr), cobalt (Co), nickel (Ni), copper (Cu) and zinc (Zn). Data generated from ICP-MS was in mg/L, which was then converted to mg/kg using the equation 3.10 (Temminghoff & Houba, 2004)

$$\text{Final concentration } \left(\frac{\text{mg}}{\text{kg}}\right) = \frac{\text{A}-\text{B}}{\text{W}\times 10^{-3}} \times \text{V} \qquad (3.10)$$

where, A is the concentration of a heavy metal in the sample (mg/L); B is the concentration of the heavy metal in the blank (mg/L); V is the total volume of the digest (ml) and W is the sample weight (kg).

3.5.4 Contamination status of soil by heavy metals

The concentrations of the analysed heavy metals were subjected to various pollution indexes to determine the level of contamination in the studied area. These pollution indexes include contamination factor index (C_F), pollution load index (PI) and integrated pollution index (IPI) which are explained in the proceeding subtopics.

Contamination factor index (C_F) and degree of contamination (Cdeg).

A modified four classes of contamination factor index (C_F) and degree of contamination (Cdeg) suggested by Hakanson (1980) was used evaluate the levels of contamination by the analysed heavy metals (Banu et al., 2013). Contamination factor was determined to

determine the extent of anthropogenic pollution and accumulation of heavy metals in the soil and PM samples. Contamination factor is the single index which is defined by relation shown in equation 3.11 (Hakanson, 1980).

$$C_F = \frac{C_m - 1}{B_m} \tag{3.11}$$

where, C_m is the mean content of the metal and B_m is the concentration of World average shale value for an individual metal. Similarly, the degree of contamination (C_{deg}) is defined as the sum of contamination for all the elements. The degree of contamination by the nine heavy metals in the radioactive dust was determined as shown in equation 3.12 (Hakanson, 1980).

$$C_{deg} = \sum_{i=1}^{9} C_F \tag{3.12}$$

The categories of contamination factors and the degree of contamination are shown are shown in Table 3.2 (Hakanson, 1980).

Table 3.2 Categories of contamination factors and degree of contamination

Class	CF	Category	Cdeg value	Category of contamination
Class 1	<1	low	<9	low
Class 2	1>CF<3	Moderate	9<Cdeg<18	Moderate
Class 3	3>CF<6	Considerable	18<Cdeg<36	Considerable
Class 4	6>	Very high	>36	Very High

Pollution load index (PLI)

The pollution load Index (PLI) is used to evaluate the level of pollution in the environment. The PLI is expressed as a concentration factor (CF) which is a quotient obtained by dividing the concentrations of each metal by its background concentration. In any given place, the PLI is calculated by obtaining the nth root from the nth- CF that were obtained for all the metals. This method was proposed by Tomlinson et al., (1980) and is shown by equation 3.13

$$\mathrm{PLI} = \sqrt[\mathrm{n}]{\mathrm{CF}_1 \times \mathrm{CF}_2 \times \mathrm{CF}_3 \cdots \mathrm{CF}_\mathrm{n}} \tag{3.13}$$

where, CF is the contamination factor, n is the number of metals, C_{metal} is the metal in polluted sample, $C_{background}$ is the background value of that metal. If the PLI is > 1, it means the soil is polluted, otherwise < 1 is unpolluted.

Enrichment ratio (ER)

The factor analysis is a method used to assess trace element concentration proposed by Simex and Helz (1981), and the its mathematically expressed by equation 3.14.

$$\text{Enrichment ratio (ER)} = \frac{(\text{X/Fe})\text{Sample}}{(\text{X/Fe})\text{Background}} \quad (3.14)$$

where, X/Fe is ratio of the element of interest (X) to iron (Fe) used as a reference element in this study because it is stable and its concentrations cannot be anthropogenically altered. i.e. it has a controlling effect on the distribution of heavy metals (Rath, 2005). The background value is world surface rock average given by Martin and Maybeck (1979). The numerical values for enrichment factors which indicate different pollution levels as proposed by Sutherland et al, 2000 are shown in Table 3.3

Table 3.3 Numerical values for enrichment factors which represents different pollution levels

EF value	Soil or dust quality
< 2	Deficiency to minimum enrichment
2 < EF < 5	Moderate enrichment
5 < EF < 20	Significant enrichment
20 < EF < 40	Very high enrichment
EF > 40	Extremely high enrichment

Geoaccumulation index (Igeo)

The Geoaccumulation Index (Igeo) was originally proposed by Muller (1979) for metal concentrations in the 2-micron fraction and was based on the world shale values and is mathematically as expressed by equation 3.15.

$$\text{Igeo} = \log_2\left(\frac{C_n}{1.5 * Bn}\right) \quad (3.15)$$

where, Cn is the measured concentration of the element in the soil or dust, Bn is the geochemical background value and the constant 1.5 allows the analysis of natural fluctuations in environmental samples and detect minute changes due to anthropogenic influence. Muller defined seven descriptive classes based on increasing Igeo values form the least polluted to the extremely contaminated i.e. Class 0 (Igeo = 0, unpolluted) to the highest Class 6 (Igeo = 6, most polluted). The Indices are illustrated on Table 3.4.

Table 3.4 Geoaccumulation index (Igeo)

Class	Value	Soil or dust quality
0	Igeo ≤ 0	Uncontaminated
1	0 < Igeo < 1	Uncontaminated to moderate contaminated
2	1 < Igeo < 2	Moderately contaminated
3	2 < Igeo < 3	Moderately to Heavily contaminated
4	3 < Igeo < 4	Heavily contaminated
5	4 < Igeo < 5	Heavily to extremely contaminated
6	Igeo ≥5	Extremely contaminated

3.6 Assessment of particulate matter (PM)

3.6.1 Sample preparation for SEM/EDX

To obtain an image of PM microstructure and identify the elements present in its composition, a scanning electron microscope with energy dispersive X-ray capabilities was used. The sample was prepared by carefully selecting and cutting a fair area of not more than 12 x 12 mm size from the dried particulate matter (PM) adsorbed on the filter paper. The piece of the selected area was handled with a tweezer to avoid contamination. A conductive graphite coating was applied to a carbon stud using a brush. This was followed by selecting a PM flake on the painted stud which was allowed to stand to dry for a short period of time. After air drying, the samples were placed in the available spaces on the equipment for further coating and the desired thickness was established on the machine. The machine was run until coating was complete and the sample was removed from the sputter coater and placed

into a petri dish for easy transportation to the SEM equipment where it was analysed for morphology and elemental composition.

3.6.2 Gravitational analysis of PM samples

The collected insoluble particulate matter (PM) samples were analysed in the laboratory following the method given by Lodge (1988). The PM samples in each bucket was filtered out (onto 125 ashes less filter) using a Buchner funnel connected to the diaphragm vacuum pump and the insoluble residue was dried before weighing. Subsequently, the filter paper was dried in an oven at 110 ^{0}C for 2 hours and afterward kept in a desiccator prior being weighed. The PM concentration was quantified using equation 3.16 which is based on the weight differences of the filter papers, the area of the PM container opening mouth (m^2) and period of exposure i.e. number of days (1 month) (Alahmr et al., 2012).

$$\mathrm{D}\ (\mathrm{mg/m2/day}) = \frac{\mathrm{W_f - W_i}}{\mathrm{AT}} \tag{3.16}$$

where; D is the particulate matter fallout rate, W_i is the weight of a filter paper without the sample (g), W_f is the weight of the dry insoluble PM sample and the filter paper (mg), A is the area of the container opening mouth (m^2), and T is the period of sampling (days).

3.6.3 The scanning electron microscopy (SEM)/ energy dispersion X-ray (EDX)

The scanning electron microscopy (SEM) is often attached to energy dispersive x-ray systems (EDX) are to give SEM/EDX. The SEM is an instrument used for observing and analysis of the surface microstructure of a bulk sample using a finely focused beam of electrons. The electron-matter beam generates a variety of signals that carry different information such backscattered electrons which produces images with contrast, and this is dependent on the atomic number of the element, secondary electrons which gives topographic information and the X-rays is important for identification of the element and measure the composition of the material. A schematic diagram the electron-matter interaction is shown in Figure 3.6. The generation of X-rays in SEM begins by bombarding a sample with an electron beam resulting in the electrons being either being excited to a higher energy level or being ejected from the atoms on the specimen surface. If such transition occurs, this results

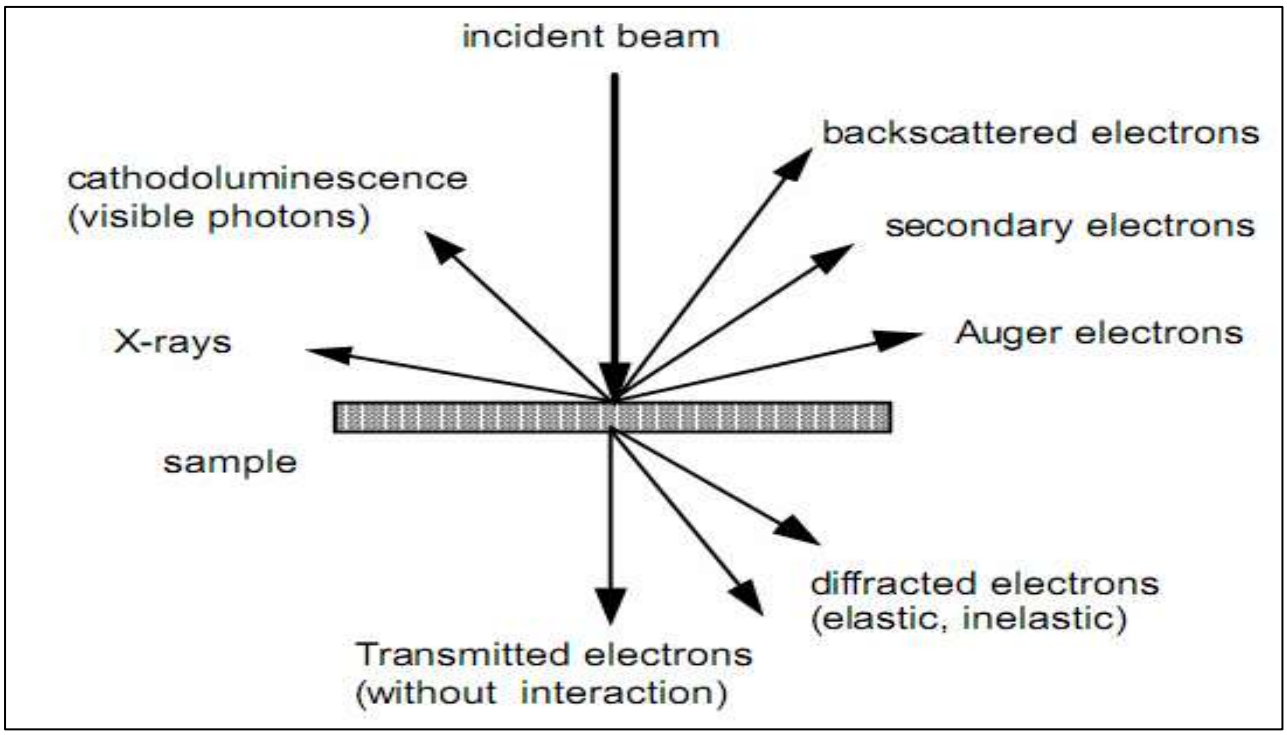

Figure 3.6 Illustration of the electron-matter interaction depicting different products (Krinsley, 1998)

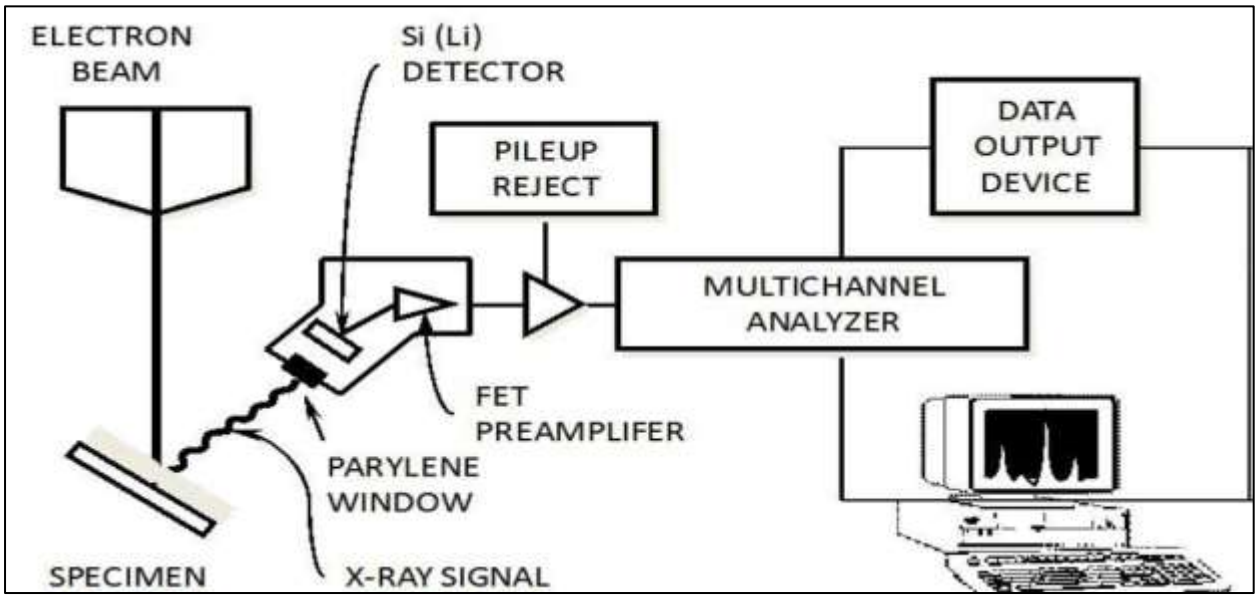

Figure 3.7: An illustration of the scanning electron microscope coupled to energy Dispersive X-ray (Krinsley, 1998)

in the formation of electron hole which is filled by an electron from a higher shell, and a characteristic X-ray is emitted to balance the energy difference between the two electrons. The EDX measures the number of emitted rays versus their energy. The energy of X-ray depends on the atomic number which is a unique proper of every element i.e. characteristic of that element from which the X-ray was emitted.

The EDX-rays is a fingerprint of each element and is often used as a qualitative elemental analysis simply to determine which elements are present and their relative abundance. Figure 3.7 shows a schematic diagram of the scanning electron microscope energy dispersion X-rays. The output from the EDX is a spectrum which is a plot to show how frequently an x ray is received for each energy level.

3.6.4 Morphological analysis of PM

The characterisation of particle morphology and composition was carried using a Scanning Electron Microscope equipped with an Energy Dispersive X-ray Spectrometer. For SEM analysis, an accelerating voltage of 5kV and a working distance of 22 mm were used. The X-ray microanalysis signal was optimised by using a specimen tilting angle of 40 ^{0}. Portions of filter (about 25 mm^{2}) were attached to aluminium stubs (diameter 12 mm) using carbon sticky tabs and subsequently carbon coated. SEM images were obtained using both secondary (SE) and back-scattered electrons. To provide representative results and minimise bias in the analysis, three randomly selected fields for each filter were examined. Manual SEM particle examinations were carried out at magnification up to 30 000 and secondary electron images were acquired, and these were later analysed with Image J software. Agglomerates with different chemical composition present in PM samples were examined in different parts. The results for the photomicrographs of individual particles and EDX data were collected for particle classification and morphological characterisation. Chemical elemental analysis was performed for crustal and toxic metals.

3.6.5 Respiratory deposition of PM (inhalability and deposition of PM)

Particulate matter is ubiquitously present in the ambient air and their unique physicochemical characteristics may pose a potential health risk. Accurate lung dose information is essential to assess the potential health risk from these particles. The potential exposure to PM particles in large concentrations is possible near the source of generation e.g. near highways or closer to a mining setting. Various studies have demonstrated that fine PM particles causes adverse health effects in animal and in vitro studies and this varies with

the particle size (Li et al., 2003; Oberdorrster et al., 1992). While there is abundant epidemiological evidence linking PM with decrease in lung function (Peters et al., 1997; Wichmann and Peters, 2000), the specific mechanism by which PM cause adverse health effects in human subjects still remain an enigma (Utell and Frampton, 2000). Respiratory deposition of PM in our lungs is necessary to evaluate their toxicity. In this study, the inhalable fraction (IF), which relates to the efficiency of the particle entry into the nose and mouth as well as the total deposition fraction (DF) in the respiratory system was evaluated by equation 3.17, 3.18 and 3.20. The meteorological data was obtained by taking the average wind speed at each sampling site (https://www.worldweatheronline.com/karibib-weather averages/erongo/na.aspx).

The inhalability data was evaluated in terms of inhalable fraction (IF) (d_a) according to the equation 3.17

$$\mathrm{IF}(d_a) = 0.5\,(1 + \exp(-0.06(d_a)) \text{ for } U_0 < 4\ \mathrm{m/s} \tag{3.17}$$

where, d_a is the aerodynamic diameter in µm. For ambient air velocity U_0 greater than 4 m/s, the inhalable fraction (IF), is given by equation 3.18 (Vincent et al, 1990).

$$\mathrm{IF}(d_a, U_0) = 0.5\,(1 + \exp\left(-0.06(d_a)\right) + 10^{-5} U_o^{2.75} \exp(0.055 d_a)) \tag{3.18}$$

while the nasal inhalability (IF_N) can be approximated according equation 3.19 (Hinds et al, 1999)

$$IF_N(d_a) = 0.035 + 0.965\exp\,(-0.0003 U d_a^{2.74})) \tag{3.19}$$

Some computer programs and equations have been developed to make calculations with International Commission on Radiological Protection (ICRP) model easier and one such equation was developed by Hinds (1998). The equation accounts for the total deposition (DF), which is the sum of the regional depositions in the respiratory system and this is illustrated in equation 3.20.

$$DF = IF\left(0.0587 + \frac{0.911}{1+\exp\,(4.77+1.485\ln d_p)} + \frac{0.943}{1+\exp\,(0.503+2.5\ln d_p)}\right) \tag{3.20}$$

where, d_p is the particle size in µm, and IF is the inhalable fraction.

3.7 External radiological risk assessment due to NORM

3.7.1 Dosimetry quantities

Exposure

Exposure can be defined as the amount of ionization that X- or gamma radiation produces in air and this is limited to only 3 MeV. Traditionally, the unit of measurement is the Roentgen (R). This unit account for 1 *esu* of electrical charge of either sign in 1 cm^3 or 0.001293 g of air at standard temperature and pressure (Turner, 2007; Lilley, 2001). Since 1 esu = 3.34 x 10-10 Coulomb (C), the exposure unit can be expressed SI system:

$$IR = 1\frac{esu}{cm^3} = \frac{3.34 \times 10^{-10} C}{1.298 \times 10^{-6}\frac{kg}{g}}$$

$$= 2.58 \times 10^{-4}\frac{C}{kg}$$

Absorbed dose (D)

The major drawback of using exposure in radiation protection is that it is applicable to photons in air but not any all types of radiation or energy deposition in tissue. However, the concept of absorbed dose may be applied to any type of radiation and any absorbing material. The absorbed dose (D) represents the quantity of energy deposited per unit mass and this can be defined by the relationship in 3.21.

$$D = \frac{\Delta\varepsilon}{\Delta m} \tag{3.21}$$

where; $\Delta\varepsilon$ is the mean energy imparted by ionising radiation to matter within a given volume element (MeV) and Δm is the mass of matter within the volume element (kg). Traditionally, the absorbed dose unit was the “rad” =100 ergs/g). The SI equivalent is the gray (Gy), which is defined as 1 joule of energy deposited per kilogram of medium (Lilley, 2001). It should be noted that the change in energy per mass becomes unpredictable as the mass of the sample becomes small.

Equivalent and effective dose

It is well documented that different types of radiation have different biological damage in an organ and so it is imperative to consider tissue weighting factor to account for that

variation. The equivalent dose, H_T in an organ or tissue is expressed as the sum of absorbed dose $D_{T,R}$ in an organ or tissue caused by different types of radiation with so called weighting factors, W_R(Lilley, 2001) as defined by the expression 3.22.

$$H_T = \sum_R W_R \times D_{T,R} \qquad (3.22)$$

The standard unit of equivalent dose is called the Sievert (Sv). The radiation weighing factor is introduced to measure the absorbed dose for biological effectiveness of the particles. The variation of radiation sensitivity of each organ is considered in the contribution of the equivalent dose in all tissues and organs of the body. Table 3.5 shows the radiation weighting for different types of radiation. The radiation weighting factors are specific to a radiation and depend on the ionizing capacity and density of radiation types.

The new terms effective dose and the tissue weighting factor (W_T) are introduced. Thus, the equivalent dose is defined as the sum of equivalent doses weighted by tissue weighting factors for each tissue as given by the following expression.

$$E(Sv) = \sum_T W_T \times H_T \qquad (3.23)$$

The effective dose considers the absorbed dose to all organs; the relative harm of the radiation and the sensitivity of each organ to radiation. Some tissue weighting factors for tissues and organs of the human body are shown in Table 3.6.

Table 3.5 Radiation weighting factor for different types of radiation (ICRP, 1991)

Type of radiation	Energy range	Weighting factor, W_R
Photons, electrons, positrons and muons	All energies	1
Neutrons	<10 KeV	5
	<10 KeV to 100 KeV	100
	>100 KeV to 2 MeV	20
	> 2 MeV to 20 MeV	10
	> 20 MeV	5
Protons	> 20 MeV	5

Alpha particles, fission fragments, non-relativistic heavy nuclei	20

Table 3.6 Tissue weighting factors (ICRP, 1991)

Tissue or organ	Tissue weighting factors, W_T
Gonads	0.20
Colon	0.12
Lung	0.12
Red bone marrow	0.12
Stomach	0.12
Bladder	0.12
Breast	0.05
Oesophagus	0.05
Liver	0.05
Thyroid	0.05
Skin	0.01
Bone surfaces	0.01
Remainder	0.05

3.7.2 Radiation protection and dose limits

The ICRP (1999) recommended that in order to reduce and avoid unnecessary radiation exposure, the doses must be kept as low as reasonably achievable (ALARA). Since stochastic effects are predicted for populations and not individuals, the ICRP Publication 60 stipulated the recommended dose limits both to the workers and members of the public and they are shown in the Table 3.7. The ICRP (1999) also made recommendations for radiation protection based on three principles and these are: Justification, optimization and dose limitation.

Dose limitation: individuals should be allowed to only receive exposure dose within the recommended limits. The dose constraints for occupational exposure for annual effective dose that the whole body is uniformly irradiated is set to 20 mSv averaged over a period of 5 years to limit the probability of non-deterministic effects and must not exceed 50 mSv in a single year.

Table 3.7 ICRP 60 Recommended effective dose limits (Santawamaitre, 2012)

Application	Dose limit	
	Occupational	Public
Whole body	20 mSv[a] per year, averaged over a period of 5 years[b]	1 mSv[a] in a year
Annual equivalent dose in;		
Lens of the eye	150 mSv	15 mSv
Skin	500 mSv	50 mSv
Hand and feet	500 mSv	-

[a] *To find the recommended limit in rem, 1 mSv = 0.1 rem*

[b] *Maximum dose in any single year do not exceed 50 mSv*

Similarly, the dose limit to members of the public is set in consideration of the critical group of the population which is the foetus and is 1 mSv per year. The reason is the children are the most vulnerable group of the population and hence the dose contracting has to be set at 1 mSv per year. The occupational equivalent dose limit due to deterministic effects of 500, 500 and 150 mSv per year were recommended for hands and feet, skin and lens of the eye respectively. The annual equivalent doses for members of the public are limited to 15 mSv for the lens of the eye and 50 mSv for the skin (Cember and Johnson, 2009; Martin etal., 2012). Since the irradiation of the body is not uniform, a term known as tissue weighting factors as shown in Table 3.4 for various organism was introduced to determine the detrimental effects that contribute to each individual organ due to differences in radiation sensitivities.

3.7.3 Assessment of absorbed dose (D)

The mean activity concentrations of ^{238}U, ^{232}Th and ^{40}K are converted into dose rate by applying factor 0.462, 0.604 and 0.0417 for radium, thorium and potassium respectively (Beretka & Matthew, 1985) as illustrated in equation 3.24

$$\mathrm{D} = (0.462\mathrm{C_U} + 0.604\mathrm{C_{Th}} + 0.0417\mathrm{C_K})\mathrm{nGy/h} \quad (3.24)$$

where, D is the absorbed dose rate in the outdoor air at 1.0 m above the ground (nGyh^{-1}), C_U, C_{Th} and C_K are the activity concentrations of ^{238}U, ^{232}Th and ^{40}K of soil samples in Bq.kg^{-1} respectively. Since absorbed dose is limited dose in the air and the dose received by the adult members of the public is taken into consideration and another term known as the annual effective dose equivalent is introduced (AEDE).

3.7.4 The annual effective dose equivalent (AEDE)

The annual effective dose equivalent (AEDE) received by a member of the public is calculated from the absorbed dose rate by applying dose conversion factor of 0.7 Sv.Gy^{1} and the outdoor occupancy factor 0.2 and an indoor occupancy factor of 0.8. It follows that the total annual effective dose (D_{tot}t) is the sum of effective indoor dose (D_{in}) and effective outdoor dose (D_{out}) and this illustrated by equations 3.25, 3.26 and 3.27 (Veiga et al., 2006).

$$D_{out}\,(mSv/y) = D_R \times DCF \times F_1 \times T \quad (3.25)$$

$$D_{in}\,(mSv/y) = D_R \times DCF \times F_2 \times T \quad (3.26)$$

$$D_{tot}\,(mSv/y) = D_{out} + D_{in} \quad (3.27)$$

where, D_R denotes the absorbed dose rate, F_1, the external outdoor occupancy factor 0.2, , F_2, the indoor occupancy factor 0.8. D_{out} , the effective out dose, and D_{in} the effective indoor dose, and T is the time which is equivalent to 8760 hours per year and DCF is the dose conversion factor of 0.7 Sv.Gyh^{-1}.

3.7.5 Radiation indices measurements

The measured activity concentrations of ^{238}U (^{226}Ra), ^{232}Th and ^{40}K were used to calculate radiation parameters and these are radium equivalent (Ra_{eq}), annual effective dose and excess lifetime cancer risk.

Radium equivalent (Ra_{eq})

Radium equivalent (Ra_{eq}) activity is used to assess the radiation hazards associated with materials containing ^{226}Ra, ^{232}Th and ^{40}K in Bq.kg^{-1} (UNSCEAR, 1982). It is well documented that these radionuclides emit gamma doses in differing amount of activities even when they are of the same amount in any material. The radium equivalent (Ra_{eq}) is calculated on the assumption that 370 Bq kg^{-1} of ^{226}Ra or 259 Bq kg^{-1} of ^{232}Th or 4810 Bq kg^{-1} of ^{40}K

produce the same gamma dose rate (Flores, Estrada, Suarez, Zerquera, & Pérez, 2008). The Ra_{eq} of the sample in Bq kg^{-1} was achieved using equation 3.28 (Ibrahiem, 1999).

$$\mathrm{Ra_{eq}} = \left(\frac{\mathrm{A_{Ra}}}{370} + \frac{\mathrm{A_{Th}}}{259} + \frac{\mathrm{A_K}}{4810}\right) \times 370 \tag{3.28}$$

where, $\mathrm{A_{Ra}}$, $\mathrm{A_{Th}}$ and $\mathrm{A_K}$ are the activity concentrations of ^{226}Ra, ^{232}Th and ^{40}K respectively. The radium equivalent is the most important reference standard for regulating safety standard on radiation protection for the public (Marr, 2012).

Hazard indices ($\mathbf{H_{ex}}$ and $\mathbf{H_{in}}$)

When radioactive materials decay, they produce either external radiation or internal radiation which results in the exposure of human being. The two indices that represent external and internal radiation hazards, are represented mathematically by equations 3.29 and 3.30 (Taskin, 2009).

$$\mathrm{H_{ex}} = \frac{\mathrm{A_U}}{370} + \frac{\mathrm{A_{Th}}}{259} + \frac{\mathrm{A_K}}{4810} \leq 1 \tag{3.29}$$

$$\mathrm{H_{in}} = \frac{\mathrm{A_U}}{185} + \frac{\mathrm{A_{Th}}}{259} + \frac{\mathrm{A_K}}{4810} \leq 1 \tag{3.30}$$

where, $\mathrm{A_U}$, $\mathrm{A_{Th}}$ and $\mathrm{A_K}$ are the radioactivity concentrations of ^{226}Ra, ^{232}Th and ^{40}K in Bq kg^{-1} of soil samples respectively. The value of this index must be less than unity for the radiation hazard to be neglible and this value corresponds to upper limit of $\mathrm{Ra_{eq}}$ of 370 Bq.kg^{-1} (Marr, 2012).

3.7.5 Excess lifetime cancer risk (ELCR)

This represent the chance of developing cancer over a lifetime at any given exposure level due to radiation. It is presented as a value representing the number of extra cancers expected in a population exposed to a carcinogen at a given dose, and this can be calculated by considering the life expectancy of a human being to be 70 years (Taskin, 2009) and is shown by equation 3.31.

$$\mathrm{ELCR} = \mathrm{AEDE} \times \mathrm{DL} \times \mathrm{RF} \tag{3.31}$$

where, AEDE = the annual effective Dose Equivalent, DL = the average duration of human life (estimated to be 70 years) and RF = the risk factor (Sv^{-1}), fatal cancer risk per sievert. For stochastic effects, which produce low background radiation, the ICRP 60 stipulates a value of 0.05 for the public exposure (Taskin, 2009).

3.8 Toxicological risk due toxic heavy metals

3.8.1 Risk assessment of toxic heavy metals

Human health risk assessment is used to determine the probability of non-carcinogenic and carcinogenic exposure after an incidental chemical exposure, and this usually follows a stratified demographic transition ranging from the most toxic and chemically sensitive group of the population-children to the less sensitive- adults. Exposure of human to heavy metals in urban soil is through three pathways: inhalation of resuspended atmospheric aerosols, dermal contact with the soil and ingestion through food or soil (Luo et al., 2012). The average daily intake (ADI) mg/kg-day for different pathways was calculated using equations 3.32, 3.33 and 3.34 described by USEPA (1989).

Ingestion of toxic heavy metals through soil

$$\mathrm{ADI}_{\mathrm{ingest}} = \frac{\mathrm{C}\times\mathrm{IR}_{\mathrm{ing}}\times\mathrm{EF}\times\mathrm{ED}}{\mathrm{BW}\times\mathrm{AT}} \times \mathrm{CF} \qquad (3.32)$$

where, $\mathrm{ADI}_{\mathrm{ingest}}$ mg/kg-day) is the average daily intake of heavy metal ingested from soil, C is the concentration of heavy metal in mg/kg for soil. $\mathrm{IR}_{\mathrm{ing}}$ (mg/day is the ingestion rate of soil (mg/kg), EF is the exposure frequency (days/year), ED is the exposure duration (years), BW is the average body weight (kg), AT is the averaging time of the dose (days) and CF is the conversion factor (1×10^{-6} kg/mg).

Inhalation of heavy metal via soil particulates

$$\mathrm{ADI}_{\mathrm{inhale}} = \frac{\mathrm{C}_{\mathrm{soil}}\times\mathrm{IR}_{\mathrm{inh}}\times\mathrm{EF}\times\mathrm{ED}}{\mathrm{PPEF}\times\mathrm{BW}\times\mathrm{AT}} \qquad (3.33)$$

where, $\mathrm{ADI}_{\mathrm{inhale}}$ is the average daily intake of heavy metal inhaled from soil (mg/kg-day), $\mathrm{C}_{\mathrm{soil}}$ is the concentration of heavy metal in for soil (mg/day). $\mathrm{IR}_{\mathrm{inh}}$ is the inhalation rate of soil

(m^3/day), EF is the exposure frequency (days/year), ED is the exposure duration (years), PPEF is the particulate emission factor (m^3/kg), BW is the average body weight (kg) and AT is the averaging time of the dose (days).

Dermal contact of soil

$$ADI_{dermal} = \frac{C_{soil} \times SA \times AF_{soil} ABS \times EF \times ED \times CF}{BW \times AT} \quad (3.34)$$

where, $\mathrm{ADI}_{\mathrm{dermal}}$ is the average daily intake of heavy metal through dermal contact from soil. C_{soil} is the concentration of heavy metal in soil (mg/kg), SA is the surface area of the skin that contacts the soil (cm^2), AF is the skin adherence factor for soil (mg/cm^2), ABS is the absorption factor (chemical specific), EF is the exposure frequency (days/year), ED is the duration of exposure (years), CF is the conversion factor (1×10^{-6} mg/kg), BW is the average body weight (kg) and AT is the averaging time (days) of the dose. The detailed description of exposure factors for children and adults used for the equation 3.32, 3.33 and 3.34 are given in Table 3.8 and Table 3.9.

3.8.2 Non- carcinogenic assessment of toxic heavy metals

The cumulative non-carcinogenic risk of heavy metals for members of the public are calculated based on the reference doses (RfD) and average daily intake for different samples.

Table 3.8 Values of exposure factors for heavy metals doses for children and adults

Factor	Description	Unit	Value		References
			Children	Adults	
C	Concentration of metal	mg/kg			Present study
BW	Body Weight	kg	15	70	(DEA, 2010; USEPA, 2001)
EF	Exposure frequency	days/year	350	350	(Peng et al., 2011)
ED	Exposure duration	years	6	30	(USEPA, 2002; DEA, 2010)
IRing	Ingestion rate of soil	mg/day	200	100	(ESAG, 2009; DEA, 2010)
IR_{inh}	Inhalation rate of PM	m^3/day	7.63	12.8	(Li et al, 2011, USEPA, 2002)
SA	Skin surface area	cm^2	1600	4350	(Zheng et al., 2010)
AF	Skin adherence factor	mg/cm^2	0.2	0.7	(Man et al., 2010)
FE	Dermal exposure ratio(soil)	unitless	0.001	0.001	(Wei et al., 2015)
PEF	Particulate emission (soil)	m^3/kg	1.36×10^9	1.36×10^9	(USEPA, 2002; DEA, 2010)
AT	Average Time	days			
	For carcinogens		365 x ED	365x70	(DEA, 2010)
	For non-carcinogens		365 x ED	365 x ED	(DEA, 2010)

Table 3.9 Reference doses (RfD) in mg/kg-day) and cancer slope factors (CSF) for the different heavy metals (Luo et, 2012; USEPA, 2002; DEA, 2010; USEPA, 2011a; USEPA, 1991; Ali et al, 2017; USEPA, 2001; USEPA, 1993; USEPA, 2010)

Risk	Heavy Metal								
	Fe	Mn	Zn	Pb	Cd	Ni	As	Cr	Cu
Ingestion (RfD)	8.40E+00	4.70E-02	3.00E-01	3.50E-03	1.00E-03	2.00E-02	3.00E-04	3.00E-03	4.00E-02
Inhalation (RfD)	2.20E-04	1.43E-05	3.00E-01	3.52E-04	1.00E-03	2.06E-02	3.01E-04	2.86E-05	4.02E-02
Dermal (RfD)	7.00E-02	1.84E-03	6.00E-02	5.25E-04	1.00E-05	5.40E-03	1.23E-04	5.00E-05	1.20E-04
Ingestion (CSF)	-	-	-	4.20E+01	-	-	1.50E+00	4.10E- 02	-
Inhalation (CSF)	-	-	-	4.20E-02	6.30E+00	-	1.51E-01	4.20E-01	-
Dermal (CSF)	-	-	-	-	-	-	1.50E+00	-	-

and these are expressed in terms of hazard quotient (HQ) and hazard Index (HI) for the different pathways (inhalation, contact and ingestion).

Hazard quotient (HQ)

Hazard quotient (HQ) is the fraction of the probable exposure to an element/ chemical level at which no negative impacts are expected. When the HQ is less than one, this means that no potential health risk are expected but when the value is more than one, it signifies that there are potential health risks due to exposure (Bermudez et al., 2011)

Hazard index (HI)

The cumulative non-carcinogenic risk, known as the hazard index (HI) is an important index that assesses the overall likely impacts that can be posed by exposure to more than one contaminant and is equal to the sum of hazard quotient (HQ) and this is illustrated by the equation 3.35.

$$\mathrm{HI} = \sum_{i=1}^{5} \mathrm{HQ} = \mathrm{HQ_{ing}} + \mathrm{HQ_{Inh}} + \mathrm{HQ_{dermal}} \quad (3.35)$$

If the value of HI is more than 1, this suggest that there is significant health risk that can results from consuming pollutants in the soil or foodstuffs (USEPA, 2002). However, if HI is less than one, it is believed that there is no significant risk of non-carcinogenic effects.
HQ is calculated as fraction of determined dose to the reference dose as illustrated in equation 3.36:

$$\mathrm{HQ\ for\ non-carcinogenic\ risk} = \frac{\mathrm{ADI}}{\mathrm{R_fD}} \quad (3.36)$$

where, ADI is the average foodstuff intake per day (mg/kg/day) and $R_f D$ is the oral reference dose of the heavy metal (mg/kg/day) and this is conservatively limited to the tolerable exposure through which an individual can sustain without any harmful effects during a lifespan. $R_f D$ is an estimation of the maximum permissible risk to human population through daily exposure by considering the sensitive group (children) during a lifetime (Ali et al., 2017).

3.8.3 Carcinogenic risk assessment of heavy metals

The carcinogenic risk represents the incremental probability of an individual developing cancer over a lifetime as a result of total exposure to the potential carcinogen and is mathematically expressed by the lifetime cancer risk equation 3.38.

$$\mathrm{Risk} = \mathrm{ADI\ x\ CSF} \quad (3.38)$$

where, “Risk” is a chance of an individual developing cancer over a lifetime and it is unitless, ADI is the average daily intake, or the dose and CSF is the cancer slope factor expressed as

(mg.kg/day). By extrapolating the cancer slope factor, the estimated daily intake of heavy metals. averaged over lifetime of exposure is converted directly to incremental risk of an individual developing cancer (USEPA, 1989). The total lifetime cancer risk (LCR) for an individual is expressed as the sum of the average contribution of individual heavy metal in the different matrix for all the pathways by applying equation 3.39.

$$\mathrm{Risk}_{(\mathrm{total})} = \mathrm{Risk}_{(\mathrm{ing})} + \mathrm{Risk}_{(\mathrm{inh})} + \mathrm{Risk}_{(\mathrm{dermal})} \quad (3.39)$$

where, $Risk_{(ing)}$, $Risk_{(inh)}$ and $Risk_{(dermal)}$ are risk contributions through different matrix i.e. soil, dust, water. Similarly, if the number of heavy metals are increased to n, for a given pathway, then the equation can be expressed as:

$$\mathrm{Risk}_{(\mathrm{pathway})} = \sum_{\mathrm{k}=1}^{\mathrm{n}} \mathrm{ADI}_{\mathrm{k}} \mathrm{CSF}_{\mathrm{k}} \quad (3.40)$$

where, ADI_k and CSF_k are the ADI and CSF for the k^{th} heavy metal. It should be noted that in this study, the assessment of health risk due to heavy metals exposure, the default reference values doses (RfD) for non-carcinogenic risk assessment and the cancer slope factor (CSF) for carcinogenic is given in Table 3.9.

CHAPTER 4 : RESULTS AND DISCUSSION

4.1 Introduction

This chapter presents and discusses the distribution of radionuclides and toxic heavy metals in PM and soil in the area under study. Furthermore, the morphological characteristic of particulate matter (PM) and the relationship between particle size and its respiratory deposition were explored. Finally, radiological and toxicological health risk due to exposure to toxic heavy metals and radionuclides were evaluated to determine the potential health risk posed to the inhabitants of these two towns. The results from this study was compared with studies conducted in other countries and the worldwide values.

4.1.2 Radioactivity in PM and soil in the Erongo region

4.1.2.1 Radioactivity in particulate matter (PM)

The activity concentrations (Bq.kg^{-1}) of ^{226}Ra, ^{238}U, ^{232}Th, ^{40}K and ^{210}Pb in PM samples collected in the residential areas in the town of Karibib and Arandis was measured by a γ – ray spectrometer and the results are presented in Figure 4.1. Detailed information about the distribution of radionuclides in the study area are given in Appendix A. As can be seen in Figure 4.1, the activity concentrations of ^{226}Ra, ^{238}U, ^{232}Th, ^{40}K and ^{210}Pb in the study area vary from 39.92±0.40 to 177.39±2.21 Bq.kg^{-1}, 19.00±0.73, to 107.91±10.78 Bq.kg^{-1}, 24.22±0.24 to 143.48± 3.96 Bq.kg$^{-1,}$ 304.00±3.69 to 1100.00±49.56 Bq.kg^{-1} and 10.38±1.19 to 120.00±20.64 Bq.kg^{-1} with mean of 81.24±1.00 Bq.kg^{-1}, 57.99±2.61, 72.10±1.67, 682.00±19.81 and 55.10±6.14 Bq.kg^{-1}, respectively. The mean activity concentrations values obtained were twice higher than the worldwide values of 33, 45 and 412 Bq/kg for ^{238}U, ^{232}Th and ^{40}K respectively. The observed results are comparable with earlier reports conducted in soil within the sample locale and elsewhere (Ademola et al., 2014; Onjefu et al., 2016). The highest activity concentrations of ^{238}U, ^{226}Ra and ^{210}Pb was found in the town of Arandis at site APM15 (107.91±10.78 Bq.kg^{-1}), APM13 (177.39±2.21 Bq.kg^{-1}) and APM24 (120.00±20.64 Bq.kg^{-1}), respectively. These sites are closer to Rössing uranium mine and high PM containing these NORM is generated from the mining activities and discharged into the nearby communities. The sites are also located in the downwind direction. High activity concentrations of ^{238}U can be also be attributed to the presence of uranium bearing ores which is common in the area while elevated levels of ^{226}Ra is due to its geochemical

speciation in the environment. However, the concentration of potassium is always high in environmental samples due to its isotopic natural abundance in the environment. Similarly, high activity concentrations of ^{232}Th and ^{40}K was found in the town of Karibib at site KPM9 (143.48± 3.96 Bq.kg^{-1}) and KPM4 (1100.00±49.56 Bq.kg^{-1}) and these sites are located in the proximity to a small-scale granite quarry mine which generate excess insoluble particulate matter from blasting and crushing of granite rocks. Granite are known to contain elevated levels of radionuclides which are inherently present during its formation.

Previous studies have shown that radioactivity is related to grain size. i.e. soil radioactivity is inversely proportional to sand content and directly proportional to clay content Several authors have reported that radioactivity concentrations in different soil aggregates is inversely proportional to the average grain size, sand and clay content (Santawamaitre et al., 2011; Hebinck et al., 2007). This proposition was asserted by Narayana & Rajashekara, 2010 who argued that radionuclides within the grain structure and grain boundaries can be more adsorbed in the fine grain than in the coarse grain. Furthermore, the activity concentrations for ^{238}U and ^{232}Th is also affected by the amount of clay and sand (Narayana & Rajashekara, 2010; Radhakrishna et al., 1993). A closer look at the radioactivity in PM and soils sample collected from the same sites revealed that the ^{238}U and ^{232}Th activity concentrations in PM was higher than the corresponding soil samples in most sites. The increase in activity concentrations in PM may be attributed to the grain size, fraction of sand and clay content and the contribution of mining activities which releases some radioactive fine particulate matter into the surrounding communities

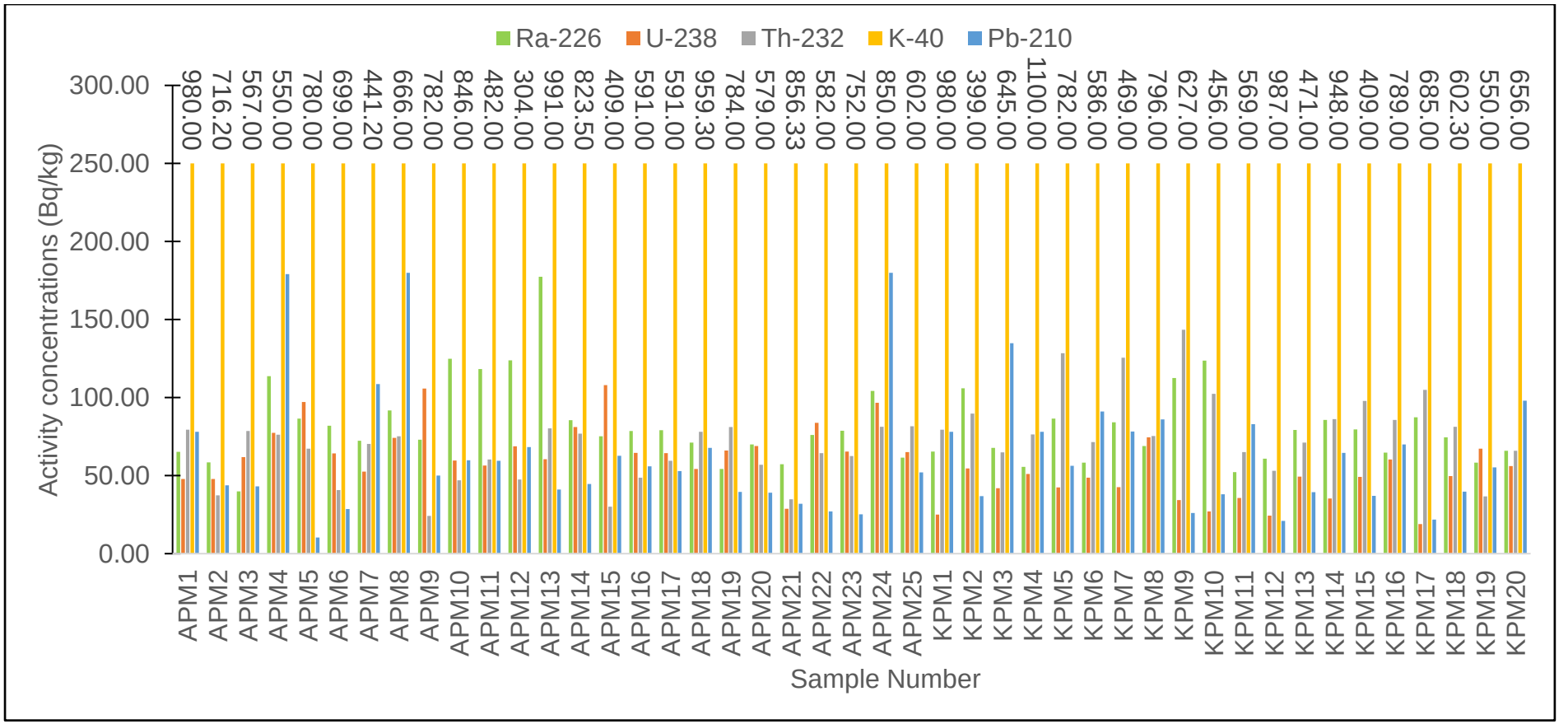

Figure 4.1 The distribution of NORM in PM from the study area

4.1.2.2 Radioactivity in soil

The measured NORM concentrations in soil from the study area are presented in Figure 4.2. Detailed information about activity concentrations are illustrated in the appendix. The data in Figure 4.2 shows the radioactivity concentrations of ^{226}Ra, ^{238}U, ^{232}Th, ^{40}K and ^{210}Pb were found to be 66.41$\pm$1.77 Bq.kg^{-1} 52.79$\pm$3.43 Bq.kg^{-1}, 71.30$\pm$2.44 Bq.kg^{-1} 780.96$\pm$18.26 Bq.kg^{-1} and 71.50$\pm$5.99 Bq.kg^{-1} respectively. Although pure ^{238}U and ^{232}Th are classified as radiotoxic, their contribution to the doses is so low due to their long half-lives. The main radiological concern emanating from these radionuclides comes from doses associated with their daughter products. For example, in ^{238}U, the key contribution comes from ^{226}Ra and its decay products which are ^{210}Pb and ^{210}Po while in ^{232}Th, it comes from the decay products of ^{212}Pb and ^{214}Bi. The obtained average activity concentration of ^{226}Ra, ^{238}U, ^{232}Th and ^{40}K in the collected soil samples from the study area were twice the world wide average values and some parts of Africa which are 33, 32, 45 and 500 Bq.kg^{-1} respectively (Sahin and Cavas, 2008; UNSCEAR, 2008). The mean activity concentrations of ^{210}Pb was higher than the mean activity concentrations of ^{226}Ra in the measured samples and this can be partly explained in terms of geochemical speciation of Pb and partly due to the chemical behaviour of ^{226}Ra. It is believed that atmospheric deposition of Pb produced by decay of ^{222}Rn and becomes aerosol occurs through wet and dry deposition and as such higher concentrations of lead Pb remain locked up in the particulate matter (Kariuki, 2018). Another reason may be pointed out to the leaching of Pb by rainwater through ^{226}Ra since ^{226}Ra is water labile and this may result in enrichment of the parent material with ^{210}Pb relative to ^{226}Ra in the soil. Pb may eventually decays to ^{210}Po and these two can attain secular equilibrium (Sheppard et al., 2008).

It can be observed that sample KS16 and KS5 have a higher activity concentration of 108.20$\pm$12.73 Bq.kg^{-1} and 157.8$\pm$5.20 Bq.kg^{-1} for ^{238}U and ^{232}Th respectively. This can be attributed to the fact that these sites are in the vicinity of a granite milling plant. Granite rocks are known to have high concentrations of uranium and thorium (AlausaShamsideen, 2014; Yang et al., 2005). Some ores of uranium and thorium were slowly in cooperated into the structure of the rocks during crystallization. The soil samples have a higher concentration of potassium-40 with an average value of 1058.00$\pm$42.00Bq.kg^{-1} and this is may be due to geological underlying rocks which are mainly composed of metasedimentary and

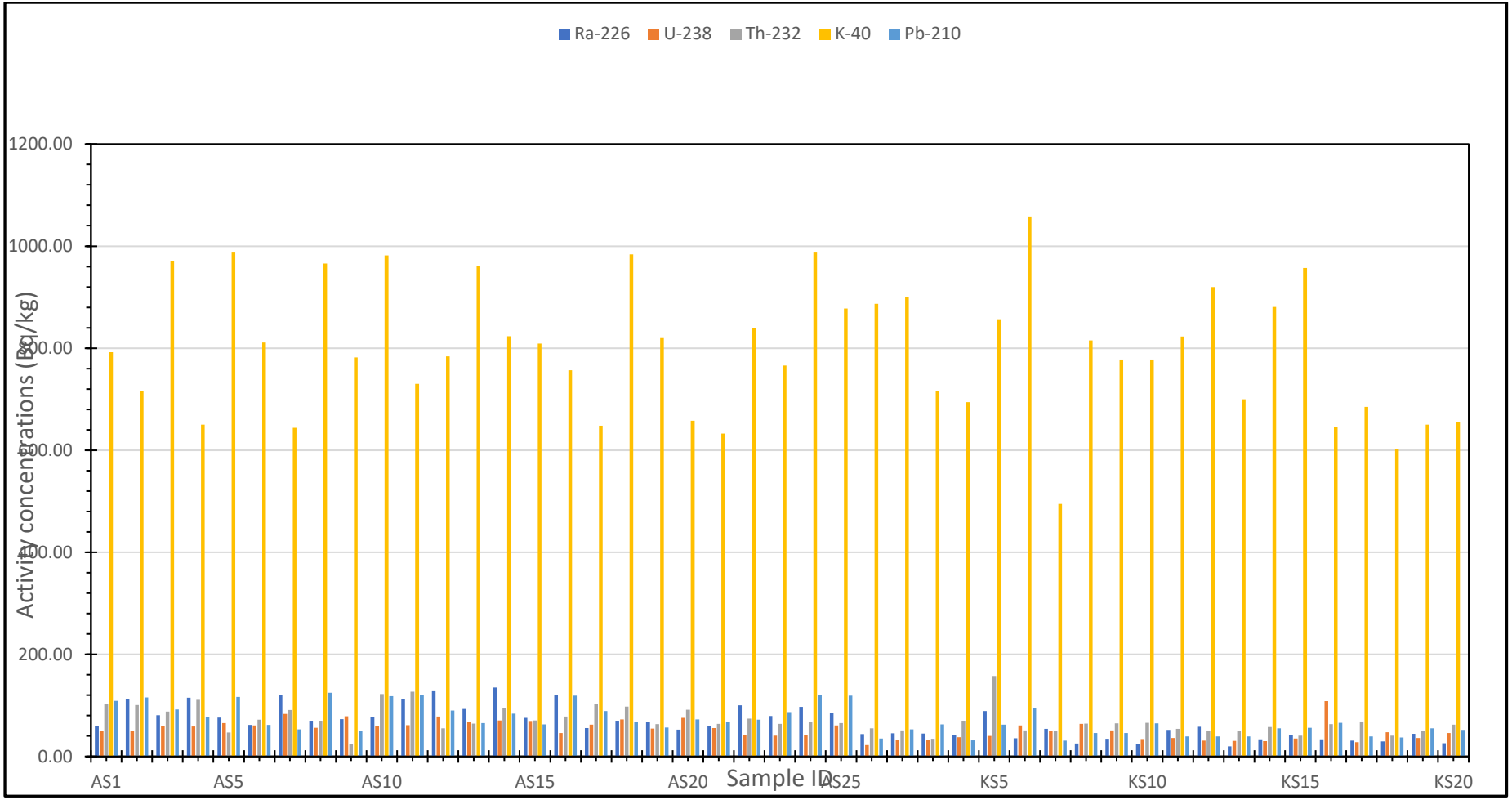

Figure 4.2 Activity concentrations of NORM in soil from the two towns of Arandis and Karibib

metavolcanics rocks with metamophosed equivalent of fluviates quartzites, limestones, marls, turbidites and shales (Brandit, 1987; Groves et al., 1990).

The long-term exposure to uranium and thorium decay series, through inhalation pathway has been linked to adverse health effects such as chronic lung diseases, acute leucopoenia, anaemia and necrosis of the mouth (ASTD, 1990). Exposure to radium has been found to cause bone, cranial and nasal tumours while exposure to thorium can cause respiratory and kidney cancer (ATSDR, 1992). It is therefore imperative that the gamma dose rate and activity concentrations should be monitored particularly in areas that are rich in uranium and thorium.

A comparison of the activity concentrations in the town of Arandis and the town of Karibib shows that the activity concentrations in Arandis are higher than in Karibib which implies that there are higher chances of cancer developing cancer due to radiation exposure from primordial radionuclides in this town. The high values of activity concentrations can be attributed to the uranium bearing ores that are found in the Erongo region. In addition, Arandis is dormitory town of Rössing uranium mine (RUM), the world fourth largest producer of uranium and it is only 10 km away from the mine. Anthropogenic activities such as mineral mining and processing may lead to the emission of particulate matter containing radioactive dust which can be blown away to the nearby community leading to an increase in natural radioactivity (Friedrich, 2009). The transport of radionuclides in the environment is governed by the chemical behaviour and its physicochemical characteristics. For example, uranium is water labile and can easily dissolve in water, where it can be attached to clay minerals and transported as particulate matter while thorium does not dissolve easily.

It is a common practice that in the measurement of radionuclides in the natural decay series, the activity of a parent radionuclide is often estimated from its daughters and vice versa (El-Daoushy & Hernández, 2002; Huy & Luyen, 2004) and this is based on the assumption that equilibrium conditions have been reached i.e. the activity concentrations of the parent and the progeny are equal in secular equilibrium and this was confirmed by determining the activity ratios of the progeny in each series of uranium, actinium and thorium which was found to be closer to one.

4.1.2.3 Comparison of radioactivity in soil in the town of Karibib, Arandis and other similar studies in the world

A comparative analysis of the distribution of radionuclides in Erongo region has shown that the town of Arandis has a higher activity concentration for all radionuclides than the town of Karibib. As can be deduced from the Table 4.1, activity concentrations of ^{238}U is two times higher while ^{232}Th is one and half times higher in Arandis town than in Karibib town and this difference can be attributed to the geological underlying rocks, the type of mineral exploited, the magnitude of mining operations, prevailing climatic conditions such as weather, wind speed and direction relative to the position and latitude. The geology of Karibib town is composed of metasedimentary and metavolcanics rocks which are rich in ^{40}K while and Arandis town is geology is impregnated with uranium bearing ores. Most parts of the bedrock in Erongo region is composed of granite rocks which are known to have high levels of ^{238}U, ^{232}Th and ^{40}K. The results from this study are comparable to worldwide values and values from other countries as illustrated in Table 4.1.

Radioactivity concentrations may differ from place to place due to difference in geochemical processes such as weathering (Verdoya et al, 2001). It is well documented that the concentration ratios of radionuclides in the environment is maintained at a steady state but any variation from the norm may be an indication of enrichment or depletion. The presence of uranium and thorium bearing minerals in the soils have led to an increase in natural background in some locale. The higher thorium content observed in this study can be as a result of the present of monazite sand soils deposits and these results are comparable to the Brazilian Guarapari locale (Aya ,2016) which experience higher background radiation. The results of this study are compared with the reported values of other locations conducted worldwide as shown in Table 4.4. While it is documented that some parts of the world such as Yangiang in China, Kerala and Madras in India, Ramsar in Iran are known to experience high background radiation (Lauria et al., 2002; Wang et al.,1990; Das et al,, 2009; Sohrabi et al., 2013), it should be noted that there is no data to link this background radiation with cancer incidence in those locales. However, there has been an increased frequency of chromosome distortion which is consistence with those seen in radiation workers and individuals exposed to high levels of doses.

Table 4.1 Comparison of the mean radionuclide concentrations (Bq.kg^{-1}) from studies conducted in other countries and results obtained in this study

Country/Region	Activity concentrations (Bq.kg^{-1})			References
	^{238}U	^{232}Th	^{40}K	
Amman, Jordan	56.4	28.8	501	Ahmed et al.,1997
Taiwan	54.0	32.4	794	Chen et al.,1993
Taiwan	30.0	44.0	431	Lin et al.,1987
Istanbul, Turkey	21.0	37.0	342	Karahn and Bayulken, 2000
Agaba-Amman	44.4	36.3	208	Al-Jundi et al., 2003
Akure, Nigeria	25.43	27.45	1015.96	Olumayede, 2016
Obajana, Nigeria	331	31.00	2189	Ajayi et al., 1999
El-Minya, Egypt	25.3	37.0	82.00	Shittu et al., 2014
Germany	ND	70	1465	Ahmed et al., 2006
Arandis, Namibia	72.4	245.7	899.7	Oyedele et al., 2010
World-wide	33	45	412	UNSCEAR, 2010
Arandis, Namibia	**63.28**	**84.77**	**785.82**	**This study**
Karibib, Namibia	**39.50**	**54.41**	**774.88**	**This study**

4.2 Indoor radon concentration in households near mining sites

4.2.1 Indoor radon concentrations in the two towns of Karibib and Arandis

Measurements of indoor radon concentrations and its progeny were made in 45 dwellings in the towns of Karibib and Arandis for a period of 3 months. These dwellings are single floor apartments, free standing houses and semi-detached houses constructed of concrete, sand, and cement bricks and the roofs are at a height of 2.5 -3.5 m above ground. The results for indoor radon concentration (C_{Rn}), effective dose from inhalation of radon and its progeny H (mSv/y) are presented in Figure 4.3 and Appendix A. The range of indoor radon concentrations varies from 71 to 98.90 to 100 Bq/m^3 with a mean of 88 Bq/m^3 which translate to an annual effective dose of 1.79 to 2.51 mSv/year and a mean of 2.22 mSv/year.

The obtained values are lower than the ICRP (1993) radon action levels of (between 200 and 300 Bq/m^3) while the mean value is about two times higher than the world average of 39 Bq/m^3 (UNSCEAR, 2000). The variation of indoor radon concentration in different dwellings is due to a variety of living style, seasonal variation, different ventilation conditions, the nature and type of building materials used during construction and the difference in radioactivity content of the soil beneath the dwelling. Figure 4.3 shows that radon concentration in all the measured dwellings were comparable to the WHO (2000) action level of 100 Bq/m^3 and these values are 3 times lower than the action level of 300 Bq/m^3 prescribed by ICRP (1993). The higher indoor radon concentrations in the dwellings could be due the geology of the rocks beneath the surfaces which are rich in uranium bearing ores.

Previous studies of soil radioactivity in Erongo region has revealed that the area experiences high background radiation due uranium bearing ores. Arandis town is a dormitory town of Rössing Uranium Mine and some of the radon may be originating from anthropogenic activities such as mining. The radon may be dispersed from the mine by wind to the surrounding residential places leading to an increased indoor radon concentration in those dwellings. Figure 4.3 illustrates the distribution of indoor radon in the selected households in the two towns of Karibib and Arandis. As observed in Figure 4.3, it can be deduced that the selected houses in Arandis have a higher randon concentrations than the houses in Karibib and these can be linked to the difference in the underlying geology and the type building material. The high concentration of indoor radon and its progeny can be attributed to thoron rich building materials derived mainly from granitic and felsite rocks which are used as a raw material for the construction of these dwellings.

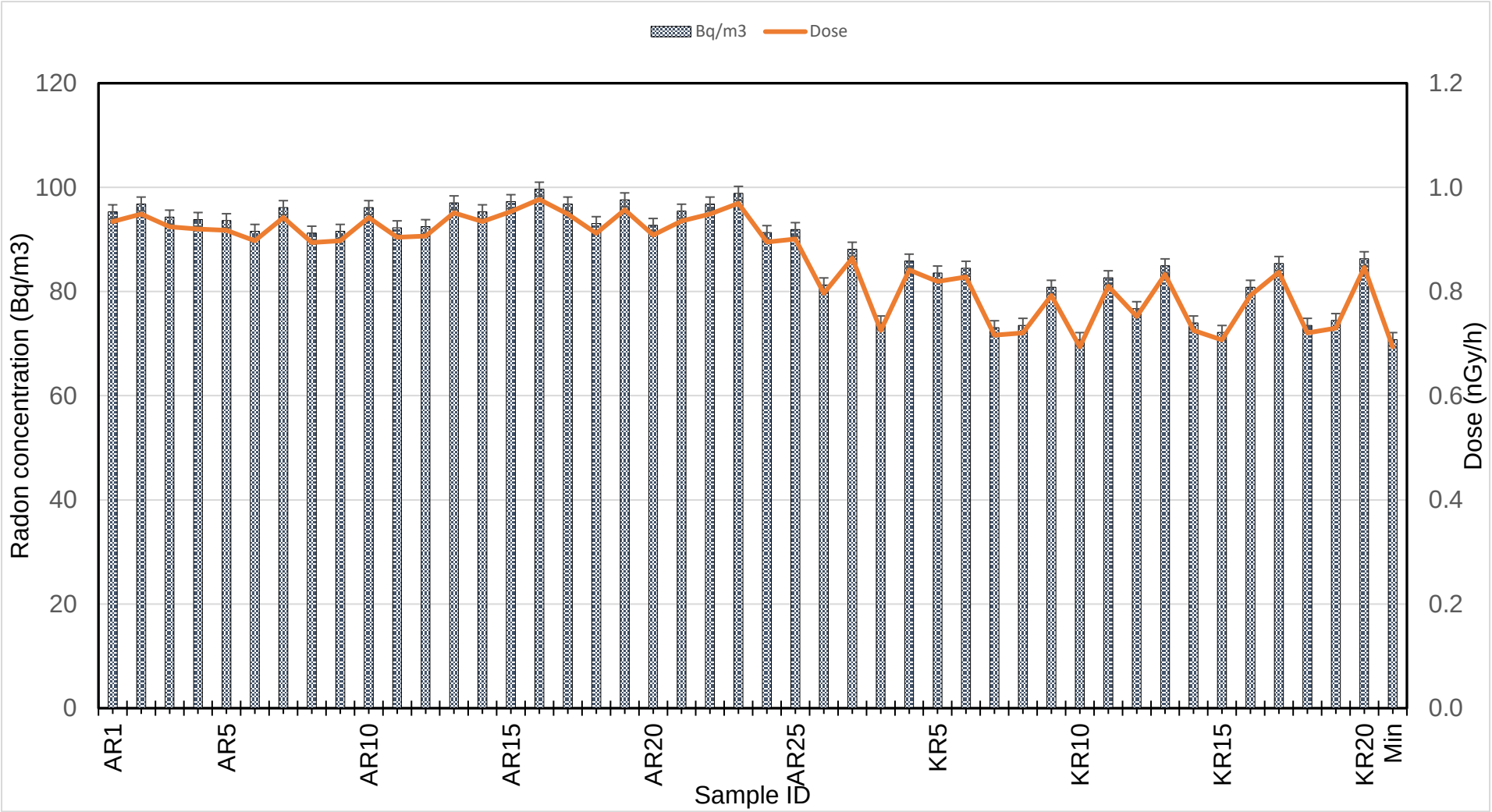

Figure 4.3 Indoor radon concentrations in some selected households in the study area

Radon can make its way through joints and cracks in buildings leading to an increase in indoor radon concentration. It has been noted that houses built of bricks and cement have low levels of uranium which imply that the radon concentration will be low. Furthermore, a low indoor radon can be due to the use of cement in the construction which makes a permanent natural barrier that prevent the easy entry of radon from underground into the building. the indoor radon concentration in the selected dwelling is fairly constant over a large area which imply that the underlying rock is homogenous. The radon flux density i.e. the ^{222}Rn exhalation rate is stochastic and it is governed by a number of parameters such as the radioactive decay of ^{226}Ra, the direction of recoil of radon in the grain, the intestinal soil moisture condition in the vicinity of the ejected radon atom and its diffusion. in the pore atom (Lawrence et al, 2009).

A number of authors have reported that the radon concentration in buildings obeys a log-normal distribution (Cosma et al., 2013); Epstein et al., 2014; Celebi et al., 2014, Bollhofer et al., 2006). If Figure 4.3 is to be extrapolated to produce a Gaussian curve, it is clear that the radon concentration in the selected buildings do not follow a normal distribution as it has a flat top. This lack of normal distribution from the measured data can be attributed to the fact that the measured buildings are not the same in terms of structure, size, age and the type of ventilation. In addition, the concentration of radon is affected by the prevailing meteorological conditions and these include humidity, temperature and wind speed.

The results from this study are agreement with earlier report obtained by Orton Von (2008), which confirms that some parts of Erongo region have high level of natural background radiation. The natural background radiation in Erongo region is 2.4 mSv/year. The mean annual effective dose in the town of Arandis is within the world-wide value of 1.0 mSv/year (UNSCEAR, 2000), however, the value is below the recommended ICRP limit which is 3-10 mSv/year, which implies there are low chances of cancer risk to the population due to inhalation of radon and its progeny. Based on the results of this study, the mean excess lifetime cancer risk is 1.56% which is substantially closer to the EPA action level of 1.43 % which corresponds to the upper boundary of 148 Bq/m^3 for enclosed places.

4.2.4 Comparison of mean indoor radon levels, annual effective dose and excess lifetime cancer risk in the towns of Karibib and Arandis and other countries.

Table 4.2 illustrates the mean indoor radon concentrations, annual effective dose and excess lifetime cancer risk reported in other countries. It can be observed that the measured indoor radon concentrations in the selected dwellings in the towns of Arandis and Karibib are

higher than those of the selected countries except India (132.84 Bq/m^3) and Nigeria (257 Bq/m^3).

Table 4.2 The comparison of mean radon concentrations (CRn), annual effective dose (H) and Excess cancer risk (ELCR) in some parts of the world.

Place Country	C_{Rn} (Bq/m^3)	H_E (mSv/y)	ELCR (%)	Reference
India	132.84	2.27	0.18	Mehra and Badhan, 2012
India	60.57	1.15	0.89	Verma and Khan, 2013
UK	20	-	-	Wrixon et al., 1988
Sudan	49	1.3	1.04	EL Zain, 2014
Jordan	39	0.99	-	Mahammad and Abumurad, 2008
Jordan	36.3	0.92	-	Al-Khateeb et al., 2012
Nigeria	257	6.5	-	Obed et al., 2012
Egypt	46	1.74	0.68	Amin, 2014
Pakistan	82	2.06	-	Rafique et al., 2012
Saudi Arabia	36	0.61	0.47	Farid, 2014
Saudi Arabia	30.80	0.79	0.44	Nazaroff, 1987
Namibia (Karibib)	79.30	2.00	1.31	Present study
Namibia (Arandis)	98.90	2.39	1.56	Present study

However, the indoor radon concentrations values from the towns of Arandis and Karibib compares well with the values from Pakistan (82 Bq/m^3). Similarly, a comparison of the indoor radon concentrations between the two towns of Arandis and Karibib shows that the Arandis town has slightly higher indoor radon concentration and this can be attributed to the differences in geological underlying rocks and the prevailing climatic conditions. The annual effective dose received by the residents of the two towns of Arandis and Karibib are less than the lower limit action level (3 -10 mSv).

The ELCR due to radon and its progeny is within acceptable limits and does not pose any serious threats to the occupants. Consequently, the development of lung cancer due to exposure to indoor radon and its progeny in these dwellings can be considered safe.

4.3 External radiological risk due to NORM

4.3.1 Radiological parameters in soil

The measured activity concentrations of ^{238}U, ^{232}Th and ^{40}K were converted into absorbed dose (D), annual effective doses equivalent (AEDE), radium equivalent (Ra_{eq}) external hazard index (H_{ex}) and excess lifetime cancer risk (ELCR) by applying equations 3.21, 3.27, 3.28, 3.29 and 3.31 respectively and the results are shown in Figure 4.4, 4.5, 4.6 and 4.7 and 4.8. Detailed information is also given in Appendix A. The measured outdoor terrestial dose rate from the soil samples collected in the study area varied from 65.95 to 149.94 nGyh^{-1} with a mean of 113.44 nGy/h and 83.66 nGy for the town of Arandis and Karibib respectively.

The obtained mean values of absorbed dose rate for both towns is about two times higher than the world value of 59 nGyh^{-1} while the measured values for the range are comparable to the world values (UNSCEAR, 2000) . The highest value of absorbed dose rate (D) of 149.94 nGyh^{-1} was found at site KS5 in Karibib town. This elevated level of absorbed dose rate in the air is due to the activity concentrations of ^{40}K which is abundantly present in the area. As can be deduced from the frequency distribution curve in Figure 4.4, the highest frequency for the absorbed dose rate is in the range of 81-90 nGyh^{-1}. The mean absorbed dose rate for all the collected samples is higher than the reported world-wide average values of 59 nGyh^{-1} (UNSCEAR 2000; Shimboyo et al., 2016). According to Radhakrishna et al., (1993), the variation in the doses is partly due to activity concentrations of radionuclides which is also dependent on the local geology and hence the soil type. It is important to estimate the external exposure to gamma-ray radiation to establish the base line of any given locale.

The International Commission on Radiation Protection (ICRP) has set a conservative annual effective dose equivalent (AEDE) limit of 1 mSvyr^{-1} for members of the public. This value was set after considering the most sensitive group of the population which is children. The calculated AEDE in soil from the study area varies from 0.40 to 0.92 mSvyr^{-1} and a mean of 0.70 mSvyr^{-1} and 0.51 mSvyr^{-1} for the town of Arandis and Karibib respectively and this is presented in Appendix A and Figure 4.5. The mean AEDE for Arandis is slightly higher than the AEDE for Karibib because of differences in geology and latitude.

The obtained mean values of AEDE in this study is higher than the average world value of 0.48 mSvyr^{-1}. Figure 4.5 shows a frequency distribution of AEDE mSv/yr in soil from

the study area. The highest frequency distribution was found in the range of 0.51-0.60 mSv/yr and the least was found in the range of 0.61-70 mSv/yr.

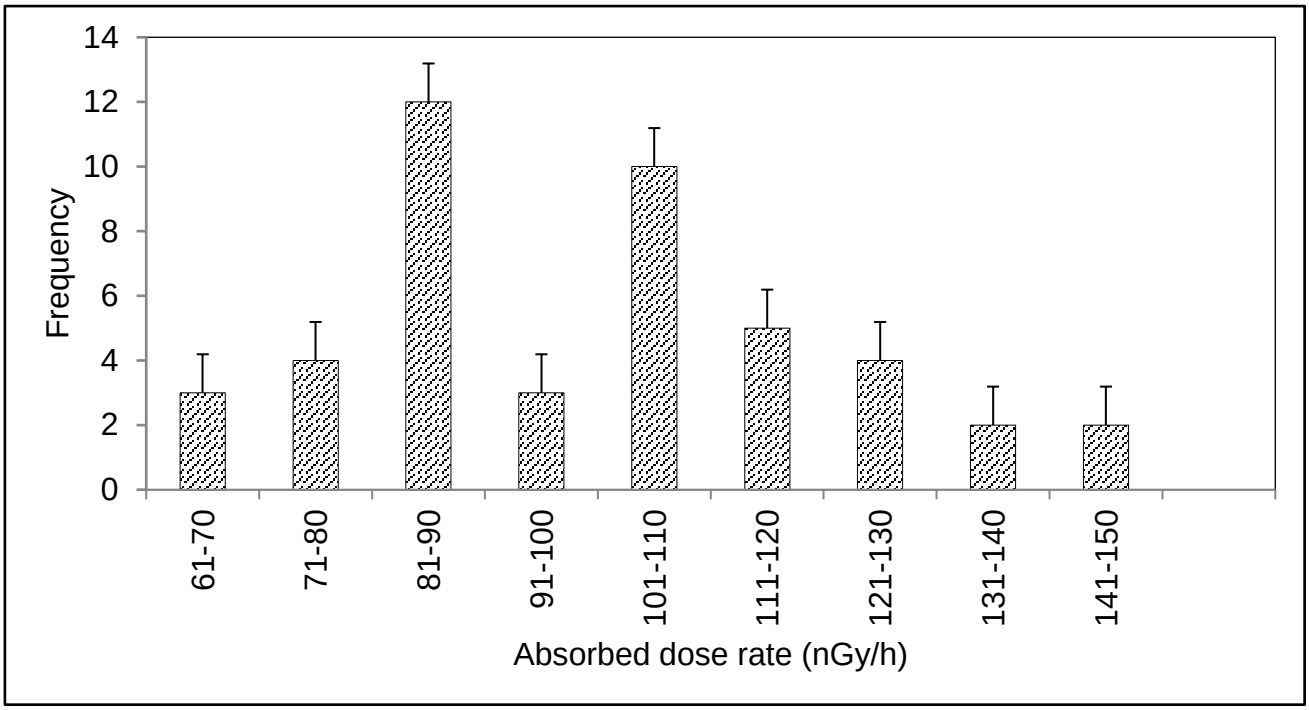

Figure 4.4 The frequency distribution of absorbed dose rate (D) in the town of Karibib and Arandis

As can observed in Figure 4.5, in all the measured soil samples the AEDE values in the two towns are less than the safe limit of 1 mSv/yr prescribed by International Commission on Radiation Protection (ICRP) which implies that the soils do not pose any radiological hazard to the inhabitants of the area.

However, it has been reported that that there is no amount of radiation doses that is safe even low doses of radiation exposure due to terrestrial radiation sources can induce chromosome aberrations which can culminate in cancer so reasonable precautions must be taken to protect the public from radiation exposure (Watson et al, 2008). The results are comparable with earlier reports by Onjefu et al., (2016), Oyedele et al.,(2010), however, they not in agreement with an earlier study by von Oertzen (2008) who reported the Erongo region as a high background radiation place. Similarly, the results for calculated radium equivalent activity concentrations (Ra_{eq}) in Bq.kg^{-1} for soil samples in the study are presented in Figure 4.6.

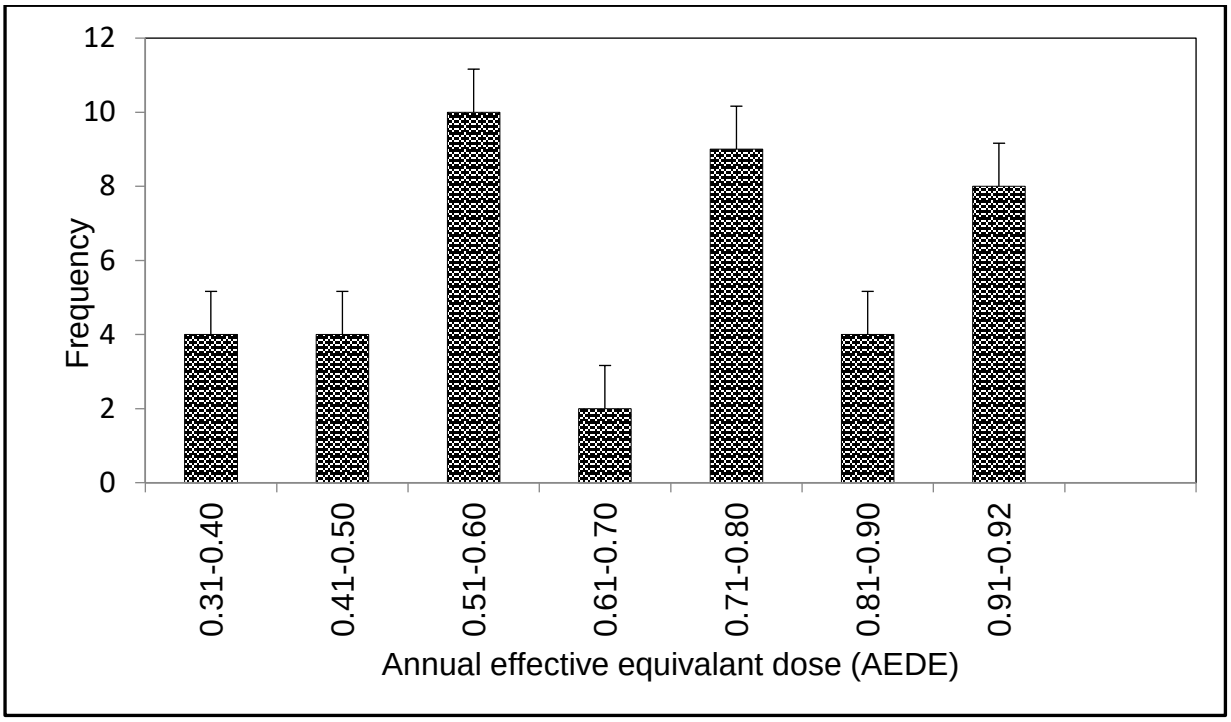

Figure 4.5 Frequency distribution for the annual effective dose equivalent (AEDE) in soil from the town of Arandis and Karibib

As can be seen in Figure 4.6, the Raeq activity concentrations in the study area in exhibit a normal distribution curve with maximum frequency appearing in 201-220 Bq.kg^{-1} range and low frequency in 321-340 Bq.kg^{-1}. Since the Raeq results in all the soil samples from the study area are less than the maximum value of 370 Bq kg^{-1} which correspond to 1 mSv/yr, the radiological safe limit established by UNSCEAR (1988), this can imply that the soils are not radiologically hazard.

In order to assess the health effects on human population due to exposure to ionising radiation due the activities of ^{238}U, ^{232}Th and ^{40}K it is important to consider external radiation sources to limit the radiation doses to 1 mSvy^{-1} (Ramasamy et al, 2011). The index value must be less than a unit to be within safe limits of radiation hazards. The calculated external hazard index in soil samples from the study area is presented in Appendix A and Figure 4.7. The calculated external hazard index varied from radiation varied from 0.37 to 0.90 with a mean of 0.66 for Arandis town and 0.48 for Karibib town. Figure 4.7 reveals that most of the soil samples have Hex values less than a unity and this implies that the soils in the study area does not constitute a health hazard to the inhabitants of area.

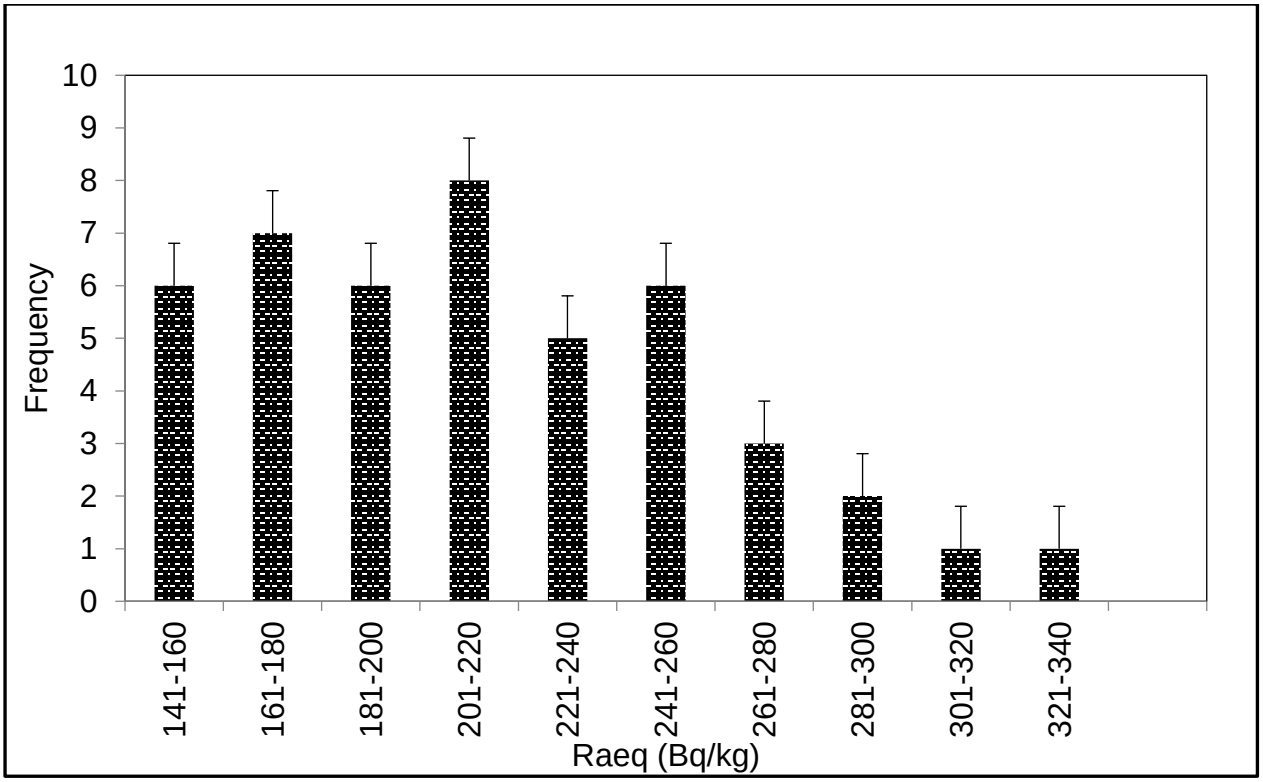

Figure 4.6 Frequency distribution of radium equivalent activity concentrations (Raeq) in the two towns of Arandis and Karibib

The excess lifetime cancer risk is defined as the probability or risk of an individual developing cancer due to exposure to deleterious substance such as radioactive substance or toxic heavy metals from multiple exposure pathways over time.

The calculated excess lifetime risk from the 45 soil samples collected from the two town of Arandis and Karibib , varies from to $0.28x10^{-3}$ to $0.64\ x10^{-3}$ with an average value of $0.49x10^{-3}$ for Arandis town and $0.36x10^{-3}$ for Karibib town as presented in Appendix A and Figure 4.8. This average value of ECLR in Arandis is 1.5 times higher than the world average of $0.29\ x\ 10^{-3}$ (Taskin et al, 2009) which can potential mean a radiation health hazards to the general populace residing in this mining towns due to radiation doses due to NORM. We were not able to evaluate the health hazards of the assessed values on the population since this information is obtained from secondary data such as mortality and morbidity of the population which was not accessible, and the study was limited to background radiations.

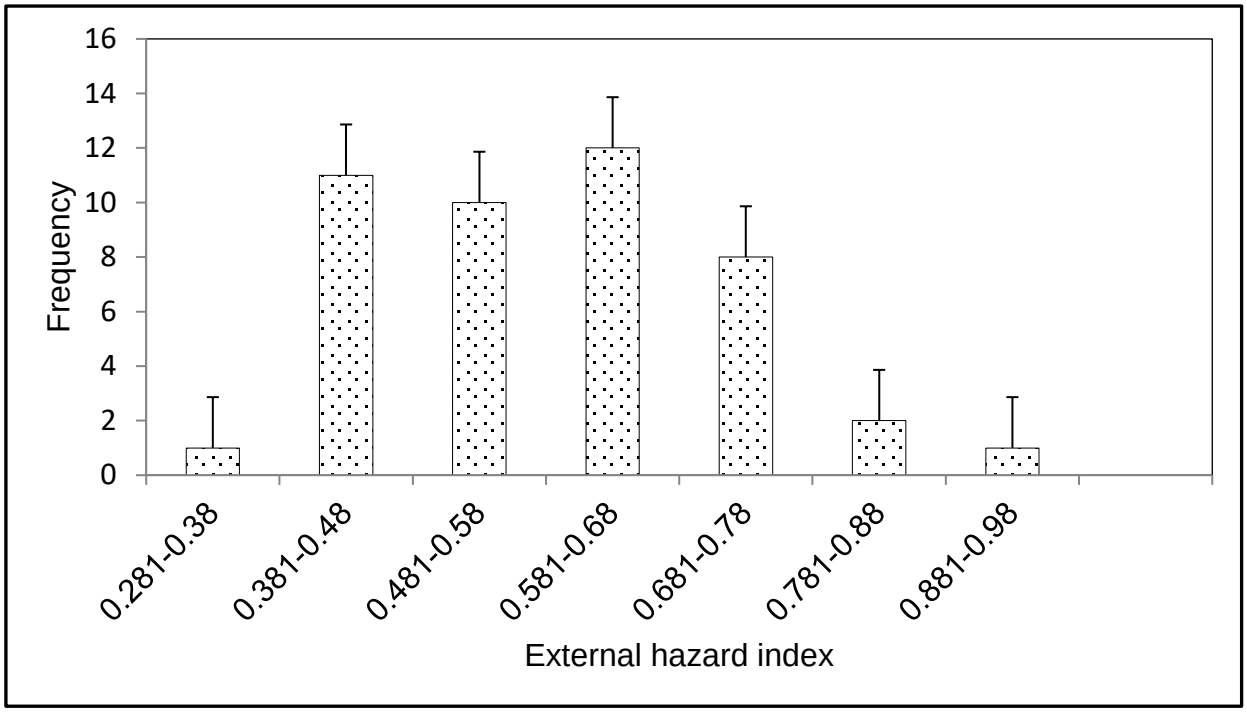

Figure 4.7 Frequency distribution for the external hazard indices in soil samples for the study area

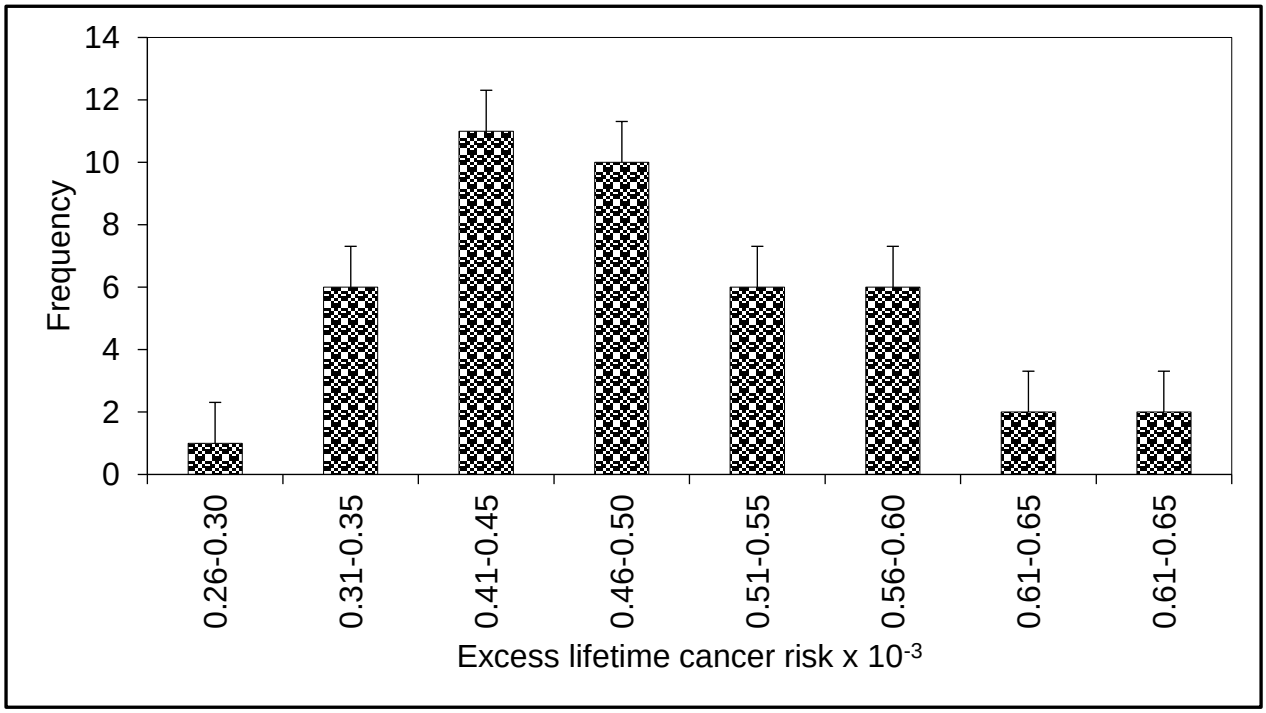

Figure 4.8 Frequency distribution for the excess lifetime cancer risk (ELCR) due to NORM in soil samples for the study area

4.3.2 Radiological parameters associated with the activity concentrations of ^{238}U, ^{232}Th and ^{40}K in PM samples

The results for the radiological parameters in PM samples collected from the town of Karibib and Arandis are listed in Appendix A and schematically presented in Figures 4.9, 4.10, 4.11, 4.12 and 4.13. These radiological parameters are measured in terms of the absorbed dose (D) rate, the annual effective equivalent dose (AEDE), radium equivalent activity($\mathrm{Ra_{eq}}$), the external hazard index $(\mathrm{H_{ex}})$, and excess lifetime cancer risk (ELCR).

The mean absorbed dose rate (D) in air at 1 m above the ground in the town of Arandis was found to be 97.98 nGy/h and 100.37 nGy/h in the town Karibib and these values are twice higher than the worldwide average value of 59 nGy/h (UNSCEAR, 2000). Figure 4.9 is a frequency distribution curve for the calculated absorbed dose rate (D) in the air from the two towns of Arandis and Karibib. As observed in Figure 4.9, the highest frequency was found in the range of 91-100 nGy/h and the least was found in the range of 131-140 nGy/h. All the samples have absorbed dose rate (D) value greater than the worldwide value of 59 nGy/h which is a concern to the inhabitants of these two towns and therefore precautionary measures must be taken to prevent exposure to ionising radiation originating from NORM. However, the absorbed dose rate in the air cannot be used to provide radiological risk conclusively, instead, the annual effective dose equivalent (AEDE) from terrestrial gamma-radiation provides a better estimate. The average AEDE which is calculated from absorbed dose rate (D) was found to be 0.61 mSv/y, which is lower than 1 mSv/yr, the safe limit promulgated by International Commission on Radiation Protection (ICRP,1993).

The annual effective dose equivalent in PM samples was found to be 0.60 mSv/y and 0.62 mSv/y for the towns of Arandis and Karibib. The obtained AEDE values are significantly lower than the safe limit of 1 mSv/y. Figure 4.10 shows the frequency distribution of annual effective dose equivalent in PM samples from the town of Arandis and Karibib. The graph is normally distributed with the highest frequency appearing in the range of 0.56-0.60 mSv/yr and thus the value is less than the safe limit given by ICRP and radiation damage due NORM is therefore not significant. It should be noted that some sampling sites have annual effective dose which is closer to a unity, and therefore may imply that prolonged exposure to radioactive PM may pose a health hazard to members of the public in these towns.

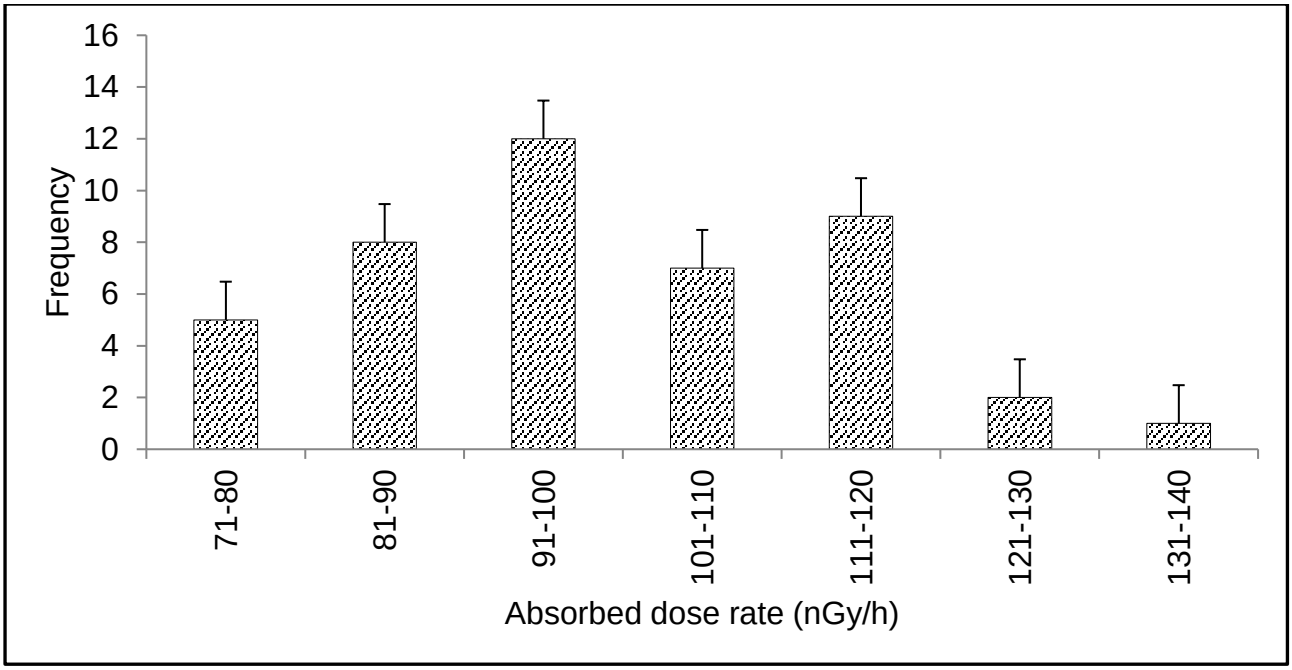

Figure 4.9 Frequency distribution for the absorbed dose rate (D) in PM samples from the two towns of Arandis and Karibib

To limit the radiation exposure due to natural radionuclides in the PM samples from the town two towns of Karibib and Arandis to a safe limit of 1 mSv/y, the internal radiation hazard (H_{in}) was introduced (ICRP, 2008). The internal radiation hazard index (H_{in}) reflects the external exposure due inhalation of alpha emitting radionuclides by members of the population which must be less than a unity in order to keep the radiation hazard below the safe limit and the maximum value of H_{ex} corresponds to the upper limit of radium equivalent activity concentrations of 370 Bq.kg^{-1} in soil (Beretka et al., 1985). The calculated mean H_{in} in this study was found to be 0.73 which is less than unity.

Figure 4.11 presents the frequency distribution of ($\boldsymbol{H_{in}}$) in the 45 PM samples collected from the two towns of Karibib and Arandis and shows that the highest frequency was in the range of 0.61-0.70, which less than unity. The H_{in} is a measure of radiation hazard emanating from radon and its short-lived products which causes more harm to internal organs.

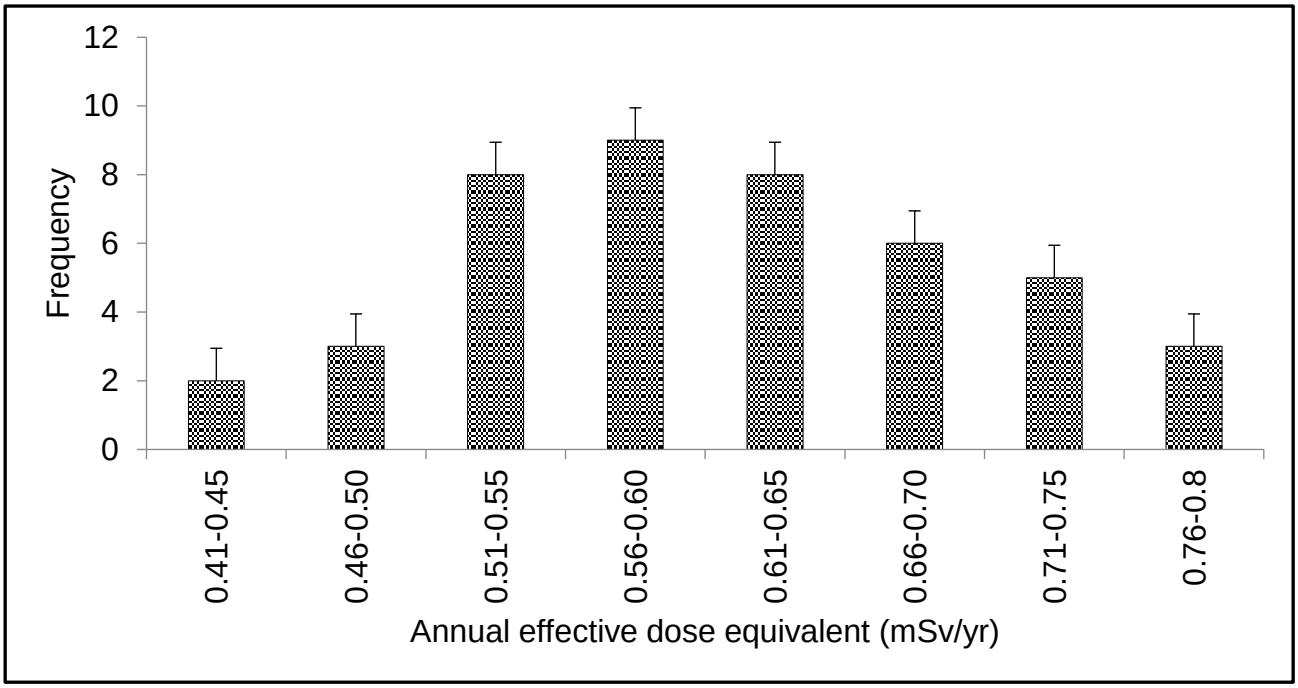

Figure 4.10 Frequency distribution of annual effective dose equivalent (AEDE) in PM samples from the town of Arandis and Karibib

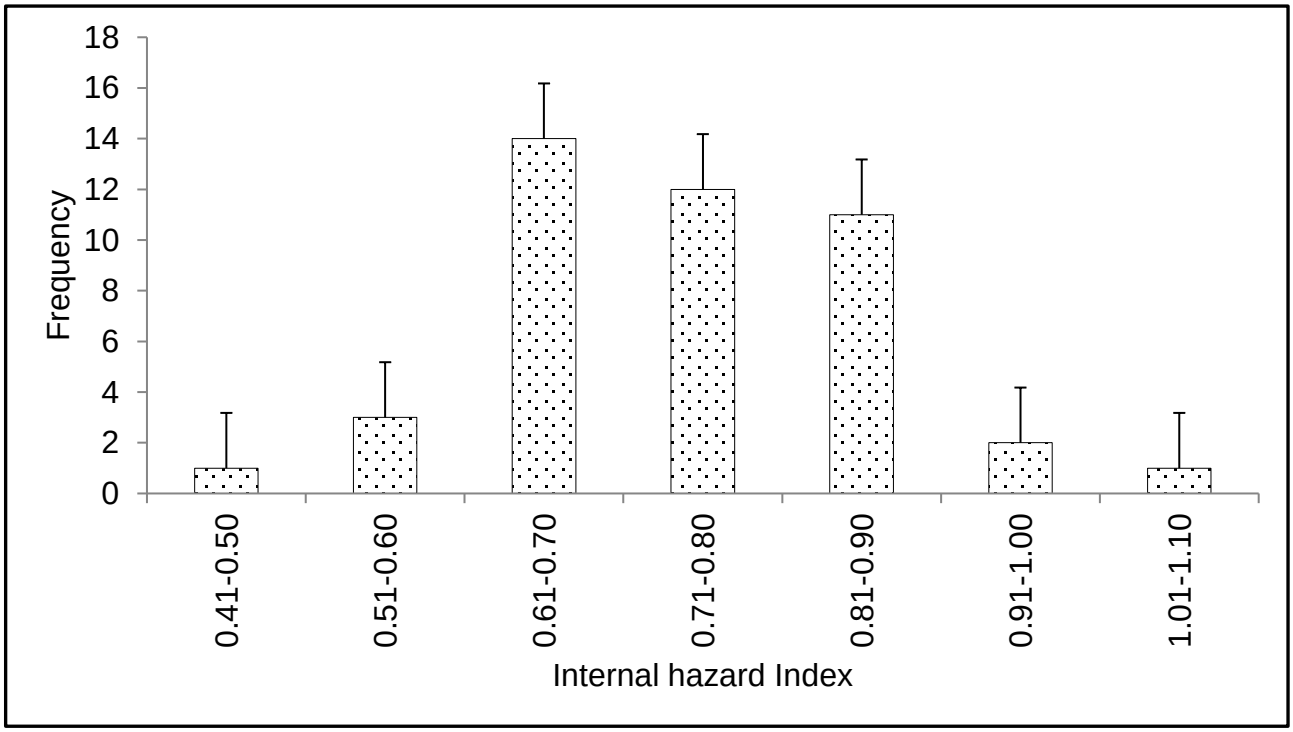

Figure 4.11 Frequency distribution for internal hazard index (H_{in}) in PM in the study area

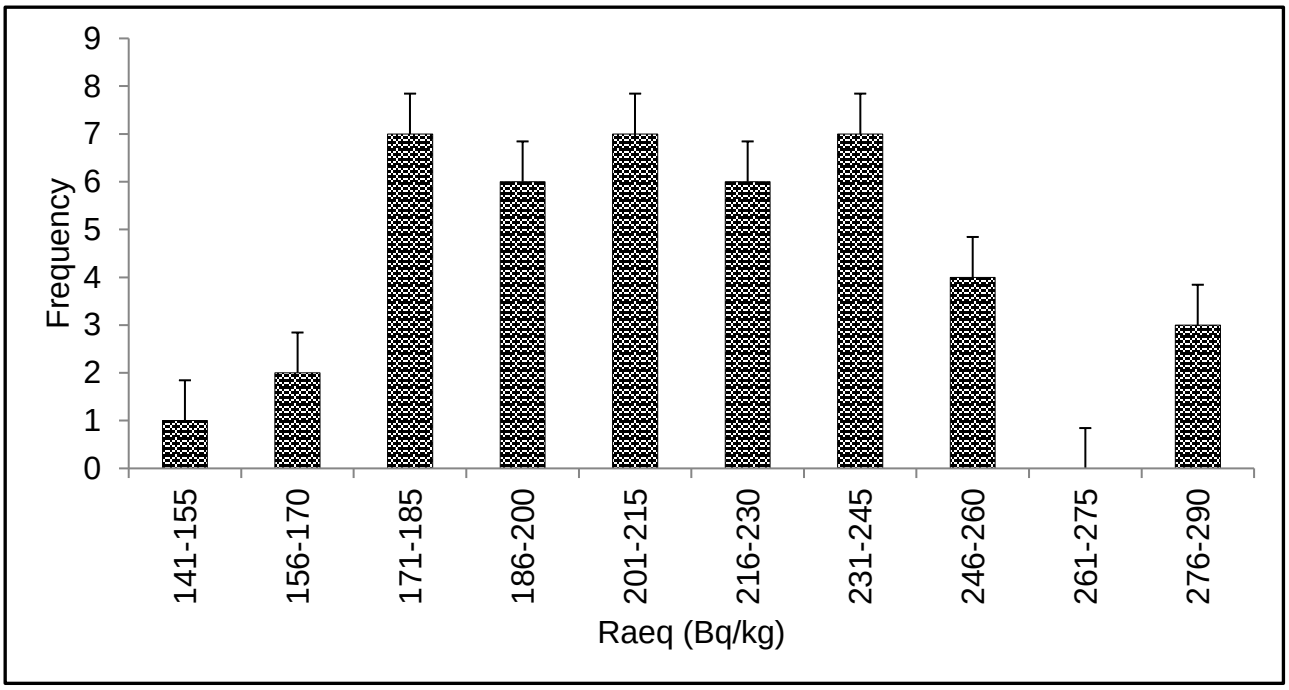

Figure 4.12 Frequency distribution for the radium equivalent activity concentrations in PM samples from the town of Karibib and Arandis

The radiation hazard indices associated with ^{238}U, ^{232}Th and ^{40}K was calculated using equations 3.29 and 3.30 and these are used to assess the radiation dose equivalent received by individuals to 1 mSv/y which correspond to the maximum permissible radium equivalent (Ra_{eq}) safe limit of 370 Bq/kg. The value was promulgated by the Organisation for Economic Cooperation and Development (OECD, 1979).

The calculated radium equivalent activity concentrations in Bq/kg in PM samples from the two towns of Karibib and Arandis was found to vary from 144.54 to 287.84 Bq/kg with mean of 209.85 Bq/kg and 218.91Bq/kg respectively. The obtained mean values of Raeq was lower than the upper safe limit of 370 Bq/kg in soil which corresponds to a value of unit and thus the PM from the two towns are not radiological hazard. It is important to keep the concentration levels below a unity to protect the delicate internal respiratory organs such as the lungs from the effects associated with radon and its decay products. The assigned value is comparable to the action level for indoor radon of 40 Bq/m^3 (UNSCEAR, 2000). The frequency distribution of Raeq in PM samples from the two towns is shown in Figure 4.12.

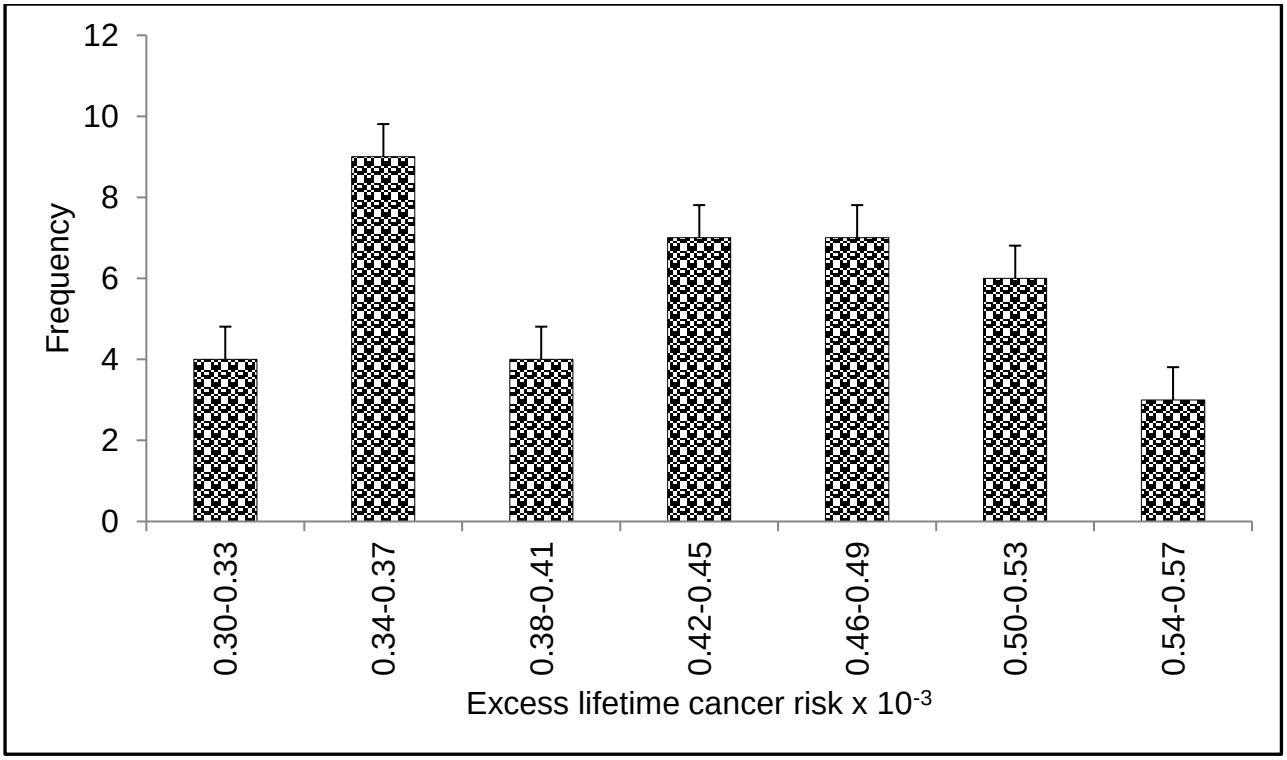

Figure 4.13 Frequency distribution of excess lifetime cancer risk in the town of Arandis and Karibib

Furthermore, the excess lifetime cancer risk (ELCR) was calculated using equation 3.31 and this is used to reflect the fatal cancer risk per sievert. For determination of stochastic effects, a value of 0.05 is applied for members of the public as per ICRP 60 recommendations. The ELCR mean value for Arandis town was found to be 0.60 x 10^{-3} while Karibib town it was 0.62 which is two times higher than the world average of 0.29 x 10^{-3} (Taskin et al., 2009). The frequency distribution of ELCR is presented in Figure 4.13 and it shows that all the samples from the mining towns have values greater than the world average value and thus there are higher chances of developing cancer by the general populace residing in these places.

4.4 Assessment of toxic heavy metals concentration in soil in Erongo region

A summary of the distribution of some heavy metals in surface soils collected from the town of Karibib and Arandis are presented in Table 4.3. Detailed information regarding the concentrations of heavy metal in each geographical site are given in Appendix B.

Table 4.3 Heavy metal concentrations (mg/kg) in the surface soil samples collected from the town of Karibib and Arandis and the comparison with World Surface Rock Average (WSRA) and World Health Organization (WHO) (Charravarty and Patgiri, 2009; Chiroma *et al*., 2014)

	Arandis town					Karibib town					WRSA	WHO
Element	Min	Max	Mean	SD	CV%	Min	Max	Mean	SD	CV%		
Cr	58.31	107.70	74.92	13.81	18.44	31.11	114.20	48.58	16.80	34.60	90	100
Mn	90.27	393.50	214.73	81.71	38.05	37.81	209.80	115.46	49.09	42.52	750	2000
Fe	8140	26550	15372	4331	28.17	1113	9309	4897.60	2356	48.12	35900	5000
Ni	15.92	71.36	24.99	12.53	50.15	6.85	216.10	24.11	46.16	19.48	50	50
Cu	18.52	37.97	27.20	5.91	21.73	2.57	39.98	11.76	7.78	66.14	45.0	100
Zn	29.10	105.30	49.52	21.69	43.79	1.53	173.40	25.52	39.14	153.4	95.00	300
As	1.71	3.74	2.67	0.58	21.76	0.46	2.56	1.22	0.50	40.65	13	20
Cd	0.52	0.79	0.60	0.06	10.38	0.37	0.71	0.56	0.09	15.38	0.3	3.0
Pb	9.30	79.68	24.10	15.71	65.19	1.44	21.10	7.30	5.37	73.00	16.0	100

The mean concentrations of toxic metals Cr, Mn, Fe, Ni, Cu, Zn, As, Cd, and Pb in the town of Arandis are 74.92, 214.52, 15372.50, 24.99, 27.20, 49.52, 2.67, 0.60, and 24.10 mg/kg while for the town of Karibib are 48.58, 115.46, 4857.60, 24.11, 11.76, 25.52, 1.22, 0.56 and 7.30 mg/kg respectively. These values are significantly lower than the World Surface Rock average (WSRA) and World Health Organisation (WHO) reference values. As can be seen from Table 4.4, the average concentrations (mg/kg) of the metals decreases in order Fe>Mn>Cr>Zn>Cu>Ni>Pb>As>Cd for the town of Arandis and Fe>Mn>Cr>Zn>Ni>Cu>Pb>As>Cd for the town of Karibib.

However, the arithmetic mean of the metals does not explain fully about the spread and variability of these heavy metals in the environment. The standard deviation (SD) was divided by the corresponding mean to give the coefficient of variation (CV). By considering the CV of the metals in this study, it can be deduced that many of the surface soils have a higher CV indicating a highly heterogenous nature of samples with elements: Ni and Zn shows the greatest variability of 50.15 and 153.37 % CV in the town of Arandis and Karibib respectively

To evaluate whether the results of the measured values are within the permissible limits, the concentrations were compared with FAO/WHO soil guidelines and other countries (Table 4.3, 4.4 and Figure 4.14). As observed in Table 4.3, the mean concentrations of most measured heavy metals are significantly lower than the FAO/WHO and WSRA soil guidelines in most of the samples. The concentrations of Fe in the town of Arandis is higher than the FAO/WHO soil guidelines and two times less than the WSRA values and this could be attributed to the nature of the parental material of soil in the study area.

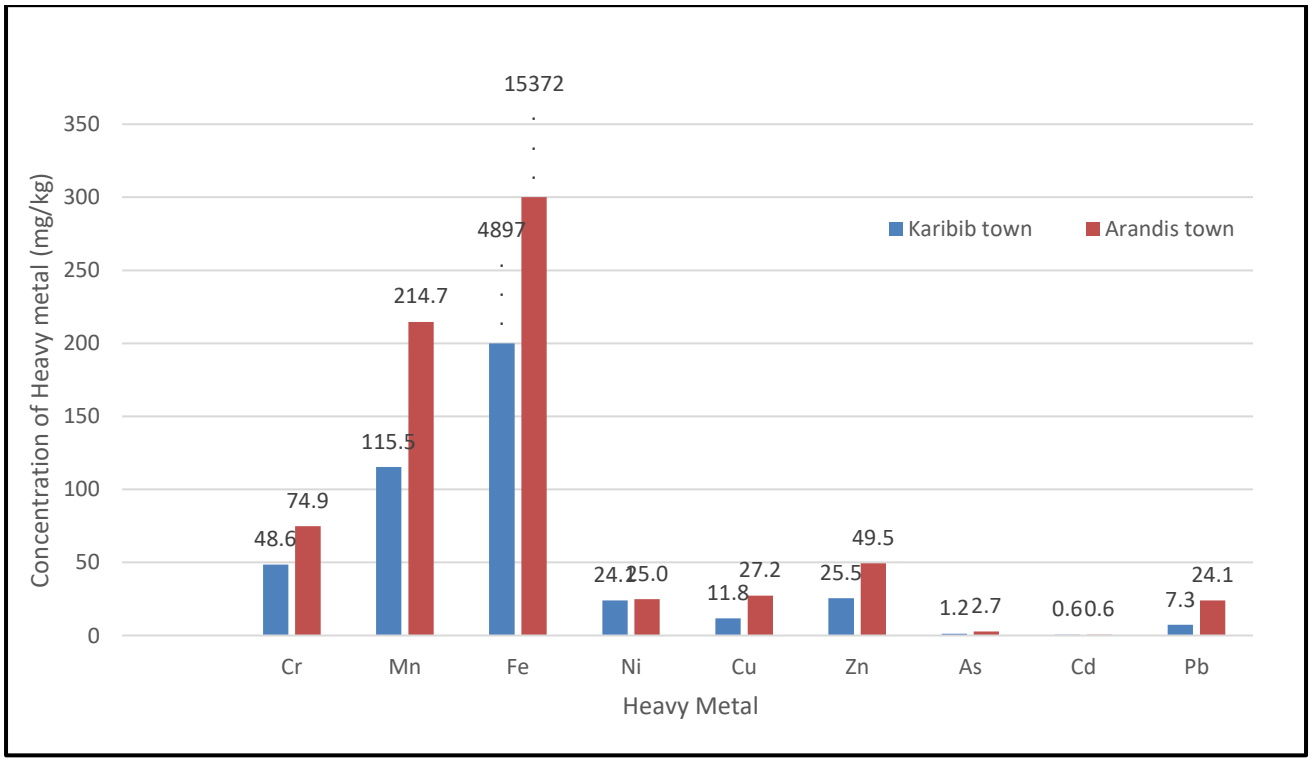

Figure 4.14 The average concentrations of Heavy metals in soils from the town of Karibib and Arandis

On the other hand, the concentration of Fe in the town of Karibib is comparable to the FAO/WHO and WSRA soil guidelines. It should be noted that most measured toxic metals in the soil samples are within the safe limit as suggested by Alloway (1995), except for Fe with a value of 4895.60 mg/kg compared to 3000 mg/kg. Detailed information about the normal concentrations of heavy metals in soil and the critical limits are given in Appendix B.

It is well documented that Cd, Cr and Pb have been ranked as the most toxic metals and have received the greatest attention from a public health point of view (Tchounwou et al., 2012). Exposure to lead (Pb) even at low concentrations have been associated with behavioural abnormalities, poor growth rate, learning impairment, decreased hearing and reduced cognitive functions in humans and even in experimental animals (Millichap, 1995) while the soluble hexavalent chromium (Cr) is widely recognised as carcinogenic, mutagen, and teratogen towards human and animal (Patlolla et al., 2009). Similarly, Cadmium and its derivative compounds interferes with calcium metabolism with consequence renal tubular dysfunction and osteoporosis (Faroon et al., 2012).

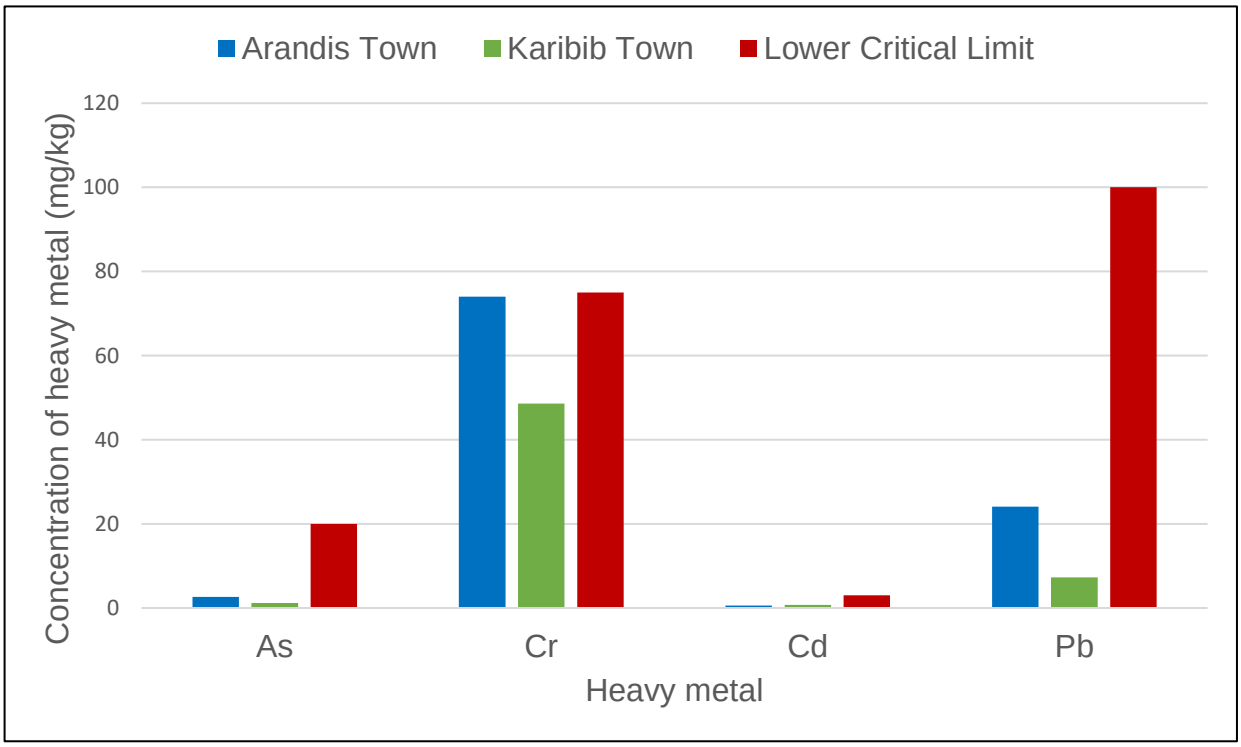

Figure 4.15 A comparison of the most toxic metals concentrations with critical limits in soil.

.

Table 4.4 Maximum allowable Limit of Heavy Metals Concentrations in Soil for Different Countries (Kamunda et al, 2016 b)

Country	Concentration limit (mg/kg)									References
	Cr	Mn	Fe	Ni	Cu	Zn	As	Cd	Pb	
Germany	60.0	50.0	40.0	150.0	50.0	1.0	70.0			Dar-Yuan & Chia Hsing, 2011
Poland	100.0	100.0	100.0	300.0	50.0	3.0	100.0			(Mtunzi et al., 2015)
UK	130.0			130.0	n.a	n.a	32.0	10.0	450.0	CLEA, 2009
Australia	50.0			60.0	100.0	200.0	20.0	3.0	300.0	EPA, 2012
Taiwan	250.0			200.0	200.0	600.0	60.0	5.0	300.0	Dar-Yuan & Chia-Hsing, 2011
China	200.0			50.0	100.0	250.0	30.0	0.5	80.0	EPMC, 2015
Canada	250.0			100.0	150.0	500.0	20.0	3.0	200.0	CME, 2009
Tanzania	100.0			100.0	200.0	150.0	1.0	1.0	200.0	He et al., 2015
WHO	100.0	2000	5000	50.0	100.0	300.0	20.0	3.0	100.0	
WSRA	90.0	850.0	35900	50.0	45.0	95.0	13.0	0.3	16.0	Martin& Maybeck, 1979 .
South Africa	6.5			91.0	16	240.0	5.8	7.5	20.0	DEA, 2010
Arandis, Namibia	74.9	214.7	15372.5	24.9	27.2	49.5	2.7	0.6	24.1	**Current study**
Karibib, Namibia	48.6	115.5	4897.5		24.1	11.8	25.5	1.2	0.6	7.3 **Current study**

Epidemiological studies have shown a close correlation of cadmium (Cd) with certain types of cancers(Tchounwou et al., 2012). A comparison of the concentrations of Arsenic (As), Cadmium (Cd), Chromium (Cr) and Lead (Pb) with the critical limits as proposed by Alloway (1995), is presented in Figure 4.15. As can be deduced from Figure 4.15, Cr concentrations value in the town of Arandis is closer to the critical limit values and as such, analysis needed to be done so as to ascertain its potential carcinogenic effects.

4.4.1 Assessment of contamination status due to heavy metals exposure

Many authors have determined the degree of metal contamination using the shale value to represent the degree of quantification of pollution (Muller, 1979, Forster and Wittman, 1983) while others have considered the background value of the study area to be the geometric mean of concentration at different sampling sites. This represent the antilog of the arithmetic mean of $\log_{10}$ of the concentration values. It has been found that the geometric mean reduces the importance of outliers and thus making it a useful indicator of background for most geochemical data. This method was not applied in this study. Instead, the world surface rock average (Martin and Meybeck, 1979) of individual metals have been taken to be the background as it helps to quantify the pollution index by converting the calculated numerical results into broad descriptive bands of pollution ranging from low to high intensity. Four indices were used to evaluate the status of the studied pollutants in the soil samples from the towns of Karibib and Arandis. Detailed results for contamination factor (CF) and degree of contamination (Cdeg), Enrichment factors (EF), Geoaccumulation Index (Igeo) are shown in Appendix C.

4.4.1.1 Contamination factor (CF)

The results for the contamination factors for the measured soil samples in the town of Arandis are presented in Figure 4.16 and Appendix B. The contamination factors (CF) in the soil samples were calculated by equation 3.11 as suggested by Hakanson (1980).

Classification of the contamination index was achieved by the criteria suggested by Hakanson (1980). Based on this criterion it can be deduced that the mean contamination factor (CF) for elements Cr, Mn, Fe, Ni, Cu, Zn, As, Cd and Pb was observed to be 0.83, 0.25, 0.43, 0.50, 0.60, 0.21, 2.01 and 1.51, respectively, in the measured soil samples which indicate low level of contamination. However, exceptions are exhibited in sample AS1, AS3, AS16 and AS20 which have moderate contamination with contamination values of 1.14, (Cr),

1.43 (Ni), 1.11 (Zn), 1.20 (Cr) and 1.00 (Zn) respectively. On the hand, Cd and Pb show moderate contamination in most samples apart from sample AS3 which have considerable contamination with an index of 4.98 (Pb). The moderate and considerable level of contamination for Cd and Pb can be partly due geological underlying rock which is rich in the metal Pb and partly due to anthropogenic activities such as mining and vehicular emissions. During mineral mining, large quantities of wastes containing different types of chemicals are accidentally or deliberately discharged into the biosphere and they may find their way into water bodies and soil which are the ultimate sinks.

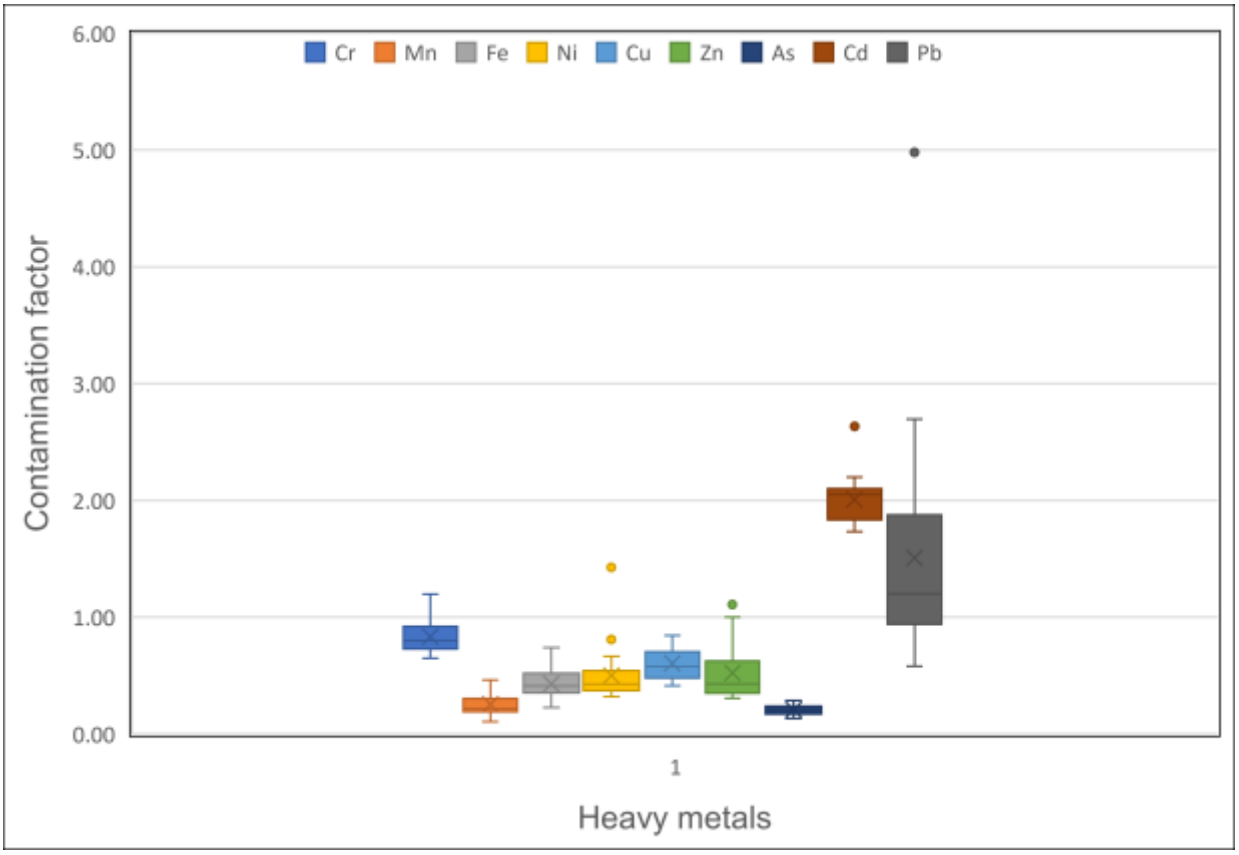

Figure 4.16 Box and whisker for the contamination factors for the measured soil samples in the town of Arandis

Contamination factors determination in soil samples may be not be conclusive to explain the extent of pollution alone, another term which sums all the contamination factors known as the degree of contamination was introduced. Appendix C also shows that the degree of contamination in the measured samples from the town of Arandis is low in most samples which imply that the extent of metals due to anthropogenic activities is insignificant.

However, only sample AS1 and AS3 have moderate contamination degree of contamination with the values of 9.34 and 11.34 respectively.

Figure 4.17 and Appendix C also illustrates contamination factors (CF) and the degree of contamination (C_{deg}) for the soil samples measured in the town of Karibib. A similar trend was observed in most of the samples from the town of Karibib. The contamination factors for Cr, Mn, Fe, Ni, Cu, Zn, As and Pb are in the low contamination category while Cd was in the moderate category. It should be noted that sample KS1 is in the moderate category with the indices of 1.27 (Cr), 2.37 (Pb) and in the considerable category for Ni with index of 4.32.

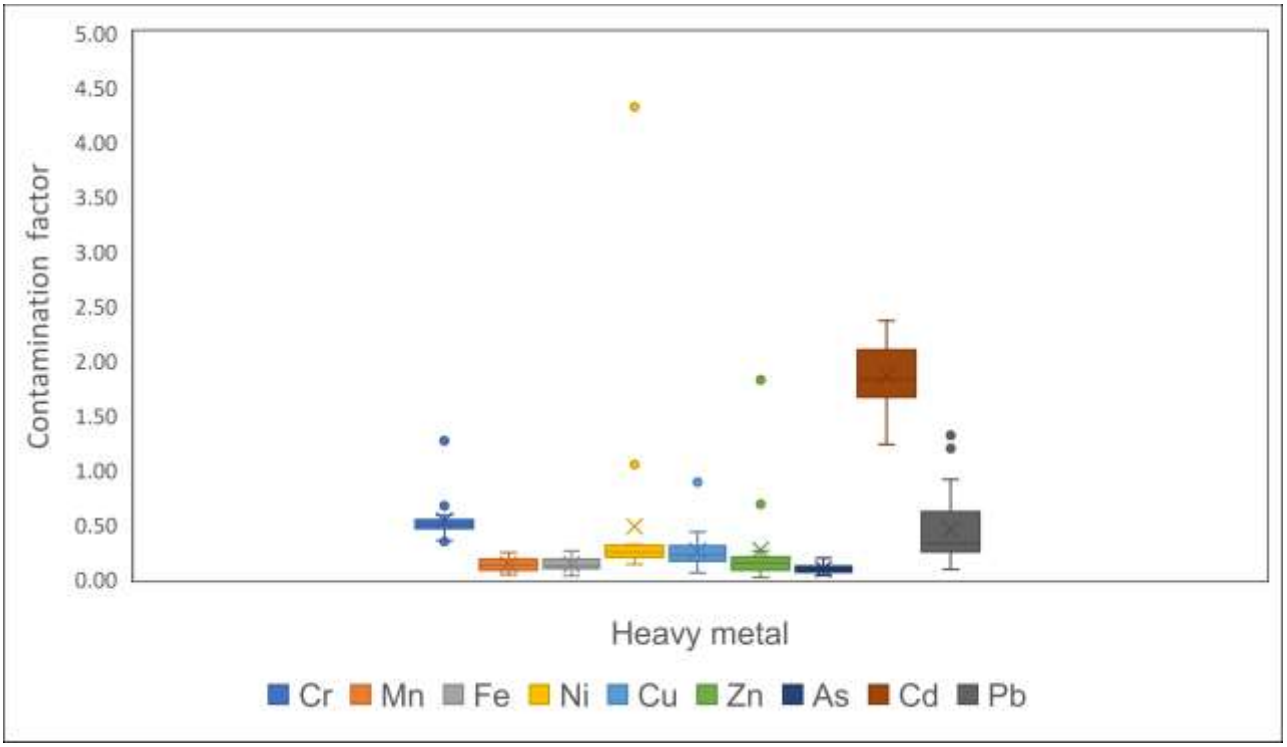

Figure 4.17 Box and whisker for the contamination factors for the measured soil samples in the town of Karibib

The measured soil samples from the town of Karibib shows that Cd is in moderate contamination category and this may be related to improper handling of waste during gold mining extraction and purification in the mine nearby the town and industrial emissions. The obtained values in this study are not in agreement with values obtained in related studies in sediments by Hu et al, 2010 where Cd showed low degree of contamination.

4.4.1.2 Pollution Load Index (PLI)

The pollution load index (PLI) in the measured soil samples in the two mining towns of Arandis and Karibib were calculated using equation 3.14 and a summary of the results are presented in Table 4.5. Detailed information of the PLI values from the two mining towns are presented in Appendix C. The mean value of PLI in Arandis from all the samples was $1.25x10^{-2}$ while in the town of Karibib it was $1.18x10^{-3}$. In all the sampling sites in both towns, the PLI was significantly lower than 1 by a magnitude of hundred folds. The measured results are comparable to a study conducted by Onjefu et al (2016) in sediments samples in the same locale. If the PLI > 1, it means the site is contaminated, PLI < 1, means no pollution and PLI = 1, means baseline pollutants are present (Tan et al, 2017). Since the PLI at different sampling points shows that all the sampling points were less than 1 which means that the soil in not polluted with heavy metals.

Table 4.5 Summary of Pollution load index in soil samples collected from the town of Arandis and Karibib

Arandis Town	Pollution Load Index	Karibib Town	Pollution Load Index
Min	2.18E-03	Min	4.17E-06
Max	3.90E-02	Max	1.32E-02
Mean	1.25E-02	Mean	1.18E-03

4.4.1.3 Enrichment factor (EF)

The enrichment factor (EF) in metals is an indicator used to assess the presence of a contaminants due to anthropogenic activities on surface soils and dust. The indices were calculated using equation 3.15 and Fe was used as a reference element. Other elements such as Al, Mn and Rb have been used as reference elements in some studies depending on the matrix and geochemical speciation of the sample and the reference material. For example, Al is an ideal reference element for use in sediment samples because it is a conservative element and a major constituents of clay minerals (Ryan et al., 1988; Sinex et al.,1988; Barbieri et al., 2014; Emmerson et al., 1997) as opposed to Fe which is not a matrix

element and its chemical speciation is similar to many other elements under oxic and anoxic environments (Emmerson, 1997).

The results for the enrichment factors in the soils of Arandis town are presented in Table in Appendix C, Table C5. As depicted in the Table C5, EF for most of the studied samples exhibit a deficiency to minimum enrichment (EF < 2) for Cr, Ni, Cu, Zn, Mn and As which suggest that the elements wholly come from natural processes such as weathering (Yongming et al., 2006). However, for the element Cd, about 50 % of the samples show a moderate contamination (EF > 2) while 50 % are significantly contaminated. A similar trend is also observed in Pb where about 90 % of the samples are moderately contaminated and 10 % are significantly contaminated. This indicate that a significant portion of the metals was delivered by other sources like point and non-point sources pollution from mining activities such blasting, excavation, drainage after mineral processing, and windblown dust (Sutherland et al., 2000; Muller, 1971). This is not surprising as Pb is a key element in the uranium tailings and depleted uranium, and Cd is widespread in chemical reagent used for the processing and purification of uranium oxide.

On the other hand, Appendix C, Table C4 presents the enrichment factors for the elements Cr, Mn, Ni, Cu, Zn, Cd and Pb in the town of Karibib. Contrary to the results in Arandis town for enrichment factors (EF) most of the samples were moderate to significant contaminated except for Mn and Cd which have deficiency to minimal enrichment (EF<2) and extremely high enrichment (EF>40), respectively, for all the samples. This suggest that that the source of these toxic metals is from anthropogenic activities. The mean EF for the measured samples were in order of Cd> As> Pb> Cu> Ni> Cr> Zn.

4.4.1.4 Geoaccumulation index (Igeo)

The intensity of heavy metal pollution in soil samples was evaluated using the Geoaccumulation index (Igeo) introduced by Muller (1979) which is illustrated by equation 3.15. The Igeo index for the 9 studied heavy metals are listed in Figure 4.18 and Appendix C.

The calculated values for the Igeo for the town of Karibib and the town of Arandis shows that most sites are unpolluted with the elements, As, Pb, Cr, Ni, Mn, Fe, Zn and Cu except for Cd which showed uncontaminated to moderately contamination. The Igeo values for Zn and Ni for site KS1 and KS10 revealed that the soil is uncontaminated to moderately contaminated and moderately contaminated. The negative values of As, Cr, Ni, Fe, Zn and Cu for Geoaccumulation index shown in Figure 4.18 are as a result of deficient to minimal

enrichment and these results are comparable earlier studies conducted by Onjefu et al., (2016) in-shore sediment samples of the Henties Bay in Erongo region. However, Fe in soil samples Fe is used because of its stability.

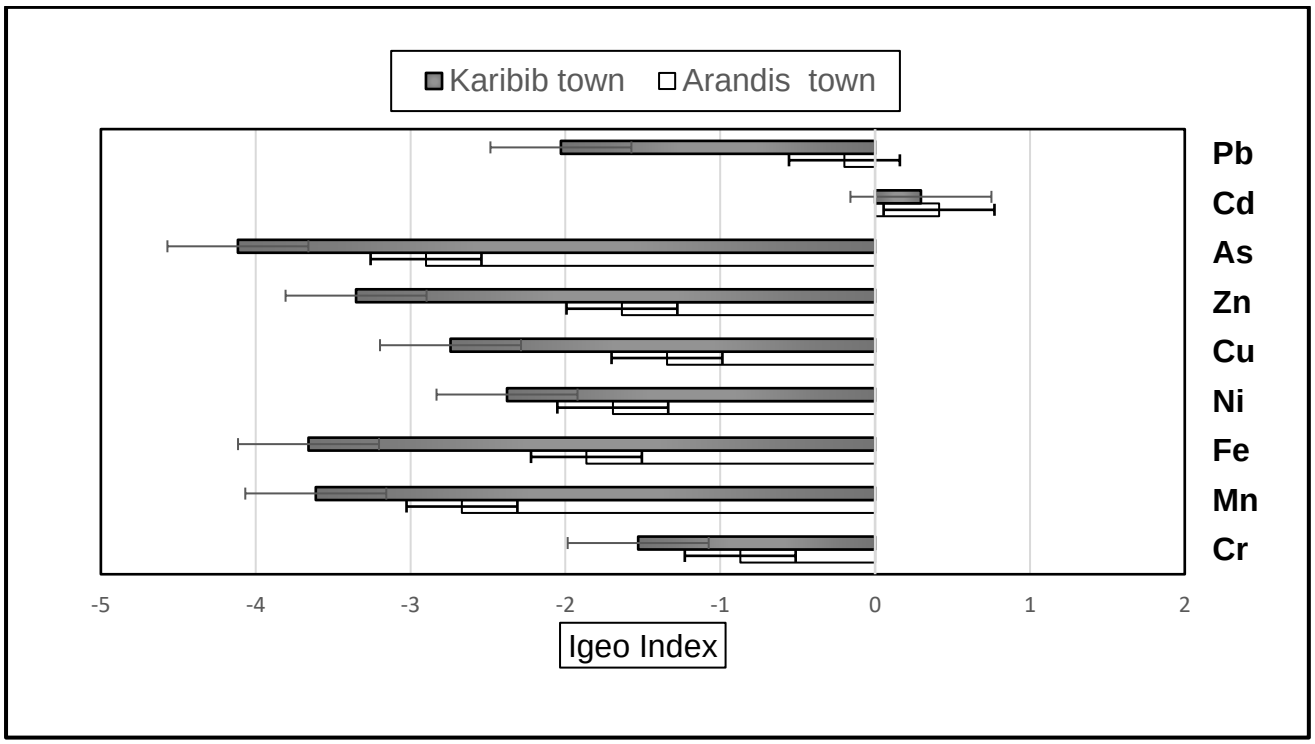

Figure 4.18: Geo-accumulation index (Igeo) values for heavy metals for soils samples collected from the town of Karibib and the town of Arandis.

4.5 Analysis of PM in Erongo region

The results for gravitational analysis, morphological and the relative number abundance (%) of the particles in the analysed PM samples collected from the town of Arandis and Karibib are presented and discussed in the proceeding sections. Figure 4.19, 4.20, 4.21 and Figure 4.22 shows the morphological characteristics of the particles detected in the town of Karibib and Arandis respectively. In addition, a correlation analysis of the relationship between respiratory inhalable fraction (IF), the deposition fraction (DF) and particle diameter of PM samples is also presented and discussed.

4.5.1 Gravitational analysis

The particulate matter fall rate was analysed by gravitational analysis. The calculation of insoluble particulate matter (D) was done using equation 3.16 and a summary of the results are presented in Table 4.6. Detailed information about the fall rate is available in Appendix

A. Table 4.7 shows the minimum, maximum and average PM fall rate in the town of Karibib was 80, 1170 and 340 mg/m^2/day and 10, 1020 and 520 mg/m^2/day for the town of Arandis, respectively.

Table 4.6 PM fall rate (D) in the town of Arandis and Karibib

Parameter	Karibib town	Arandis town
	D (mg/m^2/day)	
Minimum	70	10
Maximum	1170	1020
Mean	340	520

The values obtained in this study are significantly lower than South African Dust Control regulation (DEA, 2013) which stipulates the total amount of dust permissible in ambient air monitored in accordance with American Society for Testing and Materials standard method (ASTM D1739-98, 2004) for measuring dust fallout (particulate matter). The regulation stipulates that the dust for residential areas must be kept below 600 mg/m^2/day measured over a 30-day average and between 60 and 1200 mg/m^2/day for non-residential areas as shown in Table 4.7. In addition, the particles also include both natural and anthropogenic sources.

Table 4.7: The National Dust Control Regulations (adapted: DEA, 2013)

Restriction areas	**PM fall rate (D) (mg/m2/day averaged over 30 days)**	**Permitted frequency Exceeding dust fall rate**
Residential area	D< 600	Two within a year/not sequential months
Non-residential area	600<D<1200	Two within a year/ not sequential months

4.5.2 Morphological characteristic of PM in Karibib town

The SEM images of particles shows variation in average grain sizes and shapes. According to their average grain size, shape and elemental composition, about 80 % of the particles analysed have average grain size less than 1.0 um ($PM_{1.0}$) which is the fine fraction.

The detected particles also include a very small number with an average grain size more than 1.0 um but still less than 2.5 µm (PM2.5) while some are more than 2.5 µm as reflected in Appendix D. Appendix D shows the variation of grain size of PM samples collected from the town Karibib and Arandis.

As can be observed in Figure 4.19, the elemental composition from the X-ray energy spectra of the analysed particles shows that the most abundant elements in the PM were (C, O, Mg, Al, Si, Ca, Fe) with minute quantities of Na, Ti, P, and Cu . The morphology and chemical analysis of the PM samples collected from the town of Karibib are depicted in Figure 4.20 (a), (b), (c), (d), (e) and (f). It can be deduced that there are two classes of particles and these are: natural and anthropogenic. Natural particles consisted of mostly particulate matter from soil dust and biogenic (biological fragments, spores, pollen fungi and these particles.

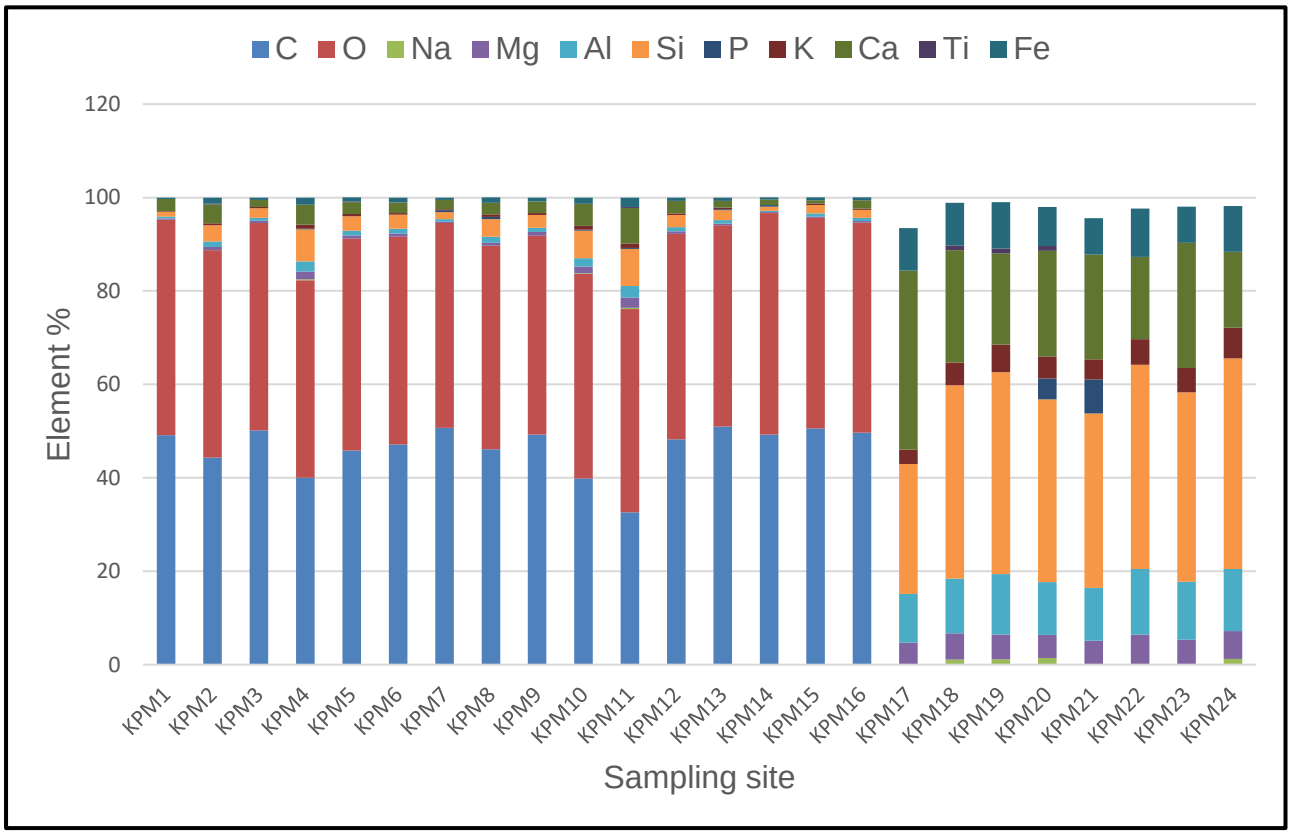

Figure 4.19 The relative number abundance (%) of the particles in the analysed PM samples collected from the town of Karibib

Dust particles have irregular shapes and sizes while biogenic particles were highly structured, with rounded shapes and smooth surfaces. These soot aggregates are characterised by a higher C content in comparison to O are thus conspicuous than the other

particles. The particles have drawn a lot of public interest because they are thought to be the largest contributor to global warming (Mico et al., 2015). The particles may originate from incomplete combustion of fuels and they are a good tracer of vehicle emissions which are used in the mines (Fruhstorfer et al., 1994). SEM photomicrographs for soot aggregates are presented in Figure 4.20 a). The variation in soot particles with fly ash from one site to the other suggest that its major source is traffic related. In closer association with the soot aggregates particles, there are biogenic particles which contain an equal amount of C and O with trace amounts of Mg, Al, Si, K, Ca and Fe and these are presented by a wide range of spores, bacteria, fungi and various types of organic fragments, with highly variable morphology (e.g. plates, spores, columns etc). The partilces are mixed, irregular, cuboidal, crystalline particles with flocks formed due to incomplete combustion as presented in Figure 4.20 (b).

The particles from site KPM17 to KPM24 with a SEM photomicrograph as given in Figure 4.20 (c) has the most abundant elements of Si, Al and Ca with minor of Na, K, Ti and Cu and the morphology of these particles' ranges from large spheroidal to irregular. The presence of Si, Al implies that the particles may have originated from weathering and breakdown of the underlying geological material as a result of mining activities. Si-rich particles are classified as quartz and contain predominantly silicon (SiO_2) with variable amount Al, Na, Mg, P and K. These particles may originate from soil and carried by wind to nearby communities. Si-rich partilces may also consists of mixed particles with a composite origin, as it can originate from deposition and heterogenous nucleation (Kandler et al, 2007) of secondary sulphates (anthropogenic component) on mineral dust (natural component).

Natural component is dominated by geogenic particles originating from crustal erosion and these are made up of aluminosilicates (mainly clay minerals), quartz and to some extent small fraction of carbonates. Aluminosilicates were present in samples KPM17, KPM18, KPM19, KPM20, KPM21, KPM22, KPM23 and KPM24 and they were characterised by high amounts of Si and Al with moderate amounts of Fe, Ca, P, Ti and other metals. These particles have irregular shapes and this shown in Figure 4.20 (c). Ca-rich particles KPM17 to KPM24 is made up of calcite particles which are dominated by Ca with minor amounts of Al, Mg, Ti, Fe and others. The particles are irregular, elongated, and have flakes which shows some lines of breakage as illustrated in Figure 4.20 (d).These particles were present in all the samples and they are as a result of geogenic origin.

The Ca-particles is an ingredient in the manufacture of cement and therefore can be coming from building construction used in the mining site. The airborne Ca particles can be derived from the earth crust. The presence of Ti, Mn and Cu and P in small amounts may suggest that the particles may come from desert dust which is common in the area

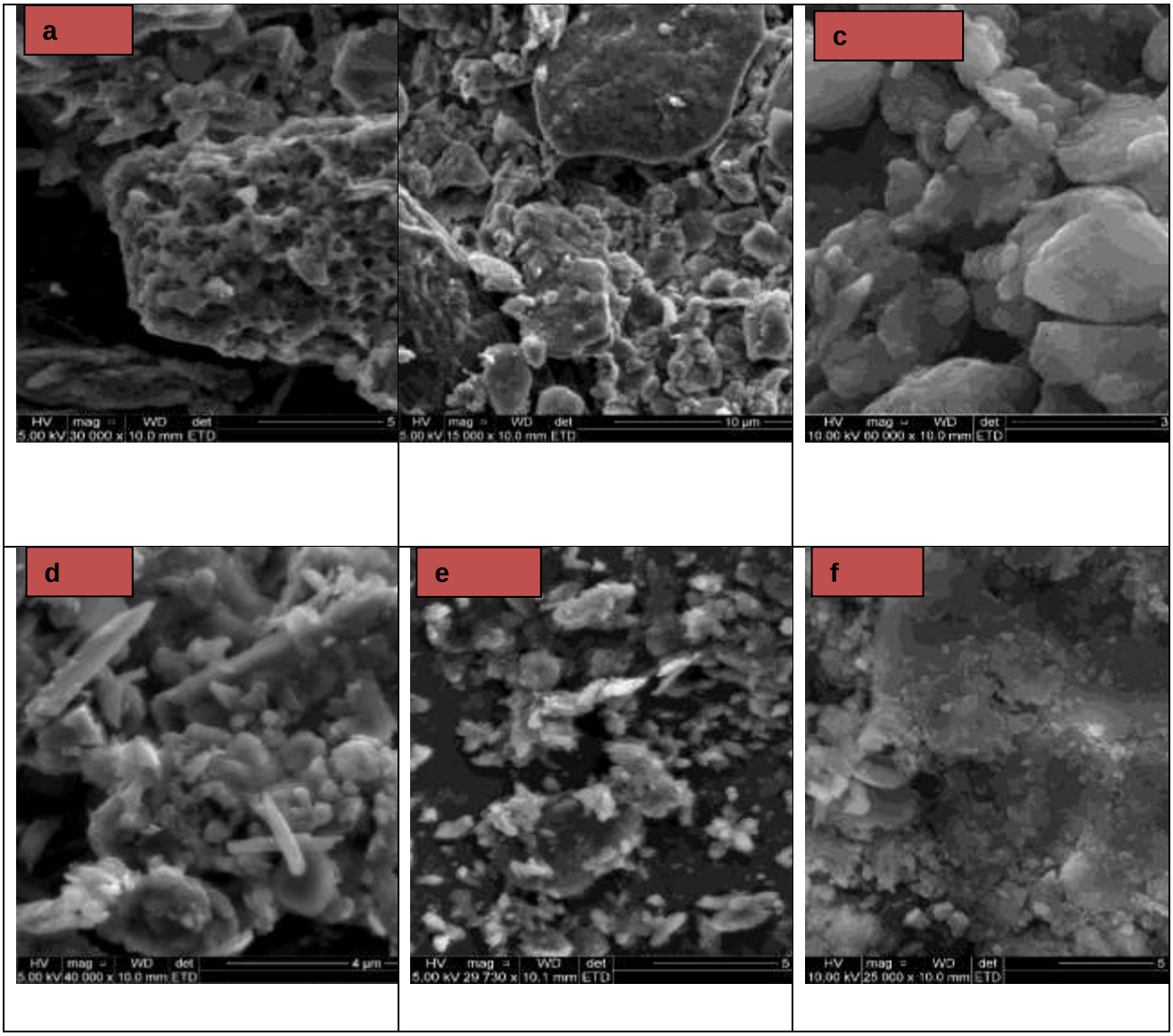

Figure 4.20 SEM photomicrographs for: a) soot aggregates; b) biogenic particles, c) Si-rich (natural quartz particles); d) Ca-rich particles ; e) Fe-rich particles; f) mixed particles

. Fe-rich particles may be of both anthropogenic and natural origin (Genge et al., 2012) and contain Fe in large concentrations with trace amounts of Cu, Ti, Na and Mg. The particles

are irregular and rounded as shown in Figure 4.20 (e). Anthropogenic process which could lead to the emission of Fe-rich particles could be industrial, mining activities and abrasion of metallic related materials and in some cases traffic related. The contributory sources of Fe was likely to be traffic related as this sites are characterised by high volume of traffic due to mining activities. In some instances, in residential places, combustion of fuel can also add Fe-particles in the atmosphere.

Mixed particles contain different combinations of elements Ca, Si, Al, Ti, Mg and Fe and they cannot be classified in any one of the described groups and they were rounded in shape. In some instances, they may also contain agglomerates of clay particles and these may either from mineral origin and transported by wind or anthropogenic origin such as construction activities. Tire wear debris and abrasion of different materials. An example of mixed partilces photomicrograph is shown in Figure 4.20(f).

4.5.3 Morphological and chemical analysis of PM samples from Arandis town

The morphology of PM collected from the town of Arandis were analysed by a scanning electron microscope with energy dispersion X- ray (SEM/EDX). The were six types of particulates identified and these are: biogenic particles, aluminosilicates, mineral particles, quartz particles, clay particles, and non-biogenic C rich particles and theses are presented in Figure 4.21. The relative amounts of several particles' morphology detected in the PM samples are shown in Figure 4.21 and the particles have high relative amounts of C and O in addition to other elements. Biogenic particles are composed of high relative amounts of C and O in equal amounts followed by small amounts of Na, Mg, K and Ti as shown in Figure 4.22 particle G. The SEM of particle G with a magnification of 5 µm collected from PM samples at site APM4 has morphology which ranges from spherical, flake irregular and flocks.

Biogenic particles are associated with flake-like particles while spherical would be an integral of pollen and ashy. The flocks are attributed to incomplete combustion of fuels and they have high concentration of carbon. These include a mixture of black, brown and clear agglomerate of small particles that are round and results from the activities from the vicinity of the mine. On the other hand, in aluminosilicates, the dominant elements are C, O, Si, Fe and Al with minor of Mg, Cl, Na and K as illustrated in Figure 4.22 particle H. The relative intensities of these elements suggest the presence aluminosilicates with traces of chloride. The consistence occurrence of Al/Si/O signals implies that the particles may have originated from natural processes such as weathering of a local geological material The SEM

micrograph of particle H with a magnification of 5 µm collected from site APM2 has morphology which ranges from clustered small to large irregular shapes

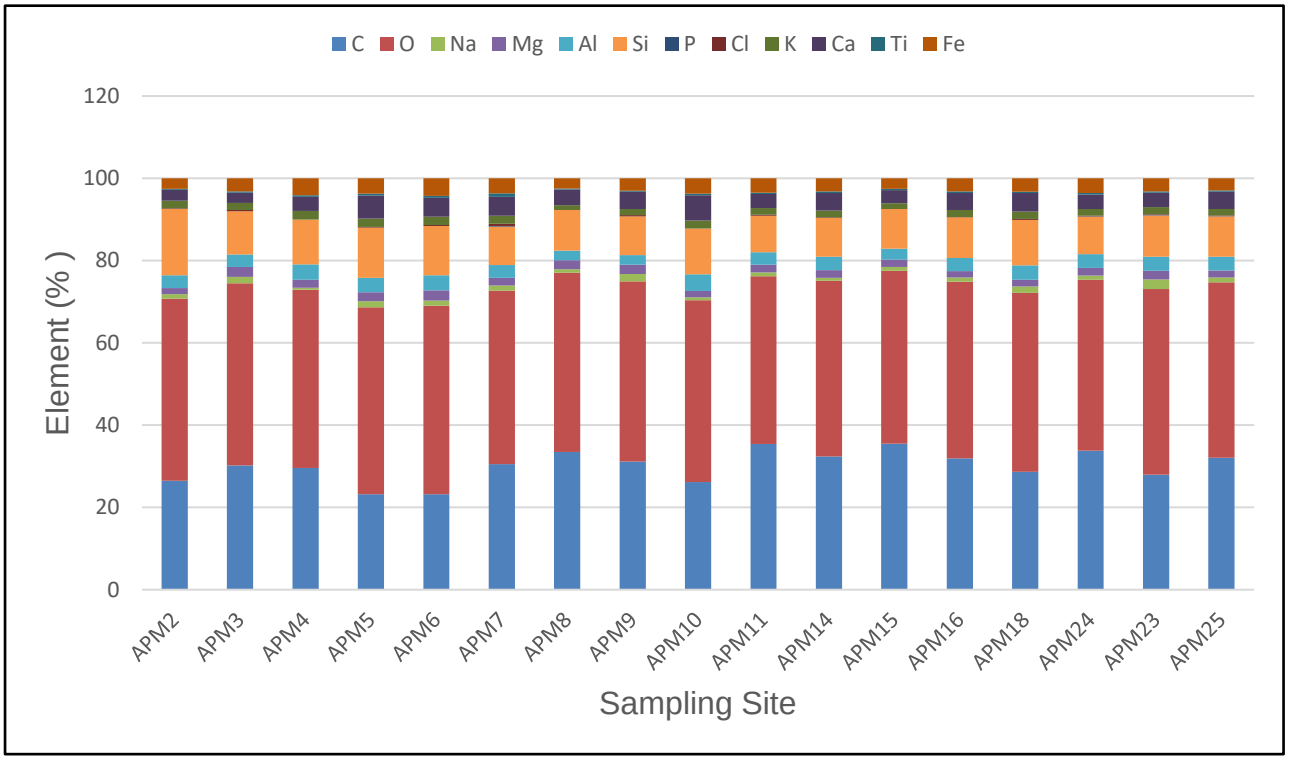

Figure 4.21 The relative number abundance (%) of the particles in the analysed PM samples collected from the town of Arandis

. The particle at magnification 2 µm collected from site APM7 in the town of Arandis shows the elemental composition of C, O, Al, Si, Ca, Fe, Na, Mg, P, K, Ti. The normalised spectrum of the spectrum shows the dominant peak of C, O, Si, Ca and Fe followed by trace elements, Ti, Cl, and P. The high presence of C and O are likely to be products of combustion.

In addition, the presence of Fe and Ti are products of mining activities such as purification of minerals which generates wastes water containing Fe and Ti as by products. Al and Si are linked to the presence of silicates and alumina silicates which are mainly derived from crustal source.

The silica particles are composed of silica and oxygen alone and these are represented by residual quartz as illustrated in Figure 4.22 (I). The presence of Fe can also be attributed to combustion of fossil fuel in vehicles (Battachayo, 2013). The morphology of this particle spheroidal to irregular with rough surfaces. The SEM micrographs of the PM samples collected from the town of Arandis were analyzed for average grain size, morphology

and elemental composition. Figure 4.22 (J) shows the SEM/EDX micrograph PM of particle from site APM14 magnified at 4 µm and shows the elemental percentages of C, O, Al, Si, Ca and Fe with minor Na, Mg, Cl, K and Ti. The dominance of Ca, Si and Al may reflect soil and ash as the source of this particle while Ca may be originating from building material that are used for construction in the mine (Xie et al, 2005) and surface soils and this suggest they are metal particles. The morphology of the particle's ranges from slates, elongated and large irregular shapes. Figure 4.22 (K) represents a SEM photo at 10 000 magnification, with a magnification of 2 µm collected from site APM20. The micrographs illustrate that there are many ultra-fine particles with most of them less than 1 um.

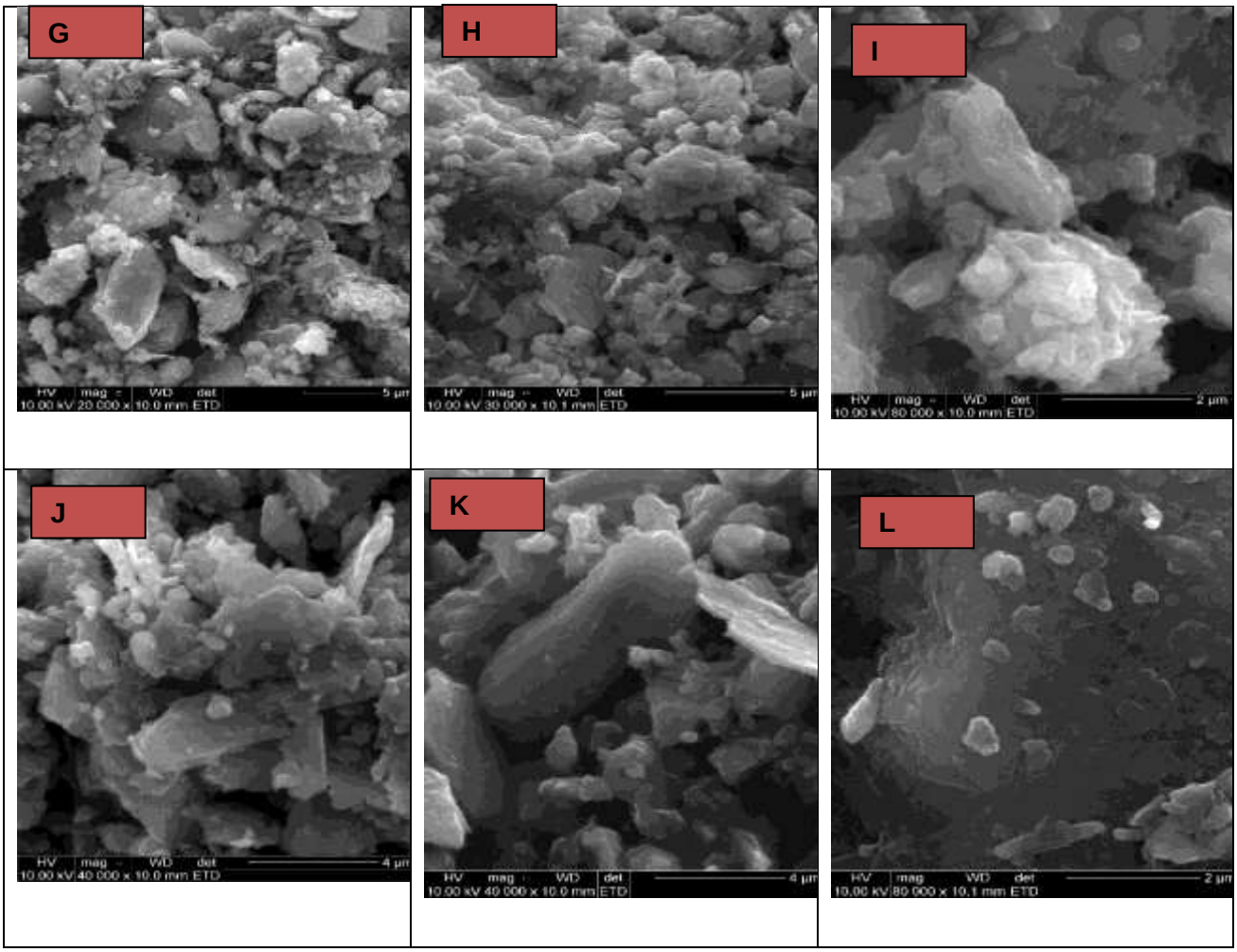

Figure 4.22 SEM micrographs of G) biogenic particles; H) aluminosilicates; I) quartz particles; J) metal particles; K) clay particles; L) non-biogenic C-rich particles

The morphology of these particles are irregular showing some triangular sharp edges, which are crushed or chamfered edges which are due to mechanical impacts due to mobilisation and transport by wind and these are clay particles. The composition of the particle is made up C, O, Al, Fe, Ca and Si which are dominant with traces of P, Cl, Na, Mg, K.

While Figure 4.22 (L) is a SEM micrograph magnified at 2 µm collected from APM24 in Arandis town. The morphology is composed of small spheroids particles with smooth edges and some of them are completely bonded forming an agglomerate state such as a platelet. These are non-biogenic C-rich particles, which are combined to form linear or branched -chain with armphous structure. The elemental composition consists of C, Al, O, K , and Fe.

4.5.4 Respiratory inhalability, deposition and particle size of PM

The inhalability fraction (IF) and deposition fraction (DF) for PM10, PM2.5 and PM1.0 of samples collected from the two mining towns of Arandis and Karibib were computed by using equation 3.17, 3.18 and 3.20 and the results are presented in Table 4.8. The inhalable fraction (IF) ranges from 0.912204 to 0.998314 while the deposition fraction (DF) varied from 0.082345 to 1.383342 in all the samples in the study area. Detailed information about IF and DF for each sample is provided in D.

Table 4.8 Inhalable, deposition and particle size in µm in PM samples

Diameter (D)	**Karibib town**		**Arandis town**	
	Inhalable Fraction (IF)	**Deposition Fraction (DF)**	**Inhalable Fraction (IF)**	**Deposition Fraction (DF)**
10	0.923841	0.09481	0.912204	0.082345
2.5	0.961347	0.267254	0.959693	0.241866
1.0	0.991937	0.969545	0.998314	1.383342
Maximum	0.923841	0.094810	0.912204	0.082345
Minimum	0.991937	0.969545	0.998314	1.383342
Average	**0.959042**	**0.443870**	**0.956737**	**0.569184**

The data from Table was subjected to polynomial regression to evaluate the relationship between deposition fraction (DF) and particle size and the results are presented in Figure 4.23 and Figure 4.24. In both Figures, it can be deduced that the that the particle size and respiratory deposition are highly correlated with values of $R^2 = 1$ for Karibib town and $R^2 = 0.94$ for Arandis town.

The polynomial regression showed a y-intercept of 1.24 for Karibib town and a y-intercept of 1.52 for Arandis town. The gradient for both towns was found to be -0.22 which illustrates an increase in respiratory deposition as particle size is decreased. The same trend was also observed with particle size and inhalability in both towns where $R^2 = 1.00$ and a gradient of -0.03 which shows an increase in inhalability as particles size becomes small and this is comparable with results reported by several authors (Kgabi, 2009; Phalen and Mendez, 2009). The relations obtained highlight the importance of particle size in relation to their potential health hazards in human beings. There is an abundance of evidence linking PM with health effects (Lee and Leu, 2013, Priya and Kuppuswami, 2012, Kumar et al, 2011; Fernandez-Navarro et al, 2012) and their toxicity depends inhalability, deposition, duration of exposure, efficiency of the exposure system delivery, the ventilation rate and sometimes gender. PM10 (particles with aerodynamic diameter $\leq$10 µm) can be attached to the upper respiratory system causing mostly sinus and sometimes asthma. PM2.5 (particles with particles with aerodynamic diameter $\leq$2.5 µm) which are inhalable particles may reach the lungs and cause lung diseases . On the other hand PM1.0 (particles with aerodynamic diameter $\leq$1.0 µm) which enters the blood stream may cause cancer and related ailment. The health problems of these PM are further compounded when the particles contain heavy metals or radioactive particles and hence it imperative to evaluate the inhalability and deposition fractions to minimise or prevent negative health associated with PM in mining communities.

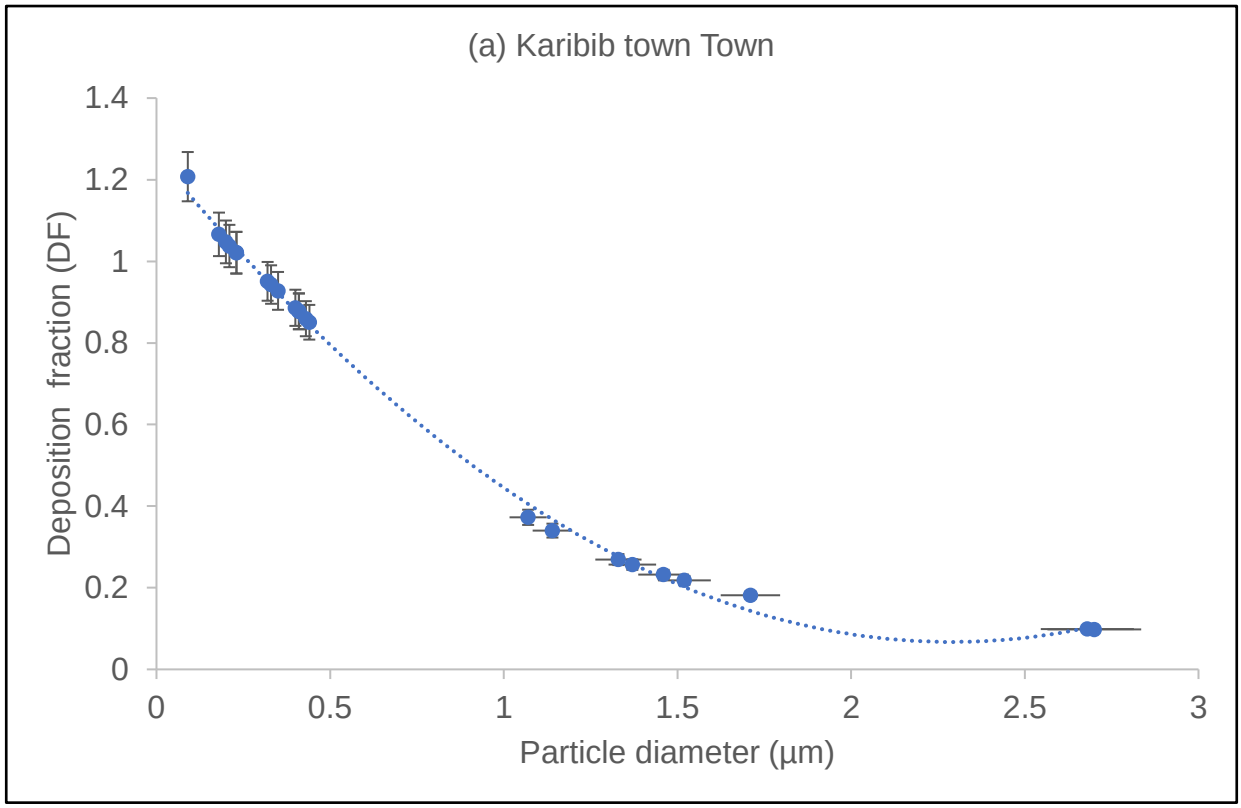

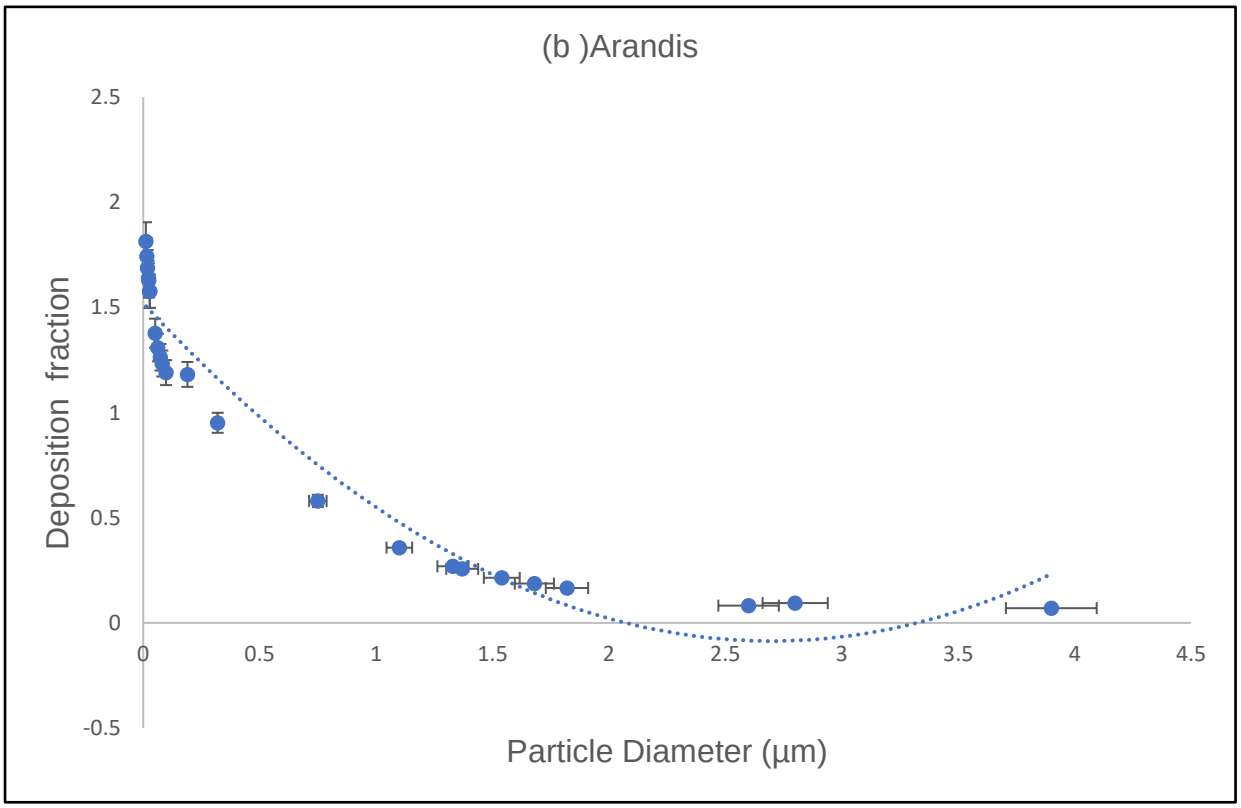

Figure 4.23 Polynomial regression of the relationship between particle diameter and deposition fraction (DF) in the town of a) Karibib town, b) Arandis town

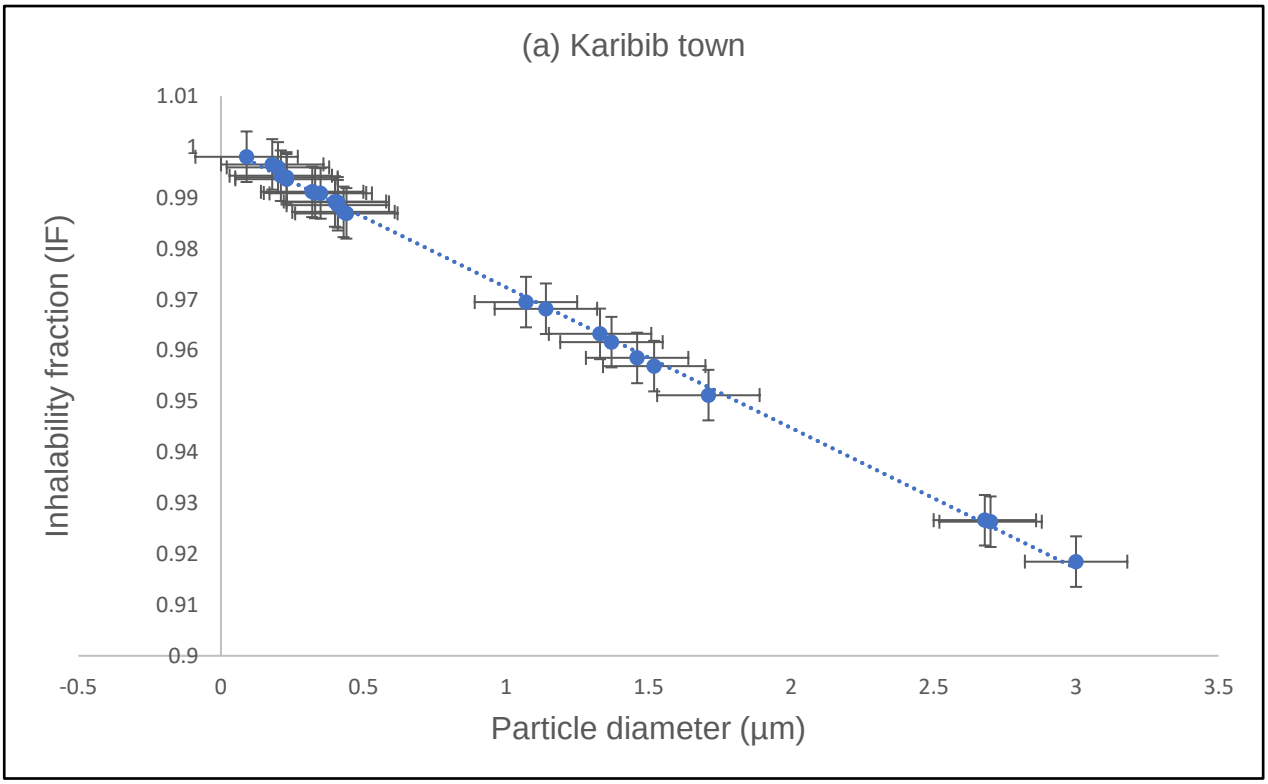

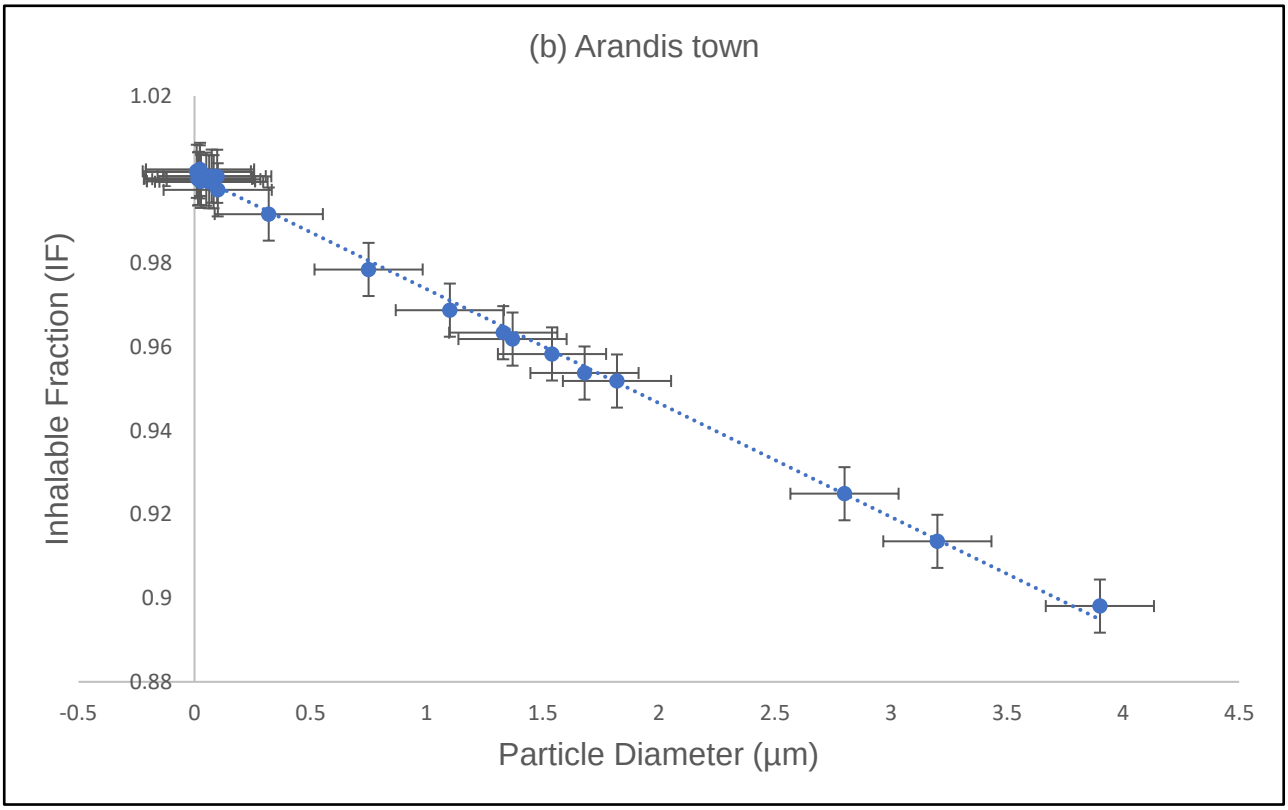

Figure 4.24 Polynomial regression of the relationship between particle diameter and inhalability fraction (DF) in the town of a) Karibib town, b) Arandis town

4.6 Toxicological risk due to toxic heavy metals

4.6.1 Introduction

Heavy metals are inherently present in the environment and they constitute an important class of toxic substance which are encountered in numerous occupational and environmental circumstances. The impact of these toxic agents on human health is a subject of intense interest due to their negative effects on health and the ubiquity of exposure. These heavy metals can induce cancer through various pathways which depends on the type of metal and time of exposure and thus it is important to prevent or reduce the exposure of individuals to contaminants that contributes directly or indirectly to increased rates of premature death, diseases or discomfort (Dockery et al., 2009) and this can be achieved through the estimation of the concentrations to which human populations may be exposed and asses the risk. The reference doses (RfD) presented in Table 5.7 and the annual daily intake (ADI) values in Table 7.6 and Table 7.7 were used to calculate non-carcinogenic human health risk exposure of heavy metals through dermal, oral and inhalation pathways.

4.6.2 Non-carcinogenic risk

4.6.2.1 The annual daily intake (ADI) for adults and children

The ADI values were calculated using equations 3.32, 3.33 and 3.34 given in chapter 3 and the results are presented in Table 4.9 and Table 4.10. The values for ingestion, inhalation and dermal routes are significantly lower than the permitted maximum tolerable daily intake (PMTDI) endorsed by WHO/FAO (Pb, 0.21 mg/person/day; Zn, 15 mg/person/day; Cu, 2.0 mg/person/day; Fe, 15.0 mg/person /day). In both adults and children population, the order of heavy metal intake in soils in the two towns of Arandis and Karibib are: Fe> Mn > Cr > Zn >Cu > Ni > Pb > As > Cd. While it is interesting to note that the ADI for all heavy metals are below the safe limit, their consumption does not imply that the health risk is eliminated. It is therefore important to evaluate the levels of heavy metals so ensure that they cannot accumulate in the food chain and illicit some health hazards. The values for ADI for all the measured metals in this study were used to calculate the Hazard quotient (HQ) and Hazard index (HI) for ingestion, inhalation and dermal pathways using equations 3.35 and 3.36.

Table 4.9 ADI values (mg/kg) for children and adult populations used for non-carcinogen Risk calculations Arandis town

Pathway	Heavy Metal									
Adults	**Cr**	**Mn**	**Fe**	**Ni**	**Cu**	**Zn**	**As**	**Cd**	**Pb**	**Total**
Ingestion	1.03E-04	2.94E-04	2.11E-02	3.42E-05	3.73E-05	6.78E-05	3.66E-06	8.25E-07	3.30E-05	**2.16E-02**
Inhalation	9.66E-09	2.77E-08	1.98E-06	3.22E-09	3.51E-09	6.38E-09	3.45E-10	7.76E-11	3.11E-09	**2.04E-06**
Dermal	3.13E-06	8.96E-06	6.41E-04	1.04E-06	1.13E-06	2.07E-06	1.12E-07	2.51E-08	1.10E-06	**6.59E-04**
Total	**1.06E-04**	**3.03E-04**	**2.17E-02**	**3.53E-05**	**3.84E-05**	**6.99E-05**	**3.77E-06**	**8.50E-07**	**3.40E-05**	**2.23E-02**
Children										
Ingestion	9.58E-04	2.75E-03	1.97E-02	3.42E-04	3.48E-04	6.33E-04	3.42E-05	7.70E-06	3.08E-04	**2.02E-01**
Inhalation	2.69E-08	7.70E-08	5.51E-06	8.96E-09	9.76E-09	1.78E-08	9.59E-10	2.16E-10	3.64E-09	**5.66E-06**
Dermal	1.53E-06	4.39E-06	3.14E-04	5.11E-07	5.56E-07	1.01E-06	5.47E-08	1.23E-08	4.93E-07	**3.23E-04**
Total	**9.59E-04**	**2.75E-03**	**1.97E-01**	**3.20E-04**	**3.48E-04**	**6.34E-04**	**3.42E-05**	**7.71E-06**	**3.09E-04**	**2.02E-01**

Table 4.10 ADI values (mg/kg) for children and adult populations used for non-carcinogen Risk calculations Karibib town

Pathway	Heavy Metal									
Adults	**Cr**	**Mn**	**Fe**	**Ni**	**Cu**	**Zn**	**As**	**Cd**	**Pb**	**Total**
Ingestion	6.66E-05	1.58E-04	6.71E-03	3.30E-05	1.62E-05	3.49E-05	1.67E-06	7.66E-07	1.00E-05	**7.03E-03**
Inhalation	6.27E-09	1.48E-08	6.32E-07	3.11E-09	1.52E-09	3.29E-09	1.57E-10	7.21E-11	9.41E-10	**6.62E-07**
Dermal	2.03E-06	4.80E-06	2.04E-04	1.01E-06	4.92E-06	1.06E-06	5.09E-07	2.33E-08	3.05E-07	**2.14E-04**

Total	**6.86E-05**	**1.62E-04**	**6.92E-03**	**3.40E-05**	**1.67E-05**	**3.60E-05**	**3.77E-06**	**7.89E-07**	**1.03E-05**	**7.25E-03**
Children										
Ingestion	6.21E-04	1.47E-03	6.26E-02	3.08E-04	1.51E-04	3.21E-04	1.56E-05	7.15E-06	9.33E-05	**6.56E-02**
Inhalation	1.74E-08	4.12E-08	1.76E-06	8.64E-09	4.23E-09	9.15E-09	4.38E-10	2.00E-10	2.62E-09	**1.84E-06**
Dermal	9.94E-06	2.35E-06	1.00E-04	4.93E-07	2.41E-07	5.22E-07	2.50E-08	1.14E-08	1.49E-07	**1.05E-04**
Total	**6.22E-04**	**1.47E-03**	**6.28E-02**	**3.09E-04**	**1.51E-04**	**3.27E-04**	**1.56E-05**	**7.16E-06**	**9.35E-05**	**6.57E-02**

4.6.2.2 The hazard quotient (HQ) and hazard index (HI) for adults and children

Human health risk assessment of heavy metals in the soils and PM from the two town of Arandis and Karibib through three different pathways (ingestion, inhalation, and dermal contact) was performed for children and adults (Table 4.11 and 4.12). As can be seen in these two Tables, the HQ values for ingestion (HQ_{Ing}), inhalation (HQ_{Inh}), and dermal (HQ_{Derm}), pathways for children and adults, the values for Arandis town was higher than Karibib town except for (inhalation, HQ_{Inh}) in adults.

Table 4.11 Hazard quotient (HQ) and hazard index (HI) values of each metal for children and adult population from the town of Arandis

Pathway	**Heavy Metal**									
Adults	**Cr**	**Mn**	**Fe**	**Ni**	**Cu**	**Zn**	**As**	**Cd**	**Pb**	**Total**
HQ_{Ing}	3.42E-02	6.26E-03	2.51E-03	1.71E-03	9.32E-04	2.26E-04	1.22E-02	8.25E-04	9.43E-03	**6.83E-02**
HQ_{Inh}	3.38E-06	1.94E-03	9.01E-03	1.56E-07	8.72E-08	2.13E-08	1.15E-06	7.76E-08	8.83E-07	**1.10E-02**
HQ_{Derm}	6.25E-02	4.87E-03	9.16E-07	1.93E-04	9.45E-05	3.44E-05	9.07E-04	2.51E-03	1.91E-03	**7.30E-02**
HI	**9.67E-02**	**1.31E-02**	**1.15E-02**	**1.90E-03**	**1.03E-03**	**2.61E-04**	**1.31E-02**	**3.34E-03**	**1.31E-02**	**1.52E-01**

Children										
HQ_{Ing}	3.19E-01	5.84E-02	2.34E-02	1.60E-02	8.69E-03	2.11E-03	1.14E-01	7.70E-03	8.80E-02	**6.38E-01**
HQ_{Inh}	9.40E-06	5.39E-03	2.51E-02	4.35E-07	2.43E-07	5.92E-08	3.19E-06	2.16E-07	2.46E-06	**3.05E-02**
HQ_{Derm}	3.07E-02	2.39E-03	4.49E-07	9.47E-05	4.64E-05	1.69E-05	4.45E-04	1.23E-03	9.39E-04	**3.58E-02**
HI	**3.50E-01**	**6.62E-02**	**4.85E-02**	**1.61E-02**	**1.51E-04**	**2.13E-03**	**1.14E-05**	**8.93E-03**	**8.90E-02**	**7.04E-01**

Table 4.12 Hazard quotient (HQ) and hazard index (HI) values of each metal for children and adult population Karibib town

Pathway	**Heavy Metal**									
Adults	**Cr**	**Mn**	**Fe**	**Ni**	**Cu**	**Zn**	**As**	**Cd**	**Pb**	**Total**
HQ_{Ing}	2.22E-02	3.35E-03	7.99E-03	1.65E-03	4.04E-04	1.16E-04	5.57E-02	7.66E-04	2.86E-03	**3.77E-02**
HQ_{Inh}	2.19E-06	1.04E-03	2.87E-03	1.51E-07	3.78E-08	1.10E-08	5.23E-06	7.21E-08	2.67E-07	**3.91E-02**
HQ_{Derm}	4.05E-02	2.61E-03	2.92E-07	1.86E-04	4.10E-05	1.77E-05	4.14E-04	2.33E-03	5.80E-03	**4.67E-02**
HI	**6.27E-02**	**7.00E-02**	**3.67E-03**	**1.84E-03**	**4.45E-03**	**1.34E-04**	**5.99E-03**	**3.10E-03**	**3.44E-03**	**8.83E-02**
Children										
HQ_{Ing}	2.07E-01	3.13E-02	7.46E-03	1.54E-02	3.77E-03	1.09E-03	5.20E-02	7.15E-03	8.67E-02	**3.52E-01**
HQ_{Inh}	6.09E-06	2.88E-03	7.99E-03	4.20E-07	1.05E-07	3.05E-08	1.45E-06	2.00E-07	7.44E-06	**1.09E-02**
HQ_{Derm}	1.99E-02	1.28E-03	1.43E-07	9.13E-05	2.01E-05	8.69E-05	2.03E-04	1.14E-03	2.84E-04	**2.29E-02**
HI	**2.27E-01**	**3.54E-02**	**1.54E-02**	**1.55E-02**	**3.79E-03**	**1.10E-03**	**5.22E-02**	**8.29E-03**	**2.70E-02**	**3.86E-01**

.

A comparison of the pathways by which heavy metals becomes hazardous to both the children and population illustrates that elements: Cr, As and Pb are more hazardous through the ingestion route ($\mathbf{HQ_{Ing}}$), Mn and Fe through the inhalation route ($\mathbf{HQ_{Inh}}$) while Cr, Mn and Cd through the dermal route ($\mathbf{HQ_{Dermal}}$). The findings show that the hazard quotient (HQ) of all heavy metals from the towns of Arandis and Karibib were less than 1 in all the collected samples. Since HQ is <1, then there is no non-carcinogenic significant risk to the populations in these towns. Although there is no noticeable health risk to local population of exposure to individual metals in soil and PM, potential risk could be synergistic when considering all the heavy metals (Sinha et al., 2006; Zheng et al., 2007). Hence it is important to estimate hazard index which assess the multiple effects of all heavy elements and routes of exposure. The calculated HQs values in the two towns of Arandis and Karibib for heavy metals for children and adults were in order of Cr > As > Pb > Mn > Fe > Ni > Cu > Cd > Zn. for $\mathbf{HQ_{Ing}}$, Fe > Mn > Cr > As > Pb > Ni > Cu > Cd > Zn. for $\mathbf{HQ_{Inh}}$, Cr > Pb > Mn > Cd > As > Ni > Cu > Zn > Fe. for $\mathbf{HQ_{Dermal}}$. The order of the heavy metals obtained was comparable to that of a previous study by Shabbaj et al., (2018) in the road dust of Jeddah, Saudi Arabia. In addition, the HQ values for the three pathways in measured results for children and adults decreased in the following order: ingestion > dermal contact > inhalation. The contributions of $\mathbf{HQ_{Ing}}$, $\mathbf{HQ_{Inh}}$ and $\mathbf{HQ_{Dermal}}$ to HI were 49.79%, 43.98% and 6.18% for adults, 90.82%, 5.41% and 3.76% for children, respectively, which demonstrate that ingestion was the route of exposure of heavy metals in soils and PM in the two towns of Arandis and Karibib. These results are in agreement with those reported in other studies (H. Li, Qian, Hu, Wang, & Gao, 2013; X. Li et al., 2013; Liu, Yan, Birch, & Zhu, 2014; Mohmand et al., 2015; Wang et al., 2016).

4.6.2 Assessment of carcinogenic health risk due to heavy metal exposure

The cancer risk (CRA) for the selected heavy metals (Cr, As, Cd and Pb) in soil was estimated for ingestion, inhalation and dermal mode of exposure for both adults and children living in the town of Arandis and the results are presented in Table 4.13. The results showed that the total cancer risk (CRA) due to exposure to soil through the three pathways was found to be 1.40×10^{-3} and 1.30×10^{-2} in both adults and children, respectively.

The main mode of exposure to heavy metals is through ingestion with a CRA value of 1.40×10^{-3} in adults and 1.30×10^{-2} in children and the least is through inhalation pathway with CRA value of 4.62×10^{-9} in adults and 8.21×10^{-8} in children. It is interesting to note exposure to Pb poses the greatest cancer risk to the inhabitants of Arandis town than any

other metals in all the measured samples. This is because Pb is widely distributed in the soil due to natural processes such as breakdown of rocks and soil and partly, it can be enriched through anthropogenic processes such as uranium mining and processing.

Table 4.13 Carcinogenic risk assessment (CRA) of each heavy metal for children and adult population living in the town of Arandis

Pathway	Heavy Metal				
Adults	**Cr**	**As**	**Cd**	**Pb**	**Total**
HQ_{Ing}	4.21E-06	5.49E-06	n.a	1.39E-03	**1.40E-03**
HQ_{Inha}	4.06E-09	5.21E-11	4.89E-10	2.64E-11	**4.62E-09**
HQ_{Dermal}	n.a	1.67E-07	n.a	n.a	**1.67E-07**
Total	**4.21E-06**	**5.66E-06**	**4.89E-10**	**1.39E-03**	**1.40E-03**
Children					
HQ_{Ing}	3.93E-05	5.13E-05	n.a	1.29E-02	1.30E-02
HQ_{Inha}	1.13E-08	1.45E-10	1.36E-09	7.35E-11	1.29E-08
HQ_{Dermal}	n.a	8.21E-08	n.a	n.a	8.21E-08
Total	**3.93E-05**	**5.14E-05**	**1.36E-09**	**1.29E-02**	**1.30E-02**

The results for carcinogenic risk assessment (CRA) of the selected heavy metals for children and adult population living in the town of Karibib are shown in Table 4.14. Table 4.14 shows that the order cancer risk exposure was: ingestion > dermal > inhalation for both children and adults. The total cancer risk for children is higher than the adults with values of 4.25×10^{-4} and 3.97×10^{-3} respectively. The higher chances can be attributed to the law of "Bergonie and Tribondeau' which states the young, actively growing and undifferentiated cells are prone to cancer than the mature, specialised and differentiated cells.

A comparison of CRA in the two towns also shows the total cancer risk is higher in the town of Arandis than in Karibib for both adults and children. Furthermore, the computed total cancer risk value for adults (1.40×10^{-3}) and children (1.30×10^{-2}) in the town of Arandis, cancer risk value of 4.25×10^{-4} in adults and 3.97×10^{-3} in children in the town of Karibib were higher than the worldwide average Excess Cancer Risk due to exposure to radionuclides from terrestrial origin (0.29×10^{-3}) (Taskin et al., 2009) and thus they are higher chances of increase in cancer among the inhabitants of Arandis and Karibib town.

Table 4.14 Carcinogenic risk assessment (CRA) of each heavy metal for children and adult population living in the town of Karibib

Pathway	Heavy metal				
Adults	**Cr**	**As**	**Cd**	**Pb**	**Total**
HQ_{Ing}	2.73E-06	2.51E-06	n.a	4.20E-04	**4.25E-04**
HQ_{Inha}	2.63E-09	2.38E-11	4.54E-10	8.00E-12	**3.12E-09**
HQ_{Dermal}	n.a	7.63E-08	n.a	n.a	**7.63E-08**
Total	**2.73E-06**	**2.58E-06**	**4.54E-10**	**4.20E-04**	**4.25E-04**
Children					
HQ_{Ing}	2.55E-05	2.34E-05	n.a	3.92E-03	**3.97E-03**
HQ_{Inha}	7.32E-09	6.61E-11	1.26E-09	2.23E-11	**8.67E-09**
HQ_{Dermal}	n.a	3.74E-08	n.a	n.a	**3.74E-08**
Total	**2.55E-05**	**2.34E-05**	**1.26E-09**	**3.92E-03**	**3.97E-03**

n.a mean that the CSF data was not available from literature.

CHAPTER 5 : CONCLUSION AND RECOMENDATIONS

5.1 Summary and conclusion

Human activities such as mineral mining and exploration may discharge large quantities of radioactive and heavy metal bound PM into the atmosphere which can be carried to nearby communities where it has negative effects on health and the environment (Hu et al, 2011; Sun et al, 2013). The aim of this study was to investigate levels of radionuclides and heavy metals in particulate matter (PM) around uranium and gold mine towns of Erongo region in Namibia. The research sheds light on methods designated for the measurement of environmental radioactivity and heavy metals and assesses their effects on human health and environment. Measurements of the samples was also performed in soil samples due to a close association between soil and PM.

One of the objectives of this study was to evaluate radionuclides concentrations and in PM and soil associated with mining activities. This objective was achieved, and results showed that the mean activity concentrations of ^{226}Ra, ^{238}U, ^{232}Th, ^{40}K and ^{210}Pb in the PM and soil in the two towns of Karibib and Arandis were two times higher than the worldwide average values. Furthermore, the activity concentrations of ^{226}Ra was always higher than ^{238}U. This is partly due to physicochemical properties of ^{226}Ra as opposed to ^{238}U. When both radionuclides are undergoing radioactive decay, ^{238}U may be deposited directly into soil surface where it can contribute to the terrestrial radiation. However, 226Ra may interact with aerosol particles and which it is deposited on soil surface, it is lost to underground water surfaces.

According to Gupta et al., (2010), the universal standards for safe limit of radionuclides in soil is prescribed with a conservative upper limit of 1000 Bq.kg^{-1} for ^{238}U, 1000 Bq.kg^{-1} and 4000 Bq.kg^{-1} for ^{40}K. Although the mean activity concentrations values of radionuclides in this study were significantly higher than the worldwide values of 33 Bq.kg^{-1} for ^{238}U, 45 Bq.kg^{-1} for ^{232}Th and 412 Bq.kg^{-1} for ^{40}K (UNSCEAR, 2000), they are within the safe limits. The radiological parameters in the study area was considered in terms of the absorbed dose(D), the annual effective dose equivalent (AEDE), the radium equivalent activity concentrations ($\mathrm{Ra_{eq}}$), the external hazard index ($\mathrm{H_{ex}}$), the internal hazard index ($\mathrm{H_{in}}$). The results show that the AEDE was less than 1 mSv.y^{-1}, the prescribed safe limits by International Commission of Radiation Protection (ICRP).

The second objective was to determine the indoor radon concentrations in selected households in the two mining towns of Arandis and Karibib. This objective was met and the

results revealed that radon concentrations in the selected dwellings varied from 70 $Bq.m^{-3}$ to 100 $Bq.m^{-3}$ while the mean indoor radon concentrations was found to be 88 Bq/m^3 which corresponds to an annual effective dose rate due to inhalation of radon and its decay products 2.22 $mSv.y^{-1.}$ This value is two times higher than the worldwide average value of 1.26 $mSvy^{-1}$. (UNSCEAR, 2000). The obtained values are not surprising as the geology of Erongo region of Namibia is composed of uranium bearing ores. Radon and its progeny will be emanating from the radioactive decay of uranium in the ores and hence elevating its concentrations in the dwellings. Other factors that can be attributed to higher concentrations of radon and its decay products include the type of building material used for the construction of these houses, ventilation, and time of the day. The high concentrations of radon and its decay products in the studied dwellings pose a health risk to inhabitants of these two towns and these factors will be elucidated on the objective of assessment of health risk due to exposure to gamma emitting radionuclides.

The third objective in this study was to investigate levels of toxic heavy metals in soil and this objective was met and the toxic heavy metal in soil samples were analysed for heavy metal loads associated with mining activities in the study area. The results revealed that mean concentrations for soil samples in $mg.kg^{-1}$ in Arandis town was Fe (15372), Mn (214.73), Cr (74.92), Zn (49.52), Cu (27.20), Ni (24.99), Pb (24.10), As (2.67) and Cd (0.60) while in Karibib town was Fe (4897.60), Mn (115.46), Cr (48.58), Zn (25.52), Ni (24.11), Cu (11.76), Pb (7.30), As (1.22), and Cd (0.56). The obtained values were compared with results from other countries, FAO/WHO soil guidelines and they were found to be within the allowable limits. The degree of heavy metal pollution was quantified by evaluation of four indices and these are: contamination factor (CF), enrichment factors (EF), pollution load index (PLI) geoaccumulation index (Igeo). Since the pollution load index (PLI) <1, the geoaccumulation index had negative values for most of the measured samples in this study, the contamination factor (CF), it can be concluded that the soils are not polluted. A correlation analysis between different metals indicates that these variables may be derived from a common origin, especially from mining activities and natural processes such as weathering.

The fourth objective was to conduct a morphological analysis of PM associated with mining activities. In addition to this objective, the respiratory inhalable fraction (IF) and deposition fraction (DF) in the PM in the two towns of Karibib and Arandis was also determined to establish their relationship with particle size as these are potentially hazardous to the inhabitants of this area. The morphology of the particles identified ranges from slate,

elongated, to irregular and with some showing some smooth edges. The PM samples in the studied area were analysed for elemental composition and characterise the major particles. All the samples collected from the two towns of Karibib and Arandis were found to composed of the following elements in different proportions: C, O, Na, Mg, Si, P, K, Ca, Ti, Fe and Cu. Based on the amount of elements present in each particle, it can be concluded that the identified major particles in PM samples in the study area were: biogenic particles, soot, aggregates, aluminosilicates, mineral particles, quartz particles, clay particles, and non-biogenic C rich particles. Furthermore, polynomial regression was applied to determine the relationship between the particle size and respiratory inhalable fraction (IF), particle size and deposition fraction in the PM. The results showed a strong correlation relationship of R^2 =0.99 between respiratory inhalabity (IF) and particle size i.e. an increase inhalable fraction as the particle diameter becomes small. Similarly, the same trend is observed between deposition fraction (DF) and particle size. The findings are consistence with previous studies on the investigation of total deposition of PM in healthy lungs under controlled breathing conditions (Jaques and Kim, 2000; Daigle et al., 2003), who have indicated that total lung deposition increases with a decrease in particle size within the ultrafine size range.

This relationship between particle size, inhalability and deposition of PM in the respiratory system is critical for assessment of potential health effects of inhaled particles. Since the findings from this study shows PM <1 are the dominant fractions, it can be concluded that there is need to take preventative measures by the inhabitants of these two mining towns so as to minize cancer induced by these particles as they can be inhaled and deposited in the alveolar lining where they can enter the blood stream and cause biological damage.

The final objective was to evaluate the human health risk due to exposure to gamma-emitting radionuclides and heavy metals associated with mining activities in the study area and this objective was achieved. The measured radionuclides in the soil and PM in the studied area were evaluated for Excess Lifetime Cancer Risk (ELCR) and the mean values was found to be 0.43 x 10^{-3}. The findings illustrate that the ELCR in the studied area is one and half times higher than the world average of 0.29 x 10^{-3} (Taskin et al., 2009). This implies that the chances of having cancer by the general populace is higher due to activity of the radionuclides.

As a complementary to assessment of health risk due to exposure to gamma-emitting radionuclides, carcinogenic and non-carcinogenic health risk exposure due to heavy metals

were also assessed in the measured samples. Non carcinogenic risk of heavy metals for adults and children through different exposure pathways in all the samples were evaluated and it was found that the total HQ children (Karibib town: 3.86 x 10^{-1} and Arandis town: 7.04 x 10^{-1}) is higher than adults (Karibib town: 8.83 x 10^{-2} and Arandis town: 1.52 x 10^{-1}). The findings show that the hazard quotient (HQ) of all heavy metals from the towns of Arandis and Karibib were less than 1 in all the collected samples. Since HQ is <1, then there is no non-carcinogenic significant risk to the populations in these towns.

Carcinogenic health risk in heavy were performed on four of the most toxic metals and these are: Cr, As, Cd and Pb. The findings on for carcinogenic risk assessment (CRA) in the selected toxic metals were in order of: ingestion > dermal > inhalation for both children and adults in the studied area. It can also be deduced that children are more vulnerable cancer due to exposure to toxic metals as compared to adults in both mining towns. For example, in Karibib town the CRA for children was 3.97 x 10^{-3} compared to 4.25 x 10^{-4} for adults and this can be attributed to the fact that children have actively growing cells which are prone to cancer induction as opposed to adults. According to US Environmental Protection Agency, the acceptable limit for cancer risk for regulatory purpose ranges between 1 x10^{-6} and 1 x 10^{-4} (USEPA, 1989) and the results from this study does not fall within these limits. It can be concluded that the radionuclides and heavy metal content in PM and soil in the two mining towns should be monitored to reduced ailment due to exposure to the pollutants.

5.2 Recommendations for future directions

The results of this study indicate the distribution of ^{226}Ra, ^{210}Pb, ^{238}U, ^{232}Th and ^{40}K in PM and soil samples in the town of Karibib and Arandis of Erongo region of Namibia. In order to obtain a statistically significance information on the distribution of these radionuclides in the environment, the number of samples and the geographical analysed can be increased. The initial intention was to take measurements at least three times a year and assess the seasonal variation of theses radionuclides in each geographical location. If the research is performed on a large scale, the results can be used to draw up a radiological map for the given geographical location. Another school of thought equally important in future studies is to evaluate the relationship between grain size of PM and radioactivity and this will be critical in assessment of the potential health hazards of these radionuclides. Physico-chemical parameters such as soil pH, temperature, electrical conductivity, type of soil also affect the

migration of radionuclides and heavy metals. The relationship between the transport, migration of radionuclides and heavy metals can be interesting areas of research in the future.

It is well documented that radon gas and its progeny contributes more than 50 % to the total natural radiation received by human beings. In this study, fewer samples were analysed by passive solid-state nuclear track detectors (SSND). There are short term and seasonal variation in radon gas and its progeny in each geographical location. The original intention was to collect samples three times a year, but this was not possible because of logistical and time limitations. Also, in important to consider is in situ measurements of indoor radon gas and its progeny as these improves the accuracy of the results. These should be considered in future studies. Further studies are also suggested in the developing a laboratory method to investigate the evaporative effect of radon exhalation rate and geochemical speciation of radionuclides such ^{238}U in the soil in Erongo region of Namibia.

In cancer risk assessment due to exposure to radionuclides and heavy metal exposure, future studies may consQider using the complementary lung model to mimic the conditions that exists in the real world. Parameters such as the inhalability of particles, deposition, ventilation rate, duration of exposure may also be considered in future studies.

A further study can also be done to include investigation the concentration of radionuclides and heavy metals in water and vegetation from the mining towns. Radionuclides and heavy metals associated with mining sites can be deposited in soil and water bodies and these can be taken up by plants via the food chain. This study could not be extended to cover radionuclides and heavy metals in plant and water bodies because of logistics and time limitations.

REFERENCES

Abidin, E. Z., Semple, S. Rasdi, I., Ismail, S. N. S., & Ayres, J. G. (2014). The relationship between air pollution and asthma in Malaysia school children. *Air qQuality aAtmospheric Health*, 7, 214-432.

Ademola, A. K., Bello, A. K., & Adejumobi, A. C. (2014). Determination of natural radioactivity and hazard in soil samples in and around gold mining area in Itagunmodi, south-western, Nigeria. *Journal of Radiation Research and Applied Sciences*, *7*(3), 249–255.

Ahad, A., Rehman, S., Rehman, S., Faheem, M., & Matiullah, X. (2004). Measurement of radioactivity in the soil of Bahawalpur division, Pakistan. *Radiation Protection Dosimetry*, 112(3), 443–447.

AHEMC (AnHui Environmental monitoring centre). (1992). The research report of background soil Environmental inAnHui Province:78.

Ahmed, N., Abbady, A., El Arabi, A., Abbady, A., Michel, R., & El-Kamel, A. (2006). Comparative study of the natural radioactivity of some selected rocks from Egypt and Germany. *Indian Journal of Pure and Applied Physics*, *44*(3), 209–215.

Ajayi, O.S and Ajayi, I.R. (1999). A survey of environmental gamma radiation levels of some areas of Ekiti and Ondo sates, Southwest Nigeria. *Nigerian Journal of Physics*, 11: 17-21.

Alahmr, F. O. M., Othman, M., Wahid, N. B. A., Halim, A. A., & Latif, M. T. (2012). Compositions of dust fall around semi-urban areas in Malaysia. *Aerosol Air Qual Res*, *12*, 629–642.

AlausaShamsideen, K. (2014). Radiological assessment of soils on the waysides of the road under construction in Ijebu-Ode, Ogun State, Southwestern Nigeria. *Journal of Natural Sciences Research*, *4*(15).

Al-Bataina, B., Ismail, A., Kullab., M, Abumurad, K., Mustafa, H., (1997). Radon measurements in different types of natural waters in Jordan. *Radiation Measurements.* 28(1), 591-594.

Al-Hamarneh, I. F., & Awadallah, M. I. (2009). Soil radioactivity levels and radiation hazard assessment in the highlands of northern Jordan. *Radiation Measurements*, 44(1), 102–110.

Alharbi, S. (2016). Measurement and monitoring of naturally occurring radioactive materials for regulation. Queensland Uuniversity of Technology Science, and engineering faculty, Phd thesis.

Ali, M. U., Liu, G., Yousaf, B., Abbas, Q., Ullah, H., Munir, M. A. M., & Fu, B. (2017). Pollution characteristics and human health risks of potentially (eco) toxic elements (PTEs) in road dust from metropolitan area of Hefei, China. *Chemosphere*, *181*, 111–121.

Aliyu, A. S., and Ramli, A. T. (2015). The world's high background natural radiation areas (HBNRAs) revisited: A broad overview of dosimetric, epidemiological and radiobiological issues. *Radiation Measurements.* 73 M 51-59

Alloway, B. J. (2013). Sources of heavy metals and metalloids in soils. In *Heavy mMetals in sSoils* (pp. 11–50). Springer.

Alloway, B., & Ayres, D. C. (1997). *Chemical pPrinciples of environmental pPollution*. CRC press.

Alloway, B.J. (1995), Soil Pprocesses and the Bbehaviour of Hheavy Mmetals. In: Heavy metals in soils (2nd edition) (B.J. Alloway ed). New York: Blackie.

Al-Masri, MS and A. Aba. (2005). "Distribution of scales containing NORM in different oilfields equipment." *Applied Radiation and Isotopes* 63 (4): 457-463.

Amin, Y. M., Khandaker, M. U., Shyen, A. K. S., Mahat, R. H., Nor, R. M., & Bradley, D. A. (2013). Radionuclide emissions from a coal-fired power plant. *Applied Radiation and Isotopes*, 80, 109–116.

Aniagyei, H., Oppon, O., & Kyere, A. (1996). Indoor radon measurement in traditionally constructed houses in Ghana. *Journal of the University of Science and Technology Kumasi*, *6*(3), 105–107.

Anon. (2013). PN Junction Diode Characteristics, Basic electron. Tutor.

APMC (Environmental protection Ministry of China). (2015). Standarnds of soil environmental quality of Agricultural land. Huangbanhang 69, Beijing, China

Appelo, C. A, J., and Postam, D. (2007). Geochemistry, groundwater and pollution, 2nd edition.

Appelo, C., & Postma, D. (2005). Geochemistry, groundwater and pollution. 2nd. *Ed. Balkema, Rotterdam*.

Appenroth, K.-J. (2010). Definition of "heavy metals" and their role in biological systems. In *Soil heavy metals* (pp. 19–29). Springer.

ASTM. (2009). Water and Environmental Technology. *American Society for testing and Materials, Philadephia*, 11, 01-02.

Asumadu-Sakyi, A., Oppon, O., Quashie, F., Adjei, C., Akortia, E., Nsiah-Akoto, I., & Appiah, K. (2012). Levels and potential effect of radon gas in groundwater of some communities in the Kassena Nankana district of the Upper East region of Ghana. *Proceedings of the International Academy of Ecology and Environmental Sciences*, *2*(4), 223.

ATSDR (Agency for Toxic Substances and Disease Registry). (1990). *Toxicological profile of Radon.* Atlanta: Public Health Service, U.S. Department of Health and Human Services.

ATSDR (Agency for Toxic Substances and Disease Registry). (1992). *Case Studies in Environmental medicine. Radon Toxicity.* Atlanta. Public Health Services, U.S. Department of Health and Human Services.

ATSDR (Agency for Toxic Substances and Disease Registry). (1999). *Toxicological profile of Uranium* (Update*).* Atlanta. Public Health Services, U.S. Department of Health and Human Services.

Avwiri, G., Enyinna, P., & Agbalagba, E. (2007). Terrestrial radiation around oil and gas Facilities in Ughelli Nigeria. *Journal of Applied Sciences, 7*, 1543-1546.

Awudu, AR, A. Faanu, EO Darko, G. Emi-Reynolds, OK Adukpo, DO Kpeglo, F. Otoo, H. Lawluvi, R. Kpodzro and ID Ali. (2012). "Preliminary studies on 226 Ra, 228 Ra, 228 Th and 40 K concentrations in foodstuffs consumed by inhabitants of Accra metropolitan area, Ghana." *Journal of Radioanalytical and Nuclear Chemistry* 1-7.

Bailey, D.L. and American Association of Physicists in Medicine (2014). *Nuclear medicine physics: A handbook of teachers and students* (Vienna: International atomic Energy Agency

Baishaw, S., Edwards, J., Daughtry, B., & Ross, K. (2007). Mercury in seafood: mechanisms of accumulation and consequences for consumer health. *Reviews on environmental health*, *22*(2), 91-114.

Banu, Z., Chowdhury, M. S. A., Hossain, M. D., & Nakagami, K. (2013). Contamination and ecological risk assessment of heavy metal in the sediment of Turag River, Bangladesh: An index analysis approach. *Journal of Water Resource and Protection*, *5*(02), 239.

Barescut, J., Gariel, J., Péres, J., Gaso, M., Segovia, N., & Morton, O. (2005). Environmental impact assessment of uranium ore mining and radioactive waste around a storage centre from Mexico. *Radioprotection*, *40*(S1), S739–S745.

Barescut, J., Gariel, J., Péres, J., Sheppard, S., Sheppard, M., Ilin, M. & Thompson, P. (2005). Soil-to- plant transfers of uranium series radionuclides in natural and contaminated settings. *Radioprotection*, 40 (S1): S253-S259.

Benetou-Marantidou, A., Nakou, S., & Micheloyannis, J. (1988). Neurobehavioral estimation of children with life-long increased lead exposure. *Archives of Environmental Health: An International Journal*, *43*(6), 392-395.

Beretka, J., Mathew, P.J. (1985). Natural radioactivity of Australian building materials, industrial wastes and by-products. Health Physics, 48:87-95.

Bermudez, G. M., Jasan, R., Plá, R., & Pignata, M. L. (2011). Heavy metal and trace element concentrations in wheat grains: Assessment of potential non-carcinogenic health hazard through their consumption. *Journal of Hazardous Materials*, *193*, 264–271.

Bhaskar, B. V., & Mehta, V. M. (2010). Atmospheric particulate pollutants and their relationship with meteorology in Ahmedabad. *Aerosol Air Qual. Res*, *10*(4), 301–315.

Boamponsem, L.K., Adam, J.I., Dampare, S. B., Owusu-Ansah E., Addae, G. (2010). Studies on the histopathological changes in selected tissues of fish (Labeo rohita to phenol. J. Chem Pharm Research 2: 504-527.

Bode, P. (1998). Detectors of radiation. Delft University of Technology, Netherlands.

Bou-Rabee, F. (1997). “Soil radioactivity atlas of Kuwait”. In Environmental International 23.1, pages 5-15.

Bradl, H. (2005). *Heavy metals in the environment: Origin, interaction and remediation* (Vol. 6). Elsevier.

Brandt, R. (1987). A revised stratigraphy for the Abbabis Complex in the Abbabis inlier, Namibia. South African Journal of Geology, 90 314-323.

Browne, E., Firestone, R.B and Shirley, V.S. (1986). “Table of radioactive isotopes” In: *Wiley-Interscience, New York.*

Brugge, D., Durant, J.L., & Rioux, C. (2007). Near highway pollutants in motor vehicle exhaust: A review of epidemiological evidence of cardiac and pulmonary health rises. *Environmental health*, 6, 23.

Burcham, W.E., (1973). *Nuclear Physics: An Introduction, 2nd edition*, Harlow: Longman.

Butcher, D.J. (2010). Advances in inductively coupled plasma optical emission spectrometry for environmental analysis. instrimentation Science and Technology 38 (6:458-469.

Cao, H., Chen, J., Zhang, J., Zhang, H., Qiao, L., & Men, Y. (2010). Heavy metals in rice and garden vegetables and their potential health risks to inhabitants in the vicinity of an industrial zone in Jiangsu, China. *Journal of Environmental Sciences*, *22*(11), 1792–1799.

Cember, H., & Johnson, T. (2009). Interaction of radiation with matter. *Introduction to Health Physics*, 143–202.

Chakraborty, S.R., Azim, R., Rahman, A.L.M., and Sarker. (2013). Radioactivity concentrations in Soil and Transfer Factors of Radionuclides from Soil to Grass and Plants in the Chittagong City of Bangladesh" *Journal of Physical Science*. 24 (1), 95 - 113.

Chandrajith, R., Seneviratna, S., Wickramaarachchi, K., Attanayake, T., Aturaliya, T., & Dissanayake, C. (2010). Natural radionuclides and trace elements in rice field soils in relation to fertilizer application: Study of a chronic kidney disease area in Sri Lanka. *Environmental Earth Sciences*, *60*(1), 193–201.

Chandrasekara. A., Ravisankar, R., Rajalakshmi, A., Eswarana, P. and Venkatraman, B. (2015). Assessment of natural radioactivity and function of minerals in soils of Yelagiri hills, Tamilnadu, India by Gamma-Ray spectroscopic and Fourier Transform Infrared (FTIR) techniques with statistical approach. Spectrochim. Acta. A Mol. Biolo. Spectroc. **136** 1734 -44

Charles, M. (2001). UNSCEAR Report (2000): Sources and effects of ionizing radiation. *Journal of Radiological Protection*, *21*(1), 83.

Chibowski, S., & Gladysz, A. (1999). Examination of radioactive contamination in the soil-plant system and their transfer to selected animal tissues. *Polish Journal of Environmental Studies*, *8*, 9–24.

Chiozzi, P., Pasquale, V., & Verdoya, M. (2002). Naturally occurring radioactivity at the Alps–Apennines transition. *Radiation Measurements*, *35*(2), 147–154.

Chiroma, T.M., Ebewele, R.O., F.K. Hymore, F.K. (2014), Comparative Assessment of Heavy Metal Levels in Soil, Vegetables and Urban Grey Waste Water Used for Irrigation in Yola and Kano, *International Refereed Journal of Engineering and Science (IRJES)* 3, 1-9.

Choppin, G. R., Liljenzin, J.-O., & Rydberg, J. (2002). *Radiochemistry and nuclearchemistry*: Butterworth-Heinemann

Choy, C. C., Korfiatis, G. P., & Meng, X. (2006). Removal of depleted uranium from contaminated soils. *Journal of Hazardous Materials*, 136(1), 53–60.

CLEA (Contaminated land exposure Assessment). (2009). Heavy metal guidelines in soil, Assessment of potentially toxic elements, Yara UK limited, technical bulletin No. 6

CME (Canadian Ministry of Environment). (2009). Soil, Ground Water and sediment standards for use under Part XV.1 of the Environment Protection Act. Canadian ministry of Environment. Canada.

Condomines, M., S. Rihs, E. Lloret and JL Seidel. (2010). "Determination of the four natural Ra isotopes in thermal waters by gamma-ray spectrometry." *Applied Radiation and Isotopes* 68 (2): 384-391.

Csavina, J., Field, J., Taylor, M. P., Gao, S., Landazuri, A., Betterton, E. A., & Sáez, A. E. (2012). A review on the importance of metals and metalloids in atmospheric dust and aerosol from mining operations. *Science of the Total Environment*, *433*, 58–73.

Darko, E.O. & Faanu, A. (2007). Baseline radioactivity measurement in the vicinity of a gold treatment plants. J. Appl. Sci. Tech, 10, 45-51.

Dar-yuan, L., Chia-hsing, L. (2011). Regulatory standards of heavy metal pollutants in soil and groundwater in Taiwan, SGWPR Act, National Taiwan University, Taiwan.

Das, A.,& Ferbel, T. (2003). Introduction to Nuclear and Particle Physics (2nd edition). London: World Scientific.

Das, A.K., Chakraborty, R, Cervera, M. L., & de le Guardia, M. (1995). Metal Speciation in solid matrices. *Talanta.* 42(8), 1007-1030.

Das, D. B., and Karuppasamy, C. V. (2009). Spontaneous frequency of micronuclei among the new-borns from high level natural radiation areas of Kerala in the south coast of India. Int. j. Radiat. Biology 85: 272-85.

Davidson, C.I., Phalen, R.F., & Solomon, P.A. (2005). Air borne particulate matter and human health, aerosol. *Science and Technology*, 39, 737-749.

DEA (Department of Environmental Affairs). (2010). The Framework for the Management of Contaminated Land, South Africa.

Dejeant, Adrien, Ludovic Bourva, Radia Sia, Laurence Galoisy, Georges Calas, Vannapha Phrommavanh and Michael Descostes. (2014). "Field analyses of 238 U and 226 Ra

in two uranium mill tailings piles from Niger using portable HPGe detector." *Journal of Environmental Radioactivity* 137: 105-112.

Desideri, D, C Roselli, MA Meli and L Feduzi. (2008). "Analytical methods for the characterization and the leachability evaluation of a solid waste generated in a phosphoric acid production plant." *Microchemical Journal* 88 (1): 67-73

Dlamini, T. (2014). Radionuclides and toxic elements transfer from Princess Dump to the surrounding vegetation in Roodepoort South Africa: Potential radiological Impact on Humans. MSc thesis.

Dockery, D. W. (2009). Health effects of particulate air pollution. *Annals of Epidemiology*, 19(4), 257–263.

Dockery, D. W., Pope, C. A., Xu, X. P., Spengler, J. D., Ware, J. H., Fay, M.E., Ferris, B.G., Speizer, F.E. (1993). An association between air pollution and Mortality in 6 United States cities, N Engl J Med 329: 1753-1759.

Dockery, D.W., Shwartz, J., Spengler, J. D. (1992). Air pollution and daily mortality: associations with particulate and acid aerosols. *Environmental Research,* 9(2), 362-373.

Dorr, W and Hendry. (2001). Consequential late effects in normal tissues. *Radiotherapy Oncology*. 66 223-31

Dowdall, M, ØG Selnæs, JP Gwynn and C Davids. (2004). "Simultaneous determination of 226Ra and 238U in soil and environmental materials by gamma-spectrometry in the absence of radium progeny equilibrium." *Journal of Radioanalytical and Nuclear Chemistry* 261 (3):513-521.

Duffus, J. H. (2002). “ Heavy metals” a meaningless term?(IUPAC Technical Report). *Pure and Applied Chemistry*, *74*(5), 793–807.

Durani, A and Bull, R.K. (1987). Solid State Nuclear Track Detection: Principles, Methods and Applications, Pergamon Press, Oxford.

Durani, A., & Ilic, R., (1997). Radon Measurements by Etched Track Detectors: Applications in Radiation Protection, Earth Sciences and Environment, World Scientific Pub Co Inc.

Duruibe, T. O., ogweugbu, M. O.C., Egwurugwu, J.N.(2007). Practical Information on surface Water Problems Int. J. Phys. Sc. 2: 112-118.

Duzgoren-Aydin, N., Wong, C., Song, Z., Aydin, A., Li, X., & You, M. (2006). Fate of heavy metal contaminants in road dusts and gully sediments in Guangzhou, SE China: A

chemical and mineralogical assessment. *Human and Ecological Risk Assessment: An International Journal*, *12*(2), 374–389.

Edwards, J. R., Srivastava, R. K., & Kilgroe, J. D. (2001). A study of gas-phase mercury speciation using detailed chemical kinetics. *Journal of the Air & Waste Management Association*, *51*(6), 869–877.

Eisenbud, M., & Gesell, T. (1997). *Environmental Radioactivity from Natural, Industrial, and Military Sources (4th edition)*. London: Academic Press.

Eisenbud, M., & Gesell, T. F. (1997). *Environmental Radioactivity from Natural, Industrial & Military Sources: From Natural, Industrial and Military Sources*: Academic Press.

El Afifi, EM, MA Hilal, SM Khalifa and HF Aly. (2006). "Evaluation of U, Th, K and emanated radon in some NORM and TENORM samples." *Radiation Measurements* 41 (5): 627 633.

El-Daoushy, Farid and Francisco Hernández. (2002). "Gamma spectrometry of 234 Th (238 U) in environmental samples." *Analyst* 127 (7): 981-989.

EPA, (2003). Assessment of Risk from Radon in Homes. Environment Protection Agency, Washington DC 402 (R03): 003.

EPA. (2011). Supplementary guidance for developing soils screening levels for superfund sites. Office of solid waste and emergency response (OSWER)

EPAA (Environmental Protection Agency of Australia). (2012). Classification and management of contaminated soil for disposal. Information Bulletin 105. Hobart, TAS 7001, Australia.

ESAG. (2009). Environmental site assessment guideline; DB11/T565-2009. Adelaide, Australia, Adelaide Airport.

Essumang, D., Obodai, E., Adokoh, C., Serfor-Armah, Y., Nyarko, B., Asabere-Ameyaw, A., & Boamponsen, L. (2012). Assessment of the levels of Manganese, Cobalt, Copper and Iron along the Coastal belt of Ghana. *Blue Biotechnology Journal*, *1*(1), 141.

Faanu, A., Ephraim, J. H., & Darko, E. O. (2011). Assessment of public exposure to naturally occurring radioactive materials from mining and mineral processing activities of Tarkwa Goldmine in Ghana. *Environmental Monitoring and Assessment*, *180*(1–4), 15 29.

Faanu, A., Kpeglo, D. O., Sackey, M., Darko, E, O., Emi-Reynolds, G.L., Lawluvi, H., Awudu, R., Adukpo, O.K., Kansaana, C., Ali, I. D., Agyeman, B., Agyeman, I., Kpodzro, R. (2013). Natural and artificial radioactivity distribution in soil, rock and

water of the Central Ashanti Gold Mine. Environ. Earth. Sci. http://dx.doi.org/10.1007/s12665-013-2244-z (Ghana).

Faires, R.A and Boswell, G.G. L. (1981), *Radioisotopes Laboratory Techniques, 4th edition*., Butterworth and Company limited., London.

Faroon, O., Ashizawa, A., Wright, S., Tucker, P., Jenkins, K., Ingerman, L., & Rudisill, C. (2012). Health effects. In *Toxicological Profile for Cadmium*. Agency for Toxic Substances and Disease Registry (US).

Feldmann, J., Salaun. P., Lombi, E. (2009). Critical review perspective: elemental speciation analysis methods in Environmental chemistry-Moving towards methodological integration. Environmental Chemistry. 6(4):275-289.

Flores, O. B., Estrada, A. M., Suarez, R. R., Zerquera, J. T., & Pérez, A. H. (2008). Natural radionuclide content in building materials and gamma dose rate in dwellings in Cuba. *Journal of Environmental Radioactivity*, *99*(12), 1834–1837.

Font, Ll, & Baixeras, C. (2003). The RAGENA dynamic model of radon generation, entry and accumulation indoors. *Science of the Total Environment*, *307*(1–3), 55–69.

Font, LL, Baixeras, C., Domingo, C., & Fernandez, F. (1999). Experimental and theoretical study of radon levels and entry mechanisms in a Mediterranean climate house. *Radiation Measurements*, *31*(1–6), 277–282.

Forstner G.T., Wittman, G.I.W. (1983), Mining Pollution in Aquatic Environment, *Journal of Natural Environment* 25 (4), 206-208.

Franchitto, N., Gandia-Mailly, P., Georges, B., Galinier, A., Telmon, N., Ducassé, J. L., & Rougé, D. (2008). Acute copper sulphate poisoning: a case report and literature review. *Resuscitation*, *78*(1), 92-96.

Friedlander, G. (1981). *Nuclear and radiochemistry*: John Wiley & Sons.

Friedrich, R. (2009). Natural and biogenic emissions of environmentally relevant atmospheric trace constituents in Europe. *Atmospheric Environment, 43*(7), 1377-1379.

Fu, Q.-L., Li, L., Achal, V., Jiao, A.-Y., & Liu, Y. (2015). Concentrations of heavy metals and arsenic in market rice grain and their potential health risks to the population of Fuzhou, China. *Human and Ecological Risk Assessment: An International Journal*, *21*(1), 117–128.

Ghiassi-Nejad, M., Beitollahi, M. M., Fallahian, N and Saghirzadeh, M. (2005). New findings in the very high natural radiation area of Ramsar, Iran. int. congr. Ser. 1276:13-6

Gilmore, G and Hemingway, J.D. (2008). *Practical gamma-ray spectrometry* (2nd edition). Wiley Online Library. ISBN: 978-0470861967.

Girigisu, S., Ibeanu, I., Adeyemo, D., & Okoh, S. (2012). Determination of Heavy Metals and Other Elements in Artisanal Gold Mining Soils. *American Journal of Applied Sciences*, *9*(7), 1014.

Godish, T. (2004). Air quality "Chapter 2: Atmospheric Pollution and Pollutants", 4th Edition in *Lewis Publishers*, ISBN: 1-56670-586-X, 23-69.

Groves, D.I., Barley, M.E., Cassidy, K.F., Fare, R.J., Hagemann, S.G., Ho, S.E., Hronsky, J.M.A., Mikucki, E.J., Mueller, A.G., McNaughton, N.J., Ridley, J.R. and Vearencombe, J.R.. Subgreen-schist to granulite-hosted Archean lodegold deposit: a depositional continuum from deep -sourced hydrothermal fluids in crustal-scale pluming systems, Third Archean Symposium, Perth, Australia, (1990)357-359.

Gruber, V. (2009). *Radiation exposure by natural radionuclides in drinking water in Upper Austria: A radioanalytical and hydrogeological research and evaluation in an international context*.

Guertin, J., (2005). Toxicity and Health Effects of Chromium (All Oxidation States), in: Guertin, J., Jacobs, J., Avakian, C. (Eds) (VI) Handbook. CRC Press, Bocca Raton London New York Washington, D.C., pp.215-234.

Gupta, M., Chauhan, R., Garg, A., Kumar, S., & Sonkawade, R. (2010). Estimation of radioactivity in some sand and soil samples. *Indian Journal of Pure and Applied Physics, 48*(7), 482-485.

Hakanson, L. (1980). An Ecological risk index for aquatic pollution control. A sediment and tological approach. Water research 14. (975-1001).

Hamby, D., & Tynybekov, A. (2002). Uranium, thorium, and potassium in soils along the shore of Lake Issyk-Kyol in the Kyrghyz Republic. *Environmental Monitoring and Assessment*, *73*(2), 101–108.

Han, S., Bian, H., Zhang, Y., Wu, J., Wang, Y., Tie, X., Y. Li, Y., Rana, S. V. S. (2006). "Environmental Pollution, Health and Toxicology: Air Pollution" in *Alpha Science International Ltd*, 10-40.

Hansen W.L. (1971), High Purity Germanium-Observations on the Nature of Acceptors *Nuclear Instrument and Methods* 94, 377-380 (3), 149-168.

Harley, N. H., Foulkes, E. C., Hilborne, L. H., Hudson, A., & Anthony, C. R. (1999). A Review of the Scientific Literature As It Pertains to Gulf War Illnesses. Volume 7 Depleted Uranium. DTIC Document.

He, Z., Shentu, .,Yang, X., Baligar, V.C., Zhang, T., Stoffella, P.J. (2015). Heavy metal contamination of soils: sources, indicators and Assessment. Journal of Environmental Indicators, 9:17-18.

Hebinck, K., Middelkoop, H., Diepen, N. van, Van der Graaf, E., & De Meijer, R. (2007). Radiometric fingerprinting of fluvial sediments in the Rhine-Meuse delta, the Netherlands–a feasibility test. *Netherlands Journal of Geosciences/Geologie En Mijnbouw*, *86*(3).

Hendryx, M. (2009). Mortality from heart. Respiratory, and kidney disease in coal mining areas of Appalachia. *Int Arch Occup Environ Health* 82:243-249.

Hinds, W.C., Kennedy, N.L., and Tatyan, K. (1998). Inhalability of large particles for mouth and nose breathing. *Journal of Aerosol Science*, 29: S277-S278.

https://www.worldweatheronline.com/karibib-weather-averages/erongo/na.aspx). Accessed 21 October 2019

Hu, Q.H., Weng, J.Q., Wang, J.S. (2010), “Sources of Anthropogenic Radionuclides in the Environment: a Review”, *Journal of Environmental Radioactivity* 101 (6) 426-437.

Hua, M., Zhang, S., Pan, B., Zhang, W., Lv, L., & Zhang, Q. (2012). Heavy metal removal from water/wastewater by nanosized metal oxides: A review. *Journal of Hazardous Materials*, *211*, 317–331.

Huda, A.A. (2011), A Determination of Natural Radioactivity Levels in the State of Qatar using High-Resolution Gamma-ray Spectrometry. PhD Thesis, University of Surrey, UK.

Hussain, R. O., & Hussain, H. H. (2011). *Natural Occurring Radionuclide Materials*. INTECH Open Access Publisher.

Huy and Luyen, (2004) Huy, NQ and TV Luyen. 2004. "A method to determine 238U activity in environmental soil samples by using 63.3-keV-photopeak-gamma HPGe spectrometer." *Applied Radiation and Isotopes* 61 (6): 1419-1424.

IAEA (International Atomic Energy Agency). (2005), International Atomic Energy Agency. “IAEATECDOC-1472”, Proceedings of an international Conference on Naturally Occurring Radioactive Materials (NORM IV), Poland: IAEA, Vienna.

IAEA (International Atomic Energy Agency). (2014). Radiation Protection Distance Learning Project, Australian Nuclear Science and Technology Organisation.

Ibrahiem, N.M. (1999). Natural Activity of ^{238}U, ^{232}Th and ^{40}K in building materials. Journal of Environmental Radioactivity 43(3) 255-258

Ibrahim, M. S., Atta, E.R. and Zakariah, Kh. M. (2014). Assessment of natural radioactivity of some quarry raw materials in EI-Minya Govemorate, Egypt, Arab Journal of Nuclear Science and Application, 47 (1): 208-216.

Ibrahim., E, Howard, C., Miles, J., (2009). Sources of Error in etched track radon measurements and a review of passive detectors using results from a series of radon intercomparisons. Radiation Measurements 44(9), 750-754.

ICRP (International Commission of Radiological Protection). (2008). ICRP Publication 103. Recommendations of the International Commission of Radiological Protection annals of the ICRP, Vol. 32, 2-4

ICRP (International Commission on Radiological Protection).(1993). Protection against radon at home and work. Oxford: Pergamon press; ICRP Publications 65; Ann ICRP 23(2).

ICRP (International Commission on Radiological Protection. (1991), ICRP Publication 60, Recommendations of the International Commission on Radiological Protection, Pergamon Press, Oxford.

ICRP, (2009). Recommendation of the International Commission on Radiological Protection. ICRP Press Release 00(902): 09.

ISU (Idaho State University). (2014). The Radiation Information Network. http://www.physics.isu.edu/radinf/index.html.USA._Accessed 15 January 2016.

Jaishankar, M., Tseten, T., Anbalagan, N., Mathew, B. B., & Beeregowda, K. N. (2014). Toxicity, mechanism and health effects of some heavy metals. *Interdisciplinary toxicology*, *7*(2), 60-72

Järup, L. (2003). Hazards of heavy metal contamination. *Br Med Bull*, *68*(1), 167–182.

Jarvis, K. (2006). National Environmental Research Center (NERC), Facility, Thermo Fisher Scientific, UK.

Jevremovic. T. (2009). Nuclear Principles in Engineering 9boston, MA: Springer US)

Kamunda, C., Mathuthu, M, Madhuku, M. (2016a). An Assessment of Radiological Hazards from Gold Mine Tailings in Gauteng Province, South Africa, Int. J. Environ. Res. Public Health, 13, 138. DOI: 10.3390/ijerph13010138.

Kamunda, C., Mathuthu, M., & Madhuku, M. (2016). Health risk assessment of heavy metals in soils from Witwatersrand gold mining basin, South Africa. *International Journal of Environmental Research and Public Health*, *13*(7), 663.

Kantele, J. (1995). *Handbook of nuclear spectrometry*: Academic Press.

Kaplan, I. (1962), Nuclear Physics (2nd edition), USA: Addison-Wesley Publishing Company Inc.

Kaplan, I., & Gugelot, P. (1955). Nuclear physics. *American Journal of Physics, 23*(8), 550-551.

Karahan, G and Bayulken. A. (2000). Assessment of gamma dose rates around Istanbul, Turkey. J. Environ. Radioact. 47 23-21.

Kariuki, M.P. (2018). The exposure of terrestial biota to naturally occurring radiation and stable elements: Case Orrefjell, a risk assessment: Faculty of Environmental Sciences and Natural resources Management, Master 'Thesis, 2018.

Kgabi, N., Shitaatala, E., & Izaaks, C. (2012). Morphological Analysis of Fallout Dust in Windhoek, Namibia. *Journal of Chemical, Biological and Physical Sciences (JCBPS)*, *2*(4), 2201.

Khan, F. M. (2010). The Physics of Radiation Therapy (Lippincott Williams & Wilkins)

Khandaker, M.U. (2011), "High Purity Detector in Gamma-Ray Spectrometry", *International Journal of Fundamental Physical Sciences*, 1 (2), 42-46.

Kinsley, David H. (1998). Backscattered scanning electron microscopy and image analysis of sediments and sedimentary rocks. Cambridge University Press.

Klement, A.W. (1982), "Natural Source of Environmental Radiation. In Handbook of Environmental Radiation, Florida: CRC Press, Inc.

Knoll, G. F. (2000). Radiation Detection and Measurement (3rd edition), USA: John Wiley & Sons Inc.

Knoll, G. F. (2010). *Radiation detection and measurement*. John Wiley & Sons.

Knoll, G.F. (1999). Radiation Detection and Measurement (new York: John Wiley and Sons, Inc.

Köhler, M, S Niese, B Gleisberg, U Jenk and K Nindel. (2000). "Simultaneous determination of Ra and Th nuclides, 238 U and 227 Ac in uranium mining waters by γ-ray spectrometry." *Applied Radiation and Isotopes* 52 (3): 717-723.

Krane, K.S. (1987). Introduction to nuclear physics. John wiley and Sons., New York, ISBN: 978-0471805533.

Krane, K.S. (1988), Introductory Nuclear Physics. Chichester: John Wiley and Sons Inc.

Lam, S. (2012). http://Large.stanford.edu/courses/2012/ph241, Accessed 18th November 2019

Lamarsh, J. R., & Baratta, A. J. (2001). *Introduction to nuclear engineering* (Vol. 3): Prentice Hall Upper Saddle River.

Lamarsh, J. R., & Bell, G. I. (2009). Introduction to Nuclear Reactor Theory. *Physics Today, 20*(3), 110-111.

Landsberger, S, C Brabec, B Canion, J Hashem, C Lu, D Millsap and G George. (2013). "Determination of 226Ra, 228Ra and 210Pb in NORM products from oil and gas exploration: Problems in activity underestimation due to the presence of metals and self absorption of photons." *Journal of Environmental Radioactivity* 125: 23-26.

L'Annunziata, M. F. (2007). *Radioactivity: Introduction and History: Introduction and History*: Elsevier.

Lapp, R.E. and Andrews, H.L. (1972). *Nuclear Radiation Physics, 4th Edition*., Sir Isaacs Pitman and Sons td, London.

Lauria, D.C., and Godoy, J.M. (2002). Abnormal high natural radium concentration in surface waters. Journal of Environmental Radioactivity. 61: 159-68.

Lawrence, C. E., Akber, R. A., Bollhofer, A., Martin, P. (2009). Radon -222 exhalation from open ground on and around a uranium mine in the wet dry tropics, J. Environ. Radioct. 100, 1-8.

Lee, E. M., Menezes, G., Flinch, E. C. (20040. Natural radioactivity in building material in the Republic of Ireland. Health Physics, 86, 378-388.

Lenka, P, SK Jha, S Gothankar, RM Tripathi and VD Puranik. (2009). "Suitable gamma energy for gamma-spectrometric determination of 238U in surface soil samples of a high rainfall area in India." *Journal of Environmental Radioactivity* 100 (6): 509-51

Lestaevel, P., Houpert, P., Bussy, C., Dhieux, B., Gourmelon, P., & Paquet, F. (2005). The brain is a target organ after acute exposure to depleted uranium. *Toxicology*, 212(2), 219–226.

Li, H., Qian, X., Hu, W., Wang, Y., & Gao, H. (2013). Chemical speciation and human health risk of trace metals in urban street dusts from a metropolitan city, Nanjing, SE China. *Science of the Total Environment*, *456*, 212–221.

Li, N., Sioutas, C., Cho, A., and Schmitz, D., Misra, C., Sempf, J., Wang, M., Oberley, T., Froines, J., and Nel, A. (2003). Ultrafine Particulate Pollutants Induce Oxidative Stress and Mitochondria Damage, *Environ. Health Perspect*. 111:455-460.;

Li, X., Chen, Z., Chen, Z., & Zhang, Y. (2013). A human health risk assessment of rare earth elements in soil and vegetables from a mining area in Fujian Province, Southeast China. *Chemosphere*, *93*(6), 1240–1246.

Li, Y. H., Yang, L.S., Wang, W.Y., Li, H.R., Lv, J. M., Zou, X.Y. 2011. Trace element concentrations in hair of healthy Chinese centenarians. Sci. Total Environ. 409, 1385-1390.

Lilley, J. (2001). Nuclear physics principles and application: Wiley, University of Manchester, New York.

Lilley, J. (2013). *Nuclear physics: Principles and applications*. John Wiley & Sons.

Liu, E., Yan, T., Birch, G., & Zhu, Y. (2014). Pollution and health risk of potentially toxic metals in urban road dust in Nanjing, a mega-city of China. *Science of the Total Environment*, *476*, 522–531.

Liu, G., Luo, Q., Ding, M., & Feng, J. (2015). Natural radionuclides in soil near a coal-Fired power plant in the high background radiation area, South China. *Environmental Monitoring and Assessment*, *187*(6), 356.

Liu, X., Song, Q., Tang, Y., Li, W., Xu, J., Wang, F., Brookes, P. C. (2013). Human health risk assessment of heavy metals in soil-vegetable system: a multi-medium analysis. Sci. Total Environ. 463-464, 530-540.

Lodge JP Jr (1988) Methods of air sampling and analysis, 3rd edn. CRC Press, Boca Raton, FL, pp 440–443

Lombardo, Andrew J and Anita F Mucha. (2008). "Measuring and Modeling Naturally Occurring Radioactive Material: Interpreting the Relationship Between the Natural Radionuclides Present-8516.

Lourens, W. Thesis: (1967). A Double Focusing Beta-Ray Spectrometer Applied in Heavy Element Studies. Technische Hogeschool Delft.

Lourtau, A. M Carrassco.,Rubio Montero, M. P., Jurado Vargas, M. (2014). “Characterisation of coal and charcoal by alpha-particle and gamma-ray spectrometry”. Radiation Physics and Chemistry.

Luo, X.-S., Ding, J., Xu, B., Wang, Y.-J., Li, H.-B., & Yu, S. (2012). Incorporating bioaccessibility into human health risk assessments of heavy metals in urban park soils. *Science of the Total Environment*, *424*, 88–96.

Lutz, G. (2001). Semiconductor radiation detectors, Berlin, Heidelberg, New York

M. Â. de. B. C. Menezes E. C. P. Maia, C. de. V. S. Sabino, J. R. Batista, O. F. Neves, C. Albinati, S. S. Filho, and S. V. de. M. Mattos. (2008). Workplace and occupational health: The fisrt metal evaluation using nuclear and analytical techniques in the state of Minas Gerais, Brazil, International Atomic Energy Agency (IAEA), 17-40.

M. Manousakas, K. Eleftheriadis, and H. Papaefthymiou. (2013). “Characterization of PM10 Sources and Ambient Air Concentration Levels at Megalopolis City (Southern Greece) Located in the Vicinity of Lignite-Fired Plants” in *Aerosol and Air Quality Research*, 13:804-817.

M. T. Ny, B. K. and Lee. (2011). “Size distribution airborne particulate matter and associated metallic elements in an urban area of an industrial city in Korea” in *Aerosol and Air Quality Research,* 11:643-653.

M. Xu, R. Yan, C. Zheng, Y. Qiao, J. Han, and C. Sheng. (2003). “Status of trace element emission in coal combustion process: A review” in *Fuel Processing Technology*, 85:215-237.

Magill, J., & Galy, J. (2004). *Radioactivity radionuclides radiation* (Vol. 1): Springer Science & Business Media, 46-49.

Man, Y. B., Sun, X. L., Zhao, Y. G., Lopez, B. N., Chung, S. S., Wu, S. C., … Wong, M.H. (2010). Health risk assessment of abandoned agricultural soils based on heavy metal contents in Hong Kong, the world’s most populated city. *Environment International*, *36*(6), 570–576.

Marillo, J., Usero, J., and Rojas, R. (2008). Fractionation of Metals and As in Sediments from biosphere reserve (Odiel salt marshes) affected by acidic mine drainage. Environmental Monitoring and Assessment, 139, 329-337.

Marr Phebe, (2012). The Modern History of Iraq, Westview press,172.

Martin, A. and Harbison, S. (2006). *An Introduction to Radiation Protection, 5th edition,* Hodder Arnold, London.

Martin, A., Harbison, S., Beach, K., & Cole, P. (2012). *An Introduction to Radiation Protection 6E*: CRC Press.

Martin, B.R. (2008). Nuclear and particle physics: [an introduction] (Chichester Willey)

Martin, J. M, Meybeck, M. (1979). “Elemental mass Balance of Materials carried by major world Rivers”: Marine Chemistry 7, 173-206.

Martins, J. V., Tanre, D., Remer, L., Kaufman, Y., Mattoo, S., & Levy, R. (2002). MODIS Cloud screening for remote sensing of aerosols over oceans using spatial variability. *Geophys. Re. Lett.* 29(12), 8009, DOI:1029/2001GL013252.

Matilda, C. S., Mannully, S. T., Viditha, R. P., & Shanthi, C. (2019). Protein profiling of metal-resistant Bacillus cereus VITSH1. *Journal of Applied Microbiology*, *127*(1), 121–133.

Mauring, A., Gäfvert, T. & Aleksandersen, T. B. (2014). Implications for analysis of 226Ra in a low-level gamma spectrometry laboratory due to variations in radon background levels. *Applied Radiation and Isotopes*, 94: 54-59.

Millichap J. (1995). Lead Neurotoxicity. Pediatr. Neurol. Briefs. 9:42. doi: 10.15844/pedneurbriefs-9-6-2.

Mirion Technologies (2017): http://www. Canberra.com, retrieved 18 November 2019

Mishra, D. P., Sahu, P., Panigrahi, D. C., Jha, V., & Patnaik, R. L. (2014). Assessment of 222 Rn emanation from ore body and backfill tailings in low-grade underground uranium mine. *Environmental Science and Pollution Research*, *21*(3), 2305–2312.

Mohmand, J., Eqani, S. A. M. A. S., Fasola, M., Alamdar, A., Mustafa, I., Ali, N., … Shen, H. (2015). Human exposure to toxic metals via contaminated dust: Bio-accumulation trends and their potential risk estimation. *Chemosphere*, *132*, 142–151.

Moon, D. S., Burnett, W. C., Nour, S., Horwitz, P., & Bond, A. (2003). Preconcentration of radium isotopes from natural waters using MnO 2 resin. *Applied Radiation and Isotopes*, 59(4), 255–262.

Morillo, J., Usero, J., & Rojas, R. (2008). Fractionation of metals and As in sediments from a biosphere reserve (Odiel salt marshes) affected by acidic mine drainage. *Environmental Monitoring and Assessment*, *139*(1–3), 329–337.

Mortzer, W., (2005). Chemistry. Geochemistry, and Geology of Chromium and Chromium Compounds, in: Guertin, J., Jacobs, J., Avakian, C. (Eds) (VI) Handbook. CRC Press, Bocca Raton London New York Washington, D.C., pp.215-234.

Mtunzi, F., Dikio, E., & Moja, S. (2015). Evaluation of heavy metal pollution on soil in Vaderbijlpark, South Africa. *International Journal of Environmental Monitoring and Analysis*, *3*(2), 44–49.

Muller, G. (1979). Index of Geoaccumulation in Sediments of the Rhine river. J. Geology, 2 (3), 108-118.

Murray, AS, R Marten, A Johnston and P Martin. (1987). "Analysis for naturally occurring radionuclides at environmental concentrations by gamma spectrometry." *Journal of Radioanalytical and Nuclear Chemistry* 115 (2): 263-288.

Namibia Statistics agency- Government of the republic of Namibia: Namibian census report (2011). http://nsa.org.na/microdata1/index.php/catalog/19/related materials. Accessed on 10 January 2016.

Narayana, Y. , Radhakrishna, A.P., Somashekarappa, H. M., Karunakara, N., Balakrishma, K. M.. and Siddappa, K. (1995). “Distribution and Enrichment of Radionuclides in the Newly Discovered High Background Area in Ullal on the Southwest Coast of India”Health Physics 69, (20), 178-186.

Narayana, Y., & Rajashekara, K. (2010). The importance of physico-chemical parameters on the speciation of natural radionuclides in riverine ecosystems. *Journal of Environmental Radioactivity*, *101*(11), 958–964.

National Council on Radiation Protection and Measurement. (1975), “Natural Background Radiation in the United State”, NCRP Report No. 45. NCRP Washington D.C.

National Nuclear Data Centre Chart of Nuclides, Brookhaven National Laboratory. http:www.nndc.bnl.gov/chart: Accessed 4 January 2018.

Neuman, C. M., Boulton, J. W., & Sanderson, S. (2009). Wind tunnel simulation of environmental controls on fugitive dust emissions from mine tailings. *Atmospheric Environment, 43*(3), 520-529.

Nickens, K.P., Paterno, S.R. Ceryak., (2010). Chromium genotoxicity: A double-edged sword. Chem. Biol. Interact. 188, 276-88.DOI:10.1016/j.cbi.2010.04.018.

Nieboer, E., & Richardson, D. H. (1980). The replacement of the nondescript term ‘heavy metals’ by a biologically and chemically significant classification of metal ions. *Environmental Pollution Series B, Chemical and Physical*, *1*(1), 3–26.

Njinga, R. L., Tshivhase, M. V., Kgabi, N. A., & Zivuku, M. (2016). Hazards index analysis of Gamma emitting radionuclides in selected areas around the Uranium Mine sites at Erongo Region, Namibia.

Norela S, Nurfatiha M, Maimon A, Ismail B (2009) Wet deposition in the residential area of the Nilai Industrial Park in Negeri Sembilan, Malaysia. World Appl Sci J 7:170–179

Noz, M., Maguire, G., & Erwin, W. D. (2008). Radiation Protection in the Health Sciences. *Journal of Nuclear Medicine, 49*(3), 509-509.

Ny, M. T., & Lee, B.-K. (2011). Size distribution of airborne particulate matter and associated metallic elements in an urban area of an industrial city in Korea. *Aerosol and Air Quality Research*, *11*(6), 643–653.

O'Neill, P.G. (1995). Arsenic. In Heavy Metals in Soil. 2nd Edition, Blackie Academic and Professional Publishing Co.

O'Toole, T. E., Conklin, D. J., & Bhatnagar, A. (2008). Environmental risk factors for heart disease. *Reviews on Environmental Health*, *23*(3), 167–202.

Oberdorrster, G., Ferin, J., Gelein, R., Sonderholm, S. C., and Finkelstein, J. (1992). Ultrafine Particles, *Environ. Health Perspect.* 97;193-199.

O'Brien, R., & Cooper, M. (1998). Technologically enhanced naturally occurring radioactive material (NORM): pathway analysis and radiological impact. *Applied radiation and isotopes, 49*(3), 227-239.

OECD. (1979). Organization of Economic Cooperation and Development, Exposure to radiation from natural radioactivity in building materials. Report by a group of experts, Nuclear Energy Agency, Paris, France.

Olumayede, E. G., Sodeinde, K. O., Akintade, C. O., Emmanuel, B. O., Akintoye, A., & Peter, O. O. (2016). Different Size Aggregates of Stone Quarry Products and Airborne Particles around a Facility in Akure, Southwestern Nigeria: Radioactivity Concentrations, Radiological Hazard and Dose Assessment. *Nature Environment and Pollution Technology*, *15*(4), 1351.

Omole, O., Akambi, A.S. (1997), "Gamma Ray Emission and the Associated Electric Field", *Journal of Mining and Geology* 33 (2), 127-134.

Onjefu, S. A. (2016). Natural radioactivity concentrations and occurrence of heavy Metals in Shore Sediments along the Coastline of the Erongo Region in Western Namibia.

Onjefu, S. A., Taole, S. H., Kgabi, N. A., Grant, C., & Antoine, J. (2017). Assessment of natural radionuclide distribution in shore sediment samples collected from the North Dune beach, Henties Bay, Namibia. *Journal of Radiation Research and Applied Sciences*, *10*(4), 301–306.

Otaviano, A. M. Helene and Vito, R. Vanin. (2007). *Update of X 9ray and Gamma-ray Decay Data Standards for Detector calibration and Other Applications*. https: //www.nds.iaea.org/xgamma_standards/crp.htm. Accessed 23 September 2019.

Ownby, D. R., Galvan, K. A., & Lydy, M. J. (2005). Lead and zinc bioavailability to Eisenia fetida after phosphorus amendment to repository soils. *Environmental Pollution*, *136*(2), 315–321.

Oyedele, J. (2006). Measurement of the natural radioactivity at the international high energy stereoscopic system (HESS) project in Southern Africa. *Applied Radiation and Isotopes*, *64*(6), 686–688.

Oyedele, J.A., Shimboyo, S., Sitoko, S., Gaoseb, F. (2010), "Assessment of Natural Radioactivity in Soils of Rossing Uranium Mine and its Satellite Town in Western Namibia, Southern Africa", *Nuclear Instruments and Methods in Physics Research* A 619, 467-469.

Pacyna, E. G., Pacyna, J. M., Steenhuisen, F., & Wilson, S. (2006). Global anthropogenic mercury emission inventory for 2000. *Atmospheric Environment*, *40*(22), 4048–4063.

Park, J. H., Kang, D. R., & Kim, J. (2016). A review on mathematical models for estimating indoor radon concentrations. *Annals of Occupational and Environmental Medicine*, *28*(1), 7.

Patlolla A.K., Barnes C., Yedjou C., Velma V.R., Tchounwou P.B. (2009). Oxidative stress, DNA damage, and antioxidant enzyme activity induced by hexavalent chromium in Sprague-Dawley rats. Environ. Toxicol. 24:66–73. doi: 10.1002/tox.20395.

Pearson, R. G. (1963). Hard and soft acids and bases. *Journal of the American Chemical Society*, *85*(22), 3533–3539.

Peng, C., Chen, W., Liao, X., Wang, M., Ouyang, Z., Jiao, W., & Bai, Y. (2011). Polycyclic aromatic hydrocarbons in urban soils of Beijing: Status, sources, distribution and potential risk. *Environmental Pollution*, *159*(3), 802–808.

PerkinElmer. (2004-2011). ICP-Mass Spectrometry, Tehnical Note.USA. www.perkinelmer.com. Accessed 10 September 2019

Peters, A., Wichmann, H.E., Touch, T., Heinrich, J., and Heyder, J. (1997). Respiratory Effects are associated with the Number of Ultrafine Particles, *Am. J. Respi.Crit. Care Med.* 155: 1376-1383.

Polichetti, G., Cocco, S., Spinali, A., Trimarco, V., & Nunziata, A. (2009). Effects of particulate matter (PM10, PM2. 5 and PM1) on the cardiovascular system. potential risk. *Environmental Pollution*, *159*(3), 802–808. *Toxicology*, *261*(1–2), 1–8.

Pradler, J and Yavin, I. (2013). Ön an unverified nuclear decay and its role in the DAMA experiment". In: physics letters B 720.4-5, pages 399-404. ISSN: 0370-2693. Prentice Hall Upper Saddle River.

Prince, J.H. (1979), "Comments on Equilibrium, Transient Equilibrium and Secular Equilibrium in Serial Radioactive Decay", *Journal of Nuclear Medicine* 20, 162-164.

Prospero, J. M., Ginoux, P., Torres, O., Nicholson, S. E., & Gill, T. E. (2002). *Environmental characterization of global sources of atmospheric soil dust derived from the nimbus7 atoms absorbing aerosol product, rev*. Presented at the Reviews of Geophysics.

Radhakrishna, A. P., Somashekarappa, H. M., Narayana, Y., & Siddappa, K. (1993). A new natural background radiation area on the Southwest Coast of India. *Health Physics*, *65*(4), 390–395. (8376119).

Rajaretnam, G. and H.B. Spitz. (2000). "Effect of leachability on environmental risk assessment for naturally occurring radioactive materials in petroleum oil fields." *Health Physics* 78 (2): 191.

Ramasamy, V., Senthil, S., Meenakshisundaram, V., Gajendran, V. (2009), "Measurement of Natural Radioactivity in Beach sediments from North East Coast of Tamilnadu, India", *Research Journal of Applied Science Engineering and Technology* 1(2), 54-58.

Ramasamy, V., Suresh, G., Meenakshisundaram, V., Ponnusamy, V. (2011), "Horrizontal and Vertical Characterization of Radionuclides and Minerals in River Sediments, *Applied Radiation and Isotopes* 69, 184-195.

Rana, M. M., Sulaiman, N., Sivertsen, B., Khan, M. F., & Nasreen, S. (2016). Trends in atmospheric particulate matter in Dhaka, Bangladesh, and the vicinity. *Environmental Science and Pollution Research*, *23*(17), 17393–17403.

Rao, C. R. M., Sahuquillo, A., & Lopez-Sanchez, J. F. (2010). Copmarison of single and sequential extraction procedures for the study of rare earth elements and remobilisation in different types of soils. Analtica Chimica Acta, 662, 128-136.

Rashki, A. (2012). Seasonality and mineral, chemical and optical properties of dust storms in the Sistan region of Iran, and their influence on human health. Retrieved from http://www.repository.up.ac.za/handle/2263/27734. Accessed 20 February 2017.

Rath, P., Panda, U.C., Sahoo, B.N. (2005). Environmental quantification of Heavy Metals in the Sediments of Brahmani and Nandira rivers, Orissa. Journal of Geol Soc Ind, 65: 487-492.

Reguigui, N. (2006). *Gamma ray spectrometry practical information*. Centre national des Sciences et Technogies Nucleares, Tunis, Tunisia. Accessed 18th November 2019

Rössing Uranium Mine- Home page of Namibia 's Rössing Mine, https://www.rosing.com: retrieved October 2018.

Santawamaitre, T. (2012). An evaluation of the level of Naturally Occurring Radioactive Materials in Soil samples along Chao Phraya River Basin, PhD Thesis, University of Surrey.

Santawamaitre, T., Malain, D., Al-Sulaiti, H., Matthews, M., Bradley, D., & Regan, P. (2011). Study of natural radioactivity in riverbank soils along the Chao Phraya river basin in Thailand. *Nuclear Instruments and Methods in Physics Research Section A: Accelerators, Spectrometers, Detectors and Associated Equipment*, *652*(1), 920–924.

Santos, I.R., Silva-Filho, E.V., Schaefer, C.E., Albuquerque-Filho, Campos, L.S. (2005), "Heavy Metal Contamination in Coastal Sediments and Soil Near the Brazilian Antartic Station, Kin George Island", *Marine Pollution Bulletin* 50, 185-194.

Sarkar, A., Ravindran, G., & Krishnamurthy, V. (2013). A brief review on the effect of cadmium toxicity: from cellular to organ level. *Int J Biotechnol Res*, *3*(1), 17-36.

Sartandel, SJ, SK Jha, SV Bara and RM Tripathi. (2014). "Assessment of 226Ra and 228Ra activity concentration in west coast of India." *Journal of Radioanalytical and Nuclear Chemistry* 300 (2): 873-877.

Shandilya, K. K., Khare, M., & Gupta, A. B. (2009). Defining aerosols by physical and chemical characteristics. *Indian Journal of Air Pollution Control*, *9*(1), 107–126.

Shang, W., Tang, Q., Zheng, L., & Cheng, H. (2016). Chemical forms of heavy metals in agricultural soils affected by coal mining in the Linhuan subsidence of Huaibei Coalfield, Anhui Province, China. *Environmental Science and Pollution Research*, *23*(23), 23683–23693. https://doi.org/10.1007/s11356-016-7599-8

Shaw, B., Sahu, S., & Mishra, R. (2004). Heavy metal induced oxidative damage in terrestrial plants. In *Heavy metal stress in plants* (pp. 84–126). Springer.

Sheppard, S. C., Sheppard, M. I., Ilin, M., Tait, J. & Sanipelli, B. (2008). Primordial radionuclides in Canadian background sites: secular equilibrium and isotopic

differences. *Journal of Environmental Radioactivity*, 99 (6): 933-946.doi: https://doi.org/10.1016/j.jenvrad.2007.11.018.

Shimboyo, S. A., Oyedele, J., & Sitoka, S. (2016). *Soil radioactivity levels and associated hazards in selected towns in uranium-rich western Namibia*.

Shittu, H.O., Olarinoye, I.O., Baba-Kutigi, A.N., Olukotun, S. F., Ojo, E, O. and Egga, A. 2015. Determination of radiological risk associated with naturally occurring radioactive materials (NORM) at selected quarry sites in abuja FCT, Nigeria, using Gamma-Ray Spectroscopy. Physic Journal of Nigeria, 1, (2): 71-78.

Siegel, P.B. 2013. "Gamma spectroscopy of environmental samples." *American Journal of Physics* 81 (5): 381.

Silberberg, R., & Tsao, C. H. (1990). Spallation processes and nuclear interaction products of cosmic rays. *Physics Reports*, *191*, 351- 408.

Simex, S.A., Helz, G.R. (1981). Regional geochemistry of trace elements in Checapeake Bay. Environmental geol, 3:315-323

Singh, S., Rani, A., Mahajan, R.K. (2005), "^{226}Ra, ^{232}Th and ^{40}K Analysis in Soil Samples From Some Area of Punjab and Himachal Pradesh, India Using Gamma Ray Spectrometry", *Journal of Radiation Measurements* 39, 431-439.

Sinha, S., Gupta, A., Bhatt, K., Pandey, K., Rai, U., & Singh, K. (2006). Distribution of metals in the edible plants grown at Jajmau, Kanpur (India) receiving treated tannery wastewater: Relation with physico-chemical properties of the soil. *Environmental Monitoring and Assessment*, *115*(1–3), 1–22.

Snyder, R. D. (1971). Congenital mercury poisoning. *New England Journal of Medicine*, *284*(18), 1014–1016.

Sohrabi, M. (2013). World high background natural radiation areas: Need to protect the public from radiation exposure. Radiat. Meas. 50: 166-171.

Sokolik, I. N., Winker, D. M., Bergametti, G., Gillette, D. A., Carmichael, G., Kaufman, Y. J., et al. (2001). Introduction to special section: Outstanding problems in quantifying the radiative impacts of mineral dust. *Journal of Geophysical Research: Atmospheres*, 106(D16), 18015–18027.

Solberg, C . (2009). Heavy Metals levels and Mercury Speciation in Water, soil, and sediments in a highly contaminated Mining area in Khaidarkan, Kyrgyzstan. M Sc. Thesis.

Stanin, F., (2005).The transport and Fate of Chromium (VI) in the Environment Frederick, in Compounds, in: Guertin, J., Jacobs, J., Avakian, C. (Eds) (VI) Handbook. CRC Press, Bocca Raton London New York Washington, D.C., pp.165-214.

Status of Namibia Economy: https://www.npc.gov.na, Accessed 15 November 2019

Strand, P., & Dowdall, M. (2010). Radioecology and environmental exposure pathways. Refresher Courses, 2982.

Strategic Environmental Assessment. (2010), “Central Namib Uranium Rush”, SEA. Geological Survey of Namibia, Ministry of Mines and Energy, Windhoek, Namibia.

Stuut, J.-B., Smalley, I., & O’Hara-Dhand, K. (2009). *Aeolian dust in Europe: African sources and European deposits. Quaternary International*, 198(1), 234–245.

Sun, K., Guo, Q., & Cheng, J. (2004). The effect of some soil characteristics on soil radon concentration and radon exhalation from soil surface. *Journal of Nuclear Science and Technology*, *41*(11), 1113–1117.

Surinder Singh, Ashna Rani, Rakesh Kumar Mahajan, 2005. 266Ra, 232Th and 40K analysis in soil samples from some areas of Punjab and Himachal Pradesh, India using gamma ray spectrometry, Radiation measurements, 39(4), pp. 431-439.

Sutton, M. W., & Weiersbye, I. M. (2008). Land use after mine closure–risk assessment of gold and uranium mine residue deposits on the Eastern Witwatersrand, South Africa. In Proceedings of the Third International Conference on Mine Closure, Mine Closure (pp. 14–17).

Sutton, M., & Weiersbye, I. (2008). *Land use after mine closure–risk assessment of gold and uranium mine residue deposits on the Eastern Witwatersrand, South Africa*. 14–17.

Tan, S. Y., Praveena, S. M., Abidin, E. Z., & Cheema, M. S. (2016). A review of heavy metals in indoor dust and its human health-risk implications. *Reviews on Environmental Health*, *31*(4), 447–456.

Taskin, H., Karavus, M., AY, P., Topuzoglu, A., Hindiroglu, S., Karahan, G. (2009),“Radionuclide Concentrations in Soil and Lifeline Cancer Risk Due to the Gamma Radioactivity in Kirklareli”, *Turkey Journal of Environment Radioactivity* 100, 49-53.

Tchounwou P.B., Ishaque A.B., Schneider J. (2001). Cytotoxicity and transcriptional activation of stress genes in human liver carcinoma cells (HepG2) exposed to cadmium chloride. Mol. Cell. Biochem. 222:21–28. doi: 10.1023/A:1017922114201.

Tchounwou, P. B., Yedjou, C. G., Patlolla, A. K., & Sutton, D. J. (2012). Heavy metal toxicity and the environment. In *Molecular, clinical and environmental toxicology* (pp. 133–164). Springer.

Temminghoff, E. E., & Houba, V. J. (2004). *Plant analysis procedures* (Vol. 179). Springer.

Thabayneh, K. M. (2015). Measurement of 222Rn concentration levels in drinking water and the associated health effects in the Southern part of West bank–Palestine. *Applied Radiation and Isotopes*, *103*, 48–53.

Thabayneh, K.M., (2005). Measurements of 222Rn concentration levels in drinking water and the associated health effects in the Southern parts of West bank-Palestine. Applied Radiation Isotope, 103, 48-53.

Thakur, M., Deb, M. K., Imai, S., Suzuki, Y., Ueki, K., & Hasegawa, A. (2004). Load of heavy metals in the airborne dust particulates of an urban city of central India. *Environmental Monitoring and Assessment*, *95*(1–3), 257–268.

Tomlinson, D., Wilson, J., Harris, C., Jeffrey, D. (1980), "Problems in the Assessment of Heavy Metal levels in Esti-arie and the Formation of a Pollution Index", *Helgoland Marine Resources 33* (1-4), 566-575.

Turner, J. E. (2007). Atoms, radiation, & radiation protection (3rd edition). Weinheim: Wiley VCH.

Tzortzis, M., & Tsertos, H. (2004). Determination of thorium, uranium and potassium elemental concentrations in surface soils in Cyprus. *Journal of Environmental Radioactivity*, 77(3), 325–338.

UNSCEAR (United Nations Scientific Committee on Effects of Atomic Radiation). (1988), "Sources and Effects of Ionizing Radiation", UNSCEAR Report to the General Assembly with Scientific Annexes, United Nations Publication, United Nation, New York.

UNSCEAR (United nations scientific committee on the effects of atomic radiation). (2000). Exposures from natural radiation sources. *Report to the General Assembly, with annexes, Annex-B*, United Nations, New York.

UNSCEAR. (1982). Ionising Radiation: Sources and Biological effect. United Nations Scientific Committee on the Effect of Atomic Radiation, United Nations, New York, ISBN: 9211422426.

UNSCEAR. (2008a). *Report of the United Nations Scientific Committee on the Effects of Atomic Radiation: Fifty-sixty Session (10-18 July 2008):* United Nations Publications

USEPA (United Nations Environmental Agency). (2014). Tittle 40 Code of Federal Regulations, Section 70.2 2009a. Available online:http:www.gpo.gov/fdsys/pkg/CFR-2009-tittle40 vol115/xml/CFR-2009-title40-vol15-part70.xml,June 2018.

USEPA (United States Environmental Protection Agency). (2002). A Review of the Reference Dose and Reference Concentration Processes. EPA/630/P-02/002F, USA

USEPA (United States Environmental Protection Agency). (2014). Priority Pollutant List [www Document. URL https://www.epa.gov/sites/production/2015-09/documents/priority-pollutant-list-epa.pdf (accessed 23.09.19).

USEPA((United States Environmental Protection Agency). (1989). Risk Asessmentassessment guidance for superfund. Human health evaluation , annual, Part (A)[r], Vol.1. Washington DC: Office of Emergency and remdialremedial response: EPA/540/1-89/002, USA.

Utell, M. J., and Frampton, M. W. (2000). Acute Hhealth Eeffects of Aambient Aair Ppollution: The Uultrafine Pparticle Hhypothesis, *J. aerosol Med.* 13: 355-259.

Van Beek, P, M Souhaut and J-L Reyss. (2010). "Measuring the radium quartet (^{228}Ra, ^{226}Ra, ^{224}Ra, ^{223}Ra) in seawater samples using gamma spectrometry.". *Journal of Environmental Radioactivity* 101 (7): 521-52.???

Van Krugten, H., E. W., (1968). Beta Ccontinuum Mmeasurements on ^{226}Ac and Ddaughter Pproducts of ^{225}Ac. Koopmann, Physics, 40: p. 253.

VanLoon, G. W., & Duffy, S. J. (2017). *Environmental chemistry: A gGlobal pPerspective*. Oxford university press.

Veiga, R., Sanches, N., Anjos, R., Macario, K., Bastos, J., Iguatemy, M., … Carvalho, C. (2006). Measurement of natural radioactivity in Brazilian beach sands. *Radiation Measurements*, *41* (2), 189–196.

Verdoya, M., Chiozzi, P., & Pasquale, V. (2001). Heat-producing radionuclides in metamorphic rocks of the Brianconnais-Piedmont Zone (Maritime Alps). *Eclogae Geologicae Helvetiae, 94* (2), 213-219.

Vincent, J.H., Mark, D., Miller, B.H., Armbruster, L and Ogden, J.L. (1990). Aerosol inhalability at high speeds. *Journal of Aerosol Science*. 21 : 577-586.

von Oertzen, D. (2008). Namibian Nnational issues report on key sector of energy with focus on mitigation. *Desert Research Foundation of Namibia, Namibia*

Wahl, W. (2007). Radionuclide handbook for laboratory Workers in spectrometry, Radiation protection and medicine, Germany: IsuS.

Wahl, W. (2007). *Radionuclide handbook for laboratory workers.* Institute for Spectrometry and Radiation Protection.

Wang D-Z, Jiang X, Rao W, He J-Z (2009). Kinetics of soil Cadmium desorption under simutaedsimuted acid rain. Ecol Ccomplex 6: 432-437. Doi:10.1016/j. ecocom. 2009.03.010.

Wang, J, J Liu, L Zhu, JY Qi, YH Chen, TF Xiao, SM Fu, CL Wang and JW Li. (2012). "Uranium and thorium leached from uranium mill tailing of Guangdong province, China and its implication for radiological risk." *Radiation Protection Dosimetry* 152 (1-3),: 215-219.

Wang, J., Li, S., Cui, X., Li, H., Qian, X., Wang, C., & Sun, Y. (2016). Bioaccessibility, sources and health risk assessment of trace metals in urban park dust in Nanjing, Southeast China. *Ecotoxicology and Environmental Safety*., *128*, 161–170.

Wang, X, Sato T, Xing, B. (2005). Health risks of heavy metals to the general public in Tianjin, China via consumption of vegetables and fish. *Sci Total Environ 350:28–37Journal of the Science Total Environment*. 350, 28–37.

Wang, Z., Boice, J. D. Jr., Beebe, G. W., Zha, Y., Kaplan, M. M., Too, Z., Maxon, H.R III., Zhang, S., Schneider, A. B., Tan, B., Wesseler, T.A., Chen, D, Ershow, A. G., Kleinerman, R.A., Littlefield, L.G., and Preston, D. (1990). Thyroid Nnodularity and Cchromosome Aaberrations Aamong Wwomen in Aareas of Hhigh Bbackground Rradiation in China. *JNCI JNatl. Cancer Inst. 82: 478-85.Journal of The National Cancer Institute.* 82, 478-85.

Ward, N.I., Dudding, A., Lyndon, M. (2004). “Platinum Eemmissions and Llevels in Mmotorway Ddust Ssamples: Influence of Ttraffic Ccharacteristics”, *Science of the Total Environment* 334-335 and, 457-463.

Watson, S., Jones, A., Oatway, W., & Hughes, J. (2005). *Ionising radiation exposure of the UK population: 2005 review*. Health Protection Agency Chilton, Oxon.

Wei, X., Gao, B., Wang, P., Zhou, H., & Lu, J. (2015). Pollution characteristics and health risk assessment of heavy metals in street dusts from different functional areas in Beijing, China. *Ecotoxicology and Environmental Safety*., 112, 186–192.

Wenquin Shang, Quan Tang., Liugen Zheng, and Hua Cheng. (2016). Chemical forms of heavy metals in agricultural soils affected by coal mining in Linhuan subsidence of Huaibei Ccoalfied, Anhui Pprovinnce, China. *Environmental Science cific Pollution Research*. 23, :23683-23693., DOI 10.1007/s 11356-016-7599-8

Whitacre, S. D., Basta, N. T., Minca, K., & Daniels, W. L. (2013). Identification of Ttoxic Aagents and Ppotential Eexposure Rroutes to Appalachian Coal Mining Communities. *Environmental Considerations in Energy Production*, 229.

WHO/FAO. WHO/FAO Ffood Aadditives Ddata Ssystems. Evaluation by the Joint Committee on Food Additives, 1956-1984. FAO Food and Nutrition Paper 30/Rev. Rome.

Wichmann, H. E. , and Peters, A (2000). Epidemiological eEvidence of the Eeffects of Uultrafine Pparticle Eexposure, *Philosophical. Transactions of the. Royal Society. London A,* 358, :2751-2769.

Wilson, W.F. (1994), A Gguide to Nnaturally Ooccurring Rradioactive Mmaterial, Oklahoma: Pennwell Books.

WNA (World Nuclear Association). (2014). "Radiation and Nuclear Energy". ,http://www.world-nuclear.org/info/inf30.html. Accessed 14th November 2018

World Health Organization, Health risks of particulate matter from long range transboundary air pollution. (2006). Joint WHO/ convention task force on the health aspects of air pollution. European Centre for Environment and Health Bonn Office. http://www.euro.who.int/data/assets/pdf file/006/78657/E88189.pdf. Accessed 15 January 2016.

World Nuclear Association (2011). In http://www. World-nuclear.org/info/inf30.html. Accessed 23 September 2019.

Xhixha, G., Bezzon, G. P., Broggini, C., Buso, G. P., Cacioli, A., Callegari, I., De Biachi, S., Fiorentini, G., Guastaldi, E., and Kaceli Xhixha, M. (2013). "The worldwide NORM production and fully automated gamma-ray spectrometer for their characterisation". *Journal of Radioanlytical and Nuclear Chemistry*, 295 (1): 445-457.

Xinwei, L., Lingqing, W., Xiaodan, J., Leipeng, Y. (2006)., "Specific Aactivity and Hhazards of Archeozoic-Cambrian Rrock Ssamples Ccollected from the Weibei area of Shaanxi, China", *Radiation Protection Dosimetry* 118, 352-359.

Yang, Y., Wu, X., Jiang, Z., Wang, W., Lu, J., Lin, J., … Hsia, Y. (2005). Radioactivity concentrations in soils of the Xiazhuang granite area, China. *Applied Radiation and Isotopes*, *63* (2), 255–259.

Yu, C., A.J. Zielen, J.-J., Cheng, D.J., LePoire, E. Krane, Kenneth S., (1988). Introductory Nuclear Physics, Kenneth S. Krane. Chichester: Wiley., New York. ISBN: 047180553X.

Zheng, N., Liu, J., Wang, Q., & Liang, Z. (2010). Health risk assessment of heavy metal exposure to street dust in the zinc smelting district, Northeast of China. *Science of the Total Environment*, *408* (4), 726–733.

Zheng, N., Wang, Q., Zhang, X., Zheng, D., Zhang, Z., & Zhang, S. (2007). Population health risk due to dietary intake of heavy metals in the industrial area of Huludao city, China. *Science of the Total Environment*, *387* (1–3), 96–104.

Zschornack, G. (2007). *Handbook of X-ray data: with 161 tables* (Berlin: Springer)

APPENDIX A

Table A1 The sample matrix, sample identities and their corresponding locations in the town of Karibib

Matrix			Geographical Position System (GIS)	
Soil Sample ID	Particulate matter Sample ID	Indoor radon Sample ID	Latitude (S)	Longitude (E)
KS1	KPM1	KR1	21°56’31.3’’	15°51’59.2’’
KS2	KPM2	KR2	21°55’39.1’’	15°52’06.4’’
KS3	KPM3	KR3	21°55’39.1’’	15°52’03.1’’
KS4	KPM4	KR4	21°55’48.2’’	15°51’37.7’’
KS5	KPM5	KR5	21°55’44.7’’	15°51’52.1’’
KS6	KPM6	KR6	21°55’45.3’’	15°51’47.0’’
KS7	KPM7	KR7	21°56’16.4’’	15°51’32.1’’
KS8	KPM8	KR8	21°56’34.7’’	15°50’46.5’’
KS9	KPM9	KR9	21°56’38.8’’	15°50’58.5’’
KS10	KPM10	KR10	21°56’39.2’’	15°50’52.1’’
KS11	KPM11	KR11	21°56’39.1’’	15°50’07.0’’
KS12	KPM12	KR12	21°56’30.1’’	15°51’14.2’’
KS13	KPM13	KR13	21°56’15.8’’	15°51’38.5’’
KS14	KPM14	KR14	21°56’15.6’’	15°51’55.8’’
KS15	KPM15	KR15	21°56’20.3’’	15°49’55.7’’
KS16	KPM16	KR16	21°56’22.0’’	15°49’01.5’’
KS17	KPM17	KR17	21°56’22.4’’	15°50’02.8’’
KS18	KPM18	KR18	21°56’23.6’’	15°50’02.9’’
KS19	KPM19	KR19	21°56’23.6’’	15°50’09.3’’
KS20	KPM20	KR20	21°56’24.6’’	15°50’09.6’’
KS21	KPM21	KR21	21°56’24.6’’	15°50’05.3’’
KS22	KPM22	KR22	21°56’32.8’’	15°50’05.4’’
KS23	KPM23	KR23	21°55’43.9’’	15°51’52.6’’
KS24	KPM24	KR24	21°55’45.5’’	15°51’56.1’’
KS25	KPM25	KR25	21°55’40.8’’	15°51’53.4’’

Table A2 The sample matrix, sample identities and their corresponding locations in the town of Arandis

Matrix			Geographical Position System (GIS)	
Soil Sample ID	Particulate matter Sample ID	Indoor radon Sample ID	Latitude (S)	Longitude (E)
AS1	APM1	AR1	22º25’15.6’’	14º58’33.5’’
AS2	APM2	AR2	22º25’05.9’’	14º58’30.7’’
AS3	APM3	AR3	22º25’01.8’’	14º58’25.6’’
AS4	APM4	AR4	22º25’07.2’’	14º58’17.7’’
AS5	APM5	AR5	22º25’05.0’’	14º58’10.5’’
AS6	APM6	AR6	22º24’56.6’’	14º58’14.2’’
AS7	APM7	AR7	22º24’52.3’’	14º58’23.0’’
AS8	APM8	AR8	22º24’48.2’’	14º58’21.1’’
AS9	APM9	AR9	22º24’42.1’’	14º58’23.7’’
AS10	APM10	AR10	22º24’42.6’’	14º58’27.8’’
AS11	APM11	AR11	22º24’51.5’’	14º58’35.2’’
AS12	APM12	AR12	22º24’51.3’’	14º58’42.5’’
AS13	APM13	AR13	22º24’52.2’’	14º58’48.1’’
AS14	APM14	AR14	22º24’55.5’’	14º58’48.2’’
AS15	APM15	AR15	22º24’57.5’’	14º58’48.6’’
AS16	APM16	AR16	22º24’54.6’’	14º58’45.2’’
AS17	APM17	AR17	22º25’00.2’’	14º58’41.0’’
AS18	APM18	AR18	22º25’03.8’’	14º58’41.1’’
AS19	APM19	AR19	22º25’04.6’’	14º58’33.8’’
AS20	APM20	AR20	22º25’10.4’’	14º58’24.5’’
AS21	APM21	AR21	22º25’12.8’’	14º58’20.4’’
AS22	APM22	AR22	22º25’17.4’’	14º58’18.5’’
AS23	APM23	AR23	22º25’20.8’’	14º58’23.0’’
AS24	APM24	AR24	22º25’23.9’’	14º58’21.5’’
AS25	APM25	AR25	22º25’04.1’’	14º58’11.6’’

Table A3 Activity concentrations in PM samples collected from the two towns of Arandis and Karibib

Sample no	Activity concentrations (Bq.kg^-1)														
	Ra-226			U-238			Th-232			K-40			Pb-210		
APM1	65.29	±	1.17	47.77	±	2.60	79.43	±	1.88	980.00	±	14.50	78.00	±	3.20
APM2	58.50	±	1.44	47.77	±	2.43	37.33	±	1.14	716.20	±	14.26	43.69	±	2.20
APM3	39.92	±	0.57	61.80	±	2.30	78.61	±	1.87	567.00	±	12.00	43.13	±	12.39
APM4	113.72	±	0.54	77.45	±	3.84	76.20	±	1.17	550.00	±	9.81	79.00	±	13.28
APM5	86.47	±	0.68	97.20	±	1.49	67.33	±	1.25	780.00	±	14.40	10.38	±	1.25
APM6	81.94	±	0.58	64.18	±	1.82	40.76	±	1.07	699.00	±	18.00	28.59	±	4.56
APM7	72.33	±	0.75	52.59	±	3.15	70.26	±	0.97	441.20	±	36.60	108.70	±	20.64
APM8	91.69	±	0.58	74.12	±	2.15	75.13	±	0.24	666.00	±	12.60	89.60	±	5.42
APM9	72.98	±	0.76	105.74	±	3.79	24.22	±	0.28	782.00	±	10.53	50.10	±	2.20
APM10	124.91	±	0.46	59.69	±	1.29	46.93	±	1.47	846.00	±	29.00	59.83	±	2.00
APM11	118.29	±	1.35	56.45	±	1.67	60.38	±	1.05	482.00	±	8.56	59.43	±	1.96
APM12	123.87	±	0.58	68.78	±	1.91	47.53	±	1.02	304.00	±	17.00	68.19	±	13.88
APM13	177.39	±	1.46	60.43	±	3.58	80.32	±	1.49	991.00	±	20.00	41.01	±	15.98
APM14	85.46	±	0.61	81.19	±	10.78	76.80	±	0.52	823.50	±	16.50	44.60	±	1.26
APM15	75.22	±	0.42	107.97	±	1.35	30.02	±	1.50	409.00	±	12.96	62.69	±	2.19
APM16	78.63	±	0.55	64.52	±	0.92	48.63	±	1.04	591.00	±	20.00	55.89	±	7.41
APM17	79.12	±	0.86	64.41	±	1.28	59.41	±	1.14	591.00	±	1.846	52.89	±	2.11
APM18	71.19	±	0.71	54.27	±	1.02	78.03	±	1.30	959.30	±	21.00	67.75	±	2.12
APM19	54.23	±	0.60	65.99	±	1.79	81.08	±	1.20	784.00	±	14.10	39.60	±	2.38
APM20	69.91	±	0.47	68.98	±	3.28	56.96	±	1.03	579.00	±	10.73	38.98	±	20.58
APM21	57.23	±	1.00	28.72	±	2.30	34.88	±	2.22	856.33	±	42.33	32.00	±	5.40
APM22	76.11	±	0.40	83.87	±	4.31	64.35	±	1.43	582.00	±	34.20	27.00	±	2.52
APM23	78.82	±	2.20	65.41	±	3.31	62.47	±	3.09	752.00	±	26.00	25.15	±	2.97
APM24	104.20	±	1.71	96.67	±	2.86	81.21	±	1.53	850.00	±	19.25	120.00	±	18.91
APM25	61.45	±	1.01	65.09	±	3.83	81.55	±	3.89	602.00	±	12.89	52.00	±	9.20
KPM1	65.47	±	1.17	25.01	±	2.09	79.34	±	1.88	980.00	±	15.00	78.00	±	12.00

KPM2	105.87	±	1.06	54.54	±	1.56	89.73	±	3.36	399.00	±	9.00	36.90	±	3.72
KPM3	67.70	±	0.73	41.84	±	1.30	64.81	±	1.51	645.00	±	21.00	38.70	±	7.40
KPM4	55.66	±	1.06	51.03	±	1.81	76.32	±	1.17	1100.00	±	49.56	78.00	±	6.89
KPM5	86.44	±	0.68	42.43	±	0.73	128.47	±	2.82	782.00	±	32.00	56.20	±	1.26
KPM6	58.22	±	1.27	48.62	±	2.91	71.52	±	1.89	586.00	±	25.00	91.00	±	2.90
KPM7	84.08	±	2.07	42.62	±	2.80	125.60	±	1.32	469.00	±	12.78	78.25	±	9.85
KPM8	68.99	±	0.49	74.55	±	2.61	75.30	±	0.38	796.00	±	17.32	86.00	±	10.26
KPM9	112.60	±	1.29	34.38	±	2.08	143.48	±	2.95	627.00	±	22.00	26.10	±	1.30
KPM10	123.67	±	0.65	26.98	±	1.80	102.43	±	3.13	456.00	±	23.00	38.00	±	2.00
KPM11	52.25	±	2.21	35.73	±	6.29	65.01	±	0.88	569.00	±	17.90	83.00	±	1.96
KPM12	60.87	±	0.81	24.33	±	3.61	53.04	±	1.12	987.00	±	3.69	21.00	±	1.94
KPM13	79.26	±	1.93	49.31	±	3.13	71.09	±	3.32	471.00	±	10.00	39.41	±	1.58
KPM14	85.67	±	0.68	35.25	±	3.13	86.18	±	1.51	948.00	±	32.00	64.50	±	6.12
KPM15	79.51	±	1.20	49.16	±	1.22	97.83	±	2.60	409.00	±	11.25	36.97	±	7.82
KPM16	64.77	±	2.03	60.38	±	3.48	85.71	±	2.32	789.00	±	49.10	70.00	±	5.67
KPM17	87.28	±	0.85	19.00	±	0.92	105.00	±	3.96	685.00	±	8.95	21.80	±	1.19
KPM18	74.47	±	0.84	49.71	±	1.81	81.35	±	1.23	602.30	±	13.00	39.70	±	9.95
KPM19	58.25	±	0.97	67.33	±	1.83	36.68	±	1.81	550.00	±	32.00	55.23	±	3.80
KPM20	65.95	±	1.70	56.18	±	3.32	65.89	±	1.02	656.00	±	20.00	98.00	±	5.80
Min	**39.92**	**±**	**0.40**	**19.00**	**±**	**0.73**	**24.22**	**±**	**0.24**	**304.00**	**±**	**3.69**	**10.38**	**±**	**1.19**
Max	**177.39**	**±**	**2.21**	**107.97**	**±**	**10.78**	**143.48**	**±**	**3.96**	**1100.00**	**±**	**49.56**	**120.00**	**±**	**20.64**
Mean	**81.24**	**±**	**1.00**	**57.99**	**±**	**2.61**	**72.10**	**±**	**1.67**	**682.00**	**±**	**19.81**	**55.89**	**±**	**6.21**

Table A4 Radiological parameters in PM samples, absorbed dose (D), Annual effective dose equivalent (AEDE), radium equivalent activity concentrations (Raeq) and external hazard index (Hex) in the two towns of Arandis and Karibib in Erongo region

Sample ID	**(D) nGy/h**	**(Raeq) Bq/kg**	**AEDE (external) mSv/y**	**(ELCR) x 10^{-3}**	**Hazard Indices (Hex)**
APM1	111.21	236.83	0.68	0.48	0.77
APM2	74.70	156.30	0.46	0.32	0.55
APM3	99.85	217.87	0.61	0.43	0.76
APM4	104.91	228.77	0.64	0.45	0.83
APM5	118.33	253.54	0.73	0.51	0.95
APM6	83.63	176.29	0.51	0.36	0.65
APM7	85.26	187.03	0.52	0.37	0.65
APM8	107.59	232.84	0.66	0.46	0.83
APM9	96.32	200.58	0.59	0.41	0.83
APM10	91.45	191.93	0.56	0.39	0.68
APM11	82.79	179.91	0.51	0.36	0.64
APM12	73.25	160.15	0.45	0.31	0.62
APM13	118.06	251.60	0.72	0.51	0.84
APM14	118.49	254.43	0.73	0.51	0.91
APM15	85.19	182.39	0.52	0.37	0.78
APM16	84.00	179.56	0.52	0.36	0.66
APM17	90.46	194.88	0.55	0.39	0.70
APM18	112.49	239.72	0.69	0.48	0.79
APM19	112.39	242.30	0.69	0.48	0.83
APM20	90.59	195.02	0.56	0.39	0.71
APM21	70.30	144.54	0.43	0.30	0.47
APM22	102.06	220.70	0.63	0.44	0.82
APM23	99.54	212.65	0.61	0.43	0.75
APM24	129.41	278.25	0.79	0.56	1.01

APM25	104.61	228.06	0.64	0.45	0.79
Mean (Arandis)	**97.88**	**209.85**	**0.60**	**0.42**	**0.75**
KPM1	100.64	213.93	0.62	0.43	0.65
KPM2	96.16	213.58	0.59	0.41	0.72
KPM3	85.57	184.18	0.52	0.37	0.61
KPM4	115.87	244.87	0.71	0.50	0.80
KPM5	130.04	286.36	0.80	0.56	0.89
KPM6	90.27	196.02	0.55	0.39	0.66
KPM7	115.25	258.34	0.71	0.49	0.81
KPM8	113.35	243.52	0.70	0.49	0.86
KPM9	128.88	287.84	0.79	0.55	0.87
KPM10	93.48	208.56	0.57	0.40	0.64
KPM11	79.67	172.51	0.49	0.34	0.56
KPM12	84.73	176.18	0.52	0.36	0.54
KPM13	85.50	187.24	0.52	0.37	0.64
KPM14	108.16	231.49	0.66	0.46	0.72
KPM15	98.98	220.56	0.61	0.42	0.73
KPM16	112.81	243.70	0.69	0.48	0.82
KPM17	100.97	221.89	0.62	0.43	0.65
KPM18	97.40	212.42	0.60	0.42	0.71
KPM19	76.36	162.13	0.47	0.33	0.62
KPM20	93.30	200.91	0.57	0.40	0.69
MEAN (Karibib)	**100.37**	**218.91**	**0.62**	**0.43**	**0.71**
Min	**70.30**	**144.54**	**0.43**	**0.30**	**0.47**
Max	**130.04**	**287.84**	**0.80**	**0.56**	**1.01**
Mean	**98.98**	**213.61**	**0.61**	**0.42**	**0.73**

Table A5 Radionuclides concentrations in soil samples from the two towns of Arandis and Karibib in Erongo region

Sample no	Activity concentrations (Bq.kg^-1)														
	Ra-226			U-238			Th-232			K-40			Pb-210		
AS1	60.44	±	0.76	50.13	±	2.76	103.07	±	1.27	792.00	±	5.50	109.00	±	5.10
AS2	112.25	±	3.01	50.13	±	3.91	100.63	±	2.57	716.20	±	9.61	115.60	±	13.10
AS3	80.59	±	2.13	59.17	±	4.71	88.13	±	2.06	971.00	±	9.70	92.00	±	6.98
AS4	115.31	±	4.87	58.57	±	2.26	110.82	±	10.70	650.00	±	8.10	76.55	±	10.43
AS5	76.17	±	3.96	65.41	±	5.76	46.76	±	1.02	989.00	±	18.70	116.80	±	23.00
AS6	61.62	±	1.07	60.55	±	7.85	71.98	±	1.07	811.00	±	9.49	62.00	±	7.80
AS7	120.84	±	1.08	83.35	±	2.05	90.91	±	1.16	644.00	±	24.00	53.20	±	3.60
AS8	69.81	±	1.56	56.15	±	16.08	70.13	±	0.24	966.00	±	6.97	125.00	±	9.46
AS9	72.98	±	0.76	78.50	±	3.79	24.22	±	0.28	782.00	±	31.00	50.10	±	2.20
AS10	77.25	±	1.29	59.69	±	2.06	122.44	±	2.10	982.00	±	20.00	118.00	±	29.50
AS11	112.06	±	3.24	61.18	±	4.10	126.72	±	5.58	729.90	±	21.60	121.00	±	16.22
AS12	129.62	±	0.85	78.32	±	1.91	55.02	±	2.43	784.00	±	15.18	89.88	±	12.60
AS13	92.81	±	1.65	68.07	±	1.96	64.17	±	2.16	961.00	±	12.64	65.13	±	9.80
AS14	135.29	±	12.82	70.50	±	4.77	95.38	±	7.73	823.50	±	23.10	84.00	±	1.26
AS15	75.56	±	2.11	69.44	±	1.35	70.41	±	1.50	809.00	±	16.82	62.69	±	2.19
AS16	120.13	±	2.60	45.66	±	2.81	78.40	±	1.53	757.00	±	10.00	119.00	±	8.04
AS17	55.79	±	1.11	62.30	±	18.59	102.77	±	17.33	648.00	±	14.80	89.00	±	5.32
AS18	70.15	±	1.72	72.77	±	2.10	97.65	±	2.05	984.00	±	11.28	67.75	±	2.12
AS19	67.03	±	1.43	54.70	±	2.59	63.47	±	3.00	820.00	±	10.00	56.78	±	2.10
AS20	52.69	±	1.01	75.47	±	5.21	91.40	±	1.03	658.00	±	7.89	72.30	±	5.80
AS21	59.25	±	0.60	55.84	±	0.79	63.83	±	2.22	633.00	±	18.00	68.00	±	3.60
AS22	100.31	±	1.42	41.39	±	2.27	73.85	±	2.67	840.00	±	21.00	72.00	±	2.60
AS23	79.04	±	2.34	40.94	±	1.36	64.02	±	2.10	766.00	±	26.00	87.00	±	3.40
AS24	97.09	±	0.83	42.43	±	0.75	67.48	±	0.71	989.00	±	22.00	120.00	±	18.91

AS25	85.96	±	0.66	60.67	±	2.01	65.25	±	0.86	878.00	±	8.90	119.00	±	9.20
KS1	43.69	±	1.09	22.24	±	0.78	55.16	±	1.19	887.00	±	12.60	35.00	±	2.60
KS2	45.35	±	1.03	33.03	±	1.25	50.92	±	2.31	900.00	±	17.30	52.94	±	0.90
KS3	44.87	±	0.67	32.59	±	0.80	34.47	±	0.79	716.00	±	26.00	62.91	±	2.90
KS4	41.99	±	0.96	37.61	±	0.80	69.86	±	0.69	694.23	±	36.10	31.62	±	3.12
KS5	88.98	±	1.61	40.31	±	0.74	157.81	±	5.20	857.00	±	32.00	62.47	±	2.60
KS6	35.77	±	0.66	60.66	±	0.94	50.80	±	0.96	1058.00	±	42.00	95.62	±	2.92
KS7	54.18	±	1.85	49.66	±	5.65	50.05	±	0.77	495.00	±	16.20	31.00	±	1.85
KS8	25.22	±	0.75	63.94	±	0.86	64.48	±	2.11	815.00	±	11.10	46.00	±	2.73
KS9	34.41	±	2.30	50.84	±	1.51	64.70	±	1.72	778.00	±	17.00	46.00	±	2.00
KS10	23.80	±	1.16	34.23	±	1.07	65.80	±	1.47	778.00	±	32.00	65.00	±	3.46
KS11	52.18	±	2.20	35.95	±	1.99	54.17	±	1.67	823.00	±	8.12	39.00	±	1.00
KS12	58.17	±	0.77	31.11	±	2.32	49.38	±	1.08	920.00	±	9.80	39.00	±	1.73
KS13	19.76	±	0.47	30.41	±	3.53	49.62	±	0.98	700.00	±	19.10	39.00	±	1.32
KS14	33.47	±	0.93	30.20	±	2.81	57.91	±	2.37	881.00	±	29.00	55.00	±	5.50
KS15	41.98	±	1.20	35.02	±	1.25	40.86	±	1.72	957.00	±	17.00	56.00	±	8.19
KS16	33.70	±	1.69	108.20	±	12.73	63.23	±	2.28	645.00	±	32.00	66.00	±	4.67
KS17	30.87	±	0.62	28.00	±	0.70	68.45	±	1.41	685.00	±	8.95	39.00	±	1.20
KS18	29.58	±	2.35	47.64	±	6.81	40.62	±	1.23	602.30	±	13.00	37.00	±	1.40
KS19	44.13	±	1.31	36.39	±	0.86	49.25	±	1.81	650.00	±	40.00	55.23	±	1.39
KS20	26.11	±	1.35	46.00	±	1.96	62.26	±	0.99	656.00	±	20.00	52.00	±	3.76
Min	**19.76**	**±**	**0.47**	**22.24**	**±**	**0.70**	**24.22**	**±**	**0.24**	**495.00**	**±**	**5.50**	**31.00**	**±**	**0.90**
Max	**135.29**	**±**	**12.82**	**108.20**	**±**	**18.59**	**157.81**	**±**	**17.33**	**1058.00**	**±**	**42.00**	**125.00**	**±**	**29.50**
Mean	**66.41**	**±**	**1.77**	**52.79**	**±**	**3.40**	**71.30**	**±**	**2.40**	**797.36**	**±**	**18.26**	**71.50**	**±**	**5.99**

Table A6 Radiological parameters in soil samples, absorbed dose (D), Annual effective dose equivalent (AEDE), radium equivalent activity concentrations (Raeq) and external hazard index (Hex) in the two towns of Arandis and Karibib in Erongo region

Sample ID	**(D) nGy/h**	**(Raeq) Bq/kg**	**AEDE (total) mSv/y**	**(ELCR) x 10^{-3}**	**Hazard Indices (Hex)**
AS1	118.68	258.50	0.73	0.51	0.70
AS2	114.02	249.17	0.70	0.49	0.67
AS3	121.35	259.96	0.74	0.52	0.70
AS4	121.29	267.09	0.74	0.52	0.72
AS5	100.00	208.43	0.61	0.43	0.56
AS6	105.51	225.93	0.65	0.45	0.61
AS7	120.47	262.94	0.74	0.52	0.71
AS8	108.87	230.82	0.67	0.47	0.62
AS9	83.74	173.34	0.51	0.36	0.47
AS10	142.77	310.39	0.88	0.61	0.84
AS11	135.46	298.60	0.83	0.58	0.81
AS12	102.34	217.36	0.63	0.44	0.59
AS13	110.57	233.83	0.68	0.47	0.63
AS14	124.77	270.30	0.77	0.54	0.73
AS15	108.59	232.42	0.67	0.47	0.63
AS16	100.24	216.05	0.61	0.43	0.58
AS17	118.07	259.16	0.72	0.51	0.70
AS18	133.93	288.18	0.82	0.57	0.78
AS19	98.04	208.60	0.60	0.42	0.56
AS20	117.71	256.84	0.72	0.51	0.69
AS21	90.94	195.86	0.56	0.39	0.53

AS22	99.00	211.67	0.61	0.42	0.57
AS23	89.76	191.48	0.55	0.39	0.52
AS24	101.90	215.09	0.62	0.44	0.58
AS25	104.31	221.58	0.64	0.45	0.60
MEAN (Arandis)	**113.44**	**245.02**	**0.70**	**0.49**	**0.66**
KS1	80.84	169.41	0.50	0.35	0.46
KS2	83.81	175.14	0.51	0.36	0.47
KS3	65.95	137.01	0.40	0.28	0.37
KS4	88.73	190.96	0.54	0.38	0.52
KS5	149.94	331.97	0.92	0.64	0.90
KS6	103.15	214.77	0.63	0.44	0.58
KS7	73.96	159.35	0.45	0.32	0.43
KS8	102.72	218.91	0.63	0.44	0.59
KS9	95.24	203.26	0.58	0.41	0.55
KS10	88.24	188.24	0.54	0.38	0.51
KS11	83.89	176.78	0.51	0.36	0.48
KS12	82.84	172.57	0.51	0.36	0.47
KS13	73.42	155.27	0.45	0.32	0.42
KS14	85.93	180.84	0.53	0.37	0.49
KS15	81.05	167.13	0.50	0.35	0.45
KS16	115.27	248.29	0.71	0.49	0.67
KS17	83.05	178.63	0.51	0.36	0.48
KS18	71.84	152.11	0.44	0.31	0.41
KS19	73.86	156.87	0.45	0.32	0.42
KS20	86.41	185.54	0.53	0.37	0.50
Mean (Karibib)	**83.66**	**176.98**	**0.51**	**0.36**	**0.48**
Min	**65.95**	**137.01**	**0.40**	**0.28**	**0.37**

Max	**149.94**	**331.97**	**0.92**	**0.64**	**0.90**
Mean (Total)	**100.94**	**216.15**	**0.62**	**0.43**	**0.58**

Table A7 MDA (Bq/kg) of the radionuclides used in the analysis

Parent nuclide	Daughter	Gamma energy line (keV)	Gamma yield (%)	MDA
^{238}U	^{234}Th	63.20	4.1	0.13
	^{234}Th	92.60	2.39	0.11
	^{234m}Pa	1001.03	0.84	0.84
^{226}Ra	^{214}Pb	351.9	38.9	0.12
	^{214}Pb	295.2	19.7	0.14
	^{214}Bi	609.3	46.10	0.19
	^{214}Bi	1120.3	15.7	0.63
^{232}Th	^{212}Pb	238.6	44.6	0.06
	^{228}Ac	338.3	11.4	0.29
	^{228}Ac	911.6	27.7	0.19
	^{228}Ac	969.1	16.6	0.12
^{40}K	-	1460.20	10.67	1.92
^{210}Pb	-	46.54	4.25	0.14

Table A8 Calculated mass concentrations of particulate matter (PM) samples collected in the town of Karibib and Arandis

Karibib town				Arandis town			
Sample ID	Mass (mg) W_i	Mass (mg) W_f	D (mass concentrations (mg)	Sample ID	Mass (mg) W_i	Mass (mg) W_f	D (mass concentrations (mg)
KPM1	796	1966	907	APM1	1006.3	1431.3	329.0
KPM2	789	1853	825	APM2	992.4	1690.7	541.0
KPM3	805	1306	388	APM3	992.0	1499.8	394.0
KPM4	764	1413	503	APM4	997.6	1135.7	70
KPM5	763	1009	191	APM5	1041.8	2051.0	782.0
KPM6	778	1192	321	APM6	1022.6	1890.2	673.0
KPM7	780	0930	116	APM7	1008.4	2059.6	815.0
KPM8	788	1235	347	APM8	1007.3	1387.8	295.0

KPM9	760	1392	490	APM9	989.5	1804.8	632.0
KPM10	797	1434	494	APM10	1034.6	2135.6	853.0
KPM11	771	2281	1171	APM11	1005.5	2060.6	818.0
KPM12	805	1006	156	APM12	1010.8	1753.8	505.0
KPM13	754	0898	112	APM13	1011.4	1022.2	80
KPM14	761	0866	081	APM14	1005.5	1789.3	608.0
KPM15	769	0921	118	APM15	998.1	1550.2	428.0
KPM16	791	1058	207	APM16	994.0	1948.0	740.0
KPM17	790	0994	158	APM17	1005.1	1281.5	214.0
KPM18	765	1036	210	APM18	1001.8	2051.3	814.0
KPM19	757	1889	878	APM19	1023.4	1408.4	298.0
KPM20	791	0908	91	APM20	992.0	1119.5	99.0
KPM21	766	0940	135	APM21	1017.2	2331.0	1018.0
KPM22	789	0895	85	APM22	992.4	1119.5	99.0
KPM23	786	1125	263	APM23	998.0	1582.2	453.0
KPM24	738	867	100	APM24	1002.8	2057.0	817.0
KPM25	795	939	112	APM25	998.4	1757.5	588.0
Min			80	Min			70
Max			1170	Max			1020
Mean			340	Mean			520

Surface area of opening of the bucket (A) = 0.043 m^2

Duration of sampling (days) (T) = 30 days

Mass (mg) W_i – net weight of the filter

Mass (mg) W_f – weight of filter + sample

Table A8 Exposure and radon gas concentration in dwellings in the town of Karibib and Arandis

SAMPLE ID	**RADON GAS**				
	Exposure (Bq. h. m^{-3})		**Radon Conc. (Bq/m^3)**		**HE**
	# Tracks	**Std. dev**	**Bq/m3**	**Std dev.**	**mSv/yr**
AR1	2.09E+05	1.99E+04	9.53E+01	9.09E+00	2.40
AR 2	2.12E+05	1.93E+04	9.68E+01	8.81E+00	2.44
AR 3	2.07E+05	2.01E+04	9.47E+01	9.15E+00	2.38
AR 4	2.06E+05	2.40E+04	9.38E+01	1.09E+01	2.37
AR 5	2.05E+05	1.44E+04	9.36E+01	6.55E+00	2.36
AR 6	2.01E+05	2.03E+04	9.16E+01	9.27E+00	2.31
AR 7	2.11E+05	2.03E+04	9.61E+01	9.27E+00	2.42
AR 8	2.00E+05	2.09E+04	9.12E+01	9.55E+00	2.30
AR 9	2.01E+05	2.23E+04	9.15E+01	1.02E+01	2.31
R 10	2.11E+05	2.19E+04	9.62E+01	9.99E+00	2.42
AR 11	2.02E+05	2.46E+04	9.23E+01	1.12E+01	2.33
AR 12	2.03E+05	2.11E+04	9.25E+01	9.63E+00	2.33
AR 13	2.13E+05	2.22E+04	9.71E+01	1.02E+01	2.45
AR 14	2.09E+05	2.27E+04	9.53E+01	1.04E+01	2.40
AR 15	2.13E+05	2.29E+04	9.73E+01	1.04E+01	2.45
AR 16	2.18E+05	2.30E+04	9.97E+01	1.05E+01	2.51

AR 17	2.12E+05	2.10E+04	9.68E+01	9.58E+00	2.44
AR 18	2.04E+05	1.06E+04	9.31E+01	4.85E+00	2.35
AR 19	2.14E+05	2.85E+05	9.76E+01	1.30E+01	2.46
AR 20	2.03E+05	2.34E+04	9.27E+01	1.07E+01	2.34
AR 21	2.09E+05	2.29E+04	9.54E+01	1.04E+01	2.41
AR 22	2.12E+05	1.47E+04	9.69E+01	6.73E+00	2.44
AR 23	2.17E+05	1.16E+04	9.88E+01	5.27E+00	2.49
AR 24	2.00E+05	2.60E+05	9.13E+01	1.18E+01	2.30
AR 25	2.01E+05	2.40E+04	9.19E+01	1.10E+01	2.32
KR1	1.78E+05	1.45E+04	8.13E+01	6.62E+00	2.05
KR2	1.93E+05	1.45E+04	8.81E+01	6.62E+00	2.22
KR3	1.62E+05	1.47E+04	7.40E+01	6.71E+00	1.87
KR4	1.88E+05	1.49E+04	8.58E+01	6.80E+00	2.17
KR5	1.82E+05	1.59E+04	8.36E+01	7.26E+00	2.11
KR6	1.85E+05	1.50E+04	8.45E+01	6.85E+00	2.13
KR7	1.60E+05	1.38E+04	7.31E+01	6.30E+00	1.84
KR8	1.61E+05	1.48E+04	7.35E+01	6.76E+00	1.85
KR9	1.77E+05	1.51E+04	8.08E+01	6.89E+00	2.04
KR10	1.55E+05	1.42E+04	7.08E+01	6.48E+00	1.79
KR11	1.81E+05	1.44E+04	8.26E+01	6.58E+00	2.09
KR12	1.68E+05	1.58E+04	7.67E+01	7.21E+00	1.94

KR13	1.86E+05	1.40E+04	8.49E+01	6.39E+00	2.14
KR14	1.62E+05	1.49E+04	7.40E+01	6.80E+00	1.87
KR15	1.58E+05	1.51E+04	7.21E+01	6.89E+00	1.82
KR16	1.77E+05	1.52E+04	8.08E+01	6.94E+00	2.04
KR17	1.87E+05	1.42E+04	8.54E+01	6.48E+00	2.15
KR18	1.61E+05	1.42E+04	7.35E+01	6.48E+00	1.85
KR19	1.63E+05	1.35E+04	7.44E+01	6.16E+00	1.88
KR20	1.89E+05	1.41E+04	8.63E+01	6.44E+00	2.18
Min			**71**		**1.79**
Max			**100**		**2.51**
Mean			**88**		**2.22**

APPENDIX B

Table B1 The concentration of Heavy (mg/kg) in soil samples collected from the town of Arandis of Erongo region

Arandis Town	The concentration of heavy (mg/kg) in soil samples								
Sample ID	Cr	Mn	Fe	Ni	Cu	Zn	As	Cd	Pb
AS1	102.5	249.5	16500	71.36	31.21	33.29	2.81	0.62	43.13
AS2	82.23	259.5	19010	33.20	32.80	56.67	3.10	0.64	31.24
AS3	58.31	166.1	14020	23.32	31.10	105.30	3.01	0.79	79.68
AS4	77.26	268.0	16570	21.61	31.75	59.59	3.48	0.66	29.86
AS5	73.88	353.4	19940	21.49	26.30	41.81	2.94	0.61	18.99
AS6	58.59	253.6	13460	18.36	23.31	29.57	2.49	0.65	16.57
AS7	67.07	177.1	13340	20.01	31.52	39.86	2.39	0.63	15.39
AS8	63.09	117.3	8510	17.00	22.82	33.14	2.51	0.62	11.23
AS9	60.42	161.3	13220	17.57	21.08	29.10	2.23	0.58	9.30
AS10	66.38	345.9	15800	21.07	21.07	30.97	2.98	0.59	11.04
AS11	92.65	393.5	26550	30.48	37.97	77.15	3.05	0.62	27.60
AS12	83.07	243.4	17670	22.00	37.96	60.22	3.74	0.63	30.06
AS13	65.41	90.27	8140	15.92	25.75	44.17	1.71	0.56	31.53
AS14	72.22	135.1	12420	19.05	20.91	35.83	1.77	0.55	17.96
AS15	77.66	179.4	15200	21.21	26.44	51.71	3.25	0.54	15.58
AS16	107.7	235	19410	40.48	33.20	58.63	3.38	0.62	24.62
AS17	67.65	164.4	12440	19.26	25.75	32.03	2.21	0.53	13.90
AS18	66.45	143.4	10870	16.54	18.52	38.29	2.28	0.53	14.91
AS19	71.89	166.9	14450	21.61	19.46	37.93	1.97	0.52	19.44
AS20	84.05	191.6	19930	28.30	25.09	95.12	2.18	0.55	19.99

Table B2 The concentration of heavy (mg/kg) in soil samples collected from the town of Karibib of Erongo region

Karibib Town	The concentration of Heavy (mg/kg) in soil samples								
Sample ID	Cr	Mn	Fe	Ni	Cu	Zn	As	Cd	Pb
KS1	114.2	154	9309	216.1	19.51	65.16	1.51	0.71	10.7
KS2	60.46	148.5	7139	52.47	11.82	20.4	1.10	0.63	5.96
KS3	49.19	157.4	6253	15.98	7.95	14.84	1.58	0.55	4.36
KS4	44.35	111.2	4028	13.06	39.98	14.43	1.08	0.58	3.99
KS5	52.66	184.7	8208	15.79	17.12	69.44	2.56	0.65	21.10
KS6	41.6	43.34	1428	10.71	11.49	4.22	0.59	0.55	1.914
KS7	45.51	157.3	5005	15.9	8.91	13.97	1.19	0.69	5.22
KS8	40.73	73.08	3557	12.62	10.41	7.99	1.67	0.47	4.36
KS9	52.43	209.8	8859	14.82	13.88	24.74	1.62	0.59	10.75
KS10	39.36	113.3	4349	12.64	13.75	173.4	0.65	0.66	14.64
KS11	47.9	158.1	6677	12.4	9.80	16.82	1.31	0.50	7.38
KS12	47.88	116.8	6396	12.57	11.25	14.75	1.18	0.63	6.91
KS13	45.12	161.1	4434	12.4	14.09	13.78	1.24	0.55	4.10
KS14	48.14	91.8	5061	11.01	7.47	14.15	0.64	0.54	5.53
KS15	44.49	99.75	4032	9.87	6.62	11.67	1.14	0.56	5.21
KS16	44.91	98.22	3785	10.07	7.38	9.99	0.94	0.52	5.26
KS17	31.11	56.72	1113	6.85	2.57	1.53	1.83	0.37	1.44
KS18	46.47	71.15	3631	10.25	7.63	6.51	1.30	0.46	3.63
KS19	43.22	65.1	3067	8.31	8.82	8.49	0.82	0.47	3.80
KS20	31.78	37.81	1621	8.34	4.81	4.11	0.46	0.50	2.43

Table B3: Concentrations of heavy metals in soils and critical concentrations in soils (Alloway, 1995)

Metals	Normal soil concentrations (mg/kg)	Critical soil concentrations (mg/kg)
As	0.1 – 40	20 – 50
Cd	0.01 – 2.0	3 – 8
Cr	5 – 1500	75 – 100
Cu	2 – 250	60 – 125
Hg	0.01 – 0.5	0.3 – 5
Mn	20 – 10000	1500 – 3000
Ni	2 – 750	100
Pb	2 – 30	100 – 400
Sb	0.2 – 10	5 – 10
Se	0.1 – 5	5 – 10
Sn	1 – 200	50
V	3 – 500	50 – 100
Zn	1 – 900	70 – 400

APPENDIX C

Table C1 Pollution load index of the soil samples collected from the two mining towns of Arandis and Karibib

Arandis Town	Pollution Load Index	Karibib Town	Pollution Load Index
AS1	2.81E-02	KS1	1.32E-02
AS2	2.29E-02	KS2	1.06E-03
AS3	2.57E-02	KS3	3.41E-04
AS4	1.80E-02	KS4	3.55E-04
AS5	1.19E-02	KS5	4.21E-03

AS6	4.78E-03	KS6	5.29E-05
AS7	5.58E-03	KS7	3.20E-04
AS8	2.18E-03	KS8	1.13E-04
AS9	2.37E-03	KS9	1.31E-03
AS10	5.71E-03	KS10	1.11E-03
AS11	3.90E-02	KS11	4.10E-04
AS12	2.07E-02	KS12	3.59E-04
AS13	2.98E-03	KS13	2.70E-04
AS14	3.19E-03	KS14	1.29E-04
AS15	7.52E-03	KS15	1.24E-04
AS16	2.59E-02	KS16	1.04E-04
AS17	3.47E-03	KS17	4.17E-06
AS18	2.72E-03	KS18	6.69E-05
AS19	4.31E-03	KS19	5.15E-05
AS20	1.32E-02	KS20	7.78E-06
Min	2.18E-03	Min	4.17E-06
Max	3.90E-02	Max	1.32E-02
Mean	1.25E-02	Mean	1.18E-03

Table C2 Contamination factors (CF) and degree of contamination in soil samples collected from the town of Karibib

Karibib Town	Contamination Factors									Degr Cont
	Cr	Mn	Fe	Ni	Cu	Zn	As	Cd	Pb	Con
KS1	1.27	0.18	0.26	4.32	0.43	0.69	0.12	2.37	0.67	10.30
KS2	0.67	0.17	0.20	1.05	0.26	0.21	0.08	2.10	0.37	5.13
KS3	0.55	0.19	0.17	0.32	0.18	0.16	0.12	1.83	0.27	3.79

KS4	0.49	0.13	0.11	0.26	0.89	0.15	0.08	1.93	0.25	4.30
KS5	0.59	0.22	0.23	0.32	0.38	0.73	0.20	2.17	1.32	6.14
KS6	0.46	0.05	0.04	0.21	0.26	0.04	0.05	1.83	1.20	4.14
KS7	0.51	0.19	0.14	0.32	0.20	0.15	0.09	2.30	0.33	4.21
KS8	0.45	0.09	0.10	0.25	0.23	0.08	0.13	1.57	0.27	3.17
KS9	0.58	0.25	0.25	0.30	0.31	0.26	0.12	1.97	0.67	4.70
KS10	0.44	0.13	0.12	0.25	0.31	1.83	0.05	2.20	0.92	6.24
KS11	0.53	0.19	0.19	0.25	0.22	0.18	0.10	1.67	0.46	3.78
KS12	0.53	0.14	0.18	0.25	0.25	0.16	0.09	2.10	0.43	4.13
KS13	0.50	0.19	0.12	0.25	0.31	0.15	0.10	1.83	0.26	3.71
KS14	0.53	0.11	0.14	0.22	0.17	0.15	0.05	1.80	0.35	3.51
KS15	0.49	0.12	0.11	0.20	0.15	0.12	0.09	1.87	0.33	3.47
KS16	0.50	0.12	0.11	0.20	0.16	0.11	0.07	1.73	0.33	3.32
KS17	0.35	0.07	0.03	0.14	0.06	0.02	0.14	1.23	0.09	2.12
KS18	0.52	0.08	0.10	0.21	0.17	0.07	0.10	1.53	0.23	3.00
KS19	0.48	0.08	0.09	0.17	0.20	0.09	0.06	1.57	0.24	2.96
KS20	0.35	0.04	0.05	0.17	0.11	0.04	0.04	1.67	0.15	2.61

Table C3 Contamination factors (CF) and degree of contamination in the soil samples collected from the town of Arandis

Arandis Town	Contamination Factors									Degr Cont
	Cr	Mn	Fe	Ni	Cu	Zn	As	Cd	Pb	Con
AS1	1.14	0.29	0.46	1.43	0.69	0.35	0.22	2.07	2.70	9.34
AS2	0.91	0.31	0.53	0.66	0.73	0.60	0.24	2.13	1.95	8.06
AS3	0.65	0.20	0.39	0.47	0.69	1.11	0.23	2.63	4.98	11.34
AS4	0.86	0.32	0.46	0.43	0.71	0.63	0.27	2.20	1.87	7.73
AS5	0.82	0.42	0.56	0.43	0.58	0.44	0.23	2.03	1.19	6.69
AS6	0.65	0.30	0.37	0.37	0.52	0.31	0.19	2.17	1.04	5.91
AS7	0.75	0.21	0.37	0.40	0.70	0.42	0.18	2.10	0.96	6.09
AS8	0.70	0.14	0.24	0.34	0.51	0.35	0.19	2.07	0.70	5.23
AS9	0.67	0.19	0.37	0.35	0.47	0.31	0.17	1.93	0.58	5.04

AS10	0.74	0.41	0.44	0.42	0.47	0.33	0.23	1.97	0.69	5.69
AS11	1.03	0.46	0.74	0.61	0.84	0.81	0.23	2.07	1.73	8.52
AS12	0.92	0.29	0.49	0.44	0.84	0.63	0.29	2.10	1.88	7.89
AS13	0.73	0.11	0.23	0.32	0.57	0.46	0.13	1.87	1.97	6.38
AS14	0.80	0.16	0.35	0.38	0.46	0.38	0.14	1.83	1.12	5.62
AS15	0.86	0.21	0.42	0.42	0.59	0.54	0.25	1.80	0.97	6.08
AS16	1.20	0.28	0.54	0.81	0.74	0.62	0.26	2.07	1.54	8.04
AS17	0.75	0.19	0.35	0.39	0.57	0.34	0.17	1.77	0.87	5.39
AS18	0.74	0.17	0.30	0.33	0.41	0.40	0.18	1.77	0.93	5.23
AS19	0.80	0.20	0.40	0.43	0.43	0.40	0.15	1.73	1.22	5.76
AS20	0.93	0.23	0.56	0.57	0.56	1.00	0.17	1.83	1.25	7.09

Table C4 Enrichment ratio for the soil samples collected from the town of Karibib

Karibib Town	Enrichment Ratio								
Sample ID	Cr	Mn	Fe	Ni	Cu	Zn	As	Cd	Pb
KS1	4.89	0.52	0.01	8.81	9.79	4.64	33.88	1468.03	27.53
KS2	3.38	0.36	0.01	6.08	6.76	3.20	23.39	1013.45	19.00
KS3	3.14	0.33	0.01	5.65	6.28	2.97	21.72	941.37	17.65
KS4	4.39	0.47	0.01	7.91	8.78	4.16	30.41	1317.58	24.70
KS5	2.56	0.27	0.01	4.61	5.12	2.42	17.72	767.74	14.40
KS6	11.62	1.23	0.03	20.92	23.24	11.01	80.45	3486.09	65.36
KS7	3.63	0.38	0.01	6.53	7.25	3.44	25.11	1088.12	20.40
KS8	4.57	0.48	0.01	8.22	9.14	4.33	31.62	1370.26	25.69
KS9	2.36	0.25	0.01	4.25	4.72	2.24	16.34	708.22	13.28
KS10	3.61	0.38	0.01	6.50	7.22	3.42	24.99	1083.03	20.31
KS11	2.86	0.30	0.01	5.15	5.72	2.71	19.81	858.47	16.10
KS12	2.99	0.32	0.01	5.37	5.97	2.83	20.67	895.82	16.80
KS13	4.06	0.43	0.01	7.31	8.12	3.85	28.10	1217.72	22.83
KS14	3.79	0.40	0.01	6.83	7.59	3.59	26.27	1138.26	21.34
KS15	4.40	0.47	0.01	7.92	8.80	4.17	30.47	1320.43	24.76

KS16	4.73	0.50	0.01	8.52	9.47	4.48	32.77	1419.88	26.62
KS17	11.15	1.18	0.03	20.07	22.30	10.56	77.19	3344.86	62.72
KS18	5.11	0.54	0.01	9.19	10.21	4.84	35.34	1531.51	28.72
KS19	5.62	0.60	0.01	10.12	11.24	5.33	38.92	1686.34	31.62
KS20	7.82	0.83	0.02	14.08	15.64	7.41	54.14	2346.09	43.99

Table C5 Enrichment ratio for the soil samples collected from the town of Arandis

Arandis Town	Enrichment Ratio								
Sample ID	Cr	Mn	Fe	Ni	Cu	Zn	As	Cd	Pb
AS1	2.48	0.64	1.00	3.11	1.51	0.76	0.47	4.50	5.87
AS2	1.73	0.58	1.00	1.25	1.38	1.13	0.45	4.03	3.69
AS3	1.66	0.50	1.00	1.19	1.77	2.84	0.59	6.74	12.75
AS4	1.86	0.68	1.00	0.94	1.53	1.36	0.58	4.77	4.04
AS5	1.48	0.75	1.00	0.77	1.05	0.79	0.41	3.66	2.14
AS6	1.74	AR 5	1.00	0.98	1.38	0.83	0.51	5.78	2.76
AS7	2.01	0.56	1.00	1.08	1.89	1.13	0.49	5.65	2.59
AS8	2.96	0.58	1.00	1.43	2.14	1.47	0.81	8.72	2.96
AS9	1.82	0.52	1.00	0.95	1.27	0.83	0.47	5.25	1.58
AS10	1.68	0.92	1.00	0.96	1.06	0.74	0.52	4.47	1.57
AS11	1.39	0.63	1.00	0.82	1.14	1.10	0.32	2.79	2.33
AS12	1.88	0.58	1.00	0.89	1.71	1.29	0.58	4.27	3.82
AS13	3.21	0.47	1.00	1.40	2.52	2.05	0.58	8.23	8.69
AS14	2.32	0.46	1.00	1.10	1.34	1.09	0.39	5.30	3.24
AS15	2.04	0.50	1.00	1.00	1.39	1.29	0.59	4.25	2.30
AS16	2.21	0.51	1.00	1.50	1.36	1.14	0.48	3.82	2.85
AS17	2.17	0.56	1.00	1.11	1.65	0.97	0.49	5.10	2.51
AS18	2.44	0.56	1.00	1.09	1.36	1.33	0.58	5.83	3.08
AS19	1.98	0.49	1.00	1.07	1.07	0.99	0.38	4.31	3.02
AS20	1.68	0.41	1.00	1.02	1.00	1.80	0.30	3.30	2.25

Table C6 The Geoaccumulation Index values(Igeo) for the heavy metals in soil samples collected in the two towns of Karibib

Karibib Town	Geoaccumulation (Igeo) index of heavy metals								
Sample ID	Cr	Mn	Fe	Ni	Cu	Zn	As	Cd	Pb
KS1	-0.241	-3.049	-2.532	1.527	-1.791	-1.129	-3.691	0.658	-1.165
KS2	-1.159	-3.102	-2.915	-0.515	-2.514	-2.804	-4.148	0.485	-2.010
KS3	-1.457	-3.018	-3.106	-2.231	-3.086	-3.263	-3.625	0.290	-2.461
KS4	-1.606	-3.519	-3.741	-2.522	-0.756	-3.304	-4.174	0.366	-2.589
KS5	-1.358	-2.787	-2.714	-2.248	-1.979	-1.037	-2.929	0.531	-0.186
KS6	-1.698	-4.879	-5.237	-2.808	-2.555	-5.078	-5.047	0.290	-0.326
KS7	-1.569	-3.019	-3.428	-2.238	-2.921	-3.351	-4.034	0.617	-2.201
KS8	-1.729	-4.125	-3.920	-2.571	-2.697	-4.157	-3.546	0.063	-2.461
KS9	-1.364	-2.603	-2.604	-2.339	-2.282	-2.526	-3.589	0.391	-1.159
KS10	-1.778	-3.492	-3.630	-2.569	-2.295	0.283	-4.907	0.553	-0.713
KS11	-1.495	-3.012	-3.012	-2.597	-2.784	-3.083	-3.896	0.152	-1.701
KS12	-1.495	-3.448	-3.074	-2.577	-2.585	-3.272	-4.047	0.485	-1.796
KS13	-1.581	-2.984	-3.602	-2.597	-2.260	-3.370	-3.975	0.290	-2.549
KS14	-1.488	-3.796	-3.411	-2.768	-3.176	-3.332	-4.929	0.263	-2.118
KS15	-1.601	-3.676	-3.739	-2.926	-3.350	-3.610	-4.096	0.316	-2.204
KS16	-1.588	-3.698	-3.831	-2.897	-3.193	-3.834	-4.375	0.209	-2.190
KS17	-2.118	-4.490	-5.596	-3.453	-4.715	-6.541	-3.414	-0.282	-4.059
KS18	-1.539	-4.163	-3.891	-2.871	-3.145	-4.452	-3.907	0.032	-2.725
KS19	-1.643	-4.292	-4.134	-3.174	-2.936	-4.069	-4.572	0.063	-2.659
KS20	-2.087	-5.076	-5.054	-3.169	-3.811	-5.116	-5.406	0.152	-3.304
Min	-2.118	-5.076	-5.596	-3.453	-4.715	-6.541	-5.406	-0.282	-4.059
Min	-0.241	-2.603	-2.532	1.527	-0.756	0.283	-2.929	0.658	-0.186
Mean	**-1.530**	**-3.612**	**-3.659**	**-2.377**	**-2.742**	**-3.352**	**-4.115**	**0.296**	**-2.029**
WSRA	90	850	35900	50	45	95	13	0.3	16

Table C7 The Geoaccumulation (Igeo) Index values for the heavy metals in soil samples collected in the two towns of Arandis

Arandis Town	Geoaccumulation (Igeo) index of heavy metals								
Sample ID	Cr	Mn	Fe	Ni	Cu	Zn	As	Cd	Pb
AS1	-0.397	-2.353	-1.706	-0.072	-1.113	-2.098	-2.795	0.462	0.846
AS2	-0.715	-2.297	-1.502	-1.176	-1.041	-1.330	-2.653	0.508	0.380
AS3	-1.211	-2.940	-1.941	-1.685	-1.118	-0.436	-2.696	0.812	1.731
AS4	-0.805	-2.250	-1.700	-1.795	-1.088	-1.258	-2.486	0.553	0.315
AS5	-0.870	-1.851	-1.433	-1.803	-1.360	-1.769	-2.730	0.439	-0.338
AS6	-1.204	-2.330	-2.000	-2.030	-1.534	-2.269	-2.969	0.531	-0.534
AS7	-1.009	-2.848	-2.013	-1.906	-1.099	-1.838	-3.028	0.485	-0.641
AS8	-1.097	-3.442	-2.662	-2.141	-1.565	-2.104	-2.958	0.462	-1.096
AS9	-1.160	-2.983	-2.026	-2.094	-1.679	-2.292	-3.128	0.366	-1.368
AS10	-1.024	-1.882	-1.769	-1.832	-1.680	-2.202	-2.710	0.391	-1.120
AS11	-0.543	-1.696	-1.020	-1.299	-0.830	-0.885	-2.677	0.462	0.202
AS12	-0.701	-2.389	-1.608	-1.769	-0.830	-1.243	-2.382	0.485	0.325
AS13	-1.045	-3.820	-2.726	-2.236	-1.390	-1.690	-3.511	0.316	0.394
AS14	-0.902	-3.238	-2.116	-1.977	-1.691	-1.992	-3.462	0.290	-0.418
AS15	-0.798	-2.829	-1.825	-1.822	-1.352	-1.462	-2.585	0.263	-0.623
AS16	-0.326	-2.440	-1.472	-0.890	-1.024	-1.281	-2.528	0.462	0.037
AS17	-0.997	-2.955	-2.114	-1.961	-1.390	-2.153	-3.141	0.236	-0.788
AS18	-1.023	-3.152	-2.309	-2.181	-1.866	-1.896	-3.096	0.236	-0.687
AS19	-0.909	-2.933	-1.898	-1.795	-1.794	-1.910	-3.307	0.209	-0.304
AS20	-0.684	-2.734	-1.434	-1.406	-1.428	-0.583	-3.161	0.290	-0.264
Min	-1.211	-3.820	-2.726	-2.236	-1.866	-2.292	-3.511	0.209	-1.368
Min	-0.326	-1.696	-1.020	-0.072	-0.830	-0.436	-2.382	0.812	1.731
Mean	**-0.871**	**-2.668**	**-1.864**	**-1.694**	**-1.344**	**-1.635**	**-2.900**	**0.413**	**-0.198**
WSRA	90	850	35900	50	45	95	13	0.3	16

APPENDIX D

Table D1 Inhalability, respiratory deposition and particle size of PM samples collected from the town of Karibib and Arandis

Karibib Town					**Arandis Town**				
Sample ID	**PM≤ 1.0μm**	Wind Speed (m/s)	Inhalable Fraction (IF)	Deposition Fraction (DF)	Sample ID	PM≤ **1.0μm**	Wind Speed (m/s)	Inhalable Fraction (IF)	Deposition Fraction (DF)
KPM1	0.23	5.10	0.994041	1.021329	APM1	0.028	4.10	0.999646	1.576453
KPM3	0.1	4.85	0.997782	1.181617	APM4	0.019	5.10	1.000314	1.688279
KPM5	0.35	5.80	0.990891	0.927558	APM5	0.01	7.22	1.001997	1.814106
KPM7	0.4	5.60	0.98931	0.886102	APM7	0.074	8.00	1.000842	1.263112
KPM8	0.32	4.70	0.991209	0.95094	APM8	0.024	8.12	1.002456	1.627963
KPM9	0.2	6.80	0.996005	1.047576	APM9	0.063	6.00	0.999498	1.308978
KPM10	0.23	4.70	0.993861	1.021144	APM11	0.028	4.00	0.999614	1.576403
KPM13	0.19	3.84	0.986973	1.046694	APM14	0.015	4.50	1.000176	1.742183
KPM14	0.43	3.87	0.987265	0.859392	APM15	0.1	4.30	0.997564	1.181359
KPM16	0.23	4.20	0.993672	1.020949	APM16	0.051	6.39	1.000118	1.377374
KPM19	0.21	4.50	0.994372	1.037539	APM17	0.023	7.50	1.001863	1.639351
KPM20	0.18	6.80	0.996596	1.066065	APM18	0.32	5.80	0.991771	0.951479
KPM21	0.09	4.90	0.998102	1.207445	APM19	0.75	4.21	0.978542	0.579946
KPM23	0.16	5.80	0.996491	1.086202	APM21	0.098	8.60	1.000803	1.189945

					APM23	0.082	6.80	0.999502	1.233205
Min	0.09	3.84	0.986973	0.850707		0.01	4	0.978542	0.579946
Max	0.44	6.80	0.998102	1.207445		0.75	8.6	1.002456	1.814106
Mean	**0.30**	**5.10**	**0.991937**	**0.969545**	**Mean**	**0.11**	**6.04**	**0.998314**	**1.383342**
	1.0<PM≤								
	$\mathbf{2.5\mu m}$								
KPM2	1.33	6.20	0.993204	0.982872	APM3	1.68	6.30	0.953788	0.18697
KPM4	1.07	4.40	0.969533	0.372672	APM10	1.37	5.80	0.9619	0.256885
KPM6	1.71	3.95	0.951244	0.181628	APM13	1.54	7.20	0.95835	0.214175
KPM12	1.52	4.10	0.956944	0.218151	APM20	1.33	6.40	0.963424	0.26913
KPM15	1.46	4.00	0.958554	0.232341	APM24	1.82	8.20	0.951877	0.165877
KPM18	1.37	5.40	0.961658	0.25682	APM22	1.1	4.71	0.968819	0.35816
KPM22	1.14	5.70	0.96822	0.340077					
Min	1.07	3.95	0.951244	0.181628	Min	1.1	4.71	0.951877	0.165877
Max	1.71	5.7	0.969533	0.372672	Max	1.82	8.2	0.968819	0.35816
Mean	**1.37**	**4.82**	**0.961347**	**0.267254**	**Mean**	**1.47**	**6.4**	**0.959693**	**0.241866**

Table D2 Inhalability, respiratory deposition and particle size of PM samples collected from the town of Karibib and Arandis continued…

Karibib Town					**Arandis Town**				
Sample ID	**1.0<PM≤ 2.5μm**	Wind Speed (m/s)	Inhalable Fraction (IF)	Deposition Fraction (DF)	Sample ID	PM≤ **1.0μm**	Wind Speed (m/s)	Inhalable Fraction (IF)	Deposition Fraction (DF)
KPM17	2.7	5.30	0.926359	0.097991	APM2	3.2	4.85	0.91357	0.08241
KPM24	2.68	4.90	0.926648	0.098789	APM6	2.8	6.80	0.924948	0.094274
KPM11	3	4.80	0.918516	0.087649	APM12	3.9	6.80	0.898094	0.07035
Min	2.68	4.80	0.918516	0.087649	Min	2.8	4.85	0.898094	0.07035
Max	3.0	5.30	0.926648	0.098789	Max	3.9	6.8	0.924948	0.094274
Mean	**2.79**	**5.30**	**0.923841**	**0.09481**	**Mean**	**3.3**	**6.15**	**0.912204**	**0.082345**

APPENDIX E

List of presentations & publications

- **Presentations**

  Title: Excess lifetime cancer risk due to natural radioactivity in soils: Case of Karibib town in Namibia. Oral presentation at the Research Week of the Faculty of Health and Applied Sciences, Namibia University of Science and Technology (FHAS Research week) 11th – 13th May 2018, Windhoek, Namibia.

- **Peer reviewed paper publications**

  1. **Zivuku. M,** Tshivhase VM, **Kgabi NA.** Excess lifetime cancer risk due to natural radioactivity in soils: Case of Karibib town in Namibia. Proceedings of the first African Conferences on fundamental Physics and Applications (2018), Namibia**.** *The African Review of Physics* (2018) 13: 0012*.*